Investigating novel aspects of the blood-brain barrier using high resolution electron microscopy

University of the Western Cape

by

Shireen Mentor

MSc Medical Biosciences, UWC

A thesis submitted in fulfilment of the requirements for the degree of ***Philosophiae Doctor*** *in the Department Medical Biosciences, Faculty of Natural Sciences, University of the Western Cape*

Supervisor:

Professor D. Fisher

Co-supervisors:

Dr F. Cummings; Professor M. Zaahl

January, 2022

ABSTRACT

The blood-brain barrier (BBB) is a restrictive interface located between the blood circulation and the central nervous system (CNS), regulating the homeostatic environment of the neuronal *milieu*, by controlling the permeability of the cerebrovasculature. Currently, we cannot fully comprehend the regulatory features and the complexity of BBB morphology to allow for intervention clinically. The thesis consists of four publications. The methodology paper proposes a novel experimental design to visualize the morphological architecture of immortalized mouse brain endothelial cell lines (bEnd3/bEnd5). The brain endothelial cells (BECs) were grown on cellulose matrices and fixed in 2.5 % glutaraldehyde in preparation for visualization of the paracellular (PC) spaces between adjacent BECs, employing high-resolution electron microscopy (HREM), with vested interest in the morphological profile of the developing BEC. The second publication addresses and reports on the nanosized detail of BEC monolayer morphology utilizing high-resolution scanning electron microscopy (HR-SEM) and published the first descriptions of the extrusion of a basement membrane from developing *in vitro* BECs. Moreover, we categorized and discussed two types of nanotubule (NT) development specific for the establishment of the BEC monolayers. NTs can occur via nanovesicle extrusion onto the BEC membrane surfaces, which fuse, forming tunneling NTs (TUNTs) between adjacent BECs. Furthermore, cytoplasmic extensions of BEC membrane leading edges give rise to tethering NT (TENTs), which result in overlapping regions across the PC spaces, resulting in PC occlusion. BEC NT communication is illuminated in a third publication utilizing immunofluorescence microscopy, which reports on the molecular, cytoskeletal elements governing NT formation. This study shows, for the first time, f-actin and α-tubulin cytoskeletal proteins extending between the soma of the cells and NT cytoskeletal structures within an *in vitro* BBB model. Thereafter, the effects depolymerizing agents, Cytochalasin D and Nocodazole, were investigated on f-actin and α-tubulin cytoskeletal protein generation,

functionality of NT morphology, cell division and permeability. For the first time, we show that f-actin possesses an additional function, key to tight junction, plaque protein organization. Moreover, it facilitates TENT formation, essential for cytoplasmic projection across PC spaces. Conversely, α-tubulin facilitates known functions: (i) transportation, (ii) cytokinesis, (iii) cellular division, and (iv) possesses a novel function as the molecular cytoskeletal backbone of TENTs, which facilitates BBB impermeability. A critical review evaluates past literature, in light of the current findings emanating from this study. The review critiques the concept of BEC cilia, which have been reported in the literature, comprised of tubulin and actin, but at low-resolution. In the light of our novel observations, nowhere in transmission electron microscopy do we observe cilia on the BECs, we postulate that NTs have been misnamed and mischaracterized as cilia. The thesis endeavors to elucidate the complexity of BEC nanostructures by examining the emerging role of the nanoscopic landscape of BBB development and the changing nature of BEC morphology, NT formation and associated cytoarchitectural underpinnings governing NT morphology. The research study attempts to, with a view to create new avenues for treating brain pathology, revolutionize our interpretation of barrier-genesis on a nanoscale.

KEY WORDS

Blood-brain barrier

Brain endothelium

Electron microscopy

Nanovesicles

Nanotubes

Cytoskeleton

Cytoarchitecture

DECLARATION

I declare that the **Investigating novel aspects of the blood-brain barrier using high resolution electron microscopy** is my own work, that it has not been submitted for any degree or examination in any other university, and that all the sources I have used or quoted have been indicated and acknowledged by means of complete references.

Shireen Mentor

27 January, 2022

ACKNOWLEDGEMENTS

I extend my sincere gratitude to my supervisors: Prof. David Fisher (PhD supervisor), for: (i) inspiring philosophical thought, (ii) molding me into a relentless researcher and (ii) for being my intellectual stress test for the past decade. The best teachers are those who tell us where to look, but not what to find.

To Dr Franscious Cummings (PhD co-supervisor), for going beyond cellular proliferation under the light microscope. Your impartation in the field of physics and electron microscopy has brought this ultrastructural narrative to light.

To the Carl and Emily Fuchs Foundation; National Research Foundation; the Fulbright program and the Confucius Institute for the financial support.

To my colleagues, family and friends (scattered across the world) for believing, with me, in every ebb and flow of this wave and for your encouragement and support. You are the reason I am still standing.

To every Neurobiology journal club, the academic purgatory is akin to the *Via Dolorosa*. It continues to floor me.

To my trusted friend and colleague, Dr Velaphi Clement Thipe for your unwavering support and being a reminder to push the frontiers of scientific research.

Dr Kim Lategan and Dr Iuliia Dubova for your assistance with the molecular aspects of this research study.

Lucinda Parsons your leadership and other-centered perspective have been a positive influence.

Breyten Rooiland for understanding the weight of journeying down a path whole-heartedly.

Gary Rhode for texturing the visual aspects of this research study. Thank you for greasing the squeaky wheels along this research journey.

Abraham Sam Udodong for your sober perspective and for epitomizing the statement, “I’ve got your back.”

Eustace Ibsen Diergaardt for egging me on through every application. Thank you for teaching me how to live through every degree. You are found between the lines.

Ryan Thebus for your encouragement and ensuring my safety to and from the lab.

Mr Moses Matthews (high school English educator), who reckoned that I would one day become a “Mad Scientist”

To my mother, Alice Pauline Mentor, for being the first person to teach me how to conduct research using an encyclopedia. For being the first to expose me to visualizing cells under a light microscope. Thank you for making me a believer in very valuable metrics (i.e. integrity, discipline, perseverance). You gave me everything. I owe you everything.

To the Genius who fashioned me - outside of time, space and matter-God is The Noblest Laureate.

DEDICATION

For my mother. Thesis dedications are soft-centered. After numerous altered versions, here is my first *tour de force* made for an audience of many, however, every single word is for you.

LIST OF PUBLICATIONS

1 **Shireen Mentor** and David Fisher (2017). Aggressive antioxidant reductive stress impairs brain endothelial cell angiogenesis and blood-brain barrier function. *Current neurovascular research*. (14): 71-81. doi: 10.2174/1567202613666161129113950.

2 David Fisher and **Shireen Mentor** (2017). Antioxidant-induced reductive stress has untoward consequences on the brain microvasculature. *Neural regeneration research*. (12): 743-744. doi: 10.4103/1673-5374.206640.

3 Duraisamy Kempuraj, Mohammad Ejaz Ahmed, Govindhasamy Pushpavathi Selvakumar, Ramasamy Thangavel, Arshdeep S. Dhaliwal, Iuliia Dubova, **Shireen Mentor**, Keerthivaas Premkumar, Daniyal Saeed, Haris Zahoor, Sudhanshu P. Raikwar, Smita Zaheer, Shankar S. Iyer, Asgar Zaheer. (2020). Brain injury-mediated neuroinflammatory response and Alzheimer's disease. *The neuroscientist*. 26 (2):134-155. doi: 10.1177/1073858419848293.

4 Duraisamy Kempuraj, **Shireen Mentor**, Ramasamy Thangavel, Mohammad E. Ahmed, Govindhasamy Pushpavathi Selvakumar, Sudhanshu P. Raikwar, Iuliia Dubova, Smita Zaheer, Shankar S. Iyer and Asgar Zaheer (2019). Mast cells in stress, pain, blood-brain barrier, neuroinflammation and Alzheimer's disease. *Frontiers in Cell Neuroscience*. 13 (54): 1-11. doi: 10.3389/fncel.2019.00054. PMID: 30837843.

5 Ahmed ME, Selvakumar GP, Kempuraj D, Thangavel R, **Mentor S**, Dubova I, Raikwar SP, Zaheer S, Iyer SS, Zaheer A. (2019). Synergy in disruption of mitochondrial dynamics by Aβ (1-42) and glia maturation factor (GMF) in SH-SY5Y cells are mediated through alterations in fission and fusion proteins. *Molecular neurobiology*. doi: 10.1007/s12035-019-1544-z.

6 Sudhanshu P Raikwar, Mohammad E Ahmed, Iuliia Dubova, **Shireen Mentor,** Daniyal Saeed, Haris Zahoor, Keerthivaas Premkumar, Ramasamy Thangavel Govindhasamy P. Selvakumar, Duraisamy Kempuraj, Smita Zaheer, Shankar S. Iyer, Asgar Zaheer (2019). Glia maturation factor gene editing improves neurocognitive function in an Alzheimer's disease mouse model. *The FASEB journal, biochemistry and molecular biology*.

7 Geofrey Omarch, Yunus Kippie, **Shireen Mentor**, Naushaad Ebrahim, David Fisher, Grace Murilla, Hulda Swai & Admire Dube (2019). Comparative *in vitro* transportation of pentamidine across the blood-brain barrier using polycaprolactone nanoparticles and phosphatidylcholine liposomes, *Artificial cells, nanomedicine, and biotechnology*. 47:1, 1428-1436. doi: 10.1080/21691401.2019.1596923.

8 Fisher D., and **Mentor S.** (2020). Are claudin-5 tight-junction proteins in the blood-brain barrier porous? *Neural regeneration research.* 15(10):1838-1839. doi:10.4103/1673-5374.280308.

9 **Mentor S.,** and Fisher D. (2021). High-resolution insights into the *in vitro* developing blood-brain barrier: Novel morphological features of

endothelial nanotube function. *Frontiers in neuroanatomy*. 15: 1–15. doi: 10.3389/fnana.2021.661065.

10 Zondagh, L.S., Joubert, J., Omoruyi, S., **Mentor, S.,** Malan, S.F., Ekpo, O., Fisher, D. (2021). Mutlifunctional edaravone-N-benzyl pyridinium derivatives: AChE inhibition kinetics, *in vitro* neuroprotective activities and BBB permeability studies. *The Journal of the Alzheimer's Association*. Drug development poster presentation. doi: 10.1002/alz.053939.

11 **Mentor S.,** Cummings F., and Fisher D. (2022). Preparation of biological monolayers for producing high-resolution scanning electron micrographs. *PLoS ONE* (in press). dx.doi: 10.17504/protocols.io.bw37pgrn.

12 V.C., Thipe, **S., Mentor**, C.S.A., Lima, L.F., Freitas, A.C.M., Fonseca, K.M., Nogueira, A.S., Rodrigues, J.G.S., Batista, A.H., Ferreira, A.B., Lugão (2022). Probiotics in the prevention and management of human diseases, A scientific perspective, Chapter 3 - The role of probiotics in maintaining immune homeostasis, Pages 41-58, doi: 10.1016/B978-0-12-823733-5.00024-6.

13 **Mentor S.,** Makhathini K.B., Fisher D. (2022). The role of cytoskeletal proteins in the formation of a functional *in vitro* blood-brain barrier model. *International journal of molecular sciences.* doi: 10.3390/ijms23020742.

14 **Mentor S.,** and Fisher D. (2022). The *ism* between endothelial cilia and endothelial nanotubules is an evolving concept in the genesis of the BBB. *International journal of molecular sciences*. 23 (5):1-16. doi:10.3390/ijms23052457.

LIST OF CONFERENCES

Shireen Mentor and David Fisher. High-resolution insights into the *in vitro* developing blood-brain barrier: Novel morphological features of endothelial nanotube function. Forty-eight Annual Congress of Physiology Society of Southern Africa (PSSA), Witwatersrand, Johannesburg, South Africa- First Virtual Congress. 12-15 September 2021- Awarded the first prize for the best publication.

Shireen Mentor and David Fisher. Morphologically mapping the development of the blood-brain barrier using high-resolution electron microscopy. 68th Lindau Nobel Laureate Meeting, Lindau Germany, 24th June 2018 – 4th July 2018.

LIST OF SELECTED ABBREVIATIONS

α-Tubulin	alpha Tubulin
°C	degrees Celsius
i.e.	Exempli gratia (for example)
v/v	volume to volume
2-D	Two-dimensional
3-D	Three-dimensional
Ab`	Antibody
ABBA protein	actin-bundling protein with BAIAP2 homology
ABC transporter	Adenosine triphosphate-binding cassette transporter
AC	Alternate current
AC3	Adenylate cyclase type III
AD	Alzheimer's disease
Ag	Antigen
AJ	Adherens Junction
ALG-2	Alpha-1, 3/1, 6-mannosyltransferase
ALIX	ALG-2 complex
AQP1	Aquaporin-1
ARP2/3:	actin-related proteins 2/3
AT	adenine thymine
ATCC	American Type Cell Collection
ATP	Adenosine triphosphate
ATPase	Adenosine triphosphatase
Au: Pd	Gold: Palladium
BAIAP2	BAR/IMD Domain Containing Adaptor Protein 2
BALB/c	Bagg Albino C57BL/6
BAR	Bin/Amphiphysin/Rvs

BBB	Blood-brain barrier
BBE	Bovine brain extract
BCSFB	Blood-cerebrospinal fluid barrier
BEC	Brain endothelial cell
bEnd3	Immortalized mouse brain endothelial cell
bEnd5	Immortalized mouse brain endothelial cell
BF	Blood flow
BM	Basement membrane
BMVEC	Brain microvascular endothelial cell
BP	Blood pressure
BSA	Bovine serum albumin
BV	Blood vessel
C4-2B	*Homo sapiens*, prostate cancer cell line
Ca^{+}	Calcium
cAMP	cyclic adenosine monophosphate
CASK	Ca^{+}-dependent serine protein kinase
Cat.	Catalogue
CDC42	Cell division control protein 42 homolog
cEND	mouse cerebral capillaries endothelial cell
CENPs	Centromeric proteins
cerebEND	cerebellar capillary brain endothelial cells
Ci	Cilium
CIP4	Cdc42-interacting protein-4
Cl^{-}	Chloride
CMECs	Cardiac microvascular endothelial cell
CNS	Central nervous system
CLSEM	Correlative scanning electron microscopy
CO_2	Carbon dioxide

CP	Critical Point
CPD	Critical Point Drying
CSF	Cerebrospinal fluid
CVA	Cerebrovascular accident
CVD	Cerebrovascular disease
CVD	Chemical vapor deposition (method paper)
DABCO	1, 4-Diazabicyclooctane
DAPI	4', 6-Diamidino-2-Phenylinole
ddH_2O	Double distilled water
DE3	*Escherichia coli* BL21 cells
DF	Depth of field
dH_2O	Distilled water
DMEM: F12	Dulbecco's Modified Eagles Medium: Hams F12
DMSO	Dimethyl sulphoxide
DNA	Deoxyribonucleic acid
dsDNA	double-stranded deoxyribonucleic acid
DSL	Dynamic light scattering
EBM	endothelial basal medium
EC	Endothelial cell
ECACC	European Collection of Authenticated Cell Cultures
ECIS	Electrical Capacitance Impedance System
ECM	Extracellular matrix
ECV304	Human umbilical vein endothelial cell
EDS	Energy dispersive spectrum
EDTA	Ethylenediamine tetraacetic acid
EMV	Extracellular microvesicles
Ena/VASP	Enabled/Vasodilator-stimulated phosphoprotein
eNOS	endothelial nitric oxide synthase

EPEC	*Enteropathogenic Escherichia coli*
etc.	*Et cetera*
e.g.	*Exempli gratia* (Latin); for example (English)
ETD	Everhart-Thornley detector (ETD)
EtOH	Ethanol
EV	Extracellular vesicles
EVOM	Electronic VoltOhmmeter
F-actin	Filamentous actin
F-BAR	FER-CIP4-homology-BAR
FBS	Fetal bovine serum
Flk-1	protein kinase (receptor)
FTase	Farnesyltransferase
FTI	Farnesyltransferase inhibitor
G250	Green tinted (dye)
GAPDH	glyceraldhehyde-3-phosphate dehydrogenase
GBD	Global Burden of Disease
GFP	Green fluorescent protein
GLUT-1	Glucose transporter – 1
Gp-120	Glycoprotein -120
G-protein	guanine nucleotide-binding protein
GTPase	Guanosine triphosphatase
GUV	Giant unilamellar lipid vesicle
H^+	Hydrogen
h	hour
H_2O	Water
hCMEC/D3	human immortalized endothelial cell line
HD	High-definition
hEGF	human epidermal growth factor

HEPES	4-(2-hydroxyethyl)-1-piperazineethanesulfonic acid
HIV	Human immunodeficiency virus
HR	High-resolution
HRas	Transforming protein p21
HREM	High-resolution electron microscopy
HRP	Horse radish peroxidase
HR-SEM	High-resolution scanning-electron microscopy
HR-TEM	High-resolution transmission-electron microscopy
HsaVEC	Human saphenous vein endothelial cell
HUVECs	Human umbilical vein endothelial cells
I	Current injected
I-BAR	Inverse BAR
ICAM-1	Intercellular adhesion molecule-1
ICC	Immunocytochemistry
i.e.	*Id est* (Latin); That is (English)
IF	Immunofluorescence
IFT	Intraflagellar transport
ILV	Intraluminal vesicles
IM	I-BAR domain
IS	Intercellular space
ISF	Interstitial fluid
JAM	Junctional adhesion molecule
LDL	Low-density lipoproteins
LP	Lamellipodia
LRP	Low-density lipoprotein receptor protein
K^+	Potassium
kDa	kilo Daltons
keV	kilo electron volts

MadCAM-1	mucosal vascular addressin
MAGI	Membrane associated guanylate kinase inverted
MAPK	mitogen-activated protein kinase
MECA-32	Panendothelial cell antigen antibody
MeOH	Methanol
min	minutes
mRNA	messenger ribonucleic acid
MSC	mesenchymal stem cells
MV	Microvesicle
MVB	Multivesicular bodies
MW	Molecular weight
Na^+	Sodium
N-BAR	Amphiphysin/endophilin BARs
NC	Neural Crest cells
NEAA	Non-essential amino acids
NH_3	Ammonia
NRK	normal rat kidney
nSMASe2	Neutral sphingomyelinase 2
NT	Nanotubule
NV	Nanovesicle
NVU	Neurovascular unit
no.	number
O_2	Oxygen
PAR	Protease-activated receptor
PBS	Phosphate buffered saline
PBECs	Porcine brain endothelial cells
PC-3	Human prostate cancer cell line
PC12	Pheochromocytoma of the rat adrenal medulla

PC	Paracellular
PCR	Polymerase chain reaction
PD	Parkinson's disease
PDX	Patient-derived xenografts
PEC	Peripheral endothelial cell
PECAM-1	Platelet endothelial cell adhesion molecule-1/CD31
Pen/Strep	*Penicillin/Streptomyocin*
pH	potential of hydrogen
PIPES	Piperazine-N, N'-bis (2-ethanesulfonic acid)
PM	Plasma membrane
PMBC	Primordial midbrain channel
pMBMEC	primary mouse brain microvascular EC
PS	Paracellular/PC space
PTU	Primordial TUNTS
PNVP	Perineural vascular plexus
PVDF	Polyvinylidene difluoride
PVP	Periventricular plexus
Rab7	Small GTPase
Rab27a	Ras-like protein in the brain 27a
Rac	Subfamily of Rho GTPases
Ras	Rat sarcoma (small GTPase protein family)
Rho	Rhodamine
RNA	Ribonucleic acid
RT	Room temperature
SDS-PAGE	Sodium dodecyl sulfate- polyacrylamide gel electrophoresis
SE	Secondary electron
SEC	Systemic endothelial cell
SEM	Scanning electron microscopy

SH-SY5Y	human neuroblastoma cell line
T-antigen	tumor-antigen
TBI	Traumatic brain injury
TBS	Tris Buffered Saline
TBS-T	Tris Buffered Saline-Tween 20
TC	Tissue culture
TE	TENT
TEER	Transendothelial electrical resistance
TEM	Transmission electron microscopy
TEMED	Tetramethylethylenediamine
TENT	Tethering nanotubule
TJ	Tight junction
TMB	Tetramethylbenzidine
TMEM30A	Transmembrane protein 30A
TNT	Tunneling nanotubule (as stated in literature)
TSG101	Tumor susceptibility gene 101 protein
TU	TUNT
TUNT	Tunneling nanotubule (as denoted in this study)
UV	Ultraviolet
V	Voltage applied
Viz	Namely
VCAM-1	Vascular cell adhesion protein -1
WB	Western Blot
WPI	World precision instruments
ZO	Zonula occludens

LIST OF FIGURES

COMMENTS ON THE MAIN TEXT

The thesis, titled: **'Investigating novel aspects of the blood-brain barrier using high resolution electron microscopy'** is outlined as a manuscript. The overall structure of the thesis takes the form of five themed chapters (four by publication).

CHAPTER ONE- An introductory **Literature review: The Blood-Brain Barrier: A Dynamic Interface**

Section one: **Literature review,** which provides background information curtailed to the existing body of knowledge pertaining to the researched and proposed functionality of the blood-brain barrier (BBB) and an introduction to nanotubules (NTs) in cell biology studies. Section two: Consolidation of the research study in the form of a: (i) Problem statement and rationale, (ii) scope of study, (iii) a hypothesis for the study and (iv) an outline of the aims and objectives.

CHAPTER TWO- Title: **'Preparation of biological monolayers for producing high-resolution scanning electron micrographs.'** The chapter is an extensive discussion on the laboratory methodology utilized for preparing biological samples for high-resolution electron microscopy analysis. The work describes, extensively, the most preeminent coating modalities for generating texturized electron micrographs of biological samples. This work was accepted for publication in the *PLoS ONE* journal (in press). All other methodologies within the thesis are included in the published manuscripts.

CHAPTER THREE- Title: **'High-resolution insights into the *in vitro* developing blood-brain barrier: Novel morphological features of endothelial nanotube function.'** This chapter describes novel morphological nanostructures involved in the development of the BBB and is the bedrock of this research study. This work was published in *Frontiers in Neuroanatomy*.

CHAPTER FOUR- Title: **'The role of cytoskeletal proteins in the formation of a functional *in vitro* blood-brain barrier model.'** The chapter evaluates the subcellular/ molecular governance of BEC NT formation. The study investigated the functional role of the brain endothelial cell's cytoskeletal proteins as cytoarchitectural/molecular backbone governing the physical functionality of tethering nanotubule (TENT) formation as a critical event in endothelial barrier-genesis. This work was published in the *International Journal of Molecular Sciences.*

CHAPTER FIVE-Title: **'The *ism* between endothelial cilia and endothelial nanotubules is an evolving concept in the genesis of the BBB.'** The review critically evaluates the current literature by analyzing the existing body of scientific knowledge and philosophical thinking (*ism*) with respect to endothelial "cilia" and comparatively evaluates it against research findings on brain endothelial nanotubes, emanating from this study. The aim is to elucidate an array of inimitable nanostructures associated with barrier-genesis. This work was published in the *International Journal of Molecular Sciences*.

CHAPTER SIX - General discussion, providing a synthesis of the research study. The chapter coalesces the main structural and molecular findings in the study in a manner that highlights the ultrastructural relevance in BBB development on a nanoscale.

CHAPTER SEVEN - General conclusions and recommendations.

The chapter summarizes the main findings by illuminating the motivation behind elucidating the morphological, nanoscopic landscape during barrier-genesis. Moreover, it provides useful suggestions for further investigation of nanovesicle biogenesis in order to endorse its role in direct/indirect cell-cell communication during BEC BBB development *in vitro*.

TABLE OF CONTENTS

CHAPTER ONE: LITERATURE REVIEW

THE BLOOD-BRAIN BARRIER: A DYNAMIC INTERFACE

1.1. Introduction

The brain's capillary endothelial cells form the anatomical basis of the cerebral microvasculature. Cerebrovascular regulatory mechanisms are nuanced and, therefore, complex in its ability to ensure that the neuronal *milieu* receives adequate blood supply. Cerebrovascular dysfunction generally encompasses disturbances in the brain vasculature (i.e., cerebrovascular accident/stroke) and brain disease progression (i.e. Alzheimer's disease (AD); Parkinson's Disease (PD) (Cai *et al.*, 2017).

Brain endothelial cells (BECs) are derived from the mesoderm, of the gastrula stage embryo (Eilken and Adams, 2010; Welti *et al.*, 2013; Okuda and Hogan, 2020). The BECs line the lumen of the brains capillaries and possess a coordinated transport system (i.e., transcellular transport) for transferring of nutrients, energy metabolites and macromolecules. Movement across the blood-brain barrier (BBB) undertakes four modes of transportation, these include:

(i) Passive diffusion, which occurs via a concentration gradient through both paracellular (PC) and transcellular (TC) routes.

(ii) Active transport, which occurs via primary, secondary of facilitative transport (i.e. movement of molecules against a concentration gradient).

(iii) Carrier-mediated transport namely (i.e. via a concentration gradient).

(iv) Endocytosis (i.e. receptor mediated, absorptive and bulk-phase endocytosis).

These basic methods of transportation are reliant on the features of and directional flow/passage of molecules (Pardridge, 2012, Al Rihani *et al.*, 2021). The strict regulation of molecule/ion flux is critical to ensure the homeostasis of the brain's microenvironment. Small molecules are pumped across specialized membrane-bound carriers namely adenosine triphosphate- binding (ATP-binding) cassette proteins (ABC-transporters), while larger molecules are transported by membrane-bound carriers (i.e., glucose transporter 1 (GLUT1); Transferrin, calveolae/clathrin-mediated) via endocytotic and exocytotic processes. This cascade of events are collectively known as transcytosis (Leite *et al*., 2020).

The PC pathway between, BECs are interconnected by intercellular tight junction (TJ) protein complexes, engaging between adjacent BMVECs, and form a critical monolayer, which restricts movement of ions, pathogens, and an array of harmful substances between adjacent BECs, thereby, protecting the chemical stability and cognitive function of the central nervous system (CNS) and constitutes the BBB. The mechanisms of adverse neurodegenerative progression are linked to a decrease in the integrity of the BBB as the frontline of defense in CNS disorders. It is, therefore, imperative to understand the physical complexity that reinforces the restrictive nature of the BBB especially when most drugs are restricted from reaching the brain's microenvironment in efficient quantities for effectively

treating brain disease (i.e. PD, AD and human immunodeficiency virus (HIV)–associated dementia) (Cai *et al.*, 2017; Upadhyay, 2014a).

Overcoming the persistent challenge with treatment modalities for CNS disorders, brain tumors, and traumatic brain injury (TBI) is critical and to date, the existing body of scientific knowledge, with respect to neurodegenerative treatment is slow growing, hitherto the lack of understanding pertaining to the morphological and molecular aptitude of the specialized endothelial cells (ECs) of our brain's capillaries.

1.1.1 The history of the blood-brain barrier

The concept of a "BBB" began in the early 1800s, by a German scientist named Paul Ehrlich. Upon conducting biological tissue staining experiments, he discovered that CNS tissue (i.e., the brain and the spinal cord) remained unstained, while the peripheral tissues stained blue. Further investigation upon injecting dye into the subarachnoid space, resulted in only CNS stained tissue while bodily tissues were unstained. Based on these findings, Ehrlich postulated that there are different structures of blood vessels (BVs) in the brain, relative to the BVs in the systemic circulation (Ehrlich, 1885). By the 1900s, Ehrlich's student, Edwin Goldmann took a keen interest in his predecessor's experimentation and followed suit with the concept of the specialized BVs residing within the CNS. Goldmann observed an accumulation of trypan blue dye within the choroid plexus of the brain, which is responsible for making cerebrospinal fluid (CSF), thus, by the 1900s we knew about the BBB and the blood-CSF-barrier (BCSFB) (Goldmann, 1913; Serlin *et al.*, 2015). The BBB or

"Blut-Hirnschranke" was termed by Max Lewandowsky, however, Lina Stern was the first person to have coined the term in the 1920s (Saunders *et al.*, 2016). To date, the concept of a regulatory interface between the blood and the brain's microenvironment has been well characterized in the literature by its high degree of impermeability across the cerebral microvessels to plethora of blood-borne substances (Reese and Karnovsky, 1967).

1.2. Differences between the systemic and brain endothelial cells

The heterogenic nature of ECs has been described on the basis of four facets: (i) structure, (ii) antigen composition, (iii) cell function, and (iv) messenger ribonucleic acid (mRNA) expression (Turner *et al*., 1987; Aird, 2007a). It is well documented that BV EC phenotypes are adapted to the underlying organ systems (i.e., the brain, heart, kidney and lung) which they supply and thus are distinctly different in their molecular profile (Aird, 2007a; Aird, 2007b;Aird, 2012).

ECs are orientated along the BV wall and exhibit select phenotypic characteristics: Thin, slightly elongated, approximately 30-50 µm in length, 10-30 µm wide and 0.1-10 µm thick with an overall cobble-stone appearance (Krüger-Genge *et al.,* 2019). Additionally, ECs from the same region of the vasculature may have structural and functional variations, which extend to subcellular organelles such as Weibel Palade bodies, which are more prevalent in the pulmonary vasculature than in the thoracic aorta (Krüger-Genge *et al*., 2019).

Two features of the cerebral capillaries contribute to its highly restrictive nature. (i) The presence of intercellular adhesion protein junctions, similarly present in

systemic endothelium and (ii) the arrangement of the protein motifs between cerebral and systemic ECs (SECs). Based on research study conducted by Reese and Karnovsky, (1967), histochemical data has illustrated a distinct feature of cerebral, inter-endothelial protein junctions as having the ability to occupy a large portion of the paracellular (PC) shunt between adjacent BECs. Furthermore, structural distinctions between ECs present in the systemic vasculature and those located in the brain capillaries exist, which serve as the anatomical foundation for understanding the innate restrictivity of the cerebrovasculature and BBB (**Figure 1.1)**.

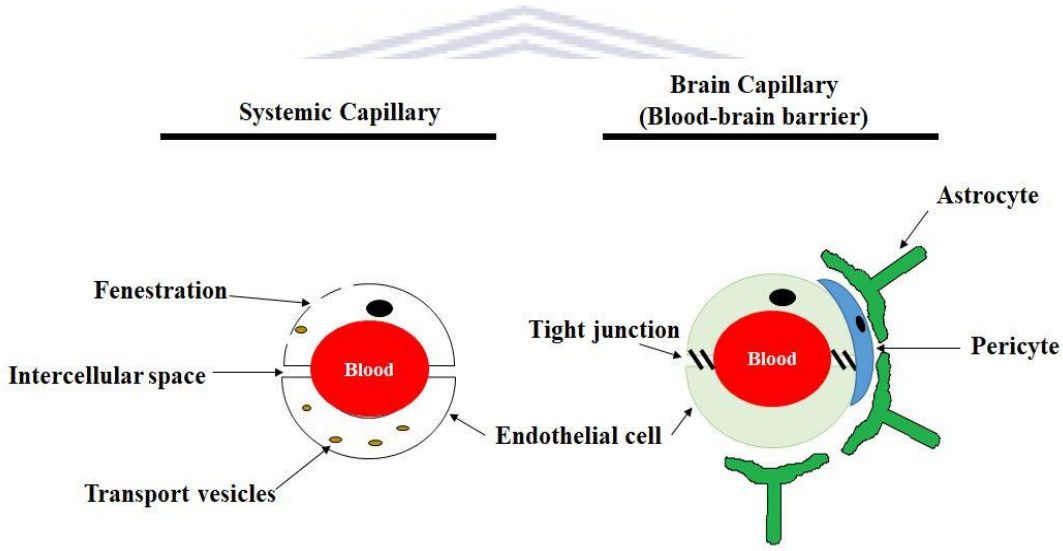

Figure 1.1. Comparison between cerebral and systemic ECs (Adapted from Neearti *et al.*, 2012 and Fisher and Mentor, 2020). Permission granted by authors.

Within the brain's microenvironment the cerebrovasculature is approximately 8-20 µm from the neural tissue, hence the ECs of the brain's capillaries exert the greatest influence on the immediate neuronal *milieu* (Abbott *et al.*, 2006; Hatherell *et al.*, 2011). The distance between the perivascular space surrounding the brain's capillaries and the brain's parenchyma is known as the Virchow-Robin

space (Serlin *et al*., 2015). The proximity is characterized by a variety of cellular interactions between microglia, astrocytes, pericytes and perivascular macrophages. The crosstalk between the BECs and these cells contribute to the formation of the neurovascular unit (Serlin *et al*., 2015).

1.3. The neurovascular unit

The neurovascular unit (NVU) enables the intercellular crosstalk between BECs, astrocytes, pericytes and neurons. The astrocytes, in some measure, envelope the BECs, hardwiring them to the neurons, (Brown *et al.*, 2015;Naranjo *et al.*, 2021) as illustrated in **Figure 1.2.**

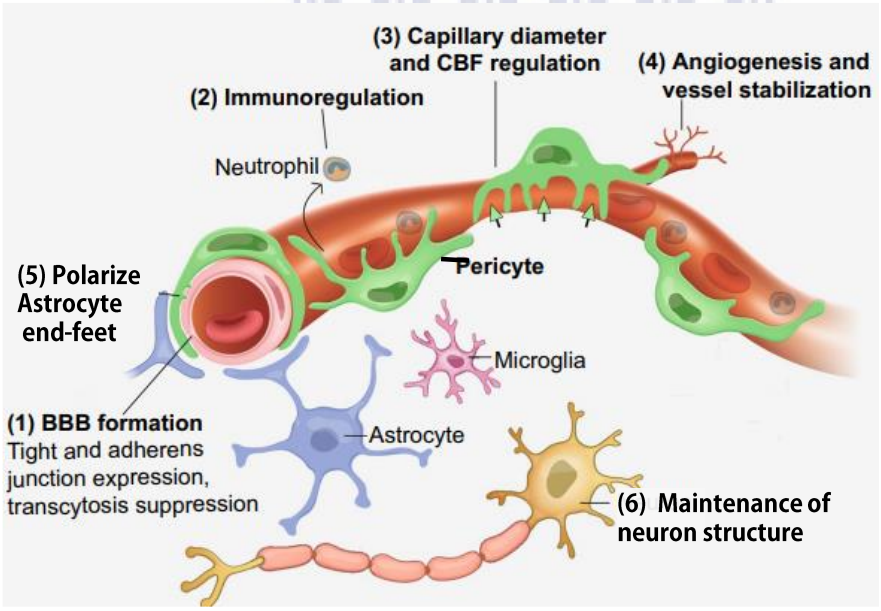

Figure 1.2. The role of the pericyte in the NVU, which constitute the *in vivo* BBB (Adapted from Cheng *et al*., 2018). Permission granted by authors.

Intercellular communication between NVU cells protects the CNS against a myriad of harmful hydrophobic compounds (MW<800 Da), by inhibiting their ability to passively diffuse into the CNS (Perrière *et al.*, 2007; Omidi *et al.*, 2003).

The dynamic interplay between cells of the NVU is reported to induce the expression of barrier specific properties in BECs (Cardoso *et al.*, 2010; Banks *et al.*, 2018) and subsequently maintain homeostasis of the brain's microenvironment by regulating ions flux via increased impermeability across the brain's capillaries (Abbott *et al.*, 2006; Naranjo *et al.*, 2021). Alterations within the NVU *in vivo* results in brain dysfunction and possible cerebrovascular pathologies, such as stroke and exacerbation of neurodegeneration, namely (viz), AD; PD and human immunodeficiency virus (HIV)-related dementia (Cai *et al.*, 2017; Upadhyay, 2014a).

1.3.1. Homeostasis of the central nervous system

It is critical to maintain homeostasis in the brain microenvironment, as changes in ionic concentration have a direct effect on the resting membrane potential of neurons. The main function of the BBB is to impede permeability between blood and interstitial fluids (ISF), functioning as a filter for essential nutrients, ions and metabolic waste products (Hawkins and Davis, 2005; Redzic, 2011; Wolburg and Lippoldt, 2002). Ions are transported both actively and/or passively across the BECs (Upadhyay, 2014b). The transport of water and water-soluble molecules, namely: sodium (Na^+), hydrogen (H^+), potassium (K^+) and chloride (Cl^-) are regulated by channels in both the apical and basolateral BEC membrane domains. Additionally, the net flux of ions such as K^+ is critical for CNS equilibrium and standard neuronal activity (Ballabh *et al.*, 2004; Redzic, 2011 ; Hatherell *et al.*, 2011).

1.3.2. Transport across the BBB

1.3.2.1. Transcellular Transport

The BECs, are interconnected by junctional protein complexes (i.e. tight junctions (TJs) and adherens junctions (AJs)) within its PC spaces. TJs and AJs are responsible for the formation of a polarized, selectively permeable, endothelial transmembrane transport system (**Figure 1.3.**). The presence of a well-regulated PC pathway endorses the formation of a specifically distributed transmembrane receptors: (i) intercellular adhesion molecule-1 (ICAM-1), (ii) vascular cell adhesion protein 1 (VCAM-1), (iii) platelet endothelial cell adhesion molecule-1 (PECAM-1), transporters (i.e. ABC-transporters; GLUT-1) and (iv) non-selective drug export pumps such as glycoprotein-120 (gp-120). These transmembrane receptors are located on the apical and basolateral surfaces of the phospholipid bilayer of the BEC membrane (Wolburg and Lippoldt, 2002).

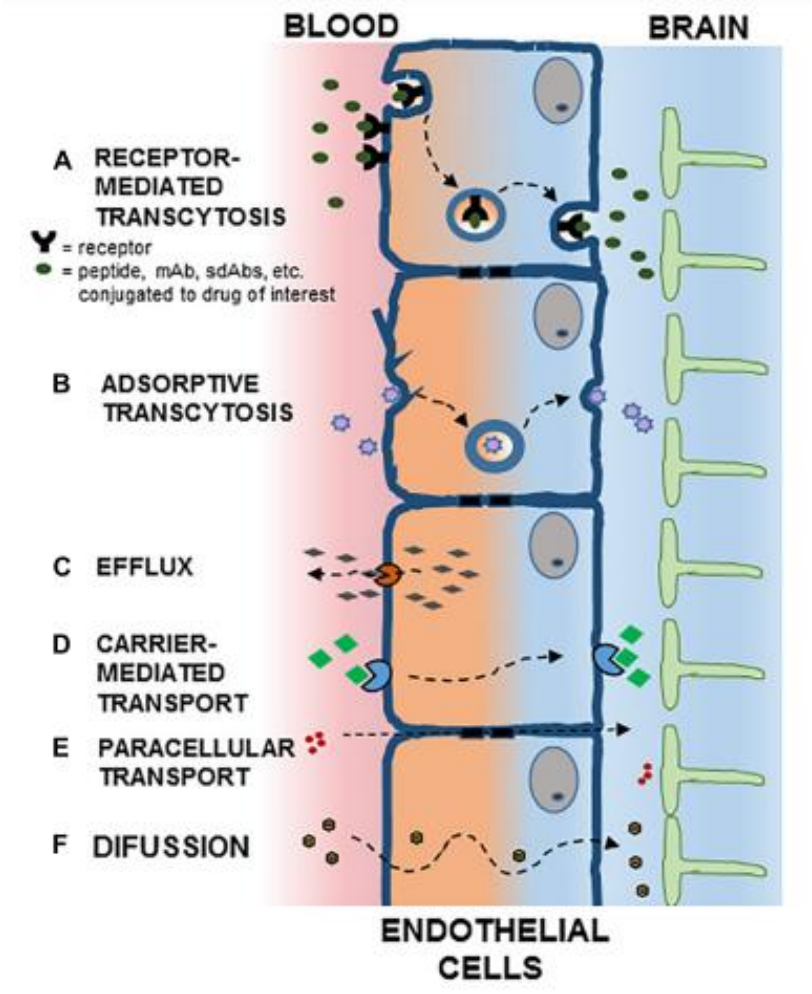

Figure 1.3. The transcellular transport system of the BBB (Pulgar, 2019). Permission granted by author.

The arrangement of receptors along the apical and basolateral membranes are asymmetrical and thus creates a polarized BECs phospholipid bilayer as the luminal (apical/blood compartment) and abluminal (basal/brain compartment) cell membranes differ in their glycoprotein composition, allowing BECs to transport substances in a polarized manner. Polarity can be assumed in two forms: Planar cell polarity (i.e. the event of migrating cells during angiogenesis) and apico-basal polarity (Worzfeld and Schwaninger, 2016).

The intercellular TJs, not only restrict BEC PC permeability, but serve a functional role in separating the apical and basal domains of BEC membranes, thus, promoting the polarized properties, found across epithelia (Abbott *et al.*, 2006). The relationship between the polarity and TJ protein complexes occur via two mechanisms of action:

(i) TJs provide docking sites for components of the apico-basal membrane, conversely

(ii) The polarity induces TJ expression.

During neurological disease, there is a propensity for BECs to lose their polarity, because of TJ disturbance, resulting in adverse effects on BBB integrity (Worzfeld and Schwaninger, 2016).

1.3.2.2. Paracellular transport

The PC pathway, located between adjacent BECs is occupied by anastomosed protein junctional complexes (i.e., TJs, AJs and junctional adhesion molecules (JAMs)) and are well reported to play a role in regulating the movement of substances and/or ions between adjacent BECs of the BBB (Ballabh, 2004; Fisher and Mentor, 2020). Research conducted by Reese and Karnovsky, (1967) has localized pores within PC TJ protein complexes, by measuring the degree of horseradish peroxidase (HRP) transport between the circulation and extravascular spaces within cardiac and skeletal muscle by diffusion. Moreover, HRP permeation displayed slower diffusion rates within the brain, concomitant with anatomical variations between systemic and cerebral endothelia (Reese and Karnovsky, 1967). Fisher and Mentor, (2020) challenged the notion of TJ proteins comprised of pores, which are accountable for ion flux by noting the unlikelihood

of pore formation in TJ protein complexes of the BBB. Their postulate was endorsed by a study conducted by Dolman *et al.*, (2005) who reported on primary rat BEC cultures having the ability to only express aquaporin 1 (AQP1) after the third passage, however, co-cultured astrocytes, suppressed AQP1 expression. The stance taken by Fisher and Mentor, (2020) supports the notion that under normal physiological conditions *in vivo* BECs do not express AQP1, or any other AQP (Dolman *et al.*, 2005; Francesca and Rezzani, 2010; Papadopoulos and Verkman, 2013; Verkman, 2013). AQPs greatly facilitate water flux in response to osmotic gradients, however, claudin TJs were postulated to have water permeability, due to its porous nature. The BECs under normal conditions, are impermeable to water due to the absence of AQPs and, thus, the water passing through the PC spaces are further regulated by astrocyte foot-like processes, which contain AQPs (Fisher and Mentor, 2020).

1.4. Intercellular tight junction interaction

It is known that intercellular tight junction (TJ) protein complexes reinforce the structural integrity of the BBB. TJ proteins are comprised of a combination of transmembrane and cytoplasmic (plaque) proteins: zonula occludens -1, -2 and -3 (ZO-1, ZO-2 and ZO-3), interlinked with the BEC's actin- cytoskeleton (Breslin *et al.*, 2015; Huber *et al.*, 2001). Moreover, transmembrane proteins include occludin and claudin-1/3, -5 and -12. The occludin is a 60-65 kDa protein with a carboxy(C)-terminal domain, which is capable of interacting with plaque proteins embedded within the actin-cytoskeleton of the BEC. In the BBB, occludin and claudin-5 are ubiquitous and contribute to the low permeability generated across both *in vivo* and *in vitro* BBB models. Junctional adhesion molecules (JAM),

namely: JAM-A, JAM-B and JAM-C are present in BECs and are important in the formation and maintenance of the TJ proteins (Schneeberger, 2004). In addition, cytoplasmic plaque proteins motifs serve as adaptor proteins with many protein-protein interaction domains (i.e. ZO-1, ZO-2 and ZO-3; the Ca^{2+}-dependent serine protein kinase (CASK) and membrane-associated guanylate kinase with inverted orientation of protein-protein interaction domains (MAGI-1, MAGI-2, MAGI-3) (Schneeberger, 2004).

The literature reports on BBB integrity as being dependent on an elevated expression of TJs: occludin and claudin-5 protein expression and intracellular signaling pathways that modulate the phosphorylation state of the TJ proteins (Rubin and Staddon, 1999; Yamashita *et al.*, 2020). This premise remains theoretical at best. The persisting gap in the current body of knowledge is located within the relationship between BEC TJ protein expression and the cytoplasmic projection of novel nanostructures, which facilitate TJ localization.

Research focused on ultrastructural dynamics of BEC communication, as the basis for barrier-genesis, will unravel structural complexities involved in attaining CNS homeostasis which, to date, has not been described in the literature. Moreover, evaluating the intracellular, molecular underpinnings, which support BBB nanostructural morphology, will nuance our understanding of cytoarchitectural mechanisms, which facilitate BEC alignment and its ability to bring about TJ protein engagement.

1.4.1. Blood-brain barrier permeability

Transendothelial electrical resistance (TEER) is the measuring index for determining the health of BEC monolayers and subsequent BBB integrity *in vitro*. Furthermore, a number of hydrophilic tracer molecules are used for PC permeability measurements, viz: Lucifer yellow (444 Da), sodium fluorescein (376 Da), sucrose (342 Da) and mannitol (180 Da) (Helms *et al.,* 2016). TEER values *in vivo*, venular endothelium are normally expected to reach between approximately 1800-2800 $\Omega.cm^2$ (Olesen *et al.,* 1987; Vigh *et al.,* 2021), whereas the human cerebrovasculature EC (hCMEC) monolayer *in vitro* range between 20-200$\Omega.cm^2$ (Hatherell *et al.,* 2011). TEER is mostly influenced by the interendothelial adhesion proteins (i.e., TJs and AJs), which are major factors regulating PC permeability (Alves *et al.,* 2018).

For most *in vitro* models, the average TEER values are approximately 100 $\Omega. cm^2$ (Malina *et al.,* 2009). The two main methods for measuring TEER across an immortalized mouse brain endothelial cell (bEnd3) monolayer are: (i) the electrical capacitance impedance system (ECIS) and (ii) a standard electrical resistance voltohmmeter (EVOM, World precision instruments/Millipore).

The literature reports on bEnd3 cells, seeded at $3x10^5$ cells/mL on microelectrodes and in $5x10^{-3}$ cm^2 polycarbonate wells, reaching Ohm's readings of up to 140Ω (Stamatovic *et al.,* 2008). Conversely, studies conducted on porcine brain endothelial cells (PBECs) grown in monoculture, generated low TEER readings, by way of cellZcope measurements (nano Analytics, Germany), a computer-controlled automated multiwall device (24-wells), which allows long-term TEER measurement and of monolayer capacitance. TEER demonstrated that only with

contact co-culture, readings more closely mimic the integrity of the *in vivo* BBB model with TEER values reaching up to 1650Ω.cm^2 (Malina *et al.*, 2009). Malina and colleagues, (2009), seeded a density of 2.5x10^5 porcine BECs (PBECs) on Transwell filter membranes. After 24h, culture medium was replaced with assay medium (containing 550nM) hydrocortisone, which resulted in TEER values reaching approximately 400Ω.cm^2. Furthermore, co-cultured BECs and astrocytes, separated by a 10µm thick polycarbonate membrane with pore size 0.4µm showed an improvement in BEC barrier properties, upon interaction with astrocytic end-feet. Co-cultures with astrocytes, therefore, have the ability to improve TEER readings, which better represents the *in vivo* resistance readings of 1500 Ω.cm^2 (Malina *et al.*, 2009).

Furthermore, Yang *et al.*, (2007), conducted an *in vitro* permeability study utilizing two cell lines: (i) human umbilical vein EC (ECV304) and (ii) immortalized mouse brain endothelial cells (bEnd3). The study reported that the bEnd3 cells, seeded on the upper surface of a polyester Transwell insert at densities of 5x10^4 and 8x10^4/cm^2, generated TEER readings of 30±2.83 Ω.cm^2 using an epithelial Voltohmmeter (EVOM) with EndOhm-12 chamber electrodes (WPI, USA). The TEER findings in this study suggested that bEnd3 monolayers were less impermeable than the ECV304 (Yang *et al.*, 2007).

Nakagawa and colleagues *et al.*, (2009), found that the BEC monolayer only reached maximum TEER at ± 70Ω.cm^2, however, when seeded with pericytes TEER was raised to 350-600Ω.cm^2. In addition, primary cultures of bovine BCECs revealed significant TEER averaging 800Ω.cm^2 (Rubin *et al.*, 1991; van der Helm *et al.*, 2016a), while several reports have demonstrated bovine BBB

models with TEER values ranging from 30-150Ω.cm^2. Alternatively, Förster *et al.*, (2008) and Helms *et al.*, (2016), reports on the ability of the cerebellar capillary brain endothelial cell (cerebEND) and mouse cerebral capillary endothelial cell (cEND) monolayers to generate TEER readings ranging between 300 – 800 Ω.cm^2. Furthermore, Hatherell and colleagues, (2011) designed a mono-cultivation of the *in vitro* human BBB by seeding 2x10^5 cells/cm^2 of a human immortalized endothelial cell line (hCMEC/D3) on the apical surface of an 8µm, fibronectin (4µg/cm^2) coated polycarbonate membrane. In this study the experimental model generated TEER readings, ranging between a minimum of ±33Ω.cm^2 and a maximum of ±42Ω.cm^2 (Hatherell *et al.*, 2011).

Conversely, *in vivo* BBB models contain a high degree of impermeability, reflected by high junctional restrictivity (i.e., high TEER). TEER measurements generated by various research groups differ and can be attributed to differences in: (i) junctional impedance (ii) measuring equipment (i.e., chopstick electrodes, cup electrodes); (iii) lab-on-chip models; (iv) temperature and (v) the handling of cells during measurement (Vigh *et al.*, 2021).

1.5. In vitro models

In vitro BBB models were first developed in 1973 in which monocultures were employed to mimic *in vivo* BBB conditions. Since then, monocultures were replaced with co-culture cellular models. Cell culture models are based on either primary or immortalized cells and have been developed in order to facilitate *in vitro* studies in drug transport, EC biology and pathophysiology (van der Helm *et al.*, 2016b; Helms *et al.*, 2016). Primary cell cultures are isolated directly from the

animal and are generally the preferred modality when studying biological tissue, as it best mimics the *in vivo* condition. The disadvantages, however, are that these cultures are expensive, susceptible to contamination, slow growing and require the regular sacrificing of animals, due to their low passage numbers. Low numbers of nucleic acids and proteins are derivatives of these cultures by biochemical or molecular assays (Brown *et al.*, 2007). Moreover, cerebral ECs are prone to losing their specific properties in culture (Nakagawa *et al.*, 2009).

The necessity for implementing *in vitro* models that are affordable, able to generate high passage numbers and able to preserve the *in vivo* conditions is critical. These factors have steered the development of continuous cell lines (i.e. immortalized cell lines). The disadvantages with employing an immortalized cell line is, however, its inability to create tightly regulated PC pathways, useful for performing pharmaceutical permeability tests (Yang *et al.*, 2007).

The *in vitro* BBB model is critical for elucidating mechanisms involved in both the establishment and breakdown of the *in vitro* BBB. These models are basic tools for discovering the passage of therapeutic agents, pathogens and cellular and subcellular dynamics during health and disease. Furthermore *in vitro* models of the BBB are able to generate high TEER and low permeability (Helms *et al.*, 2016; Erickson *et al.*, 2020). In addition, *in vitro* models provide higher throughput screening; lower cost and enables the study of specific, individual molecular mechanisms underlying permeability across the BBB (Lundquist *et al.*, 2002; Hatherell *et al.*, 2011).

In addition, BECs of porcine origin, form functional EC monolayers, which generate high TEER readings. Moreover, BECs of rat and mouse origin are advantages to utilize as they are derived from well-characterized species and are often employed in pre-clinical studies. However, *in vivo* models are critical for obtaining long-standing knowledge on BBB integrity, which would in turn promote the evaluation of tissue cross-reactivity profiles in human tissues (Helms *et al.*, 2016).

The organ-on-chips are innovative micro-engineered *in vitro* models, which enabled the study of human cells within a simulated physiological environment in real-time. This model provides features such as geometrics, sensors and fluid flow, however, the burgeoning challenges are a lack of standardized measuring parameters such as barrier permeability and shear stress, which limits the ability to comparatively analyze different, BBB-on-chip models (van der Helm *et al.*, 2016a; van der Helm *et al.*, 2016b; Vigh *et al.*, 2021).

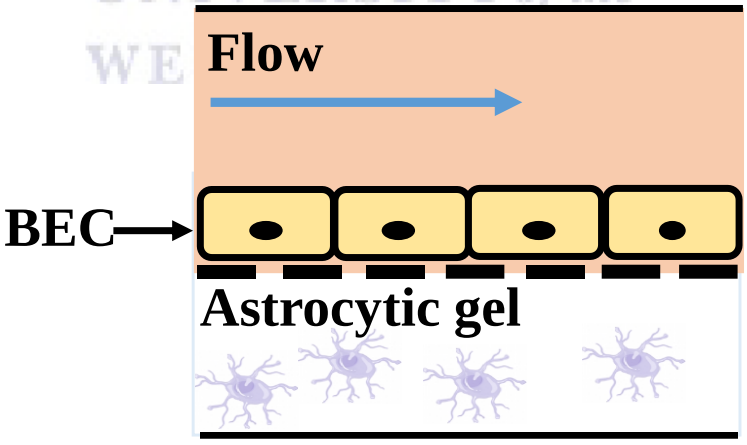

Figure 1.4. An illustration of a co-culture of BEC bEnd3s and astrocytes utilizing a microfluidic model (Adapted from Sellgren *et al.*, 2015). Permission granted by author.

Moreover, an additional *in vitro* model as proven useful in order to overcome challenges to maintain reproducibility of barrier functionality. One such model is the "BBB organoid" which are constructed utilizing co-cultures with ECs, pericytes and astrocytes. The organoid is able to mimic BBB properties (i.e. TJ expression/molecular transporters and drug efflux pumps (i.e. glycoprotein-120). The most common of this ilk of *in vitro* models are the bicameral systems constructed by growing BECs in the upper, apical compartments (top/luminal side) of Millicell/Trans-well inserts (Brown *et al.,* 2015; Mentor and Fisher, 2017).

Microfluidic devices such as the micro-on-chip and/or the organoid BBB models stimulates both a dynamic and realistic simulation of the *in vivo* scenario as it incorporates flow and shear stress. A few advantages are: (i) The ability to generate immediate permeability measurements, (ii) it closely mimics the *in vivo* BBB by providing fluid flow, which permits real-time study of the BBB in 3D and (iii) improves PC barrier functions (Sivandzade and Cucullo, 2018). The disadvantage, however, is the utilization of highly specialized equipment (Bergmann *et al.,* 2018).

In this research study, immortalized mouse BEC lines (i.e. bEnd3/bEnd5) are utilized in the construction of an *in vitro* BBB model as the BEC forms the anatomical basis of capillary beds of the cerebromicrovasculature (Daneman and Prat, 2015). The bEnd3 cell line has been reported to be the less popular cell line for studying the BBB transport mechanisms, compared to a bEnd5 cell line, as it expresses plaque proteins, i.e. ZO-1, ZO-2, occludin and the cytoskeletal element

actin (Brown *et al.,* 2007). The TEER readings for monolayer bEnd3 cells is 110-140 Ω.cm^2 compared to the *in vivo* TEER of >1000 Ω.cm^2. Brown *et al.,* (2007) surmised that bEnd5 cells are suitable as an *in vitro* model of the BBB when cultured in serum free media on the abluminal surface and is allowed to reach confluence for several days (Brown *et al.,* 2007).

1.6. Functional establishment of the blood –brain barrier

Elucidating the step-by-step development of the BBB from the perspective of cell-cell interaction involves: (i) BEC cytoarchitectural organization (ii) BEC orientation, attributed to the secretion of an extracellular matrix (ECM) (i.e. basement membrane (BM)) and (iii) BEC alignment. Investigating these aspects of development, both qualitatively and quantitatively are imperative when describing the process of barrier-genesis. Redefining the genesis of BBB formation, within the context of the cytoarchitectural and ultrastructural development of the BEC, enables better comprehension of the physical functionality of the BBB interface.

1.6.1. Morphological development of the BBB

The lateral domains of BECs are large surfaces, thus, its correct orientation is essential for BEC alignment (Mentor and Fisher, 2021). Appropriate BEC orientation into apical and basal domains provides a suitable exemplar for studying the phenotypic profile and localization of intercellular TJ protein engagement.

During the early stages of BEC development, the cell secretes an extracellular matrix (ECM), which constitutes an amorphous basement membrane (BM) comprised of 30-40µm lamina tissue consisting of select proteins: (i) collagen type IV; (ii) heparin sulfate; (iii) proteoglycans; (iv) laminin; (v) fibronectin among other ECM proteins as shown in **Figure 1.5.** In an *in vivo* scenario, the BM envelopes the cells of BECs and pericytes, enclosing the brain capillaries (Hawkins and Davis, 2005; Serlin *et al.*, 2015).

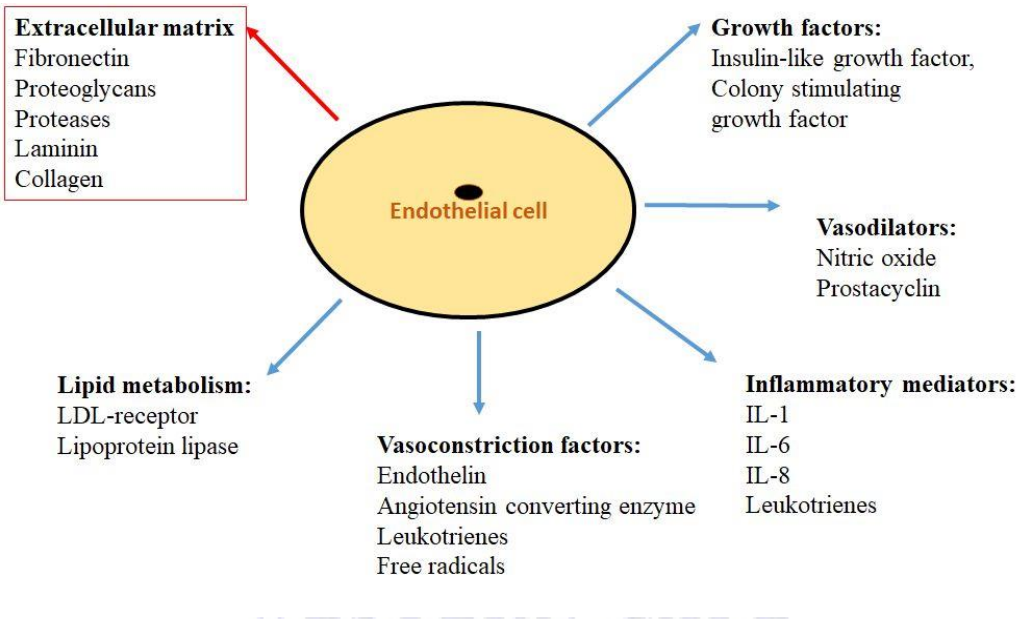

Figure 1.5. The extracellular matrix as a critical baseline for cellular orientation (Adapted from Galley and Webster, 2004). Permission granted by authors.

Mentor and Fisher, (2021) reports, for the first time, on the visualization of BECs secreting an amorphous BM within its basolateral domain in an *in vitro* BBB (bEnd5) model. This morphological finding endorses the notion that BM formation is critical for BEC orientation into apical and basolateral domains and subsequently creates an ideal environment (closely mimics the *in vivo* scenario) that enables appropriate ultrastructural BBB development *in vitro*.

In an *in vivo* scenario, the molecular underpinnings of lumen formation involve the following role players: the cytoskeleton, cell adhesion, junctional complexes and cell-matrix interactions. Moreover, the vascular lumen depends on EC cell polarity which is reliant on the formation of the BM. EC polarity is, therefore, critical during BV lumen formation, as it establishes molecular and morphological distinctions between basal, lateral and apical sides and ensures for the proper molecular engagement between cells and cell-matrix adhesion pathways (Iruela-Arispe and Beitel, 2013). Establishing apico-basal cell orientation is requisite for spatiotemporal organization of cellular processes (i.e. endocytosis, exocytosis and localized adhesion of cell membranes via protein-protein interaction (Xu *et al.*, 2012).

1.6.2 Tubulogenesis and cellular polarity

Tubulogenesis involves the evolution of an angioblast into flat shaped cells and concomitant protein junctional rearrangement as they develop into ECs, which line the blood vessel's (BV's) lumen (Xu *et al.,* 2012). The cytoskeletal proteins and its associated guanosine triphosphatase (GTPases) enzymes constitute a set of lumen regulators, namely hydrolase enzymes, which include Rac, a subfamily of the Rho family of GTPases, small (21 kDa) signaling G-proteins and the cell division control protein 42 homolog (Cdc42). Small GTPases are critical for regulating cellular processes (i.e. cytoskeletal dynamics, cellular proliferation, cellular adhesion, EC vascular morphogenesis *in vivo* and EC lumen formation *in vitro* (Koh *et al.,* 2008, Xu *et al.*, 2012; Zovein *et al.*, 2010).

Investigating the morphology and intracellular, molecular mechanisms underpinning BEC monolayer development, as a basis for *in vitro* BBB development, will facilitate our ability to comprehend the mechanobiology involved in both angiogenesis, tubulogenesis, and consequently barrier-genesis, all of which require intricate cell-cell communication between adjacent BECs of the brain's capillaries.

1.7. Cell-cell communication

Intercellular interaction requires the existence of very specific directives/factors, which exist endogenously by way of the paracrine system. Paracrine communication is an essential form of intercellular communication between unicellular models (i.e. cell monolayers of a particular cell type). Intercellular communication is typically achieved by soluble paracrine and endocrine factors (i.e. growth factors, clotting factors) and direct cell-cell contact, mediated by synapses (i.e. neuronal), in the case of typical epithelial-like cells it utilizes the gap junctions (Lucas *et al.,* 2009; Abounit and Zurzolo, 2012).

The ability of a cell to receive, process and respond to information is essential for a variety of biological processes (i.e. proliferation, division and apoptosis). Our brain's reflect a complex network of intercellular links, provided by gap junctions and neural synapses (Gurke *et al.,* 2008). In the brain, specific biomarkers are released from the CNS into the circulatory system during pathological conditions, transcytosis of blood-borne molecules into the brain, and in cell-cell communication within the NVU via extracellular microvesicles (EMVs) (Haqqani *et al.,* 2013). According to a study conducted by Haqqani *et al.,* (2013) the EMVs of BECs possess 1179 proteins. EMVs were validated by the identification of

approximately 60 known markers (i.e. Alix, TSG101 and the tetraspanin proteins). Furthermore, the surface proteins on EMVs have the ability to interact with both primary astrocytes and cortical neurons, as cell-cell communication vesicles (**Figure 1.6.**). Moreover, EMVs of the BECs exhibited several receptors previously shown to carry macromolecules across the BBB, these included: transferrin receptor, insulin receptor, low-density lipoprotein (LDL) receptor proteins (LRPs), LDLs and cell cycle transmembrane protein 30A (TMEM30A) (Haqqani *et al.*, 2013).

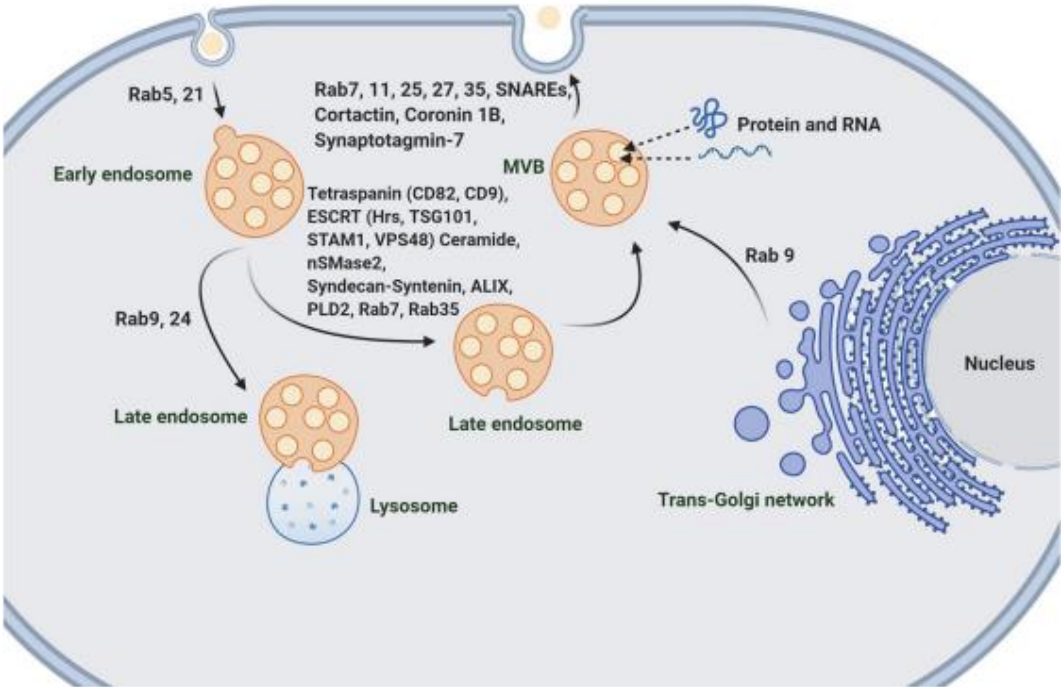

Figure 1.6. Extracellular vesicle/exosome formation within BECs MVB denotes multivesicular bodies (Heidarzadeh *et al.*, 2021) Permission granted by authors.

Extracellular vesicles (EVs) shed from cells are enclosed by a lipid bilayer creating its own precinct within the cellular environment. Three types of EVs exist: (i) microvesicles (ii) apoptotic bodies (iii) Exosomes/ nanovesicles (NVs) (Raposo and Stoorvogel, 2013; Mentor and Fisher, 2021). The second, most

abundant EV is the exosomes/NV, which possesses a 30-150 nm diameter (György *et al.*, 2011; Abels and Breakefield, 2016). The exosomes/NVs are derived from the inward budding of endosomes within intraluminal vesicles (ILV). ILVs assemble into multivesicular bodies (MVB), which fuse with the plasma membrane and release NVs, which fuse onto the plasma membrane surface (Abels and Breakfield, 2016). The biogenesis of the NV is facilitates by Rab GTPases (i.e. Rab27A, Rab27b, Rab11, Rab 35) Furthermore, the NVs formed by Rab 27A/Rab27b contain endosomal proteins (ALIX, TSG101 and CD63) (Abels and Breakfield, 2016; Heidarzadeh *et al.*, 2021).

Furthermore, vesicles are able to be extrude from nanotubular (NT) structures, which project or originate from the cells plasma membrane (Rilla *et al.*, 2013). Recently, a novel type of cell-cell communication reported on the *de novo* formation of BEC membrane-bound NV structures, which are able to induced tunneling NTs (TUNTs) were discovered for the first time, in Mentor and Fisher, (2021), during BEC (bEnd5) monolayer establishment. The TUNTs appear to be critical for BEC alignment and membrane interaction during the establishment of a BEC barrier interface.

1.8. The role of the cytoskeleton in establishing BEC morphology

To date, much elucidation is required, with respect to morphological, nanoscopic landscape of endothelial barrier establishment. Furthermore, the molecular underpinnings of its ultrastructural profile remains moot. It is well documented in the literature that immortalized mouse BECs (bEnd5) exhibit a longitudinal pattern of filamentous-actin (f-actin) distribution compared to the more organized orientation of apical rings in the primary mouse brain microvascular ECs (pMBMECs), throughout the entire cell body (Steiner *et al*., 2011). Moreover, BEC bEnd5s express spindle-shape cell morphology compared to the pMBMECs (Steiner *et al.*, 2011). Despite the phenotypic characterization of BECs,

Cytoskeletal elements (i.e., microfilaments and microtubules) are known to play a critical role in establishing cell shape/morphology. Recent findings by Rajakylä *et al.,* (2020) discusses the role of actin-myosin bundles in facilitating the assembly of the AJ within the PC space. The study described two types of actin filament populations within the PC shunts of epithelial cultures which display indistinguishable filamentous sheets of cytoplasmic projections as a means of direct cell-cell (Rajakylä *et al.*, 2020).

Furthermore, the literature reports on cell membrane's leading edges, which are denoted as actin-rich lamellipodia (LP) and function in spearheading, cell migration as shown in **Figure 1.7.** LP are mediated by actin-related proteins 2/3 (ARP2/3). Actin filaments are small microfilaments, with a diameter of approximately 6 nm, comprised of f-actin. F-actin is a 42 kDa, microfilament protein found in the cytoarchitecture of eukaryotic cells. LP are generally found in

motile cells (i.e., endothelial cells, neurons, immune cells and epithelial cells) (Breslin *et al.*, 2015). *In vitro* cultures of EC monolayers are reported to display frequent localized LP, which is critical in cell-cell membrane migration and interaction during monolayer establishment (Ballestrem *et al.*, 2000).

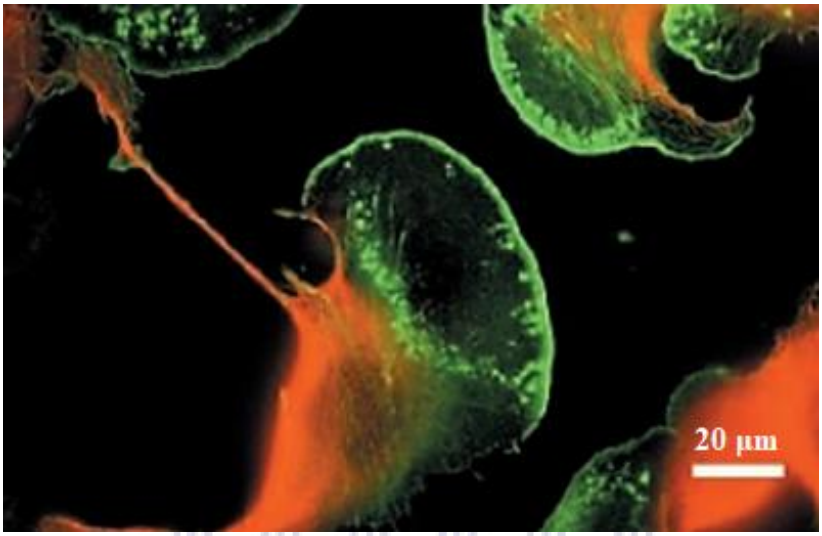

Figure 1.7. An IF micrograph illustrating lamellipodia (LP) cytoarchitectural dynamics of murine melanoma cells (B16). Actin (green) and Tubulin (red), showed actin-rich, membrane leading edges/LP, devoid of tubulin. Tubulin, however, appeared in the tubular cell-cell contact points between adjacent B16 cells growing in culture (Ballestrem *et al*., 2000). Permission granted by author.

Within the ECs, cytoskeletal proteins and associated GTPases (i.e., Rac and Cdc42) control actin cytoskeleton and microtubule assembly. This modulation contributes to the formation of the lumen of BVs. Moreover, cytoskeletal proteins regulate vesicular trafficking and facilitate cellular morphogenesis endorsing lumen size (Bayless *et al.*, 2000; Iruela-Arispe and Beitel, 2013; Koh *et al.*, 2008).

Further protrusion out of the LP give rise to filopodial structures, which hover between cells.

Paralleling these filopodia are novel ultra-structures, denoted as the nanotube (NTs) (Mentor and Fisher, 2021). In this study Mentor and Fisher, (2021) describe, for the first time, the potential role of NT scaffolding in the alignment of BECs (i.e., bEnd3/bEnd5) during BBB development *in vitro*. Tunneling NTs have been described in various cell types: neurons (Rustom *et al.*, 2004; Wang *et al.*, 2010), myeloid cells (Wang *et al.*, 2010), mesenchymal stem cells (Rajan *et al.*, 2020), endothelial progenitor cells (Koyanagi *et al.*, 2005) and more recently, similar in behavior to the filamentous actin structures observed within epithelial cells (Rajakylä *et al.*, 2020).

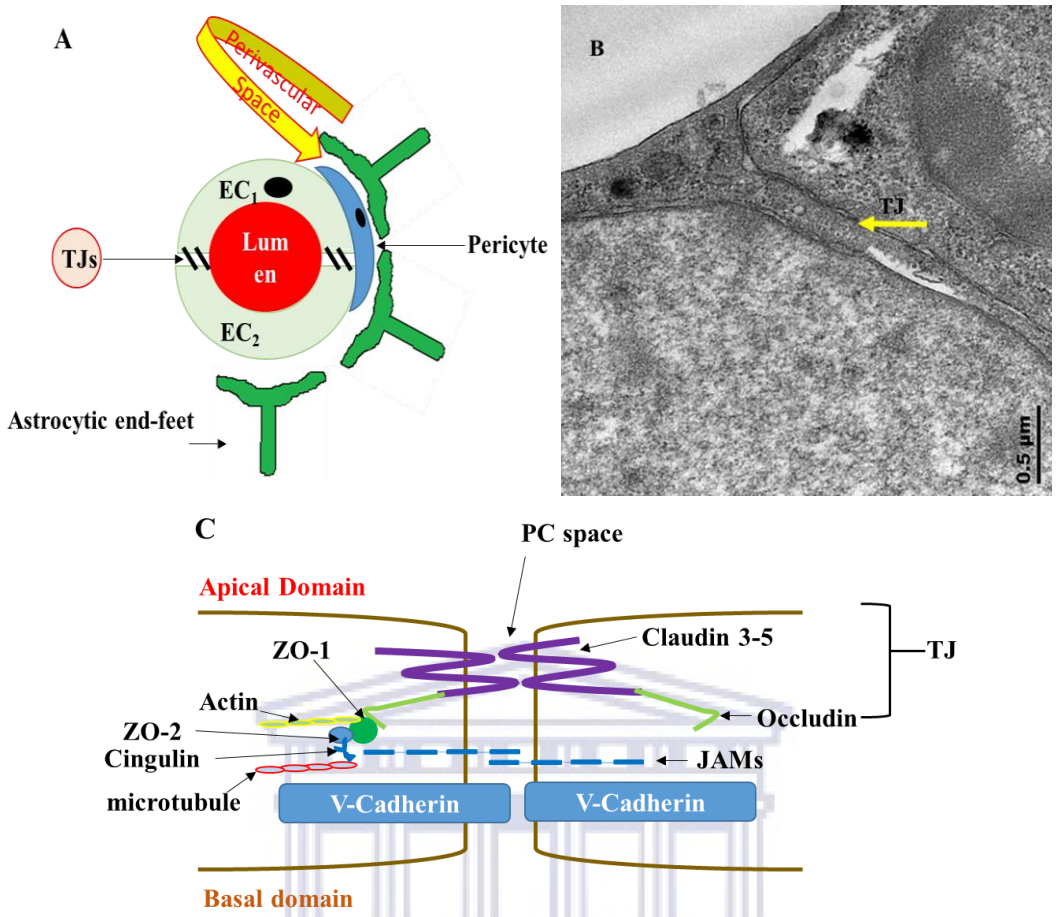

Figure 1.8. Actin involvement in the BEC interaction with plaque proteins to facilitate transmembrane TJ protein alignment. (A) Represents the NVU demonstrating TJ engagement between adjacent BECs, EC_1 and EC_2 denotes endothelial cells and TJ denotes tight junctions (Adapted from Fisher and Mentor, 2020). Permission granted by authors; (B) A transmission electron micrograph displaying zones of TJ interaction (Mentor and Fisher, 2021). Permission granted by authors; (C) An illustration of zones of TJ interaction. (Adapted from Heidarzadeh *et al*, 2021) Permission granted by authors.

Furthermore, literature reports on high-resolution transmission electron micrographic (HR-TEM) data of *in vivo* BEC, which has shown distinct electron dense regions, covered by overlapping regions of membranous leading edges which appear to reinforce occlusion of the EC barrier. HR-TEM studies observed

bead-like structures, now reported to be the TJ protein localization, which exists within the PC space as shown in **Figure 1.9.** (Salman *et al.*, 2020).

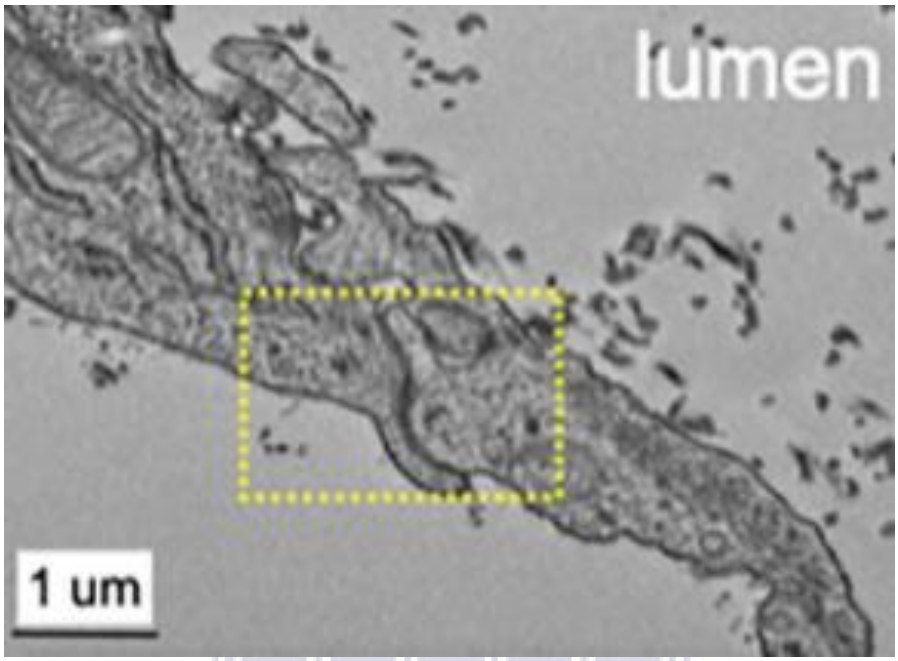

Figure 1.9. An HR-TEM micrograph displaying a capillary EC presented with electron dense region between two adjacent human BECs grown on a microchip, represented within the perforated yellow square. The micrograph displays overlapping membranous structures, between adjacent BECs of the cerebromicrovasculature (Salman *et al.*, 2020). Permission granted by authors.

1.8.1. Role of cytoskeletal microtubules in establishing BEC morphology

Microtubules are the largest type of filament, with a diameter of about 25 nm, and are composed of a protein called tubulin (55kDa) as shown in **Figure 1.10.** Tubulin polymerizes into long chains or microtubules, which constitute the cytoarchitecture of living cells. Cytoskeletal proteins namely f-actin and α-tubulin are not, however, limited to functioning as components of the BEC cytoskeleton. Additionally, it is involved in the formation of nanostructural deformations (i.e.

invaginations or protrusions) of the leading edges of the cell's membrane (i.e. LPs, filopodia and nanotubules (NTs)).

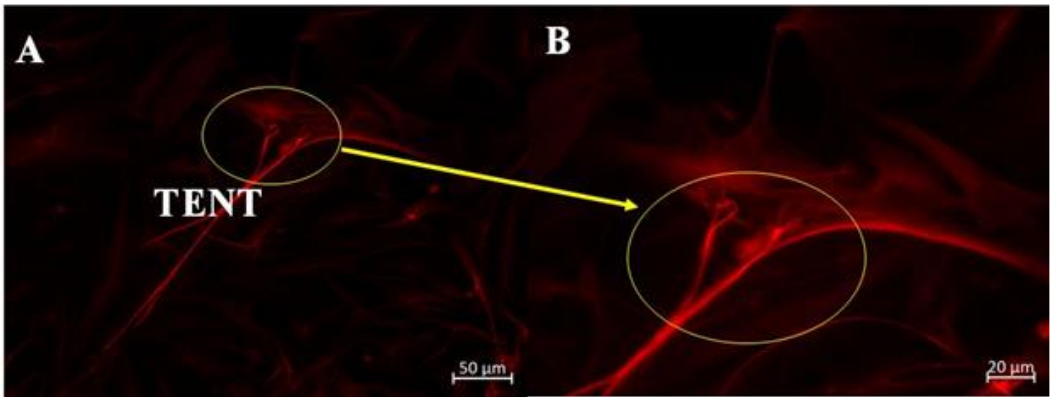

Figure 1.10. (**A**) **Micrographic display showing (red fluorescence/Alexa Fluor 568 stained) α-tubulin-rich microtubule involvement in the formation of NT structures between adjacent BECs (bEnd3); (B) A magnified depiction of (A) illustrating NT distal ends contacting a neighboring BEC** (Mentor *et al.,* 2022). Permission granted by authors.

Furthermore, an additional protein, f-actin is ubiquitous in the cytoplasm, influencing cell shape. Immunofluorescence (IF) micrograph of the subcellular cytoarchitecture within cardiomyocytes **(Figure 1.11)** endorses the notion that the cell's cytoskeleton is f-actin rich, providing cell shape and cell-cell contact between adjacent cells by the formation of intracellular, molecular, scaffolding extending from within the cell cytoplasm, guiding the cells cytoplasm towards making contact cells growing in close proximity (Acquistapace *et al.,* 2011; Mentor *et al.,* 2022).

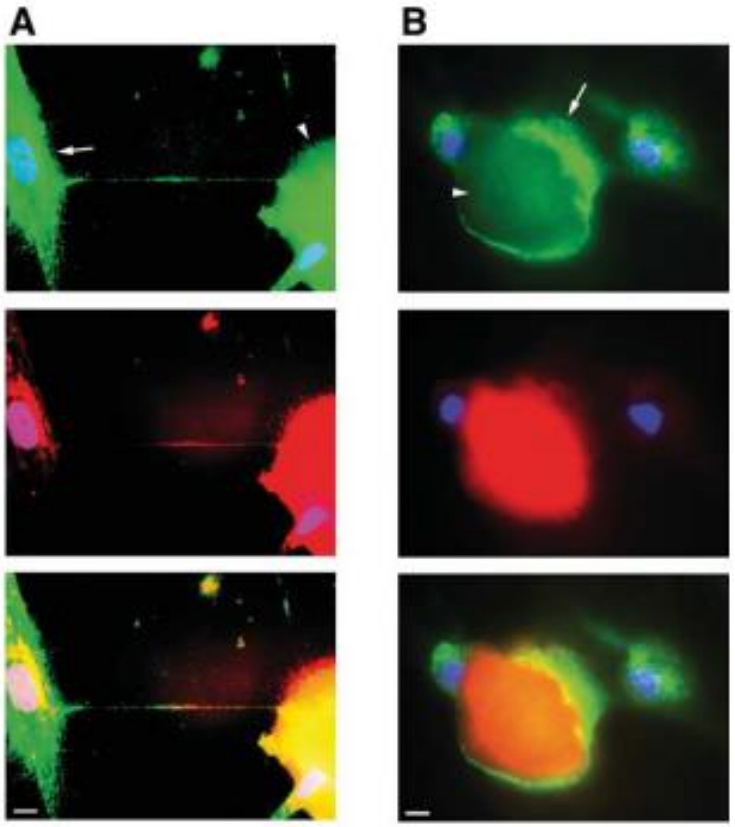

Figure 1.11. The cytoarchitectural backbone of cardiomyocytes. (**A**): Thin membranous protrusions extending from the leading edges of cardiac cells (arrow) containing both f-actin (rhodamine-phalloidin staining, red) and tubulin (fluorescein isothiocyanate–conjugated a tubulin, green); (**B**): Cardiac cells expressing intercellular cytoplasmic cross-bridges, which are f-actin rich **(red**) and tubulin rich (**green**). Scale bar: 10 μm (Acquistapace *et al.,* 2011). Permission granted by authors.

1.8.2. Effect of depolymerization on cytoarchitectural proteins

1.8.2.1. The role of Cytochalasin D in the inhibition of cytoarchitectural microfilament formation

Cytochalasin D represented in **Figure 1.12.** forms part of a class of structurally related fungal metabolites (i.e. mycotoxins), an alkaloid produced by Helminosporium and other molds. It is a cell-permeable and potent inhibitor of actin polymerization by binding to the barbed ends of actin filaments (i.e. at the f-actin polymer) and prevents elongation of the microfilaments (Natarajan *et al.*, 2000).

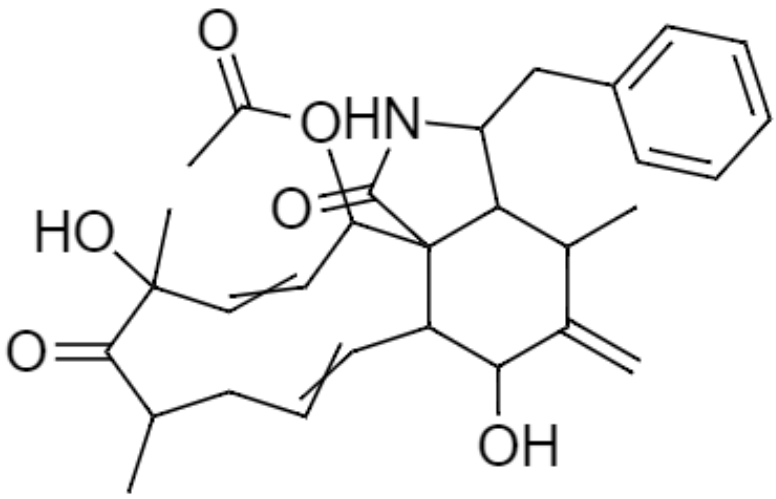

Figure 1.12. The chemical structure of the mycotoxin, Cytochalasin D, with a MW of 507.6g/mol.

1.8.2.2. Mode of action of Cytochalasin D

The literature reports on the ability of polymerizing suppressive agent, Cytochalasin D, to suppress the formation of f-actin microfilaments at 0.5µM in cardiomyocytes (Acquistapace *et al.*, 2011). This is achieved by disrupting cytoskeleton network filaments (i.e. actin-filaments, actin microfilaments and microtubules) resulting in the formation of filamentous aggregates when the

fungal toxin binds to the barbed ends of actin and inhibits polymerization (Schliwa, 1982) as illustrated in **Figure 1.13.**

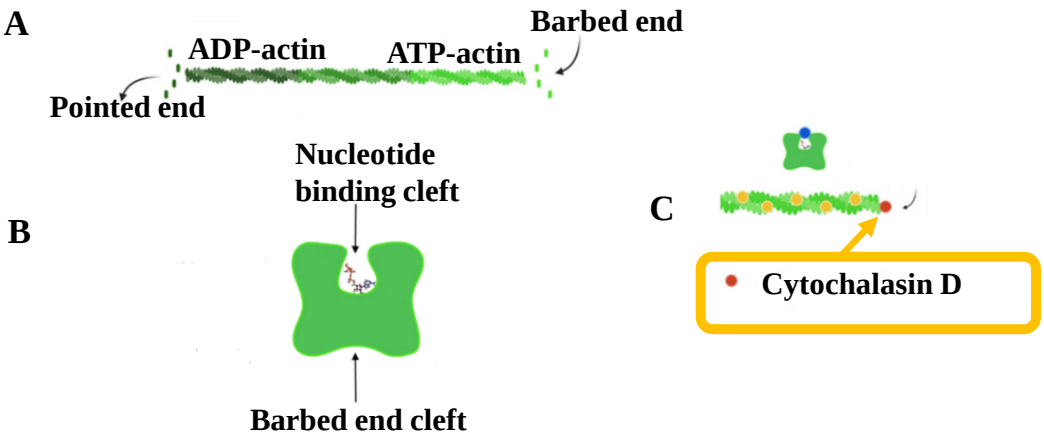

Figure 1.13. Mechanism by which Cytochalasin D inhibits microfilament polymerization or elongation through ATP hydrolysis, which inhibits G-actin monomers from binding to the barbed ends of the microfilament. (A) An illustration of filamentous actin; (B) An illustration of a G-protein monomer and; (C) An illustration of Cytochalasin D binding to the barbed end of a microfilament (Adapted from Gentile *et al*, 2022). Permission granted by authors.

1.8.3. The role of Nocodazole in the inhibition of cytoarchitectural microtubule formation

A recent study by Mentor and Fisher, (2021) has shown thin membranous stems/NTs form between BECs growing *in vitro*, and have since investigated the subcellular, cytoarchitectural backbone of these connections. Molecular findings in this study suggested that cell-cell connections are formed by transient α-tubulin rich tethering NTs (TENTs) resulting in membrane apposition and PC occlusion between adjacent BECs. The study alludes the molecular mechanisms underpinning ultrastructural TENT dynamics, which is a functional imperative when elucidating barrier-genesis. The study introduced the treatment of BECs

with Nocodazole as a known depolymerizing agent (**Figure 1.14.**) in order to inhibit the formation of α-tubulin (Acquistapace *et.al*. 2011). The aim of this study was to test the postulated role of α-tubulin-rich microtubules in NT formation (Acquistapace *et al.*, 2011; Mentor *et al.*, 2022; Önfelt *et al.*, 2006).

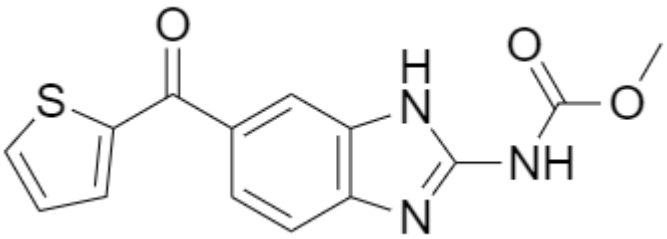

Figure 1.14. The chemical structure of Nocodazole, which has a MW of 301.3g /mol, is a member of thiophenes and benzimidazoles; a carbamate ester and an aromatic ketone.

1.8.3.1.Mode of action of Nocodazole

Microtubules are comprised of isometric monomers of tubulin (i.e., α-tubulin and β-tubulin) which, concomitantly, forms the functional and structural units making up the whole microtubule composite (**Figure 1.15.**).

Nocodazole, is a synthetic tubulin-binding agent and/or microtubule-active agent). It is an antineoplastic agent, which functions in preventing centromere spindle fiber formation during mitosis and thus inhibits cellular division and proliferation; it acts by inhibiting microtubule formation through depolymerization of α-tubulin subunits (Rajendraprasad *et al.,* 2021). A study conducted by Acquistapace *et al.*, (2011) reports on Nocodazole's ability to inhibit the polymerization of α-tubulin at 1µM. Depolymerization occurs by increasing tubulin GTPases, and reduces the delivery of apical membrane proteins (Eilers *et al.*, 1989).

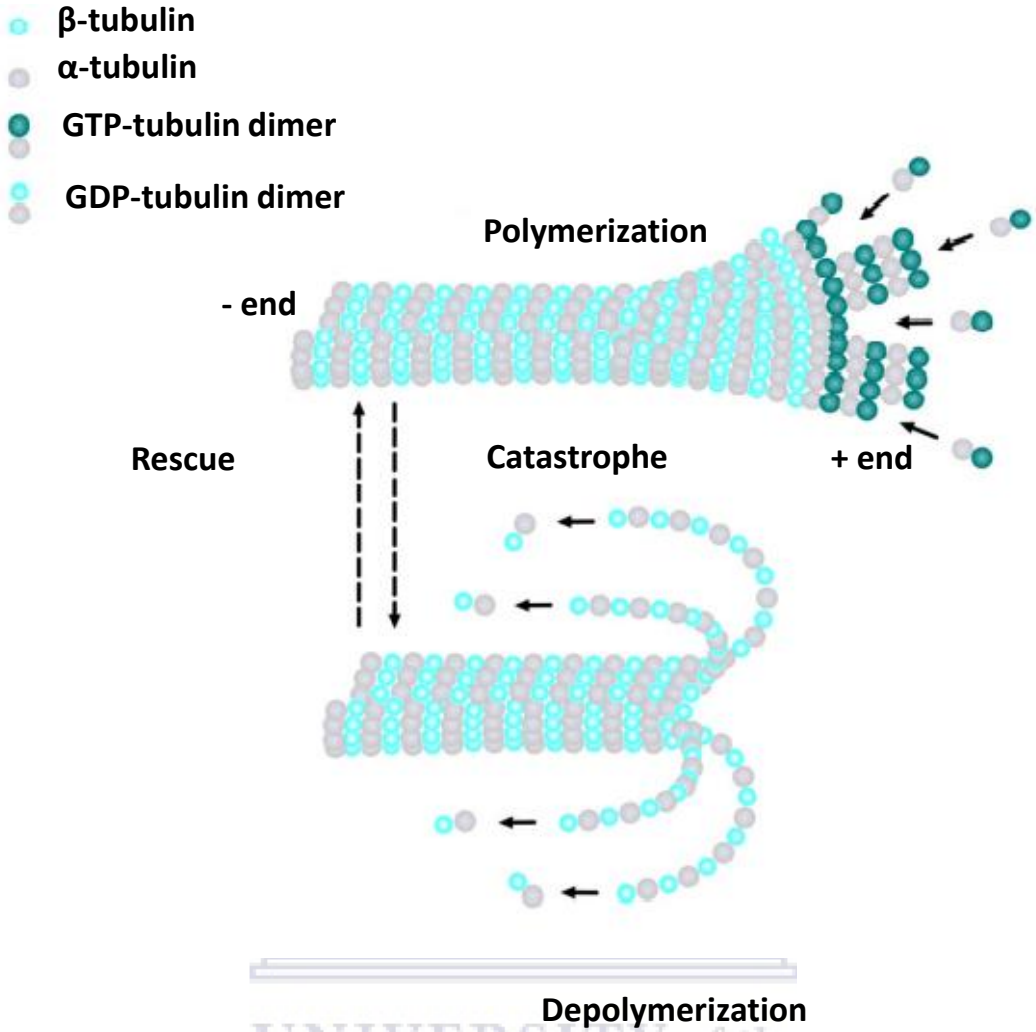

Figure 1.15. Mechanism of polymerization and depolymerization of α-tubulin. Microtubules within the cytoskeleton of all cells and are comprised of the monomers α-tubulin heterodimers and β-tubulin. The anabolism of the microtubule designates polymerization and the process labelled as 'rescue'. Conversely, the catabolism of the microtubule designates depolymerization and the deconstruction process denotes a 'catastrophe.' The breaking down and building up of the tubules are catalyzed by GTPases (Lasser *et al.*, 2018). Permission granted by authors.

1.9. Nanotubules

Intercellular communication is functionally necessary for the cell to perform coordinated physiological processes, such as proliferation, migration and the formation of neuronal networks (Lasser *et al.,* 2018). Moreover, in a recent study conducted by Mentor and Fisher, (2021) discusses the significance of a novel form of direct cell-cell communication in the form of nanotubular (NT) cross-bridges which form transiently between adjacent BECs, during *in vitro* BBB development. The study characterized two distinct NTs: (i) tunneling nanotube (TUNT) and tethering NT (TENT) formation (Mentor and Fisher, 2021). It has been previously reported that NTs are f-actin-rich structures, which form the subcellular architecture for the leading edges of the cells membrane and have been described as mediators of membrane continuity between pheochromocytoma (PC12) cells (Rustom *et al.*, 2004;.Gerdes *et al.*, 2008). F-actin dependent NTs have been reported to function as facilitators in intercellular transport of various cellular components (Gurke *et al.,* 2008; Mentor and Fisher, 2021).

NTs, therefore, represents a form of f-actin and α-tubulin based tubular connections between adjacent cells growing in close proximity (Mentor *et al.*, 2022), and are implicated in various essential physiological processes, such as: development, tissue regeneration and signal transduction (Kimura *et al.*, 2012).

In the literature, NTs function as a facilitator in the transfer of an array of cargo, such as organelles, plasm membrane machineries, pathogens and calcium (Ca^{2+}). In addition, a recent functionality is its ability to transfer electrical signals, via gap junctions (Abounit and Zurzolo, 2012). NTs are different from filopodia or LP, as

mentioned previously in the text, unlike the other filament bridges; they mediate continuity between the cytoplasm of remote cells and are suspended structures within the PC spaces, never contacting the substrate. **Figure 1.16.** illustrates these dynamic structures which form transiently and display an *in vitro* half-life ranging from minutes to hours (Rustom *et al.*, 2004; Abounit and Zurzolo, 2012). There are two main reasons for this relatively recent discovery: (i) They have very small diameters ranging from 20-500 nm and can reach lengths spanning diameters of cells and (ii) *in vitro*, these connections are momentary, fragile and light-sensitive and sensitive to shear stress and chemical fixation (Rustom *et al.*, 2004)

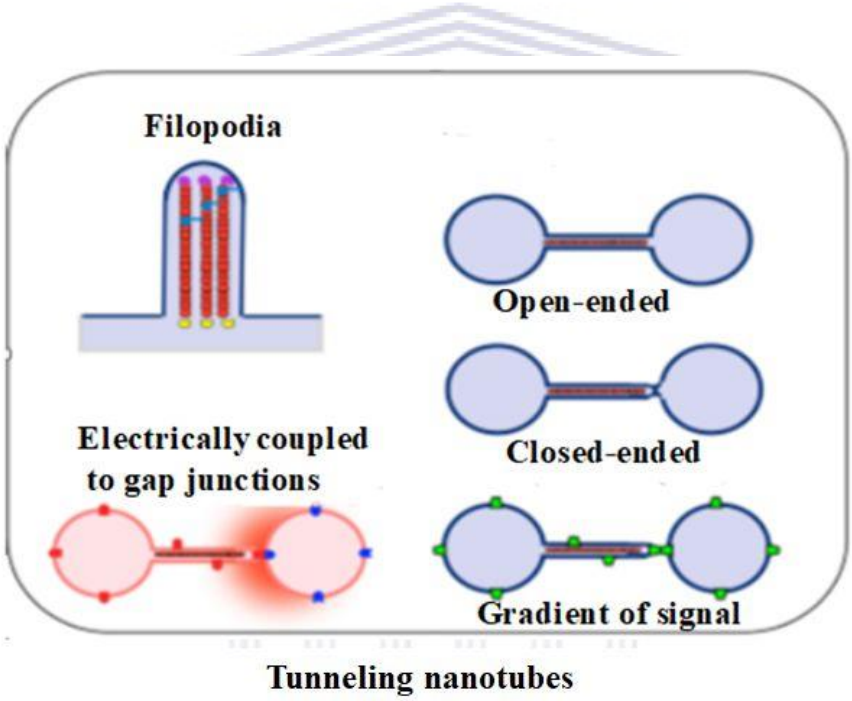

Figure 1.16. An illustration of three NT profiles (Abounit and Zurzolo, 2012). Permission granted by authors.

Filopodia are exploratory cytoplasmic projections (containing parallel bundles of f-actin). The machinery involved in filopodia includes actin nucleation complex, containing Rho GTPase CDC42 and at the end of the f-actin tip, barbed end

proteins, such as capping proteins and Ena-VASP proteins which regulate actin polymerization (Abounit and Zurzolo, 2012).

To date, the hallmark of BBB integrity is attributed to interendothelial TJ protein engagement. The BBB ECs are, however, morphologically complex and its complexity must be properly elucidated if we want to achieve successful treatment of the CNS. The importance of BEC cytoplasmic projections (i.e. nanotubules) as an essential part of BEC alignment must be further investigated in order to establish its relevance in the process of barrier-genesis and the establishment of the BBB.

1.10. Problem statement and rationale

The chemical stability of the brain's parenchyma (i.e. neurons) is critical as it directly implicates our decision-making aptitude and, therefore, must be well regulated. Local communities within Cape Town, South Africa, are rife with drug abuse (i.e. Methamphetamine, alcohol, cannabis) (Mushanyu *et al.,* 2015; van Heerden *et al.,* 2009), which affects the brain's microenvironment by disrupting its protective properties. One of the main protective properties is the BBB, which comprises of brain capillary endothelial cells (BECs) (Naranjo *et al.,* 2021). Cellular differentiation of the BECs is an important parameter to consider when elucidating the structural establishment of BBB integrity, which is grounded in the BECs ability to occlude its PC spaces through the expression of intercellular TJ proteins. The impermeability of these PC spaces is crucial in the regulation of transcellular transport systems across the BECs to achieve homeostasis of the CNS.

The BBB has two aspects to consider: (i) It is highly restrictive and (ii) its restrictivity is an inhibitory factor in the treatment of CNS disorders (i.e. AD, PD etc.) (Zorkina *et al.*, 2020).

To date, elucidating the physical functionality of nanostructures in reinforcing BBB integrity remains moot. The dissertation attempts to comprehend the nanostructural relevance in BBB development. Ultrastructural investigation at high-resolution will illuminate the nanostructural behaviour of the developing BBB *in vitro*. Ultrastructural and molecular findings will provide a level of understanding that will illuminate the role of nanotubules (NTs) in facilitating the alignment of BECs in a manner that promotes intercellular TJ engagement during *in vitro* BBB development.

The necessity to develop novel therapeutic strategies, which are able to traverse the BBB is critical for the successful treatment of CNS disorders. To-date the literature has not emphatically described all structural interfaces, which exist between the blood and the brain. The dissertation, thus, takes the form of a morphological study, utilizing high-resolution microscopy and challenges the existing theoretical premise that BBB integrity is attributed to intercellular TJ proteins, transcellular ionic flux and enzymatic components (Cecchelli *et al.*, 2007).

Furthermore, the research study investigates the role of cytoskeletal proteins f-actin and α-tubulin in the formation of BEC ultrastructural NTs by treating cells with selected depolymerizing agents, Cytochalasin D and Nocodazole to

investigate the BEC cytoarchitectural influence on nanostructural development and permeability of the BBB *in vitro*.

1.11. Scope of study

This research study investigates the structural dynamics involved in barrier construction of BECs in order to elucidate the restrictive physical nature of the cerebromicrovasculature. Furthermore, subcellular research investigations will analyze the molecular underpinnings of BECs morphology (i.e. NTs) in order to establish its functional role in the developing *in vitro* BBB. The research study is, therefore, a structural account, of the developing *in vitro* BBB from an ultrastructural and cytoarchitectural perspective. The aim is to transcribe and define the physical functionality of BBB morphology within a nanoscopic landscape. The study seeks to generate novel insights into BEC ultrastructural development and to coalesce the topographical and molecular underpinning of these ultra-structures in a manner that redefines BBB integrity. This study reports on the role of NVs, TUNTs and TENTs in BBB development utilizing an *in vitro* BBB model employing immortalized mouse brain endothelial cell lines (i.e. bEnd3 and bEnd5 cells). Furthermore, it challenges the existing theoretical premise of BBB formation. The use of high-resolution electron microscopy (HREM) aids in distinguishing between several nanoscopic BBB ultrastructures. More importantly, this *in vitro* BBB model serves as a useful modality to employ when evaluating the effects of neurodegeneration, CVA and drug treatment on the BBB.

1.12. Hypothesis

The theoretical premise of the existing BBB model is that intercellular TJ proteins form a scaffolding between adjacent BECs during barrier-genesis, which occludes PC shunts, and is thus critical for establishing a well-regulated BBB. This research study hypothesizes that novel NT ultrastructure's assist in a polarized sheet of BECs by: (i) eliciting direct cell-cell communication; (ii) alignment of adjacent BECs and (iii) juxtapositioning its apico-lateral membranes, which allows for TJ protein-protein engagement and the occlusion of the PC spaces, subsequently establishing a highly restrictive BBB.

1.13. Research aims and objectives

1.13.1. Aims:

i. Identify, analyze and compare the morphological and topographical ultrastructural NVs, tunneling NT (TUNT) and tethering NT (TENT) differences between brain microvascular and systemic microvascular ECs.

ii. Determine the effect of depolymerization of cytoskeletal proteins on BEC percentage viability, percentage toxicity and cell division.

iii. Determine the effect of depolymerizing agents on BBB permeability.

iv. Determine the physical functionality of TENT formation in facilitating TJ protein-protein interaction along the PC pathways of a bEnd5 cells, upon treatment with select depolymerizing agents.

v. To determine the effect of the cytoskeleton on the formation of TENTs by visualization of BEC cytoarchitecture, upon treatment with select depolymerizing agents.

vi. To quantify the expression of f-actin and α-tubulin in BEC cytoarchitecture upon treatment with select depolymerizing agents.

1.13.2. Objectives:

i. High-resolution electron microscopy (HREM) was utilized to investigate the micrographical anatomy of the *in vitro* BBB BECs as a 3-D construct and was compared to systemic ECs. HREM findings would aid in making inferences about the role of NVs, NTs in BEC alignment and TJ localization compared to the ECs of systemic rat cardiomicrovascular ECs (CMECs).

ii. Trypan blue exclusion assay studies were utilized for assessing percent cell viability, percent cell toxicity and BEC numbers upon exposure to the inhibitors of cytoskeletal proteins (i.e. f-actin and α-tubulin) utilizing Cytochalasin D (0.1, 0.25, 0.5, and 1 μM) and Nocodazole (0.25, 0.5, 1, and 2 μM) , relative to control groups (untreated).

iii. Transendothelial electrical (TEER) studies were performed to assess barrier integrity/permeability upon treatment with Cytochalasin D (0.1, 0.25, 0.5, and 1 μM) and Nocodazole (0.25, 0.5, 1, and 2 μM), relative to control groups (untreated).

iv. Micrographical analysis to endorse the ultra-structural role of NTs in cell-cell communication within the *in vitro* BBB utilizing high-resolution

scanning electron microscopy (HR-SEM) to visualize NT /deformation during BBB development upon stimulation with Cytochalasin D (0.1, 0.25, 0.5, and 1 μM) and Nocodazole (0.25, 0.5, 1, and 2 μM), relative to controls (untreated).

v. Qualitatively investigate the role of cytoskeletal protein (i.e. f-actin and α-tubulin) polymerization in TENT formation between adjacent bEnd5 cells utilizing immunocytochemistry (ICC) upon stimulation with Cytochalasin D (0.1, 0.25, 0.5, and 1 μM) and Nocodazole (0.25, 0.5, 1, and 2 μM), relative to control groups (untreated).

vi. Quantify protein (i.e. f-actin and α-tubulin) expression or inhibition upon stimulation with microfilament-active depolymerizing agent Cytochalasin D (0.1, 0.25, 0.5, and 1 μM) and microtubule-active depolymerizing agent Nocodazole (0.25, 0.5, 1, and 2 μM), utilizing Western blot analysis.

Cell-based *in vitro* BBB models are useful for supplementing the existing knowledge on the typography of developing BEC monolayers. Furthermore, the employment of high -resolution scrutiny will revolutionize our interpretation of BEC barrier-genesis by the exploitation of novel, morphological ultrastructures, which are involved in reinforcing BBB integrity. The findings in this research study will dramatically aid our understanding of the *ad hoc*, reversible opening of the BBB, which would set new targets for drug access to disease sites in the brain.

REFERENCES

Abbott, N. J., Rönnbäck, L., and Hansson, E. (2006). Astrocyte-endothelial interactions at the blood-brain barrier. *Nature reviews neuroscience*, 7(1): 41–53. doi: 10.1038/nrn1824.

Abels, E. R., and Breakefield, X. O. (2016). Introduction to extracellular vesicles: Biogenesis, RNA cargo selection, content, release, and uptake. *Cellular and molecular neurobiology*, 36(3): 301–312. doi: 10.1007/s10571-016-0366-z.

Abounit, S., and Zurzolo, C. (2012). Wiring through tunneling nanotubes - from electrical signals to organelle transfer. *Journal of cell science*, 125(5): 1089–1098. doi: 10.1242/jcs.083279.

Acquistapace, A., Bru, T., Lesault, P., Figeac, F., Coudert, A.E., le Coz, O., Christov, C, Baudin, X, Auber, F., Yiou, R., Dubois-Randé, J., Rodriguez, A. (2011). Human mesenchymal stem cells reprogram adult cardiomyocytes toward a progenitor-like state through partial cell fusion and mitochondria transfer. *Stem cells*, 29(5): 812–824. doi: 10.1002/stem.632.

Aird, W. C. (2007a). Phenotypic heterogeneity of the endothelium: I. Structure, function, and mechanisms. *Circulation research*, 100(2): 158–173. doi: 10.1161/01.RES.0000255691.76142.4a.

Aird, W. C. (2007b). Phenotypic heterogeneity of the endothelium: II. Representative vascular beds. *Circulation research*, 100(2): 174–190. doi: 10.1161/01.RES.0000255690.03436.ae.

Aird, W. C. (2012). Endothelial cell heterogeneity. *Cold spring harbor perspectives in medicine,* 2(1): a006429–a006429. doi: 10.1101/cshperspect.a006429.

Al Rihani, S.B., Darakjian, L.I., Deodhar, M., Dow, P., Turgeon, J., and Michaud, V. (2021). Disease-induced modulation of drug transporters at the blood-brain barrier level. *International journal of molecular sciences,* 22 (7):3742. doi: 10.3390/ijms22073742.

Alves, N.G., Motawe, Z.Y., Yuan, S.Y., and Breslin, J.W. (2018). Endothelial protrusions in junctional integrity and barrier function. *Curr. Top. Membr,* 82:93-140. doi: 10.1016/bs.ctm.2018.08.006.

Ballabh, P., Braun, A., and Nedergaard, M. (2004). The blood-brain barrier: An overview: structure, regulation, and clinical implications. *Neurobiology of disease,* 16(1): 1–13. doi: 10.1016/j.nbd.2003.12.016.

Ballestrem, C., Wehrle-Haller, B., Hinz, B., Imhof, B.A. (2000). Actin-dependent lamellipodia formation and microtubule-dependent tail retraction control-directed cell migration. *Molecular biology of the cell*, 11(9): 2999–3012. doi: 10.1091/mbc.11.9.2999.

Banks, W. A., Kovac, A., and Morofuji, Y. (2017). Neurovascular unit crosstalk: Pericytes and astrocytes modify cytokine secretion patterns of brain endothelial cells. *Journal of cerebral blood flow & metabolism*, p. 0271678X1774079. doi: 10.1177/0271678X17740793.

Bayless, K. J., Salazar, R., and Davis, G. E. (2000). RGD-dependent vacuolation and lumen formation observed during endothelial cell morphogenesis in three-

dimensional fibrin matrices involves the alpha (v) beta (3) and alpha (5) beta (1) integrins. *The American Journal of Pathology,* 156 (5): 1673-1683. doi: 10.1016/s0002-9440(10)65038-9.

Bergmann, S., Lawler, S.E., Qu, Y., Fadzen, C.M., Wolfe, J.M., Regan, M.S., Pentelute, B.L., Agar, N.Y.R., Cho, C. (2018). Blood–brain-barrier organoids for investigating the permeability of CNS therapeutics. *Nature protocols*. Springer Nature, 13, (12): 2827–2843. doi:10.1038/s41596-081-0066-x.

Breslin, J. W., Zhang, X.E., Worthylake, R.A., Souza-Smith, F.M. (2015). Involvement of local lamellipodia in endothelial barrier function. *PLoS ONE*, 10(2): 1–30. doi: 10.1371/journal.pone.0117970.

Brown, R. C., Morris, A. P., and O'Neil, R. G. (2007). Tight junction protein expression and barrier properties of immortalized mouse brain microvessel endothelial cells. *Brain research*, 1130 (1): 17–30. doi: 10.1016/j.brainres.2006.10.083.

Brown, J. A., Pensabene, V., Markov, D.A., Allwardt, V., Neely, M.D., Shi, M., Britt, C.M., Hoilett, O.S., Yang, Q., Brewer, B.M., Samson, P.C., McCawley, L.J., May, J.M., Webb, D.J., Li, D., Bowman, A.B., Reiserer, R.S., and Wiskwo, J.P. (2015). Recreating blood-brain barrier physiology and structure on chip: A novel neurovascular microfluidic bioreactor. *Biomicrofluidics,* 9(5). doi: 10.1063/1.4934713.

Cai, W., Zhang, K., Li, P., Zhu, L., Xu, J., Yang, B., Hu, X., Lu, Z., Chen, J. (2017). Dysfunction of the neurovascular unit in ischemic stroke and

neurodegenerative diseases: An aging effect. *Ageing research reviews*, 34: 77–87. doi: 10.1016/j.arr.2016.09.006.

Cardoso, F. L., Brites, D., and Brito, M. A. (2010). Looking at the blood-brain barrier: Molecular anatomy and possible investigation approaches. *Brain research reviews*, 64(2): 328–363. doi: 10.1016/j.brainresrev.2010.05.003.

Cecchelli, R., Berezowski, V., Lundquist, S., Culot, M., Renftel, M., Dehouck, M., and Fenart, L. (2007). Modelling of the blood-brain barrier in drug discovery and development. *Nature reviews drug discovery,* 6 (8): 650-661. doi: 10.1038/nrd2368.

Cheng, J., Korte, N., Nortley, R., Sethi, H., Tang, Y., and Atwell, D. (2018). Targeting pericytes for therapeutic approaches to neurological disorders. *Acta neuropathological,* 136(4): 507-523. doi: 10.1007/s00401-018-1893-0.

Daneman, R., and Prat, A. (2015). The blood-brain barrier. *Cold spring harbor perspectives in biology*,7(1):a020412. doi:10.1101/cshperspect.a020412.

Dolman, D., Drndarski, S., Abbott, N.J., Rattray, M. (2005). Induction of aquaporin 1 but not aquaporin 4 messenger RNA in rat primary brain microvessel endothelial cells in culture. *Journal of neurochemistry,* 93(4): 825–833. doi: 10.1111/j.1471-4159.2005.03111.x.

Ehrlich, P. (1885). Das Sauerstoff-Bedürfniss des Organismus: eine farbenanalytische Studie, Hirschwald, Berlin, p. 167. Available at: https://www.pei.de/SharedDocs/Downloads/DE/institut/veroeffentlichungen-von-paul-ehrlich/1877-1885/1885-sauerstoff.pdf?__blob=publicationFile&v=2.

Eilers, U., Klumperman, J., and Hauri, H. P. (1989). Nocodazole, a microtubule-active drug, interferes with apical protein delivery in cultured intestinal epithelial cells (Caco-2). *Journal of cell biology*, 108(1): 13–22. doi: 10.1083/jcb.108.1.13.

Eilken, H. M., and Adams, R. H. (2010). Dynamics of endothelial cell behavior in sprouting angiogenesis. *Current opinion in cell biology*. Elsevier Ltd, 22(5): 617–625. doi: 10.1016/j.ceb.2010.08.010.

Erickson, M. A., Wilson, M. L., and Banks, W. A. (2020). *In vitro* modeling of blood-brain barrier and interface functions in neuroimmune communication. *Fluids and barriers of the CNS*, 17(1): 1–16. doi: 10.1186/s12987-020-00187-3.

Fisher, D., and Mentor, S. (2020). Are claudin-5 tight-junction proteins in the blood-brain barrier porous? *Neural regeneration research*, 15(10): 1838–1839. doi: 10.4103/1673-5374.280308.

Förster, C., Burek, M., Romero, I.A., Weksler, B., Couraud, P.O., and Drenckhahn, D. (2008). Differential effects of hydrocortisone and TNF-alpha on tight junction proteins in an *in vitro* model of the human blood-brain barrier. *The journal of physiology*, 586 (7): 1937-1949. doi: 10.1113/jphysiol.2007.146852.

Francesca, B., and Rezzani, R. (2010). Aquaporin and blood brain barrier. *Current neuropharmacology*, 8(2): 92–96. doi: 10.2174/157015910791233132.

Galley, H. F., and Webster, N. R. (2004). Physiology of the endothelium. *British journal of anaesthesia*, 93(1): 105–113. doi: 10.1093/bja/aeh163.

Gentile, J.E., Carrizale, M.G., and Koleske, A.J. (2022). Control of synapse structure and function by actin and its regulators. *Cells,* 11 (4): 603. doi: 10.3390/cells11040603.

Gerdes, H. H., and Carvalho, R. N. (2008). Intercellular transfer mediated by tunneling nanotubes. *Current opinion in cell biology*, 20(4): 470–475. doi: 10.1016/j.ceb.2008.03.005.

Goldmann, E.E. (1913). Vital staining on the central nervous system: contribution to the physio-pathology of the choroid plexus and meninges (1). *Königl. Academy of Sciences*.

Gurke, S., Barroso, J. F. V., and Gerdes, H. H. (2008). The art of cellular communication: Tunneling nanotubes bridge the divide. *Histochemistry and cell biology*, 129(5): 539–550. doi: 10.1007/s00418-008-0412-0.

György, B., Szabó, T.G., Pásztói, M., Pál, Z., Misják, P., Aradi, B., László, V., Pállinger, E., Pap, E., Kittel, A., Nagy, G., Falus, A., Buzás, E.I. (2011). Membrane vesicles, current state-of-the-art: Emerging role of extracellular vesicles. *Cellular and molecular life sciences*, 68(16): 2667–2688. doi: 10.1007/s00018-011-0689-3.

Haqqani, A. S., Delaney, C.E., Tremblay, T., Sodja, C., Sandhu, J.K., Stanimirovic, D. (2013). Method for isolation and molecular characterization of extracellular microvesicles released from endothelial brain cells. *Fluids and barriers of the CNS*, 10(1):4. doi: 10.1186/2045-8118-10-4.

Hatherell, K., Couraud, P., Romero, I.A., Weksler, B, Pilkington, G.J. (2011). Development of a three-dimensional, all-human *in vitro* model of the blood-brain

barrier using mono-, co-, and tri-cultivation Transwell models. *Journal of neuroscience methods*, 199(2): 223–229. doi: 10.1016/j.jneumeth.2011.05.012.

Hawkins, B. T. and Davis, T. P. (2005). The blood-brain barrier / neurovascular unit in health and disease. *Pharmacological reviews,* 57(2): 173–185. doi: 10.1124/pr.57.2.4.173.

van Heerden, M.S., Grimsrud, A.T., Myer, L., Williams, D.R. (2009). Patterns of substance use in South Africa: Results from the South African stress and health study. *South African medical journal*, 99 (5 Pt 2): 358-366.

Heidarzadeh, M., Gürsoy-Özdemir, Y., Kaya, M., Abriz, A.E., Zarebkohan, A., Rahbarghazi, R., and Sokullu, E. (2021). Exosomal delivery of therapeutic modulators through the blood-brain barrier; promise and pitfalls. *Cell & bioscience,* 11:142. doi:10.1186/s13578-021-00650-0.

van der Helm, M. W., Odijk, M., Frimat, J., van der Meer, A.D., Eijkel, J.C.T., van den Berg, A., Segerink, L.I. (2016a). Direct quantification of transendothelial electrical resistance in organs-on-chips. *Biosensors and bioelectronics.* Elsevier, 85: 924–929. doi: 10.1016/j.bios.2016.06.014.

van der Helm, M. W., van der Meer, A. D., Eijkel, J.C.T., van den Berg, A. and Segerink, L.I. (2016b). Microfluidic organ-on-chip technology for blood-brain barrier research. *Tissue barriers*, 4(1). doi: 10.1080/21688370.2016.1142493.

Helms, H. C., Abbott, N.J., Burek, M., Cecchelli, R., Couraud, P., Deli, M.A., Förster, C., Galla, H.J., Romero, I.A., Shusta, E.V., Stebbins, M.J., Vandenhaute, E., Weksler, B., and Brodin, B. (2016). *In vitro* models of the blood–brain barrier: An overview of commonly used brain endothelial cell culture models and

guidelines for their use. *Journal of cerebral blood flow & metabolism*, 36(5): 862–890. doi: 10.1177/0271678X16630991.

Huber, J. D., Egleton, R. D., and Davis, T. P. (2001). Molecular physiology and pathophysiology of tight junctions in the blood-brain barrier. *Trends in neurosciences*, 24(12), pp. 719–725. doi: 10.1016/S0166-2236(00)02004-X.

Iruela-Arispe, M. L., and Beitel, G. J. (2013). Tubulogenesis. *Development*, 140 (14): 2851–2855. doi: 10.1242/dev.070680.

Kimura, S., Hase, K., and Ohno, H. (2012). Tunneling nanotubes: Emerging view of their molecular components and formation mechanisms. *Experimental cell research*, 318(14): 1699–1706. doi: 10.1016/j.yexcr.2012.05.013.

Koh, W., Mahan, R. D., and Davis, G. E. (2008). Cdc42- and Rac1-mediated endothelial lumen formation requires Pak2, Pak4 and Par3, and PKC-dependent signaling. *Journal of cell science*, 121(7): 989–1001. doi: 10.1242/jcs.020693.

Koyanagi, M., Brandes, R.P., Haendeler, J., Zeiher, A.M. Dimmeler, S. (2005). Cell-to-cell connection of endothelial progenitor cells with cardiac myocytes by nanotubes: A novel mechanism for cell fate changes? *Circulation research*, 96(10): 1039–1041. doi: 10.1161/01.RES.0000168650.23479.0c.

Krüger-Genge, A., Blocki, A., Franke, R., Jung, F. (2019). Vascular endothelial cell biology: An update. *International journal of molecular sciences*, 20(18). doi: 10.3390/ijms20184411.

Lasser, M., Tiber, J., and Lowery, L. A. (2018). The role of the microtubule cytoskeleton in neurodevelopmental disorders. *Frontiers in cellular neuroscience*, 12: 1–18. doi: 10.3389/fncel.2018.00165.

Leite, D.M., Matias, D., and Battaglia, G. (2020). The role of BAR proteins and the glycocalyx in brain endothelium transcytosis. *Cells*, 9(12): 2685. doi: 10.3390/cells9122685.

Lucas, W. J., Ham, B. K., and Kim, J. Y. (2009). Plasmodesmata - bridging the gap between neighboring plant cells. *Trends in cell biology*, 19(10): 495–503. doi: 10.1016/j.tcb.2009.07.003.

Lundquist, S., Renftel, M., Brillault, J., Fenart, L., Cecchelli, R., and Dehouck, M. (2002). Prediction of drug transport through the blood-brain barrier *in vivo*: A comparison between two *in vitro* cell models. *Pharmaceutical research*, 19(7):976-981. doi: 10.1023/a:1016462205267.

Malina, K. C. K., Cooper, I., and Teichberg, V. I. (2009). Closing the gap between the *in-vivo* and *in-vitro* blood-brain barrier tightness. *Brain research*, 1284: 12–21. doi: 10.1016/j.brainres.2009.05.072.

Mentor, S., and Fisher, D. (2017). Aggressive antioxidant reductive stress impairs brain endothelial cell angiogenesis and blood brain barrier function. *Current neurovascular research*, 14(1): 71–81. doi: 10.2174/1567202613666161129113950.

Mentor, S., and Fisher, D. (2021). High-resolution insights into the *in vitro* developing blood-brain barrier: Novel morphological features of endothelial

nanotube function. *Frontiers in neuroanatomy*, 15: 1–15. doi: 10.3389/fnana.2021.661065.

Mentor S., Makhathini, K.B., Fisher, D. (2022). The role of cytoskeletal proteins in the formation of a functional *in vitro* blood-brain barrier model. *International journal of molecular sciences*. doi: 10.3390/ijms23020742.

Mushanyu, J., Nyabadza, F., and Stewart, A. G. R. (2015). Modelling the trends of inpatient and outpatient rehabilitation for methamphetamine in the Western Cape province of South Africa, *BMC Research Notes*, 8(1): 1–13. doi: 10.1186/s13104-015-1741-4.

Nakagawa, S., Deli, M.A., Kawaguchi, H., Shimizudani, T., Shimono, T., Kittel, A., Tanaka, K., Niwa, M. (2009). A new blood-brain barrier model using primary rat brain endothelial cells, pericytes and astrocytes. *Neurochemistry international*, (54) (3-4): 253-263.

Naranjo, O., Osborne, O., Torices, S., Toborek, M. (2021). *In vivo* targeting of the neurovascular unit: Challenges and advancements. *Cellular and molecular neurobiology*, (Zlokovic 2010). doi: 10.1007/s10571-021-01113-3.

Natarajan, P., May, J.A., Sanderson, H.M., Zabe, M., Spangenberg, P., Heptinstall, S. (2000). Effects of cytochalasin H, a potent inhibitor of cytoskeletal reorganization, on platelet function. *Platelets*, 11(8): 467–476. doi: 10.1080/09537100020027842.

Neearti, P., Mohammada, R., Bangarua, R., Devde, R., R, J.K. (2012). The effects of verapamil, curcumin, and capsaicin pretreatments on the BBB uptake clearance of digoxin in rats. *Article in journal of pharmacy research*, 5(4): 2126–2133.

Okuda, K. S., and Hogan, B. M. (2020). Endothelial cell dynamics in vascular development: Insights from live-imaging in zebrafish. *Frontiers in physiology*, 11. doi: 10.3389/fphys.2020.00842.

Olesen, S.P. (1987). Regulation of ion permeability in frog brain venules. Significance of calcium, cyclic nucleotides and protein kinase C. *The journal of physiology*, 387:59–68. doi: 10.1113/jphysiol.1987.sp016562.

Omidi, Y., Campbell, L., Barar, J., Connell, D., Akhtar, S., Gumbleton, M. (2003). Evaluation of the immortalised mouse brain capillary endothelial cell line, b.End3, as an *in vitro* blood-brain barrier model for drug uptake and transport studies. *Brain research*, 990(1–2): 95–112. doi: 10.1016/S0006-8993(03)03443-7.

Önfelt, B., Nedvetzki, S., Benninger, R.K.P., Purbhoo, M.A., Sowinski, S., Hume, A.N., Seabra, M.C., Neil, M.A.A., French, P.M.W., Davis, D.M. (2006). Structurally distinct membrane nanotubes between human macrophages support long-distance vesicular traffic or surfing of bacteria. *The journal of immunology*, 177(12): 8476–8483. doi: 10.4049/jimmunol.177.12.8476.

Papadopoulos, M. C. and Verkman, A. S. (2013). Aquaporin water channels in the nervous system. *Nature reviews neuroscience*, 14(4): 265–277. doi: 10.1038/nrn3468.

Pardridge, W.M. (2012). Drug transport across the blood-brain barrier. *Journal of cerebral blood flow and metabolism*, 32 (11): 1959–1972. doi:10.1038/jcbfm.2012.126.

Perrière, N., Yousif, S., Cazaubon, S., Chaverot, N., Bourasset, F., Cisternino, S., Declèves, X., Hori, S., Terasaki, T., Deli, M., Scherrmann, J.M., Temsamani, J.,

Roux, F., Couraud, P.O. (2007). A functional *in vitro* model of rat blood-brain barrier for molecular analysis of efflux transporters. *Brain research*, 1150(1): 1–13. doi: 10.1016/j.brainres.2007.02.091.

Pulgar, V.M. (2019). Transcytosis to cross the blood brain barrier, new advancements and challenges. *Frontiers in neuroscience, 12: 1019* doi:10.3389/fnins.2018.01019.

Rajakylä, E. K., Lehtimäki, J.I., Acheva, A., Schaible, N., Lappalainen, P., Krishnan, R., Tojkander, S. (2020). Assembly of peripheral actomyosin bundles in epithelial cells is dependent on the CaMKK2/AMPK pathway. *Cell reports*, 30 (12): 4266-4280.e4. doi: 10.1016/j.celrep.2020.02.096.

Rajan, T. S., Gugliandolo, A., Bramanti, P., Mazzon, E. (2020). Tunneling nanotubes-mediated protection of mesenchymal stem cells: An update from preclinical studies. *International journal of molecular sciences*, 21(10). doi: 10.3390/ijms21103481.

Rajendraprasad, G., Eibes, S., Boldú, C.G., and Barisic, M. (2021) TH588 and low-dose Nocodazole impair chromosome congression by suppressing microtubule turnover within the mitotic spindle. *Cancers*, 13(5995):1-17. doi:103390/cancers13235995.

Raposo, G., and Stoorvogel, W. (2013). Extracellular vesicles: Exosomes, microvesicles, and friends. *Journal of cell biology*, 200(4): 373–383. doi: 10.1083/jcb.201211138.

Redzic, Z. (2011). Molecular biology of the blood-brain and the blood-cerebrospinal fluid barriers: Similarities and differences. *Fluids and barriers of the CNS*, 8(1): 3. doi: 10.1186/2045-8118-8-3.

Reese, T. S., and Karnovsky, M. J. (1967). Fine structural localization of blood-brain barrier to exogenous peroxidase. *The journal of cell biology*, 34(1): 207–217. doi: 10.1083/jcb.34.1.207.

Rilla, K., Pasonen-Seppänen, S., Deen, A.J., Koistinen, V.V.T., Wojciechowski, S., Oikari, S., Kärnä, R., Bart, G., Törrönen, K., Tammi, R.H., Tammi, M.I. (2013). Hyaluronan production enhances shedding of plasma membrane-derived microvesicles. *Experimental cell research*, 319(13): 2006–2018. doi: 10.1016/j.yexcr.2013.05.021.

Rubin, L.L., Hall, D.E., Porter, S., Barbu, K., Cannon, B.C., Horner, H.C., Janatpour, M., Liaw, C.W., Manning, K., Morales, J., Tanner, L.I., Tomaselli, K.J., and Bard, F. (1991). A cell culture model of the blood-brain barrier. *The journal of cell biology*, 115(6):1725-35. doi:10.1083/jcb.115.6.1725.

Rubin, L.L., and Staddon, J.M. (1999). The cell biology of the blood-brain barrier. *Annual review of neuroscience*, 22:11-28. doi: 10.1146/annurev.neuro.22.1.11.

Rustom, A., Saffrich, R., Markovic, I., Walther, P., and Gerdes, H. (2004). Nanotubular highways for intercellular organelle transport. *Science*, 303(5660): 1007–1010. doi: 10.1126/science.1093133.

Salman, M. M., Marsh, G., Kusters, I., Delincé, M, Di Caprio, G., Upadhyayula, S., de Nola, G., Hunt, R., Ohashi, K.G., Gray, T., Shimizu, F., Sano Y., Kanda, T, Obermeier B, Kirchhausen, T. (2020). Design and validation of a human brain

endothelial microvessel-on-a-chip open microfluidic model enabling advanced optical imaging. *Frontiers in bioengineering and biotechnology*, 8: 1–16. doi: 10.3389/fbioe.2020.573775.

Saunders, N. R., Habgood, M.D., Møllgård K., Dziegielewska K.M. (2016). The biological significance of brain barrier mechanisms: Help or hindrance in drug delivery to the central nervous system? *F1000 Research,* 5(0): 1–15. doi: 10.12688/f1000research.7378.1.

Schliwa, M. (1982). Action of Cytochalasin D on cytoskeletal networks, *The journal of cell biology*, 92(1): 79–91. doi: 10.1083/jcb.92.1.79.

Schneeberger, E. E. (2004). The tight junction: a multifunctional complex, AJP: *Cell physiology*, 286(6): C1213–C1228. doi: 10.1152/ajpcell.00558.2003.

Sellgren, K. L., Hawkins, B. T., and Grego, S. (2015). An optically transparent membrane supports shear stress studies in a three-dimensional microfluidic neurovascular unit model. *Biomicrofluidics*, 9(6): 1–4. doi: 10.1063/1.4935594.

Serlin, Y., Shelef, I., Knyazer, B., Friedman, A. (2015). Anatomy and physiology of the blood-brain barrier. *Seminars in cell and developmental biology*, 38: 2–6. doi: 10.1016/j.semcdb.2015.01.002.

Sivandzade, F., and Cucullo, L. (2018). *In-vitro* blood-brain barrier modeling: A review of modern and fast-advancing technologies. *Journal of cerebral blood flow and metabolism,* 38 (10): 1667-1681. doi: 10.1177/0271678X18788769.

Stamatovic, S. M., Keep, R. F., and Andjelkovic, A. V (2008). Brain endothelial cell-cell junctions: how to “open” the blood brain barrier. *Current neuropharmacology*, 6(3): 179–92. doi: 10.2174/157015908785777210.

Steiner, O., Coisne, C., Engelhardt, B., Lyck, R. (2011). Comparison of immortalized bEnd5 and primary mouse brain microvascular endothelial cells as *in vitro* blood-κ Brain barrier models for the study of T cell extravasation. *Journal of cerebral blood flow and metabolism*, 31(1): 315–327. doi: 10.1038/jcbfm.2010.96.

Turner, R.R, Beckstead, J.H., Warnke, R.A., Wood, G.S. (1987). Endothelial cell phenotypic diversity. *In situ* demonstration of immunologic and enzymatic heterogeneity that correlates with specific morphologic subtypes. *American journal of clinical pathology*, 87(5):569-75. doi:1093/ajcp/87.5.569.

Upadhyay, R.K. (2014a). Drug delivery systems, CNS protection and the blood brain barrier. *BioMed research international*, (2014):869269. doi: 10.1155/2014/869269.

Upadhyay, R.K. (2014b). Transendothelial transport and its role in therapeutics. *International scholarly research notices*, 2014: 1-39. doi:10.1155/2014/309404.

Verkman, A.S. (2013). Aquaorins. *Current biology*, 23(2):R52-55. doi: 10.1016/j.cub.2012.11.025.

Vigh. J.P, Kincses, A., Ozgür, B., Walter, F.R., Santa-Maria, A.R., Valkai, S., Vastag, M., Neuhaus, W., Brodin, B., Dér, A., and Deli, M.A. (2021). Transendothelial electrical resistance measurement across the blood-brain barrier:

A critical review of methods. *Micromachines*, 12 (6): 685. doi: 10.3390/mi12060685.

Wang, X., Veruki, M.L., Bukoreshtliev, N.V., Hartveit, E., and Gerdes, H. (2010). Animal cells connected by nanotubes can be electrically coupled through interposed gap-junction channels. *PNAS*, 107 (4): 17194-17199. doi: 10.1073/pnas.1006785107.

Welti, J., Loges, S., Dimmeler, S., and Carmeliet, P. (2013). Recent molecular discoveries in angiogenesis and antiangiogenic therapies in cancer. *Journal of clinical investigation*, 123(8): 3190–3200. doi: 10.1172/JCI70212.

Wolburg, H., and Lippoldt, A. (2002). Tight junctions of the blood-brain barrier: Development, composition and regulation. *Vascular pharmacology*, 38(6): 323–337. doi: 10.1016/S1537-1891(02)00200-8.

Worzfeld, T., and Schwaninger, M. (2016). Apicobasal polarity of brain endothelial cells. *Journal of cerebral blood flow and metabolism*, 36(2): 340–362. doi: 10.1177/0271678X15608644.

Xu, K., and Cleaver, O. (2012). Tubulogenesis during blood vessel formation. *Seminars in cell developmental biology*, 22(9): 993–1004. doi: 10.1016/j.semcdb.2011.05.001.

Yang T., Roder K., Abbruscato T.J. (2007). Evaluation of bEnd5 cell line as an *in vitro* model for the blood–brain barrier under normal and hypoxic/aglycemic conditions. *Journal of pharmaceutical science*, 96 (12): 3198- 3205. doi:10.1002/jps.21002.

Yamashita, K., Mizuno, K., Furukawa, K., Hirose, H., Sakurai, N., Masuda-Hirata, M., Amano, Y., Hirose, T., Suzuki, A. and Ohno, S. (2020). Phosphorylation and dephosphorylation of ser852 and Ser889 control clustering, localization and function of PAR-3. *Journal of cell science,* 133 (22): jcs244830. doi: 10.1101/2020.05.04.075952.

Zorkina, Y., Abramova, O., Ushakova, V., Morozova, A., Zubkov, E., Valikhov, M., Melnikov, P., Majouga, A. and Chekhonin V. (2020). Nano carrier drug delivery systems for the treatment of neuropsychiatric disorders: Advantages and limitations. *Molecules*, 25(22). doi: 10.3390/molecules25225294.

Zovein AC, Luque A, Turlo KA, Hofmann JJ, Yee KM, Becker MS, *et al.* (2010). Beta1 integrin establishes endothelial cell polarity and arteriolar lumen formation via a Par3-dependent mechanism. *Developmental cell,* 18:39–51. doi: 10.1016/j.devcel.2009.12.006.

CHAPTER TWO: 'PREPARATION OF BIOLOGICAL MONOLAYERS FOR PRODUCING HIGH-RESOLUTION SCANNING ELECTRON MICROGRAPHS'

Preparation of biological monolayers for producing high-resolution scanning electron micrographs

Short title: Preparing HR-SEM biological samples

Shireen Mentor [1¶], Franscious Cummings [2], David Fisher [1,3¶*]

1. Department of Medical Biosciences, Faculty of Natural Sciences, University of the Western Cape, Cape Town, South Africa.

2. Department of Physics and Astronomy, Electron Microscopy Unit, University of the Western Cape, Cape Town, South Africa.

3. Adjunct Professor, School of Health Professions, University of Missouri, , Columbia, Missouri, United States of America.

*Corresponding author

EMAIL: dfisher@uwc.ac.za

¶These authors contributed equally to the paper

Abstract

Scanning electron microscopy (SEM) provides a technical platform for nanoscopic mapping of biological structures. Correct preparation of SEM samples can provide an unprecedented understanding of the nexus between cellular morphology and topography. This comparative study critically examines two coating methods for preparing biological samples for scanning electron microscopy, while also providing novel advice on how to prepare *in vitro* epithelial or endothelial samples for high-resolution scanning-electron microscopy (HR-SEM). Two obstacles often

confront the biologist when investigating cellular structures grown under tissue culture conditions, namely, how to prepare and present the biological samples to the HR-SEM microscope without affecting topographical membrane and cellular structural alterations. Firstly, our use of the Millicell cellulose inserts on which to grow our cellular samples in preparation for HR-SEM is both novel and advantageous to comparing the permeability function of cells to their morphological function. Secondly, biological material is often non-conducting, thermally sensitive and fragile and, therefore, needs to be fixed correctly and coated with thin conducting metal to ensure high-resolution detail of samples. Immortalized mouse brain endothelial cells (bEnd5) was used as a basis for describing the preferences in the use of the protocol. We compare two biological sample coating modalities for the visualizing and analysis of texturized, topographical, membranous ultrastructures of brain endothelial cell (BEC) confluent monolayers, namely, carbon and gold:palladium (Au:Pd) sputter coating in preparation for HR-SEM. BEC monolayers sputter-coated with these two modalities produced three-dimensional micrographs which have distinctly different topographical detail from which the nanostructural cellular data can be examined. The two coating methods display differences in the amount of nanoscopic detail that could be resolved in the nanosized membrane cytoarchitecture of BEC monolayers. The micrographical data clearly showed that Au:Pd sputter-coated samples generate descript imagery, providing useful information for profiling membrane nanostructures compared to carbon-coated samples. The recommendations regarding the contrast in two modalities would provide the

necessary guidance to biological microscopists in preparing tissue culture samples for HR-SEM.

Keywords: scanning electron microscopy, sputter coating, profilometry, nanostructural cytoarchitecture

Introduction

The successful generation of electron micrographs largely depends on the preparation of the specimen under investigation. Early ultrastructural investigations were limited due to resolution limitations and investigators were restricted in their ability to observe the ultrastructural details of cell membranes and their extracellular topography. This severely limited both the theoretical and experimental approaches to cell biology.

High-resolution scanning electron microscopy (HR-SEM) allows much higher-resolution of the cell's plasma membrane surface, allowing for the visualization of nanosized morphological structures. Tissue-culture based samples also provide numerous challenges to the microscopists in preparing the samples for HR-SEM. One of the main problems in presenting endothelia or epithelia is that they have to be grown on a biological basement-like material to orientate themselves morphologically into distinct basolateral and apical domains. These domains are both morphologically and functionally different from each other. Therefore, growing the cells on non-physiological surfaces namely, glass or plastic produces endothelial/epithelial cells that are morphological and physiological disorientated. We, therefore, grew our BECs on a cellulose-based insert (Millicell) which allowed our cells to grow into correctly orientated cellular monolayers. These inserts

allowed for the measurement of permeability across the monolayer as well as a platform to fix the cells in preparation for HR-SEM.

We further describe two acceptable preparatory coatings of biological tissue and compare the structural differences between the two protocols. For a specimen to yield high-resolution micrographs, the surface of the specimen requires electrical conductivity. Biological material is often non-conducting, thermally sensitive and fragile, therefore, fixation of biological samples must be performed correctly and coated with thin conducting metal such as gold:palladium (Au:Pd) (5 nm), contrary to carbon (15 nm) [1, 2].

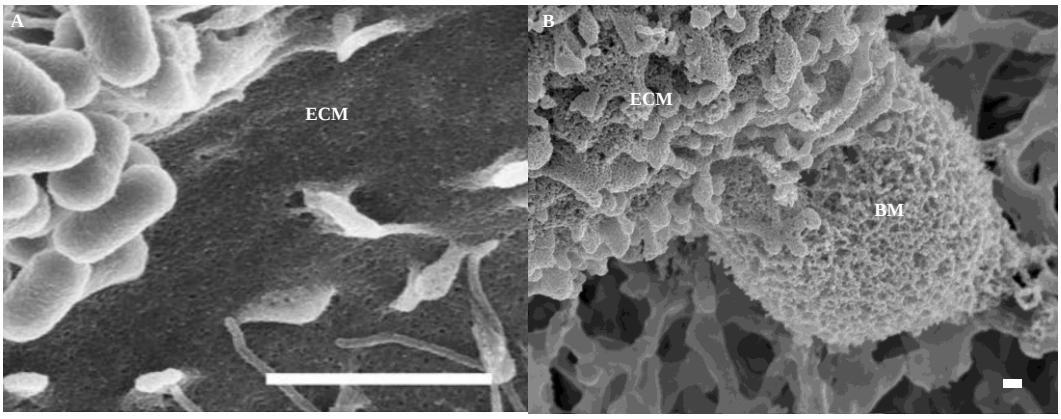

Fig 1. Scanning electron micrographs displaying the apical surface of a polarized epithelial cell interacting with *Escherichia coli* bacteria, grown on gold mesh grids, dried and coated with carbon, scale bar = 2000 nm [3]. **ECM** denotes the epithelial cell membrane (**A**); A polarized brain endothelial cell (bEnd5), grown in our laboratory, on an insert membrane, dried and coated with Au:Pd, scale bar = 2000 nm. **ECM** denotes the endothelial cell membrane and the basement membrane of the BEC is denoted as **BM** (**B**).

We used **Figs 1A-B** to illustrate the relative lack of high-resolution detail in a recent HR-SEM micrograph [3] compared with the resolution we routinely are able to generate in our HR-SEM micrographs. **Fig 1A**, depicts a carbon-coated micrograph showing the interaction between correlative light and scanning electron microscopy

(CLSEM) of *Enteropathogenic Escherichia coli* (EPEC) with the surface of a polarized epithelial monolayer. The micrograph lacks nanoscaled detail of the ultrastructural profile of an epithelial cell membrane [3]. The preparatory process of this epithelial cell sample may have caused structures to appear obscured and lack three-dimensionality which could be due to the type of coating material utilized and how excessively it has been applied. Conversely, during monolayer development of the BEC, as seen in **Fig 1B** of a BEC published in a recent study by [4] more nanoscopic details can be observed, as the micrograph displays a detailed plasma membrane surface and the extrusion of an amorphous extracellular matrix, showing molecular details of the plasma membrane, after utilizing the Au:Pd alloy coating material on the BEC membrane. In this methodology paper, we report on the comparison of using both carbon/graphite (C) and Au:Pd coating methods and its ability to yield a greater resolution of ultrastructural detail of the biological sample surfaces /plasma membrane topography.

The electron microscope was utilized due to its ability to generate high-definition (HD) micrographs, at nanometer scaled resolution. In light microscopy, the maximum resolution is approximately 0.2 µm, as opposed to 0.1 mm for the unaided eye (at a standard viewing distance of 25 cm [5]. HR-SEM, on the other hand, enables 3-dimensional (3-D) visualization of biological specimens to a resolution of approximately 10 nm [6]. Therefore, both HR-SEM and HR transmission-EM (HR-TEM) bridge the gaps between resolution produced with light microscopy, which is limited in generating high-resolution micrographs. HR-SEM produces images with a substantial amount of ultrastructural information which illuminates the physical (molecular) composition of a specimen's surface

topography [4-5]. The *in situ* HR-SEM analysis of BEC monolayer growth was conducted to extrapolate nanostructural dynamics involved in BEC-cell interaction. However, upon analysis with carbon-coated samples, we observed large carbon grains which distorted the 3-D nature of the endothelial micrographs. The findings were endorsed in a study conducted by [7] who reported altered morphology of a biological specimen after being coated with carbon. For this comparative study, HR-SEM was employed as a tool for the analysis of the ultrastructural dynamics of the BEC monolayer of the *in vitro* blood-brain barrier (BBB) development. To date, an existing issue that persists in micrographical findings found in the literature to as recent as 2019 is the excessive use of metals applied during sputter coating, thus, it is critical to consider finer and/or lower atomic number elements such as iridium (atomic number = 77) or palladium (atomic number = 46 in contrast to gold (atomic number = 79) [1]. The use of metals with high atomic numbers tend to result in the obscurity of nanoscopic details and, more often than none, biological sample surface appears bulky [1,3]. Inadequate to poor coating choices for biological sample imaging in HR-SEM remains the current *status quo* for biological sample preparation.

Modern high-resolution microscopy requires a re-evaluation of its current methodological approaches. The objective of this study was to compare two coating modalities to visualize high ultrastructural dynamics of BEC plasma membrane-associated nanostructures. The utilization of an inadequate coating method would lose vital micrographical detail which is a disadvantage to an HR-SEM narrative for describing novel BEC ultrastructures. The detail seen in **Fig 1B** is much more apparent, displaying greater molecular resolution upon coating with Au:Pd (**Fig**

1B), in comparison to carbon (**Fig 1A**). The novelty in this study is not the utilization of a Au:Pd alloy per sé, but in its recommended employment for visualizing ultrastructures, when superficially studying the cell's plasma membrane surface. The study aims to alert microscopy scientists to make use of the Au:Pd alloy as opposed to non-metal carbon-coating as it obscures a plethora of morphological detail that we can and/or should be observing. The study investigated BEC ultrastructural variation utilizing two coating modalities for HR-SEM studies: (i) metal coating Au:Pd 80:20 application (as opposed to 60:40) and (ii) non-metal, Carbon-coating to decipher between samples exhibited detailed morphological features using two different coating modalities.

Materials and methods

The protocol described in this peer-reviewed article is published on protocols.io, Updated November 6 2021 dx.doi.org/10.17504/protocols.io.bw37pgrn and is included for printing as supporting information file 1 with this article.

High-resolution scanning electron microscopy

When using HR-SEM, the signal generating the image occurs as a result of the interaction of the primary electron beam with the biological specimen. Briefly, upon interaction, the primary beam electrons induce ionization of the sample's atoms and the subsequent emission of secondary electrons (SE) from the top-most region of the specimen. The surface-emitted SEs are detected by a scintillator-based Everhart-Thornley detector (ETD), also known as secondary or SE detector. Modern SEMs, however, are more frequently manufactured with in-lens SE

detectors, which have the ability to detect fine structures that are invisible to traditional ETDs [8].

For biological materials, which are predominantly hydrocarbons, a low, primary beam energy is desirable to minimize the interaction volume depth in accordance with equation (1). A small volume allows the operator to study finer specimen surface detail while simultaneously minimizing sample charging caused by secondary electron build-up on the surface. One drawback, however, is a low signal-to-noise ratio caused by the reduced secondary electron emission. This can, however, be solved by coating the sample surface with a thin layer of conducting material such as gold or graphite. The nexus of structural biology is achieving three-dimensionality and investigating the correlation between the morphological framework and its molecular underpinnings. The macromolecular structure is concomitant with its physiology as the shape of any given structure determines its function. Studying both the nanostructural and/or molecular machinery that governs the phenotypic evolution of a BEC unifies our understanding of BBB construction. The volume created by electron beam when incident on the specimen surface is called the interaction volume and is dependent on the following important parameters: (i) the primary electron beam energy (E_0), (ii) the average atomic number (Z), (iii) density (ρ) and (iv) average atomic mass (A) of the specimen under investigation [9]. A semi-empirical model of the interaction volume depth, R_p is given by [10].

$$R_p[in\ \mu m] = \left(\frac{0.0276A}{\rho Z^{0.889}}\right) {E_0}^{1.67} \quad (1)$$

In this study, specimens were analyzed using a Zeiss Auriga high-resolution field-emission gun SEM (FEG-SEM), operated at an electron beam energy of 5 keV, a nominal working distance of 5 mm and using an in-lens SE detector for high-resolution imaging.

Biological sample preparation

The bEnd5 cell line was purchased from the European collection of cell cultures (Sigma-Aldrich, 96091930). The cells were cultured in Dulbecco's Modified Eagles medium (Whitehead Scientific, Cat no. BE12-719F, South Africa), supplemented with 10% fetal bovine serum (FBS) (Celtic/Biowest, Cat no. S181G-500, South America), 1% *Penicillin/Streptomycin* (Whitehead Scientific, Cat. no. DE17-602E, South Africa), 1% non-essential amino acids (Whitehead Scientific, Cat no. BE13-114E, South Africa) and 1% sodium pyruvate (Whitehead Scientific, Cat no. BE13-115E, South Africa).

bEnd5 Cells were seeded at $5x10^5$ cells/insert on a Millicell, mixed cellulose esters insert membrane (Millipore/Merck, Cat no. PIHA01250, Germany). After exposure of the cell monolayers to the standard culture medium (i.e. supplemented DMEM:F12), at respective time intervals (24-48h), the bEnd5 cells were fixed with 2.5% glutaraldehyde made by adding 10 ml of a 25% solutions of glutaraldehyde (Fluka/ Sigma, Cat no. 49626, Switzerland) in 90 ml of 1X phosphate-buffered saline (PBS) solution (Life Technologies, Cat. no. 20012019 , South Africa). Buffers and fixatives used in culture were maintained at pH 7.2 and an osmolality which mimicked that of blood plasma (280-300 mOs/kg) utilizing a Vapor pressure osmometer (VAPRO) (Wescor, South Africa, ser. no. 55201671, Germany), as

BECs form the anatomical basis of the brains capillaries and its luminal surfaces are naturally exposed to circulating blood *in vivo*.

Chemical fixation

Once bEnd5 monolayers reached confluence the inserts were removed using a lancet and were placed in protein and lipid cross-linking reagent such as 2.5% solution of glutaraldehyde (Fluka/ Sigma-Aldrich) was prepared in standard cell culture buffer- 1X PBS solution. [1, 11]. Following a 1 h incubation period at room temperature (RT). The sample could be stored in a 2.5% glutaraldehyde fixative at 4°C overnight. Thereafter, the specimen was washed in 1X PBS (devoid of glutaraldehyde) for 2x5 minutes (min) each. Then samples were washed twice in de-ionized water (H_2O), each time for 5 min [1].

Biological specimens were removed from the de-ionized H_2O and placed in a series of graded ethanol (EtOH) (KIMIX, Batch no. 185/11/67 K08/0911) solutions: 50%, 70%, 90%, 95% and twice in 99.9% EtOH for 10 min each. All EtOH solutions were prepared by diluting absolute EtOH in de-ionized H_2O v/v.

Critical point drying

Biological samples are composed largely of H_2O and sample desiccation using a critical point dryer (CPD) allows for the phased drying of wet, delicate samples from liquid to gas form, by using liquid carbon dioxide (CO_2), which functions as 'transitional fluid'. Since H_2O is not miscible with CO_2, the alternative is EtOH which serves as the 'intermediate fluid'/ 'dehydration fluid.' Following the dehydration of the fixed samples, it is required that the sample be dry before further processing could occur, this was performed using the Hitachi HCP-2 CPD. Evaporative drying of biological specimens could cause deformation and collapse from the native state of the sample. The deformities in the sample are often due to the surface tension of water, relative to evaporating air [1]. Therefore, CPD was performed by immersing biological samples in liquid with a lower surface tension to air (i.e. CO_2).

The dehydrated samples were transferred to and retained inside 10 mm diameter aluminium baskets. The basket holders were placed inside the CPD chamber and filled with liquid CO_2. This step is critical, as the amount of liquid CO_2 injected into the chamber must be between 50% and 80% of the total chamber volume. The chamber would not reach the critical point (CP) with inadequate liquid CO_2. The temperature was set to 20˚C for 15 min and then 38°C for 5 min until the critical pressure was reached (73 kg/cm^2).

Bio-organic specimen coating for HR-SEM

It is imperative to ensure that the coating material does not compromise the surface details of the specimen during analysis. The coating's main function is to ensure sufficient surface conductivity, reduction of beam heating and radiation damage, as well as specimen volatility [12]. Post CP drying, the BEC monolayers are coated with either a gold: palladium(Au:Pd) alloy by means of sputter-coating using a Quorum Q150T ES sputter coater, or with a thin layer of carbon during thermal evaporation of a carbon rod using an Emitech K950X carbon coater.

Sputter coating using gold:palladium

A Au:Pd alloy in an atomic ratio of 80:20 (Au:Pd 80:20) was used as the sputtered target material.The use of Au:Pd 80:20 is much *en vogue* compared to traditional gold only coatings. Palladium prevents Au agglomeration, which is known to produce large islands between 8 nm and 12 nm which result in an uneven coating, especially around the tallest structures in the specimen. This non-homogeneous coating invariably restricts resolution performance [13]. Conversely, Au:Pd 80:20 produces a finer, homogenous film with a particle grain size between 4 nm and 8 nm [14]. This information is supported by a study that involved the imaging of blood capillaries using SEM by [13]. In their study the luminal cell surface of a fenestrated adrenocortical endothelial cell after deposition of a thick metal film of Au:Pd 60:40 is reported, as indicated in the high-resolution micrograph of **Fig 2** [13]. However, although this micrograph shows a fair amount of detail regarding the magnitude of the textured topography of the biological sample, the molecular details are obscured.

For the purpose of this study, the thickness of the Au:Pd 80:20 coating is controlled by sticking to a standard sputtering time of 60 s. A chamber pressure of 10^{-5} mbar is maintained beforehand, with a sputtering pressure of 10^{-2} mbar used during coating. A sputtering current of 40 mA and tooling factor for Au:Pd of 2.3 are used with a quartz, crystal thickness monitor used to measure the thickness of the coating during sputtering. At the above experimental conditions, a deposition rate of roughly 5 nm/min is achievable at a sample-to-target distance of 50 mm. During deposition, the sample stage is rotated at a speed of 70 rotations per minute to ensure even coating across the specimen surface. Based on the above, a nominal coating thickness of 5 nm is, thus, deposited.

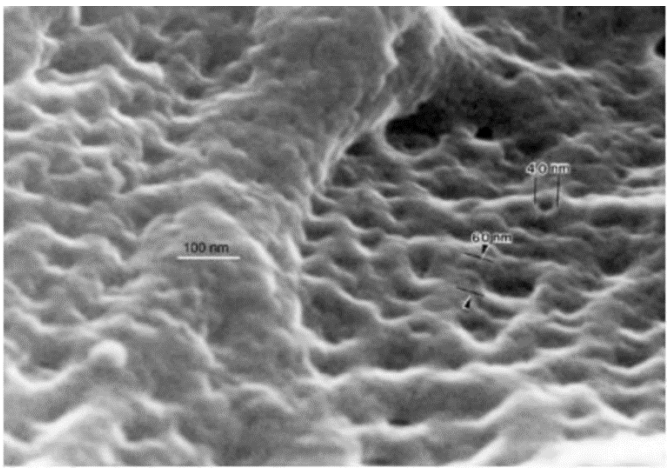

Fig 2. High-resolution SEM of the luminal surface of a capillary coated with Au:Pd [13]. Here the molecular detail on the luminal surface appears obscured, due to bulky coating, thus resulting in loss of ultrastructural detail.

The deposition of layers of material (i.e. metal/non-metal) are denoted as films that range from nanometers to micrometers. Films can be classified into Physical Vapor Deposition (PVD) and Chemical Vapor Deposition (CVD) [15]. To investigate the exact sample thickness, three different sputtering thicknesses are shown in **Fig 3**

below. From left to right, Au:Pd layers sputtered on soda-lime glass substrates for 30 s, 60 s and 120 s (s: seconds) are displayed. The reflectivity of the films decreases with increasing sputtering times, readily suggesting an increase in thickness of the films, with the sample deposited at 120 s exhibiting a very dark tinge.

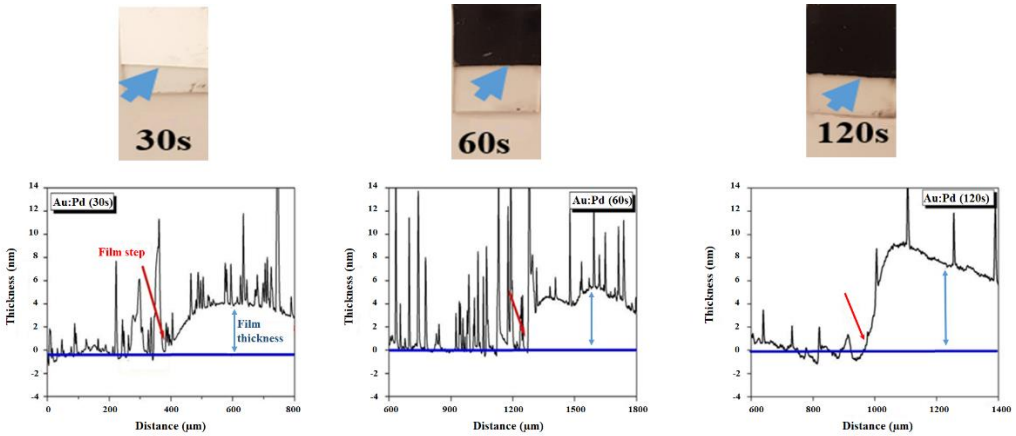

Fig 3. Optical images of the Au:Pd 80:20 coatings sputtered on soda-lime glass for 30 s, 60 s and 120 s (s: seconds) with correlative profilometry measurements after 30 s, 60 s and 120 s sputter-coated by Au:Pd films approximately 4 nm, 5 nm and 8 nm thick. The glass level, which refers to the soda-lime glass, is indicated by the blue baseline, with the film step indicated by red arrows. The film step refers to the sputter-coated material and the red and blue arrows correspond with each other and indicate the same place where the coating has taken place. The blue double-ended arrow, indicates the film thickness.

To validate the sputtered thicknesses, surface profilometry was performed using a Veeco Dektak 6M Stylus Profilometer. A diamond stylus tip, with an average diameter of 12.5 µm, was scanned at a step-size of 0.333 µm across the film for a total length of 3 mm. The thickness of the Au:Pd layer was determined by scanning the stylus across the film step, as indicated by the arrows in **Fig 3**.

As shown in **Fig 3,** a sputter time of 30 s produces a film thickness of approximately 4 nm (shown by the red double arrows) which increases to roughly 5 nm after 60 s

and 8 nm after 120 s. The spikes observed in the profilometry profiles are due to Au:Pd flakes attaching to the stylus tip. This is very common and indicative of the soft nature of the sputtered film surface. It must be noted that the above results on reasonably flat soda-lime glass produce even coatings, which is not always the case for specimens that are highly textured topographically. Previous results show that coatings of 30 s or less produce specimens that are unevenly coated and still experience surface charging during SEM analysis. Hence, to ensure evenly coated BEC monolayers and to avoid the previously mentioned challenges, a sputter coating time of 60 s (and thus Au:Pd 80:20 coating of 3-5 nm) is recommended for coating biological samples.

Thermal evaporation of carbon

In comparison, the BEC monolayers were coated with carbon during thermal evaporation. A 3 mm thick carbon rod is sharpened to a diameter (d) of 1.1 mm, with an evaporation length (L) totaling approximately 2 mm. The sharpened rod is mounted against a spring-loaded counter electrode in a vacuum, with the specimen placed a distance, r, from the carbon source. During evaporation, the chamber is pumped down to a vacuum of 10^{-3} mbar, which increases to 10^{-1} mbar for deposition. The current is then slowly increased to a max of 20 A and passed through the carbon rod, thereby heating it beyond the vaporization temperature of carbon; the vaporized carbon plumes subsequently coat the specimen. **Fig 4** shows a schematic representation of this set-up.

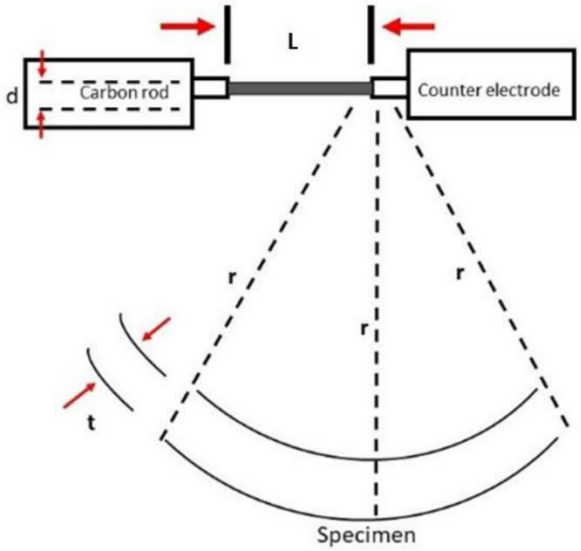

Fig 4. Schematic layout of the thermal evaporation set-up used to deposit carbon layers using the Emitech carbon coater. The *t* symbol denotes the time in seconds, *r* denotes the radius between the rod and the specimen, *d* refers to the diameter of the rod and L denotes the evaporation length.

From **Fig 4**, the average thickness of the deposited carbon film, *t*, can be estimated using simple geometry and the inverse square law as follows:

$$\frac{\pi d^2 l \rho}{4} = 4\pi r^2 t \rho \quad (1)$$

or

$$t = \frac{d^2 l}{16 r^2} \quad (2)$$

where ρ is the density of the source material. **Fig 5** shows optical images of three carbon films deposited on soda-lime glass. From left to right, the films were deposited at a distance of 15 mm, 25 mm and 40 mm from the carbon source. As shown, the transparency of the films decreases with increasing distance, suggesting

a decrease in film thickness. To confirm this, profilometry is once more employed and shown in **Fig 5**.

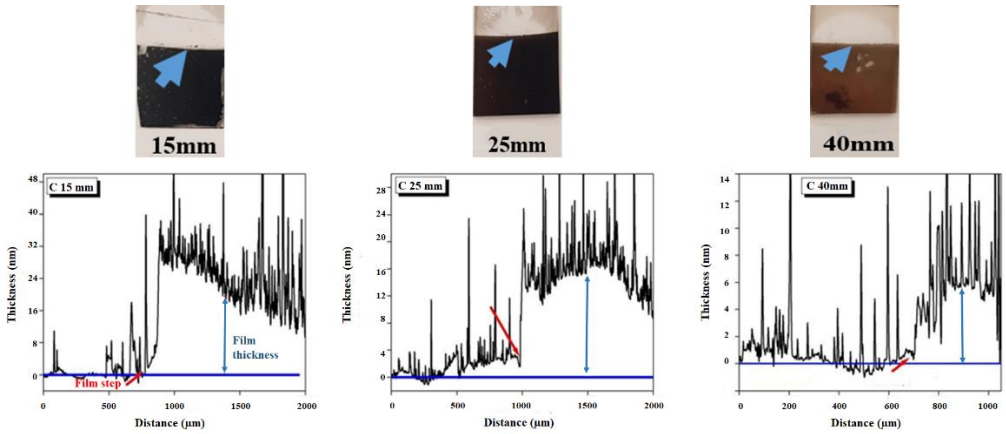

Fig 5. Optical images of carbon coatings deposited on soda-lime glass at a distance of 15, 25 and 40 mm from the carbon source with correlative profilometry measurements of carbon films deposited on soda-lime glass placed 15, 25 and 40 mm from the carbon rod. The glass level is indicated by the blue baseline, with the film step indicated by red arrows. The red and blue arrows correspond with each other, indicating the same place where the coating has taken place. The blue double-ended arrow, indicates the film thickness.

An average thickness of approximately 20 nm is deduced from the stylus profile of **Fig 5** for the sample placed at 15 mm from the source, which reduces to approximately 16 nm and 6 nm for the 25 mm and 40 mm placed samples, respectively. Closer inspection reveals that the carbon film roughness is more pronounced compared to the Au:Pd 80:20 coatings of **Fig 3** as the spikes in the profiles are more closely spaced and more frequent compared to the Au:Pd coatings. In addition, from the optical images of **Fig 5**, the carbon film integrity is of inferior quality than the Au:Pd films, which had high reflectivity indicative of a compact layer. A simple swab test also reveals that the carbon film is more powdered compared to the metal layers, as they delaminate far easier from the glass slides

than the Au:Pd sputtered films. This is to be expected and can be explained by the relative chamber pressures (namely, the metal coatings were deposited in a cleaner chamber (10^{-6} mbar) compared to the carbon coating at a pre-deposition vacuum of (10^{-3} mbar)). Based on the above analysis, a standard sample distance of 25 mm was maintained for all specimens, implying a nominal carbon coating of 16 nm.

Results and discussion

To date, HREM studies producing 3-D volume images remains scant. The current issue with the loss of resolution, especially with respect to nanoscopic topographical detail, has remained a largely unresolved microscopy problem. Moreover, mapping the membrane pore sizes, nanovesicles and the complex interactive PC spaces of BECs have been thwart with technical difficulty. The absence of these HR-SEM micrographs is a glaring omission in the literature with regards to describing biological surfaces on a nanoscopic level. In parallel, there is a dearth of information regarding the preparation of biological material. Given this lack of crucial preparatory methodology, we utilize the preparation of BECs in monolayers grown on insert cellulose membranes as an exemplar technique. The insert cellulose membrane mimics the basement membrane of epithelia/endothelia. This allows for epithelia or endothelia to express and orientate themselves morphological into distinct basolateral and apical functionality. Our use of these *in vitro* techniques is essential to viewing how cells interact with each other and also cellular interaction within an epithelial/endothelial cell monolayer. These techniques provide much greater insight into how these cells would behave within the *in vivo* environment, which is critical for developing *in vitro* models of

biological structures to mimic *in vivo* tissues and to further investigate regulatory mechanisms to treat pathological states of disease. The greater the detail that we can observe in cells under normal physiological states the better we can elucidate how these nanoscopic details change within the pathological states. Therefore, the selected and recommended methodology proposed in this paper should tremendously advance the study of biological structures at the nanoscopic level.

Sputter coating cellular surfaces for high-resolution

The loss of ultrastructural, topographical detail of biological specimens using the incorrect coating modality gives an obscured impression of how these nanostructures are presented within their native state. The incorrect view of a structure would subsequently lead to an incorrect view of its functionality.

We present a series of HR-SEM micrographs to compare two modalities for coating cellular surfaces of monolayers of immortalized mouse brain endothelial cells (bEnd5). In **Fig 6** the topographical data generated between a carbon-carbon coat and a Au:Pd coat show stark differences in ultrastructural definition. **Fig 6B** was able to generate an image that allows for the visualization of detailed features of a phospholipid membrane surface with numerous pore formation and vesicular bodies accrued on the cell membrane surface, compared to **Fig 6A** which shows visible obscurity of HD detail, producing an almost 2-D interpretation of the cell surface.

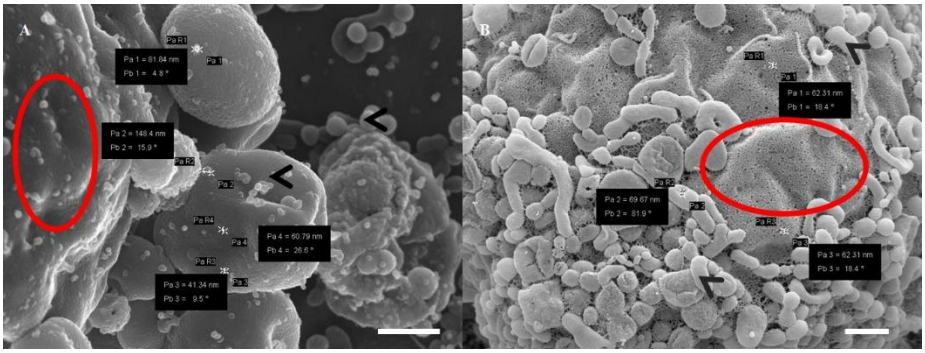

Fig 6. A micrograph representing BEC plasma membrane (PM) surfaces. (A) An image of carbon-coated PM and microvesicle (MV) formation. Scale bar = 1000 nm; (B) An image of a Au:Pd coated PM and vesicle formation. Scale bar = 200 nm. The "red circles" indicate distinct differences in the PM: (A) shows a smooth membrane surface, devoid of pores; (B) displays a porous membrane surface. Pore sizes range between 62-70 nm. The "black arrows" indicate the formation of microvesicles (A) reveals smooth vesicles; (B) exhibits textured vesicles on the PM surface.

Enabling nanoscopic cytoplasmic projections observations:

In this study we utilized cytoplasmic projections as an exemplar for this technique, comparing carbon and Au:Pd coated samples to illustrate the discrepancies between the ultrastructural information gathered using a non-metal vs a metal sputter coating modality.

Figs 7A and C (carbon-coated), relative to **Figs 7B and D** (Au:Pd coated), shows stark differences in the detailed development of nanotubes (NT) between PC spaces of the BECs. In the carbon-coated micrographs, there are projecting membrane edges that appears continuous with the cell membrane material (**Figs 7B and D**). The membrane appears roughly textured and porous, while the projecting NTs are smooth in texture. In addition, extracellular membranous structures visibly suffuse

the BEC membrane surfaces in Au:Pd coated samples thus more morphological data is able to be extrapolated from an Au:Pd coating.

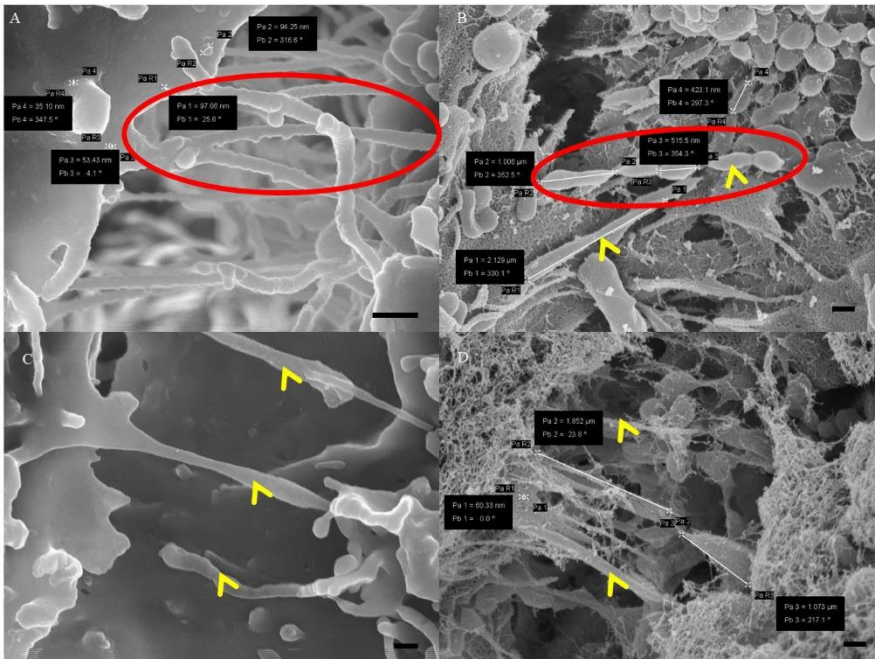

Fig 7. A micrograph representing apicolateral membranous projections between adjacent BECs grown on a Millicell insert membrane. (A) An image of a carbon-coated NT formation, showing smooth, indistinct leading edges, continuous with the cell membrane, see "red circle." Scale bar = 300 nm; (B) An image of a Au:Pd coated leading edges where more textured lateral vesicles fuse into distinct cytoplasmic projections, see "red circle," within the PC space, as indicated by the "yellow arrows." Scale bar = 300 nm; (C) An image of a carbon-coated cytoplasmic projections (CPs) within the PC spaces, see "yellow arrowheads." Scale bar = 200 nm; (D) An image of Au:Pd coated CPs, indicated by the "yellow arrows." Scale bar = 300 nm.

Enabling tight junction interaction observations:

When tight junction (TJ) proteins interact between adjacent BECs it forms contact points with its counterparts. These intercellular adherens junctions were, therefore, coated and compared.

The use of Au:Pd coating in **Fig 8B** clearly demonstrates the interaction of TJs between adjacent BEC membranes, within its PC shunt. Conversely, **Fig 8A** demonstrates that carbon–coating obscures the detailed fusion of adjacent BEC membranes at the paracellular (PC) shunt. In **Fig 8B** the Au:Pd coating enables the visualization of textured surface structures on a nanoscale, such as membranous tent-like leaflets (see "purple circle") forming what would eventually be overlapping regions across the TJ zones which measured approximately 60-90 nm, occluding the PC shunt.

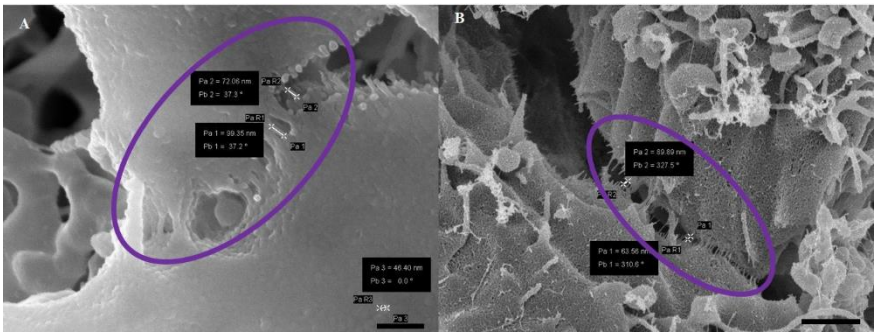

Fig 8. A micrograph representing juxtaposing BEC PMs within the PC spaces. (A) An image of carbon-coated juxtaposed PMs. Scale bar = 1000 nm; (B) An image of Au:Pd coated juxtaposed PMs as seen in the "purple circles". Scale bar = 1000 nm. (A) When coating with carbon the detail of the membrane is obscured by the coating process,with the membrane presenting an amorphous appearance; (B) shows definitive TJ interaction of two adjacent BECs . This technique provides an unprecedented level of biological detail, making it possible to observe these molecular interactions at the level of the surface of the plasma membrane.

Viewing paracellular spaces under HR-SEM

To comprehend the convoluted nature of the paracellular (PC) spaces between BECs during monolayer establishment, the study attempts to elucidate the complexity of the PC space using carbon coating and Au:Pd.

Carbon coating seen in **Fig 9A** produced blunt membrane edges, with a smooth finish of the membranous material, which does not resemble the rich *in situ* biological topography. This is a disadvantage as the morphological data that can be extrapolated remains infinitesimal, thus limiting our understanding of the nanoscaled structural dynamics at play within the PC spaces of BECs. **Fig 9B**, however, exhibits a nuanced, multi-layered PC space enabling the visualization of an array of membranous surface structures, mono-vesicles and multiple vesicular fusion to form nanotubes between adjacent BECs. The Au:Pd, thus, generates more useful, 3-D topographical data that can be investigated and incorporated when describing PC dynamics during BEC monolayer establishment.

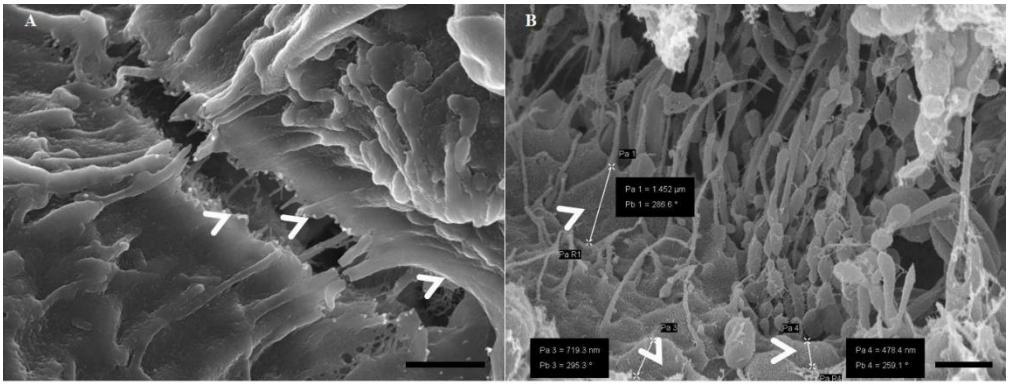

Fig 9. A HR-SEM micrograph representing multiple layers of PM interaction within the PC spaces of BECs. (A) An image of a carbon-coated PM interaction; (B) An image of Au:Pd coated PM interaction as seen by the "white arrowheads." Scale bar = 1000 nm.

Coating the samples with Au:Pd (**Fig 6B-9B**) produced more detailed micrographs, revealing ultrastructural data on the membrane surfaces of BEC monolayers. In addition, Au:Pd prevented charging of images, compared to **Fig 6A-9A**, which produced a membrane surface that obscured a substantial amount of topographical data. The images generated in this study suggest that coating samples with Au:Pd improved bulk conductivity and generated well contrasted topographical imagery.

To develop high-quality micrographical information, sputter-coating the biological sample with the correct alloy is imperative as it enables the elucidation of ultrastructural, morphological and/or topographical data of a developing BEC in high-resolution. The most frequently used sputter coating material has been gold, iridium, tungsten and carbon which are common choices for low-resolution. Gold particles, however, allow viewing at both low and high magnification [1]. It possesses a high conductivity and relatively small grain size, which makes it ideal for HR imaging. However, the use of Au:Pd, as a metal alloy coating, provides more detail and is advantages in that it provides greater contrast within an HR-SEM micrograph, compared to non-metal carbon coating. Sputter coating with metal alloys are advantages in that it visibly produce greater contrast and HD micrographs and thus it is more beneficial for coating biological samples as it is able to: (i) reduce microscope beam damage, (ii) increase thermal conduction, (iii) reduce sample charging (increased conduction), (iv) improve secondary electron emission, as the metal coat generates higher secondary electrons than samples with no metal/conducting coated (v) reduce beam penetration with improved edge resolution and (vi) protect beam sensitive specimens [12, 14, 16]. It is, thus, critical to ensure that the biological specimen and its environment are modified by the

correct sputter-coating. Specimen modification entails coating specimens to increase their conductivity which precludes problems such as electric charge build-up; thermal and radiation damage by the primary beam and thickness of the metallic coating [2, 12]. To retain the biological sample's authentic characteristics, care should be taken during the fixation process namely: the pH, temperature and osmolality should be within physiologically relevant ranges for the specific cell type. Moreover, strict adherence to timeframes for fixation ensures the preservation of the native state of the biological material under investigation.

The Au:Pd has a significant impact on the quality of the image generated in HD. It illuminates the presence of a porous membrane surface, detailed surface topography, down to individual molecules, jutting out of the cell.

Conversely, the carbon coat obviates analysis of high-resolution, ultrastructural biological data as it reduces the ability to see new, textured nanosized structures during cellular development as it is inclined to produce 2-D planar surfaces and subsequently results in less 3-D anatomizing of the ultrastructures under investigation. HR-SEM utilizing well coated Au:Pd allows for the visualization of a smooth/rough or hollow surface, allows for morphological studies, allows the study of surface texture, whether the structure has pores and pore sizes, normally at a micron size or a nano size.

Coating thickness is a critical aspect to take into account. Based on the profilometry analysis the lowest amount of coating was 15 mm for carbon. The advantage of using Au:Pd is that a coating of a meagre 5 nm is able to produce an even spread of coating over 60 s producing high-resolution ultrastructures which, for the first time, closely presents nanostructures found in its native state.

Conclusions

When preparing biological samples for HR-SEM imaging the goal is to minimize the aberration of structures found within the native state of the sample. We show that using the tissue-culture technique of growing cellular structures on the cellulose membrane provides novel and optimal experimental conditions for preparing samples for HR-SEM. Given the success we had in elucidating the *in vitro* nanoscopic structure of the endothelial BBB model [4], we have provided a detailed experimental procedure to enhance further investigation of such biological *in vitro* structures (e.g., monolayers of retinal epithelium, germinal epithelium of the blood-testis barrier, endothelial layers of both the systemic and brain endothelia, etc). These structures have not yet been investigated using the methodology we recommend.

Furthermore, the use of Au:Pd sputter-coating, enables the nanostructures of biological specimens to be studied at high-resolution, at a molecular level, whereas carbon-coated samples tend to lose a significant amount of ultrastructural detail. Carbon thermal evaporation may, however, be useful in determining the dimensions of biological structures given its 2-D attributes. In summary, our experimental data recommends using cellulose-based inserts to biologically prepare samples for HR-SEM and Au:Pd sputter-coating as the superior technique that allows for clearly defined nanostructures without adding extrinsic defects, when acquiring HR-SEM nanoscopic topographical details of biological samples. It is recommended that biological material is grown in a manner that mimics the *in situ* situation when preparing it for HR-SEM. This is critical, and if not done correctly, factors such as hypertonicity, osmolality, pH and temperature could result in the severe aberration

or/and tearing of tissue/cell samples. We strongly recommend correct coating to preserve the detail of biological samples. Lastly, we recommend Au:Pd sputter-coating, as per our descriptions in the methodology and protocol, to illuminate ultrastructural data in order to study the molecular detail of the BEC membrane surfaces.

Acknowledgements

This chapter was accepted for publication in *PLoS ONE* (in press). The work was supported by the infrastructural and academic support provided by the Department of Medical Biosciences at the University of the Western Cape (UWC) and the Electron Microscopy Unit at the University of the Western Cape, Cape Town, South Africa.

References

1. Fischer ER, Hansen BT, Nair V, Hoyt FH, Dorward DW. Scanning electron microscopy. *Curr Proto in Micro*, 01 May 2012, Chapter 2:Unit 2B.2. Nihms-375012;2013.doi:10.1002/9780471729259.mc02b02s25.
2. Giurlani W, Berretti E, Innocenti M, Lavacchi A. Measuring the thickness of metal coatings: A review of the methods. *Coatings*. 2020; 10: 1–36. doi:10.3390/coatings10121211.
3. Kommnick C, Lepper A, Hensel M. Correlative light and scanning electron microscopy (CLSEM) for analysis of bacterial infection of polarized epithelial cells. *Sci. Rep*. 2019; 9: 17079. doi:10.1038/s41598-019-53085-6.
4. Mentor S, Fisher D. High-resolution insights into the *in vitro* developing blood-brain barrier: Novel morphological features of endothelial nanotube function. *Front. Neuroanat*. 2021; 15: 1–15. doi.org/10.3389/fnana.2021.661065.
5. Postek MT, Howard KS, Johnson AH and McMichael KL. Scanning Electron Microscopy: A Student's Handbook, edn. Ladd Research Industries: Postek, M.T. Jr. 1980.
6. Raval N, Maheshwari R, Kalyane D, Youngren-Ortiz SR, Chougule B. and Tekade,R.K. Importance of physicochemical characterization of nanoparticles in pharmaceutical product development. In basic fundamentals of drug delivery,

   ISBN 9780128179093, Chpt 10. 2019. pp 369-400. doi: 10.1016/B978-0-12.
7. Park JB, Kim YJ, Kim SM, Yoo JM, Kim Y, Gorbachev R, *et al.* Non-

destructive electron microscopy imaging and analysis of biological samples with graphene coating. *2D Mater.* 3. 2016. doi:10.1088/2053-1583/3/4/045004.

8. Griffin BJ. A comparison of conventional Everhart-Thornley style and in-lens secondary electron detectors-a further variable in scanning electron microscopy. *Scanning* 2011; 33: 162–173. doi:10.1002/sca.20255.
9. El Azzouzi M, Khouchaf L, Achahbar A. Monte Carlo study of the interaction volume changes by the beam skirt in Vp-Sem. *Acta Phys. Pol. A.* 2017; 132: 1393–1398. doi.org/10.12693/APhysPolA.132.1393.
10. Kanaya K, Okayama S. Penetration and energy-loss theory of electrons in solid targets. J. Phys. D. Appl. Phys. 1972; 5: 43–58. doi:10.1088/0022-3727/5/1/308.
11. Faso L, Trowbridge RS, Quan W, Yao XL, Jenkins EC, Maciulis A, *et al.*. Characterization of a strain of cerebral endothelial cells derived from goat brain which retain their differentiated traits after long-term passage. *Vitr. Cell. Dev. Biol. - Anim.* 1994; 30: 226–235. doi:10.1007/BF02632044.
12. Goldstein JI, Newbury DE, Echlin P, Joy DC, Romig AD, Lyman CE, *et al.*. Coating and conductivity techniques for SEM and microanalysis. Scanning electron microscopy and X-Ray microanalysis. 1992. pp 671–740. doi:10.1007/978-1-4613-0491-3_13.
13. Zhou W, Apkarian R, Wang ZL, Joy D. Fundamentals of scanning electron microscopy (SEM). *Scanning Microsc. Nanotechnol. Tech. Appl.* 2007; 1–40. doi:10.1007/978-0-387-39620-0_1.
14. Heu R, Shahbazmohamadi S, Yorston J, Capeder P. Target material

selection for sputter coating of SEM samples. *Micros. Today* 2019; 27: 32–36. doi:10.1017/s1551929519000610.

15. Rath SS. Growth and characterization of gold-palladium thin-films on a silicon substrate. *Ijert*. 2014; 3: 261–264.
16. Sputter coating brief: Available from: http://www.iitk.ac.in/meesa/SEM/coater_manual_technical.pdf [Cited 21 May 2021].

Supporting information

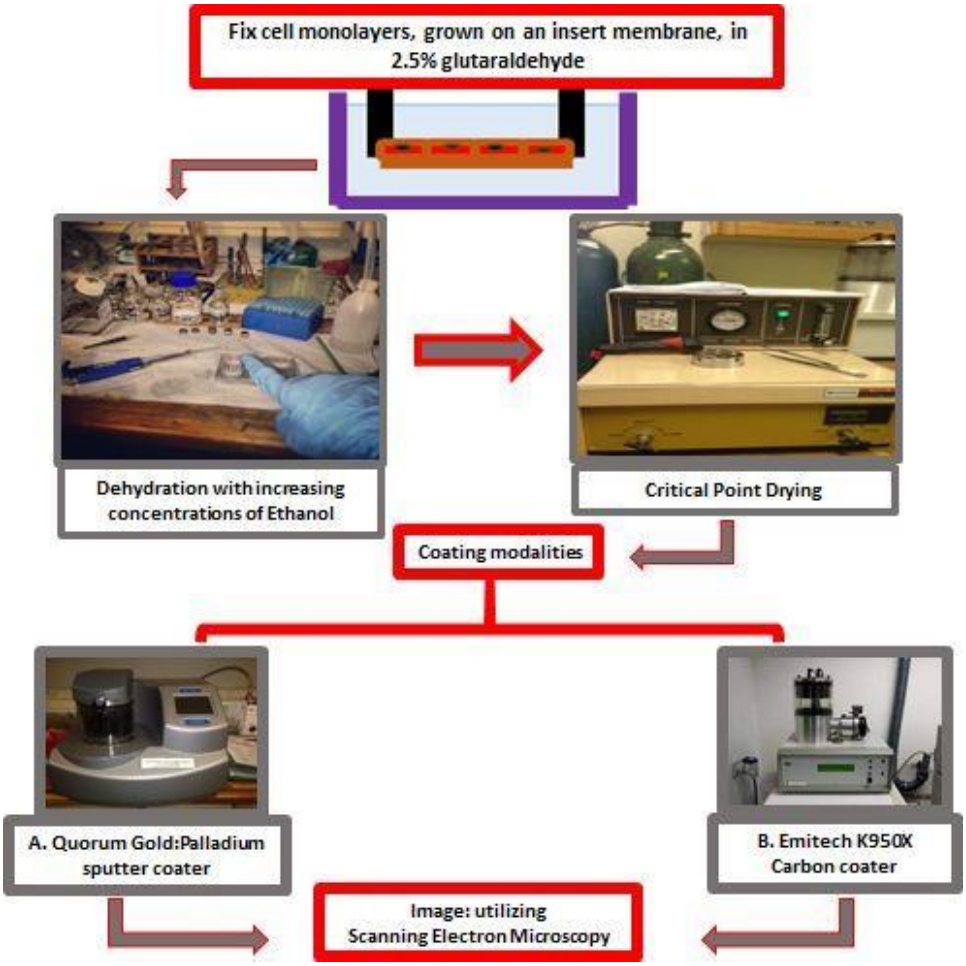

S1 Fig. A **flow-diagram illustrating the preparation of brain endothelial cell monolayers for imaging using high-resolution electron microcopy.** The flow-diagram illustrates the process of monolayer development on a mixed cellulose esters insert membrane, fixation of the BEC monolayer. Fixation was followed by dehydration within a series of graded ethanol concentrations and, thereafter, it underwent critical point drying, replacing ethanol with liquid carbon dioxide at high pressure and regulated temperature until the critical point was reached. After drying, the biological samples were sputter-coated with carbon and Au:Pd in order to ensure the preservation of the sample in its native state when viewed under HR-SEM.

S1 File. PDF version of the protocol submitted on Protocols io.

CHAPTER THREE: 'HIGH-RESOLUTION INSIGHTS INTO THE *IN VITRO* DEVELOPING BLOOD-BRAIN BARRIER: NOVEL MORPHOLOGICAL FEATURES OF ENDOTHELIAL NANOTUBE FUNCTION'

frontiers in Neuroanatomy

ORIGINAL RESEARCH
published: 25 June 2021
doi: 10.3389/fnana.2021.661065

High-Resolution Insights Into the *in vitro* Developing Blood-Brain Barrier: Novel Morphological Features of Endothelial Nanotube Function

Shireen Mentor[1] *and David Fisher*[1,2]*

[1] *Neurobiology Research Group, Department of Medical Biosciences, Faculty of Natural Sciences, University of the Western Cape, Cape Town, South Africa,* [2] *Adjunct Professor in School of Health Professions, University of Missouri, Columbia, MO, United States*

High-resolution electron microscopy (HREM) imaging of the *in vitro* blood-brain barrier (BBB), is a promising modality for investigating the dynamic morphological interplay underpinning BBB development. The successful establishment of BBB integrity is grounded in the brain endothelial cells (BEC's) ability to occlude its paracellular spaces of brain capillaries through the expression of the intercellular tight junction (TJ) proteins. The impermeability of these paracellular spaces are crucial in the regulation of transcellular transport systems to achieve homeostasis of the central nervous system. To-date research describing morphologically, the dynamics by which TJ interaction is orchestrated to successfully construct a specialized barrier remains undescribed. In this study, the application of HREM illuminates the novel, dynamic and highly restrictive BEC paracellular pathway which is founded based on lateral membrane alignment which is the functional imperative for the mechanical juxtapositioning of TJ zones that underpin molecular bonding and sealing of the paracellular space. For the first time, we report on the secretion of a basement membrane *in vitro*, which allow BECs to orientate themselves into distinct basolateral and apicolateral domains and establish a 3-dimensional BEC construct. We report for the first time, on the expression of nanovesicles bound to the plasma membrane surfaces of the BECs. These membrane-bound vesicles are reported to possess an array of DNA/RNA constituents and chemotaxic properties affecting the formation of nanotubes that span the paracellular space between BECs, facilitating BBB construction, alluding to a functional role in mediating cell-to-cell communication. This study suggests that novel, ultrathin nanotubular (NT) structures are involved in functional roles in bringing into alignment the paracellular space of BECs. Immortalized mouse BECs (b.End3, b.End5) and primary rat cardiac microvascular ECs were used to further validate the *in vitro* BBB model by profiling variances in peripheral EC monolayer development. These cardiac capillary ECs presented with an opposite topographical profile: large fenestra and intercellular spaces, devoid of morphological ultrastructures. This comparative study alludes to the role of NT facilitation in TJ-induced hemifusion of apicolateral BEC membranes, as a structural event forming the basis for establishing a polarized BBB.

Keywords: blood-brain barrier, exosomes, nanovesicles, tunneling nanotubes, tethering nanotubes

OPEN ACCESS

Edited by:
Zhuhao Wu,
Icahn School of Medicine at Mount Sinai, United States

Reviewed by:
Mayumi Nishi,
Nara Medical University, Japan
José L. Ferran,
University of Murcia, Spain

***Correspondence:**
David Fisher
dfisher@uwc.ac.za

Received: *30 January 2021*
Accepted: *21 April 2021*
Published: *25 June 2021*

Citation:
Mentor S and Fisher D (2021) High-Resolution Insights Into the in vitro Developing Blood-Brain Barrier: Novel Morphological Features of Endothelial Nanotube Function. Front. Neuroanat. 15:661065. doi: 10.3389/fnana.2021.661065

INTRODUCTION

Endothelial cells (ECs) originate from the mesoderm, a germ layer that forms at gastrulation, during early embryonic development (Dyer and Patterson, 2010) and are essential for capillary formation. Vasculogenesis involves the formation of major vessels in the embryonic midline from angioblasts that originate in the lateral plate mesoderm (Risau and Flamme, 1995; Okuda and Hogan, 2020). The vascularization of the brain and spinal cord begins before birth, by way of angiogenic sprouting networks, namely the perineural vascular plexus (PNVP) and the periventricular plexus (PVP) (Ruhrberg and Bautch, 2013). The PNVP arises from the mesoderm-derived angioblasts (endothelial precursor cells) and conceals the entire central nervous system (CNS) by embryonic day 9.0 (E9.0) (Engelhardt and Liebner, 2014; Gupta et al., 2021). Brain endothelial cells (BECs) grow in close proximity forming restrictive capillary tubes due to the presence of barrier points. The literature denotes these contact points as "kissing points" which is further supported by freeze-fracture studies (Haseloff et al., 2015). In the current morphological study it is referred to as "stitching points." Based on the literature, this partial "stitching" of the BEC membrane appears to be a central part of blood-brain barrier (BBB) CNS vascularization. The development of the BBB is dependent on BECs aligning themselves along their lateral membranes in such way that an array of transmembrane tight-junction (TJ) molecules from adjacent BECs can physically connect, very specifically apicolaterally, sealing the paracellular (PC) space. Although the TJs are fundamental to the integrity of BBB, the mechanisms involved in the alignment between two adjacent cells, has not been described in the literature.

In the current study, the key focus is on how the BBB is forged, primarily, by the BECs of the cerebromicrovasculature interconnected by intercellular TJ protein complexes (Saunders et al., 2014; Qosa et al., 2016). BECs are key components to BBB integrity and regulates the homeostatic *milieu* of the brains microenvironment, by the strict control of the permeability of its capillaries. The BBB regulatory mechanisms, despite its overall strength, is a persistent impediment in the successful treatment of CNS associated diseases (i.e., Alzheimer's Disease, Parkinson's Disease, Brain Cancer etc., actively precluding the entry of drugs to target areas within the diseased brain).

Previously, imaging the molecular interplay between BBB-ECs was encumbered by methodological difficulty. We, hereby, utilize an innovative experimental design to visualize the molecular architecture of brain capillary endothelium development, and with the utilization of high-resolution scanning electron microscopy (HRSEM), the visualization of *in vitro* BBB morphogenesis into a functional monolayer has dramatically enlightened our understanding with regards to how morphological ultrastructures orchestrate adjacent BEC alignment to facilitate the molecular interaction between TJ proteins.

Intercellular communication between BECs is essential to accomplish molecular alignment and the proliferating environment of the brain capillary EC is highly dependent on paracrine signaling molecules, which includes an array of growth factors, e.g., tissue necrotic factor beta, and vascular endothelial growth factor etc. (Lucas et al., 2009). In angiogenesis, cell-to-cell communication is achieved by way of paracrine, autocrine, endocrine factors and by direct cell-to-cell contact, but how this contributes to aligning cells to accomplish the molecular connection between corresponding PC rows of TJs within the cerebromicrovasculature, was until now, still largely unknown.

In vitro models of the BBB have long been used to elucidate the physiological functioning of the *in vivo* BBB, as well as the mechanisms involved in various experimental and clinical treatment procedures. However, except for a few studies, information on the development of the formation of the functional *in vitro* monolayer has remained theoretical at best. Based on our HRSEM studies on the immortalized mouse brain endothelial cells (b.End3 and b.End5), we introduce a novel technique to report, how nanovesicles (NV) induced nanotubular (NT) structures (Gerdes et al., 2007; Gurke et al., 2008; Gerdes et al., 2013) extending from the plasma membrane, can contribute to the alignment of apical membrane proteins during BBB development. To date, there are a plethora of terms used to coin the varying sizes of extracellular vesicles exocytosed from cells (Tamkovich et al., 2016; Schwich and Rebmann, 2018). It is thus propitious to bring clarity to the manner in which we denote these extracellular vesicles (EVs). Different sources use different terms (viz. microparticles, microvessesls, ectosomes, shedding microvesicles, NV, exosomes, exosome-like particles, dexosomes, texosomes, and oncosomes etc.) each term employed according to the various biological material in which they reside [(7) Tamkovich et al., 2016] (**Table 1**).

TABLE 1 | The four major categories of extracellular vesicles.

Vesicle	Mechanism of generation	Size (nm-μm)	References
1. Exosomes	Microvesicular endocytic process; endosomal membrane particle	30–100 nm 70–150 nm	Tamkovich et al., 2016; Schwich and Rebmann, 2018
2. Nano vesicles (NV)	Exocytosed extracellular vesicles	30–300 nm	Novel
3. Microvesicles (μm)	Outward budding and scission of plasma membrane	50–500 nm 100 nm-1,000 μm	Tamkovich et al., 2016; Schwich and Rebmann, 2018
4. Oncosomes and blebbing/apoptotic bodies	Generated from apoptotic bodies and amoeboid cancerous cells	>500 nm	Schwich and Rebmann, 2018

Abbreviations: ATCC, American Type Culture Collection; BALB/c, Bagg Albino C57BL/6; BBB, blood-brain barrier; BEC, brain endothelial cells; b.End3, immortalized mouse brain endothelial cells; b.End5, immortalized mouse brain endothelial cells; BM, basement membrane; CMEC, rat cardio microvascular endothelial cells; DMEM:F12, Dulbecco's Modified Eagles Medium:Hams F12; EC, endothelial cell; ECACC, European Collection of Authenticated Cell Cultures; ECM, Extracellular matrix; Ev, Extracellular vesicle; Flk-1, receptor for vascular endothelial growth factor; HREM, high resolution electron microscopy; HRSEM, high resolution scanning electron microscopy; HRTEM, High resolution transmission electron microscopy; ICAM-1, Intercellular Adhesion Molecule 1; MadCAM-1, mucosal vascular addressin; MECA-32, Panendothelial Cell Antigen Antibody; NT, nanotube; NV, nanovesicle; PC, paracellular; PNVP, perineural vascular plexus; PVP, periventricular plexus; TC, tissue culture; TEM, Transmission electron microscopy; TENT, tethering nanotube; TJ, tight junction; TUNT, Tunneling nanotube.

NTs can be further classified into tethering NTs (TENTs) and tunneling NTs (TUNTs), which are crucial to the intercellular interplay which mobilizes the molecular alignment of TJs between adjacent BEC; requisite to the mechanical juxtapositioning of the BECs and its alignment into a physiological BBB which begins with qualitative and quantitative assessment of the biophysical properties of BECs during development and proliferation, enabling the step-by-step analysis of the evolution of a highly restrictive, continuous membranous structure.

MATERIALS AND METHODS

Bio-Reagents

The immortalized mouse brain endothelial cells (b.End3) were pre-incubated in standard Dulbecco's Modified Eagles Medium: Hams F12 DMEM: F12 nutrient mixture (Thermo Fisher, Cat no. 2176317) supplemented with 1% *Penicillin-Streptomycin* (Whitehead Scientific (Pty) Ltd., Cat no. 17-745E) and 0.117 g of L-glutamine (4 mM) (Sigma-Aldrich, Cat no. G-3126) and b.End5 cells were grown in DMEM: F12 (BioWhitakker/Lonza®, Cat no.12-719F), supplemented with 1% *Pen/Strep*, 1% non-essential amino acids (BioWhitakker/Lonza®, Cat no.13-114E), 1% Sodium pyruvate (Gibco®, Cat no. 11360) and 10% Fetal bovine serum (Celtic Diagnostics/BioWest, Cat no. S181G-500).

Tissue Culture

Immortalized Mouse Brain Endothelial Cell

Both brain endothelial cell lines were derived from BECs of BALB/c mice (Watanabe et al., 2013). The only difference designated to each cell line is the company from which each was purchased. The b.End3 was purchased from American Type Culture Collection, Cat no. CRL-2299 and are positive for gene expression of: von Willebrand factor, Intercellular Adhesion Molecule 1; Vascular cell adhesion protein 1 (VCAM-1) and the mucosal vascular addressin (MAdCAM-1). The MAdCAM-1 and CD62 antigen-like family member E. The b.End5 cell lines was purchased from the European Collection of Authenticated Cell Cultures, Cat no. 96091930 and are positive for gene expression of endothelial specific proteins: Platelet endothelial cell adhesion molecule, Endoglin, Panendothelial Cell Antigen Antibody (MECA-32) and a receptor for vascular endothelial growth factor (Flk-1) tested by fluorescence activated cell sorting. Inflammatory cytokines are able to induce the expression of proteins such as: VCAM-1 and E-selectin.

Primary Rat Cardiac Microvascular Endothelial Cell

The primary rat cardiac microvascular endothelial cell (CMEC) line is a primary line, was donated by Dr. A. Genis, at Stellenbosch University-Tygerberg campus, Tygerberg, Cape Town, South Africa.

CMEC Cell Culture

The CMECs are seeded on TC plates that are pre-coated for an hour with attachment factor (basically gelatin), from Life Technologies. The confluent plates are trypsinized with 0.25% Trypsin-EDTA solution (Whitehead Scientific, Cat no. BE 02-007E) and suspended cells are removed and re-plated in a 1:2 ratio. Suspended cells are centrifuged at 1000 rpm for 3 min to obtain a pellet. The pellet is re-suspended in a specialized growth medium. Microvascular Endothelial Cell Growth Medium-2 (Whitehead Scientific-Lonza®, Cat no. CC-3156) and supplemented with the Bullet Kit (Whitehead Scientific-Lonza®, Cat no. CC-4147), when ordered together as one package, the Cat no. is CC-3202.

The *in vitro* Bicameral System

Immortalized mouse BECs and primary rat CMECs were grown on an insert membrane with a 12 mm diameter, a pore size of 0.45μm and an effective filtration area of 0.6 cm^2. The membrane of the insert was comprised of mixed cellulose esters, according to the manufacturers' specifications (Millicell® insert, (Merck), Cat no. PIHA01250). Inserts were placed in 24-well tissue culture microtiter plates (Adcock Ingram). BEC monolayers (b.End5) were seeded on the inserts at a low cell density (1×10^4 cells/insert/well), to allow for sparse location of cells, and both CMECs and BECs were seeded at cell densities ranging from $1 \times 10^4 - 1 \times 10^6$ cells/insert/well, respectively, so that the close proximity of cells could facilitate monolayer confluence, and also to promote cell-to-cell communication over a 24–48 h timeframe.

To identify PC structures, we designed a cell culture experiment that provided the BEC with a slightly hypertonic tissue culture environment (330–340 mosmol/kg) to promote subtle crenation of the BEC body. The slight crenation allowed for the PC space to be uncovered which better permits TUNT and TENT ultrastructural investigation along the adjacent, lateral cell membranes.

Scanning Electron Microscopy

We introduce a novel technique that involves growing BECs to confluence on inserts and, thereafter, image monolayer development utilizing HRSEM. BECs (b.End5 cells) were grown at 37°C, at 5% CO_2 on Millicell filter inserts (at 1×10^4 and 1×10^6 cells/insert/well). Upon cellular confluence, cell monolayers were fixed with 2.5% glutaraldehyde solution (BioChemika/Fluka- Sigma-Aldrich) (Faso et al., 1994). The biological sample was dehydrated in a graded series of ethanol concentrations and critically dried using a Hitachi HCP-2 critical point dryer. Samples were coated with gold-palladium (Au: Pd) and imaged using a Zeiss Auriga high-resolution field-emission gun SEM. All images were captured using an in-lens secondary electron detector.

Transmission Electron Microscopy

The b.End3 cells were grown at 5×10^5 cells/insert/well at 37°C and 5% CO_2 ($n = 3$; day = 0) in supplemented DMEM: F12. Cells were allowed to attach and expand to confluence for 24 h. The samples were chemically fixed in 2.5% glutaraldehyde solution (BioChemika/Fluka- Sigma-Aldrich), in 100 mM phosphate buffer at pH 7.2) for 2–24 h at 4°C (Faso et al., 1994). Samples were washed twice in 100 mM phosphate buffer that has been adjusted to the osmolarity of the sample to prevent tissue damage. Post-fixation was conducted using 1% Osmium tetroxide made

in 100 mM phosphate buffer 1–2 h, at 4°C. Specimens were incubated in 2% aqueous uranyl acetate and dehydrated in a graded series of ethanol concentrations. Samples were embedded using a series of resin-ethanol mixes during the infiltration process. Ultrathin thin sections (∼60 nm) slices of sample embedded in resin were prepared using a Reichert Ultracut S ultramicrotome. Sections were imaged on a FEI/TECNAI T20 transmission electron microscope.

RESULTS

This study strongly suggests how novel, nanosized ultrastructures functionally cooperate in the formation of a physiologically functional *in vitro* BBB model. Furthermore, we discuss novel mechanisms showing how tunneling and tethering nanotubules (TUNTs and TENTs) may play an important role in aligning the brain capillary endothelial cells to form sealed PC pathways. This study describes how BECs develop morphologically in an *in vitro* environment designed to model the BBB using HRSEM to morphological describe cellular membrane ultrastructures on a nanoscale. This is especially pertinent to a more informed perspective of the *in vivo* formation of the BBB.

In vitro Secretion of the Basement Membrane

BECs were grown at a low cell density (1×10^4 cells/insert/well) to track its development progressively over 24 and 48 h. At these low cell densities, the BECs were sparsely located, allowing for the investigation of three-dimensional development of cells before exponential cell division resulted in the close approximation of cells in culture and their interaction (**Figure 1**). The mixed cellulose ester insert membrane mimics a biological surface which allowed cells to orientate themselves and to differentiate functionally into distinct morphological apical and basolateral domains. After the attachment of BECs to the insert membrane the secretion of an amorphous extracellular material from the basal surface of the cell was observed (**Figure 1**). The HRSEM enabled the viewing of the cell membrane, in which pore-like structures could be identified (**Figure 1**).

Nanovesicles

Following repetitive divisions of cells on the insert membrane, it became apparent that the surface or membrane morphology of the cells became increasingly more complex. Two structures became abundant on the cell surface: copious amounts of NVs and the subsequent emergence of primordial, nano-sized filaments emanating from the extracellular apicolateral membrane surfaces.

There are two types of NVs, which we categorized according to possible functions:

Chemotaxic Nanovesicles

These NVs have membranes that are "adhesive" and are characterized by prominent membrane pores and "sticky" filamentous surface structures. The images suggest that NVs are able to facilitate additional anchorage onto the parent cell membrane (**Figure 2**). Their membrane structure appears to be identical to the parent cell's membrane. Although we have not been able to report on the actual formation of these NVs, within a closed cell culture environment, its origins preclude any other contingency other than the cultured cells. It is also of interest to note that initially, upon the seeding of the BECs, there is an absence of NVs; its pervasion only increases upon the formation of denser cell populations. The formation of the NVs are limited to cells growing in close proximity (**Figure 2**).

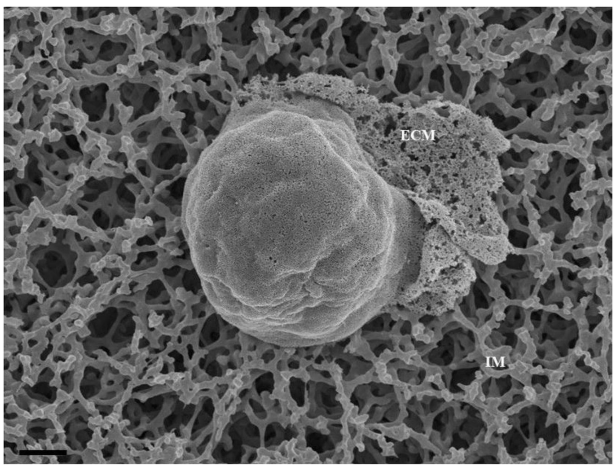

FIGURE 1 | An HRSEM micrographic illustration of a b.End5 cell seeded on a mixed cellulose insert membrane establishing 3-dimensional cellular architecture (Scale bar = 2000 nm). The micrograph exhibits the secretion of a basement like extracellular matrix (ECM). The insert membrane is denoted as "IM."

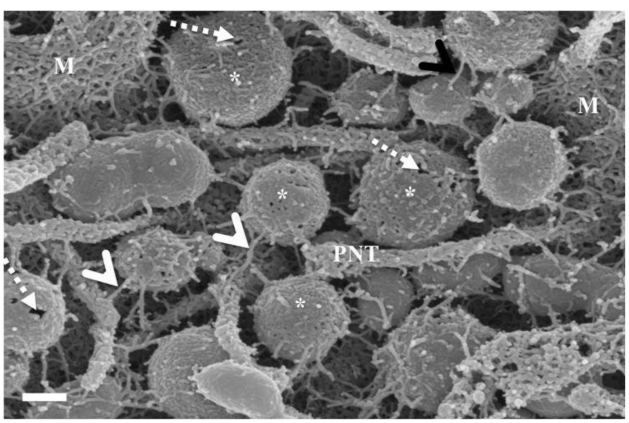

FIGURE 2 | The HRSEM micrograph depicts nanovesicular structures emanating from the b.End5 cell (Scale bar = 200 nm). This category of EV is porous in nature enabling them to act as generators of a chemotaxic gradient and also protrude sticky filaments (white arrowheads), further enabling it to be anchored close to their area of formation. These EVs range from 30 to 300 nm in size and thus are categorized as nanovesicles. The "perforated white arrows" indicate the pores of the exosomes. "**M**" denotes the plasmalemma outer surface, the * asterisk denotes the nanovesicle (NV) and "**PNT**" denotes primordial NTs.

Nanovesicle-Induced Nanotubules

A novel finding of this study showed that closely approximated NVs, which have been classified into two sub-populations of membrane-bound vesicles, was integrally involved in regulating PC cell-to-cell communication. This study proposes the following: (i) NVs are porous in nature, possessing "sticky" tentacles which allow for the vesicle to attach to the cell membrane (**Figure 2**), and (ii) a clearly different category of NVs which fused to each other to form nanotubes (NTs), with their proximal ends firmly attached to the surface membranes of the parent cell, while the distal ends, initially forming close-ended, "sticky" ends on the cell membranes of adjacent BECs (see **Figures 4A–C**), and later these proximal and distal ends fuse with the plasma membranes, connecting the cytoplasm of adjacent cells (refer to **Supplementary Figure 1**). These NTs appeared to have hollow lumens which stretched across

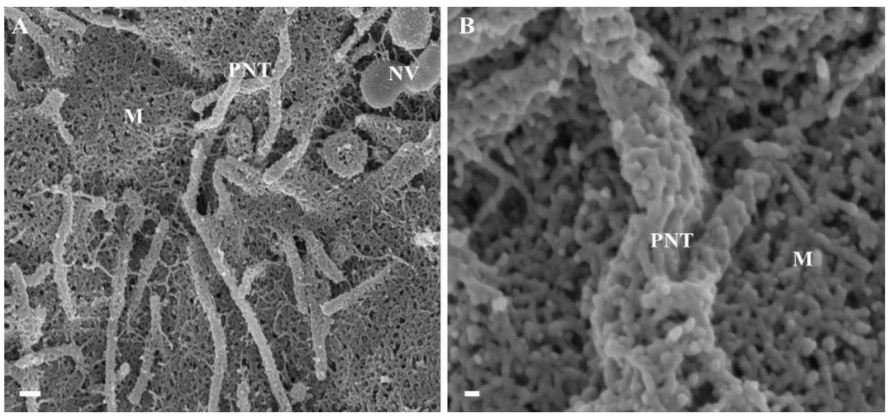

FIGURE 3 | The *de novo* formation of primordial nanotubules on the membrane surface of BECs. **(A)** Depicts a micrograph showing elongated NT structures emanating from the plasmalemma of a b.End5 cell (Scale bar = 200 nm). Membranous protrusions from the cell surface morph into rope-like, tethering NTs on the apical surface of a b.End5 cell membrane. **(B)** Illustrates the formation of dense NT distensions' originating from the cell membrane surface (Scale bar = 100 nm). "M," denotes the porous membrane, "NV" denotes the nanovesicle and "PNT," denotes the primordial nanotubule.

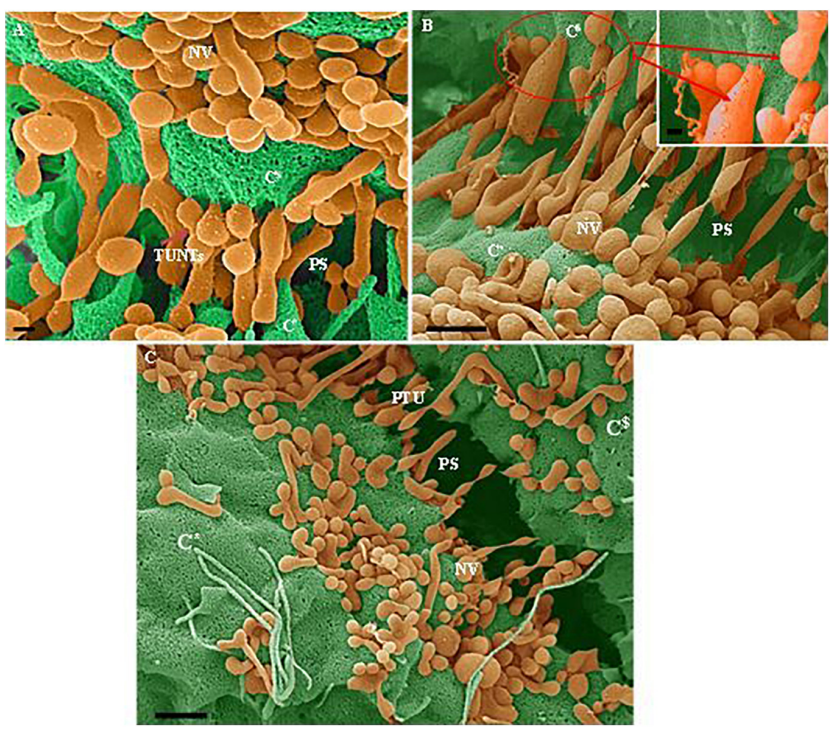

FIGURE 4 | (A–C) Indicate both the porosity and the sticky filaments of NVs found along the lateral walls lining the PC space. C* and C$ are denoted as cell 1 and cell 2, "**NV**" denotes the nanovesicle, "**PS**" denotes the PC space and "**PTU**" denotes the primordial TUNTs. **(A)** Scale bar = 200 nm; **(B,C)** Scale bar = 1,000 nm.

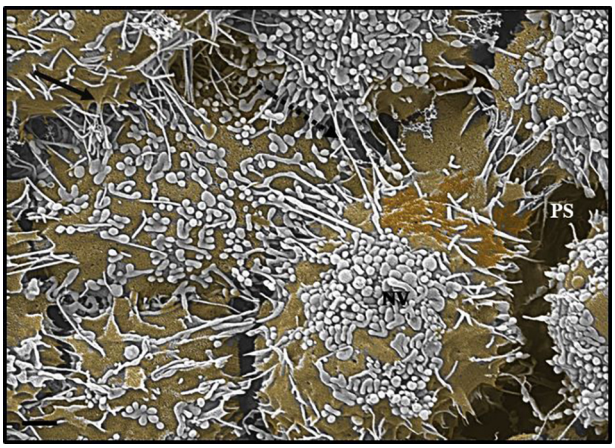

FIGURE 5 | An HRSEM micrograph 24 h after seeding b.End5 (BECs) in close proximity (1×10^6 cells/insert/well) (Scale bar = 1000 nm). The nanovesicle is denoted by an "**NV,**" **TUNTs** are indicated by the perforated, black arrow and **TENT** formation is indicated by the solid, black arrow and the "**PS,**" denotes the PC space.

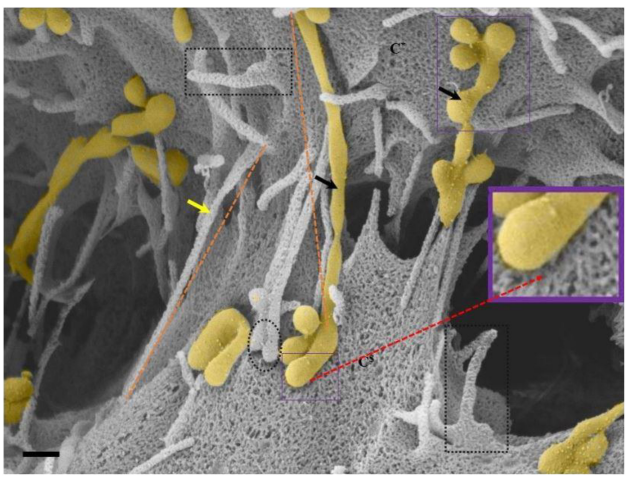

FIGURE 6 | An HRSEM micrograph of two BECs utilizing TENTs to facilitate occlusion of the PC space (Scale bar = 200 nm). Proximal ends of short developing TENTs (**perforated rectangles**) are observed alongside fully extended and developing TUNTs, on each of the juxtaposed lateral membrane surfaces of two BECs in close proximity. TENTs are indicated by the "**yellow arrow,**" its distal ends are indicated by "**black perforated circles**" and TUNTs are indicated by the "**black arrows**." The proximal and distal ends of TUNTs are indicated by the "**solid purple squares**." The micrograph depicts the interplay between flanked TENTs and TUNTs which results in the continuity of BEC membrane topography.

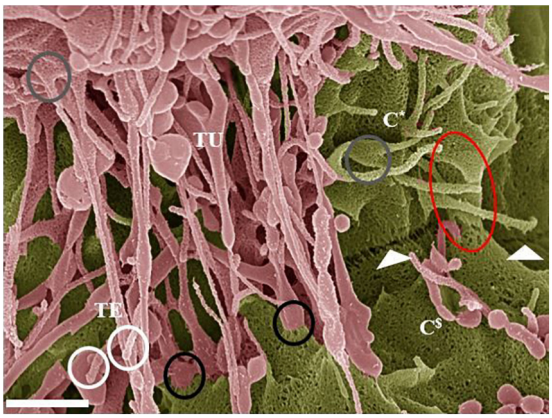

FIGURE 7 | Hemifusion across the PC space between two juxtaposing BECs (Scale bar = 1,000 nm). The HRSEM micrograph depicts juxtapositioning adjacent b.End5 cell membranes and subsequent TJ protein alignment facilitated by TUNT and TENT formation denoted as "**TU**" and "**TE**" within 24 h of monolayer establishment. The occurrence of TENTs and TUNTs together is a clear observation that they have distinctly different functions. The "**white circles**" highlight the extremities of the TENT structures which exhibit bulb-like distal ends. The "**gray circles**" highlight the proximal ends of TENTs, which form tent-like leaflets from the leading edges of the cell membrane. The "**black circles**" highlight the distal ends of TUNTs, which fuse with the surface membrane of the adjacent/target cell, the lower black circle illustrates the short fibers tethering the foot process to the membrane. The "**white arrows**" indicates an additional, novel feature that presents itself throughout the BEC cultures as a partial "stitching" together of adjacent BECs across the PC space (partial fusion). This hemifusion of adjacent BEC cell membranes indicates the site for TJ protein interaction and the "**red circle**" illustrates the beginning of membrane overlapping. The **C*** denotes cell one and the **C$** denotes cell two (the target cell).

the PC spaces of adjacent BECs appearing to connect the two cells, forming a framework of tubes across the PC space of adjacent BECs.

Primordial TENTs

HRSEM analysis after 24–48 h of seeding of 1 million b.End5 cells on a cellulose insert membrane showed the *de facto* initiation of projecting cytoplasmic tube-like extensions from the surface of cells (**Figures 3A,B**). These micrographs illustrate the primordial formation of NT structures extending from the cell membrane surface, eventually developing into NT cross-bridges across the PC space. The outer surface of the primordial NTs appears to be consistent with the molecular structures of the cell membrane (**Figure 3B**). Sparsely distributed BECs did not express the elaborate membranous structures and are devoid of structures involved in cell-to-cell communication, including exocytotic vesicles and subsequent NT formation (**Figure 1**), which was only observed when cell populations grew to the close proximity of each other (**Figure 3**).

In **Figures 4A–C** NVs are exocytosed onto the BEC PM surface and remain "attached" to the cell membrane. The NVs progress from mono-vesicular structures, by a process of fusion, to form bi-vesicular, tri-vesicular and multi-vesicular structures which adjoin to form elongated, NTs. These NTs morph into "tunneling tubes which have a clear trans-paracellular space lineament as it propagates across the PC space along the apicolateral domain. This NV-induced, tubular formation appears to be the *de novo* synthesis of a tunneling NT (TUNTs) and to the best of our knowledge, it has never been described before in the literature. The TUNT, thus comprises of all amalgamated contents housed within individual NV packages.

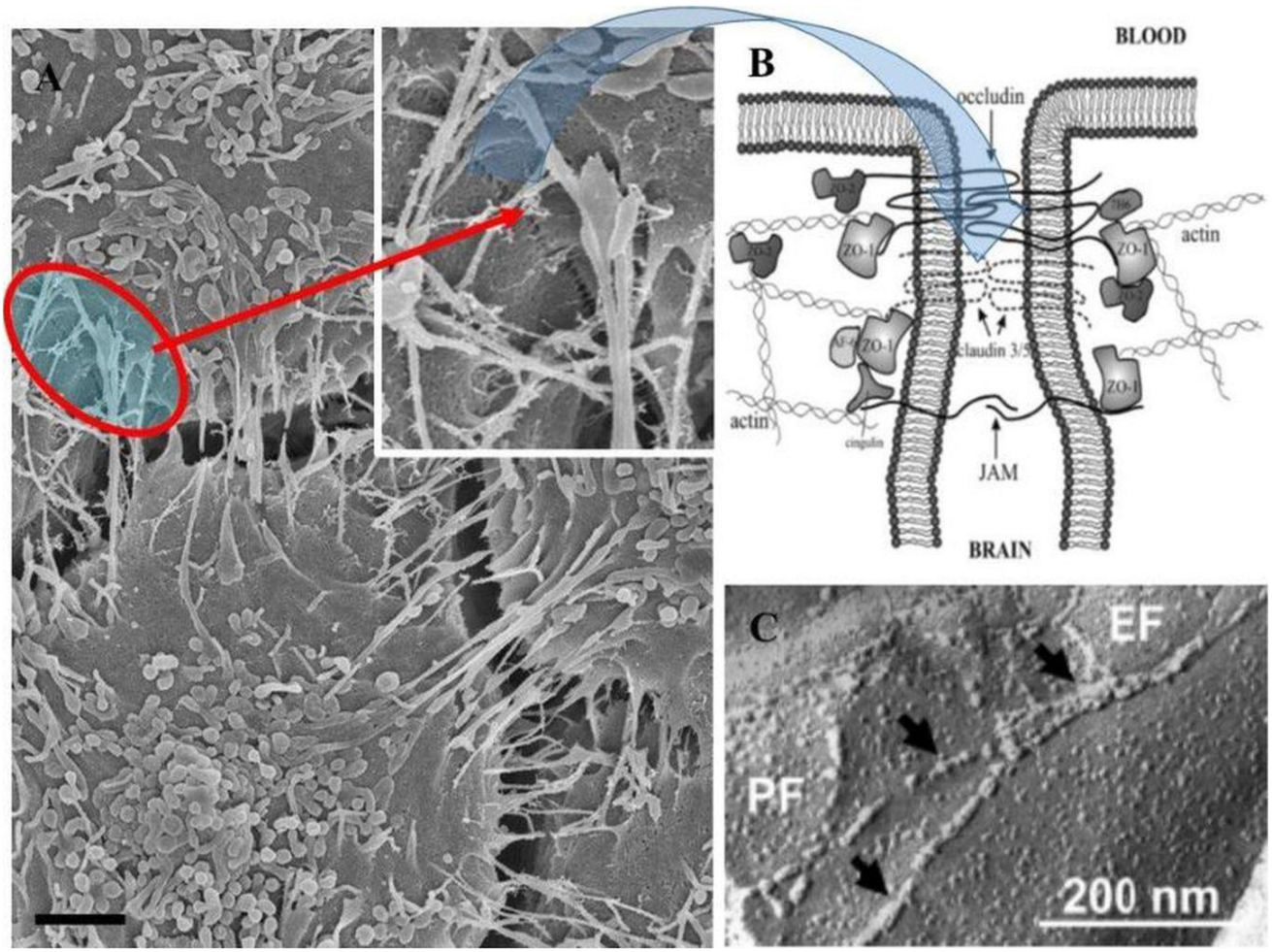

FIGURE 8 | The role of TUNTs in aligning and juxtaposing the adjacent lateral membranes (Scale bar = 2,000 nm). **(A)** Illustrates membrane interaction at the apical domains which are achieved when two juxtaposed BECs are localized in close proximity (see the "red circle"), which shows membranes positioned close. **(B)** Is an annotated diagram of TJ interaction which occurs when adjacent cell membranes are closely position (**B**; Hawkins and Davis, 2005). **(C)** Depicts freeze-fracture electron microscopy of TJ interaction of ECs of the BBB (Haseloff et al., 2015).

In **Figure 5**, we see cells have been purposefully crenated to expose some of the morphological topography between adjacent cells. During the crenation process, some of the NTs which have been attached to adjacent cells have been broken. This process exposed the molecular and morphological membrane processes involved in aligning and joining these PC spaces (**Figure 5**).

BEC Tethering Nanotubules

Observations of the PC spaces of closely juxtaposed b.End5 cells revealed that NTs are characterized by thin, rope-like structures which functions by mechanically aligning the PC space and subsequently pulling over or securing of plasma membranes across the PC space, playing an important role in the occluding of the PC pathway (**Figures 5**, **6**). Based on the function and the morphological description of the NT we, hereafter, denoted these NTs as tethering NTs (TENTs).

TENTs are characterized by thin filamentous structures (see **Figure 6** "yellow arrows," below), have mechanical integrity and extend with focus intent to project across the PC space and make contact with the adjacent lateral cell membrane its distal ends anchor to the membrane of the adjacent cell.

Proximal ends (origin of the TENT): Scrutiny of the origin of the TENT's shows that TENTs are continuous and have similar surface cytoarchitecture with the cell's PM. Furthermore, the proximal origins of TENTs are clearly characterized by triangular membrane leaflets, the apex of which continues to form an NT projecting toward the adjacent cell (see the perforated black frame in **Figure 6**). Conversely, the proximal end of a TUNT is formed by the fusion of multiple NVs (see **Figure 6**: purple frame).

Distal ends: the distal end of the TENT is bulb-shaped and appears "sticky" (see the black perforated circle in **Figure 6**). Initially, close observation of the distal bulb of the TENT shows tiny filaments which appear to anchor the TENT to the lateral membrane of the adjacent cell. With time the distal ends of the TENT appear to be reabsorbed adjacent cell membrane, resulting in the bulb end to disappear. Conversely, the distal end

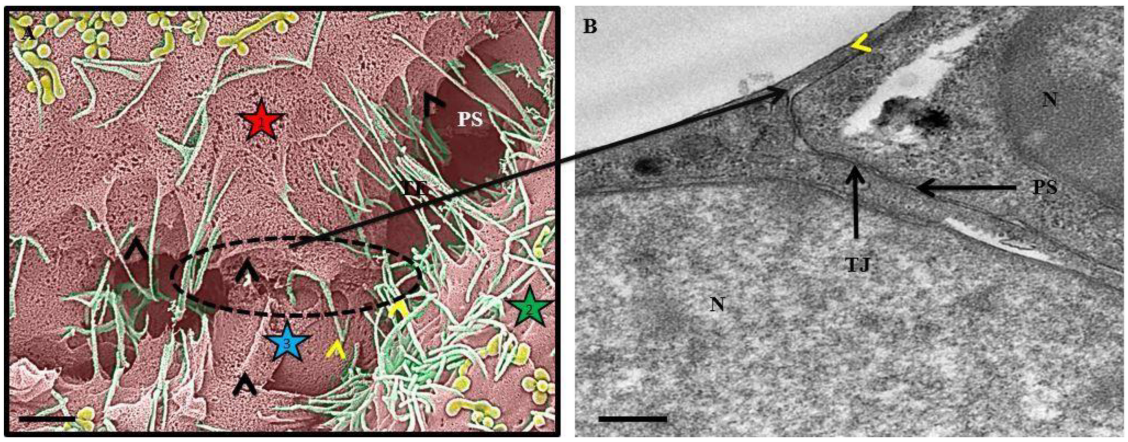

FIGURE 9 | An HRSEM and HRTEM micrograph of tethering nanotubule formation on b.End3 and b.End5 cells. In **(A)** the HRSEM micrograph depicts the formation of membrane tethers which progress into overlapping leaflets between adjacent b.End5 (BECs). The "**black arrowheads**" indicate direct cell-to-cell communication by way of lateral cytoplasmic protrusions of tethering NTs (TENTs). The "**yellow arrowheads**" indicate the overlapping membranous regions generated by TENTs on the lateral borders between adjacent b.End5, BECs. The stars 1, 2, and 3 designate three different cells (Scale bar = 1,000 nm). In **(B)** the HRTEM micrograph depicts an apical membranous region on a b.End3 monolayer, establishing an apparent, continuous membrane surface by the fusion of overlapping membrane regions as indicated by the "**yellow arrowhead**." "**N**," denotes the nucleus of the cell, "**PS**," denotes the PC space and "**TJ**" denotes the region of tight junction localization (Scale bar = 0.5 μm).

of a TUNT forms foot-like ends which interact with the plasma membranes of the target cell (see purple frame, **Figure 6**).

The distal ends appear to be continually reabsorbed by the cell's lateral plasma membranes, inevitably resulting in the shortening of the TENT. The shortening of the TENT appear to have three functions: one, to mechanically pull the membranes of adjacent cells toward each other, and secondly, to align the zones of TJs on the lateral cell walls (see **Figures 6**, **7**), resulting in the hemifusion of adjacent cells. Thirdly, tethering also involves the cell membrane (marginal-folds) being pulled across the PC space by TENTs (**Figures 6**, **9**, **10**).

The stem of NTs: The stem is represented along the "perforated orange line." Visually, the TUNT appears larger in diameter and is generated by the fusion of NVs. The TENT is much smaller in diameter, forming tethers, from membranous leading edges of the BEC, as shown by the "perforated black squares," extending across the PC space. TUNTs and TENTs appear similar in length.

Hemifusion/Point Cell-to-Cell Interaction

Hemifusion, by definition, refers to the TJ-induced "stitching" together of plasma membranes across the PC space. We hereby document that when b.End5 cells are in close proximity to each other on a monolayer, the plasma membranes of adjacent cells, becomes attached to each other in a "stitched" process across the PC space (**Figures 7**, **8A**). This stitching occurs in the apicolateral domain of the PC space, and each "stitch" has a molecular appearance resembling molecules from opposing lateral membranes "sticking" to each other. It conforms to the theoretical and molecular description for TJs between BECs, the PC freeze-fracture histology of BECs and BEC fluorescence immunocytochemistry postulates of the zone of TJs.

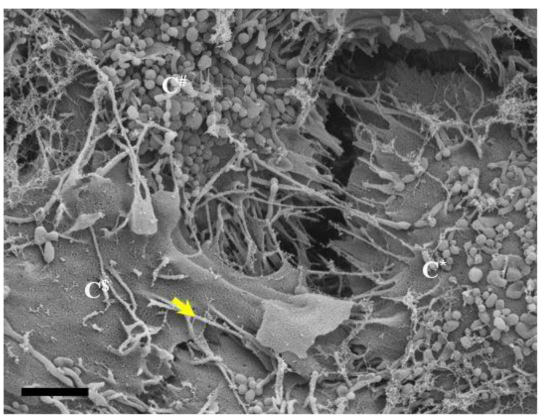

FIGURE 10 | An HRSEM micrograph of two BECs utilizing TENTs to facilitate occlusion of the PC space (Scale bar = 2,000 nm). Short developing TENTs are observed alongside fully extended TENTs, on each of the juxtaposed lateral membrane surfaces of two BECs in close proximity. TENTs are indicated by the "**yellow arrow**." The micrograph suggests, together with the additional evidence in this paper, that overlapping TENTs may have an important role in BEC membrane continuity. **C***, **C$**, and **C#** denote three different adjacent cells.

The HRSEM micrograph in **Figure 8A** illustrates the alignment of the b.End5 cells' junctional border between the apicolateral domains of two adjacent BECs within the cell monolayer (cell density 1×10^6 cells/insert). The micrograph (**Figure 8A**) shows that TUNTs and TENTs are candidates to have a role in aligning the PC spaces between adjacent cells, allowing for both mechanical forces to stabilize the PC space, and at the same time, align the adjacent cells to permit interaction between molecular structures (e.g., TJs).

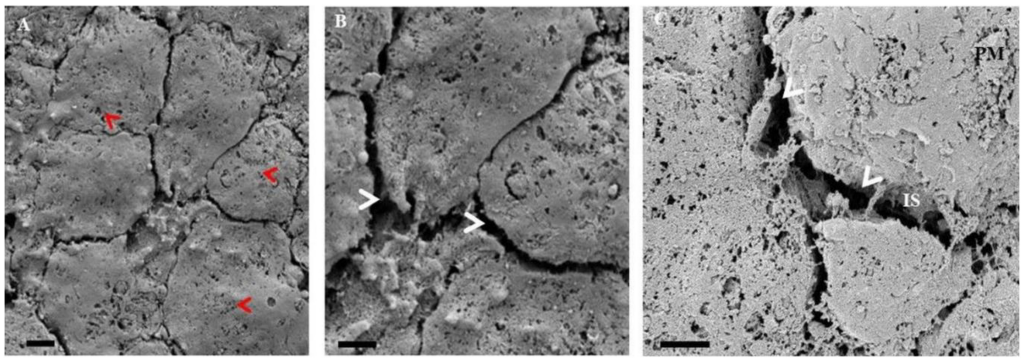

FIGURE 11 | A series of HRSEM micrographs of early stages of the primary rat cardiac microvascular endothelial cell, illustrating the ultrastructural topography of a confluent CMEC monolayer, growing in close proximity. In **(A)** the "red arrows" indicate the pervasive fenestra on the rat CMECs (Scale bar = 2,000 nm). Furthermore, in **(B)** apparent, is the conspicuous absence of TENTs and TUNTs and surface NVs. The "white arrows" indicate the multiple intercellular spaces (IS) devoid of NTs and TJ protein-protein interaction (Scale bar = 2,000 nm). In **(C)** the HRSEM micrograph displays a PC space between CMECs grown in close proximity. The CMEC monolayer is devoid of NVs as indicated by the "white arrows" (Scale bar = 1,000 nm).

The Overlapping Apical Membrane

Leading edges of the cell membrane develop into overlapping membrane leaflets. The leaflets are formed by the proximal ends of TENTs. The shaft of the TENT is formed by rope-like, slender tethers that fuse with the adjacent cell's surface membrane. The TENTS serve to create a series of connections between the apical surfaces of endothelia as a means to cover the zones of apicolateral TJs and further mechanically occlude the PC space.

It is well established in the literature that the apical membranes of BEC, as seen in *in vitro* transmission electron micrographs, form overlapping regions across the PC space (Martins et al., 2013; Haseloff et al., 2015).

TENTs, resembling rope-like tethers, are integrally involved in "pulling across" of the plasma membranes, across the BEC's PC space, as indicated by the yellow arrows (**Figures 9**, **10**). TENTs have a rigid structure and grow in a targeted direction from the leading edges of the cell membrane across the PC space eventually resulting in the distal ends attaching to the lateral membrane of the adjacent cells. TENT distal ends are not "open-ended" in their architectural make-up, instead, they resemble "closed-ended" nanostructures with "sticky," distal ends that pull the leading edges of the BEC membrane, generating tent-like overlapping membranous leaflets. The micrograph (**Figure 10**) depicts the initial stages of cellular communication whereby cells are being drawn toward each other by way of TENTs. The generation of overlapping membrane continuity, in turn, results in an occluded PC space and the protection of the underlying TJ molecular attachments (**Figure 10**).

Primary Rat Cardiac Microvascular Endothelial Cell Communication

We postulated that the elaborate intercellular topography we observed in the development of the BEC monolayer was crucial to the formation of a "tight" epithelium where the alignment of TJs were pivotal to the functionality of a "tight" endothelium. The functionality of systemic endothelium, in contrast, is characterized by an absence of TJs, high levels of porosity and permeability. We cultured cardiac capillary endothelium to study *in vitro* monolayer development.

After an initial seed (24 h) of the rat CMECs, on a Millicell mixed cellulose esters insert membrane; minimal cell-to-cell interaction is observed. Distinct features of a typical systemic ECs (SEC) display a "cobblestone" appearance when forming a lawn of cells attached to the insert membrane. SECs are distinctly different from the BECs showing a visible reduction in the amount of cell-to-cell communication between adjacent SECs (Plate 11 A). There is a visible absence of ultrastructural NT extracellular projections, in comparison to the complexed PC spaces seen between adjacent BECs (**Figures 6–8A**). In addition, notable paucity of surface membrane structures and extracellular vesicles are seen on the CMECs, limiting the adhesion of CMECs to both the mixed cellulose esters filter membrane and adjacent SECs growing in close proximity (Plate 11 A). In Plate 11 B, CMECs display clear, uninterrupted PC spaces between CMECs are simple and displays no hemifusion and TJ occlusal interaction, thus demonstrating a typical "leaky"/permeable monolayer expected of systemic capillary endothelia. Furthermore, the CMECs present with multiple fenestra on its membrane surface. Since CMECs do not exhibit exosome formation; little to no NT formation is observed, in contrast to the BECs (**Figures 9**, **10**) of the *in vitro* BBB. Plate 11 C displays reduced intercellular communication, compared to BEC communication. The absence of exosome expression on the cell membrane surface illustrates a very low degree of cell-to-cell communication between CMECs growing in close proximity. A lack of exosome expression subsequently culminated in a lack of direct cell-to-cell contact in the form of TUNT and TENT extracellular protrusions. The paucity of NT formation resulted in the noticeable failure to induce the juxtapositioning of CMEC membranes amounting to no hemifusion of the CMEC apicolateral borders (**Figures 11A–C**).

DISCUSSION

Many studies allude to tunneling NTs (TUNTs) being the nexus of biochemical signaling between cells that exhibit extracellular cytoplasmic projections from cell membrane surfaces. This is well-documented in diverse tissues, and crucial for a myriad of physiological processes such as embryogenesis, stem cell differentiation, cell migration and wound healing (Gerdes et al., 2013). Although BECs are central to the establishment of a highly regulated BBB, little is known about the cellular interaction at the level of the PC space. We observed two types of these NTs involved at the PC juncture between adjacent BECs. Using HRSEM to document the sequential interaction at the PC space we postulate the role that these membrane structures play in the formation of a "tight" PC space. In theory, BBB models describing intercellular TJ functionality has been over-simplified. This has been especially conspicuous when analyzing the development of the BBB *in vitro*, using HREM. The micrographical HREM analysis, in this study, documents the snapshot development of the BEC monolayer, as the anatomical basis of the *in vitro* BBB. Nevertheless, these *in vitro* intercellular mechanisms have to correlate closely to the *in vivo* mechanisms of BBB angiogenesis. Direct cell-to-cell communication via ultrastructural interaction of NVs and NTs are novel and special to this study in our pursuit to elucidate, morphologically, the evolution of the BEC into a functional BBB construct.

EC heterogeneity throughout the human body is influenced by its extracellular matrix (ECM), which is promoted by the diverse composition of its basement membrane (BM). Establishing appropriate spatial orientation of a BEC, in culture is paramount to accurately map the progression and orientation of cells during the establishment of the endothelium. The main factor affecting the EC orientation is in selecting a suitable "physiological" base on which BECs can attach themselves *in vitro*. The mixed cellulose esters insert membrane serves as a viable proxy endorsing BM development of the b.End3 and b.End5 cells. In this study, we observe the "secretion" of an amorphous BM which allowed BEC consolidation into a perfectly orientated monolayer, an essential prerequisite for proper expression of domain-specific BBB ultrastructures and protein expression during its development and subsequent angiogenesis (**Figure 1**). We postulate that this feature is central to the functional orientation of BECs and the TJ enabled sealing of the PC space, a key component of BBB regulation (Fisher and Mentor, 2019).

During growth and development, it is well-reported that cells are inclined to release extracellular vesicles (EVs) of varying sizes (Delmas et al., 2003; Iraci et al., 2016; Datta et al., 2018). We observe, for the first time, EVs sized within an average range of 3–300 nm and, thus, we denote these EVs as NV (refer to **Table 1**). NVs that have the ability to remain bound to target ECs were reported to transfer proteins anchored within the vesicle membranes, into the plasma membranes of recipient cells according to an early study conducted by Rieu et al. (2000) the literature gives heed to the presence of α4βL-integrin found on reticulocyte exosomes which could bind to the vascular cell adhesion molecule-1 (VCAM-1) on ECs which lead to the cargoing of glycosylphatidylinositol-bound proteins (i.e., acetylcholine) into the plasma membranes of recipient cells, moreover, exosomes are reported to play a functional role in the delivery of prostaglandins to target cells (Samanta et al., 2018). The surface of these membrane-bound, nanosized vesicles are reported to be comprised of saccharide groups, rich in polylactoseamine, α2.6 sialic acid and N-linked glycans (Rieu et al., 2000; Samanta et al., 2018). Similarly, EVs are vehicles for a large number of miRNAs involved in cardiovascular disorders. In the literature, EVs, treated with miR-150 was reported to increase EC migration and miR-126 elevated various types of EVs, promoting re-endothelialization *in vivo*, making EVs an important regulator of angiogenesis and vascular integrity (Samanta et al., 2018) this illuminates the important role for EVs/NVs in a plethora of physiological and pathophysiological functions.

Relationship Between Exosomes and Nanotubules

By using backscattered secondary electrons, HRSEM allows a resolution of structures approximately 10 nm or less, which permitted us to ascertain sizes of exosomes (Zhou et al., 2007). Upon HRSEM analysis of BECs, grown to 70–80% confluence, enabled the visualization of a myriad of EVs. With reference to **Table 1**, it is still unclear as to which accepted categorization standards are utilized when classifying the EVs according to function, size and shape. In this study, the micrographical data alludes to potential exosome formation (30–100 nm), however, due to the irregular variation in size from 30 to 300 nm coining these vesicles "exosomes" as the definitive nomenclature utilized becomes imprecise (**Figures 2**, **4A–C**). In terms of its physical properties, the NV exhibits a sticky topographical surface (**Figure 2**) and attaches to the plasma membrane on its apicolateral surface. Studies conducted by Purushothaman et al. (2016) reports on heparin sulfate material found on exosome membranes which suggests that heparin sulfate acts as a target for fibronectin on the cell surface, alluding to the mechanism whereby these exosomes are "sticky" (Sarrazin et al., 1965; Purushothaman et al., 2016).

Although there have been no reports in the literature regarding the secretion or function of vesicle/exosome secretion from BECs, the phenomenon of exosomes being extruded from cells is supported by work described in LeBleu et al. (2007) and György et al. (2011) and are reported to originate from endocytic vesicles which have been exocytosed onto the cell surface. The contents within a typical exosome depend greatly on the intracellular mechanisms whereby the endosome is reported to be enriched with many bioactive molecules, i.e., proteins, lipids, mRNA and miRNA (Cheng et al., 2017). Cheng et al. (2017), goes on to report that the exosome possesses the ability to traffic paracrine factors, i.e., vascular endothelial growth factor, matrix metalloproteinase, these are proteins vital for angiogenesis within an EC. Also, exosomal studies on mesenchymal stem cells (MSC) reports on its exosomes possessing over 900 proteins. Moreover,

exosomes have the capacity to influence the mediation of molecular signaling, by intercellular transferring of information in major biological processes such as cell survival, apoptosis, immune disease and neurological disease (Cheng et al., 2017; LeBleu and Kalluri, 2020).

This study explores an additional class of EVs that form a hybrid vesicle exceeding the size of a typical exosome but does not reach the 1000 nm size as those of the microvesicles. We, therefore, introduce the taxonomic term, "nanovesicle" (NV). The micrographs in **Figures 2**, **4** suggests that these NVs are of the first nanostructures that appears as BEC populations grow more proximally and its porous nature suggests that it plays an integral role in paracrine communication between cells, a pre-requisite for the transformation of the plasmalemma's leading edges into NT cross-bridges, therefore, serving as a mediator of cell-to-cell communication. This study proposes that the *de novo* synthesis of the NVs of BECs appears to be triggered by extrinsic paracrine factors released from closely approximated neighboring BECs and is supported by the absence of NVs and NTs on cells growing in sparse populations (**Figure 1**).

Primordial TUNTs and TENTs

Actinmyosin bundles have recently been documented in the literature to facilitate adhesion junctions (AJs) within the PC space (Rajakylä et al., 2020). Rajakylä et al. (2020) discriminate between two distinct actin filamentous populations which are separated in semi-confluent epithelial cultures, but upon cell-to-cell contact, morph into indiscriminate cortical actin rings of polarized epithelial cells. It is well reported in the literature that peripheral protuberances of cellular cytoplasm are comprised of actin-myosin bundles, which are contractile and are modulated by Rac1, CDC42 and RhoA activity. These filaments have been documented as running parallel to cell-cell junctions (i.e., TJs, AJs and desmosomes) (Vaezi et al., 2002; Zhang et al., 2005; Gomez et al., 2011; Rajakylä et al., 2020). Conversely, in our study, we observe for the first time, cell membranous NT projections "tunneling" toward target cells, which display distinctly different phenotypical characteristics when compared to the membranous, actin-based leading edges of epithelial cell membranes.

The micrographical data in this study animates two novel NTs which exhibits cellular extensions gravitating toward target PM surfaces of the PC space. It is important to note that NT formation can assume both close-ended and open-ended structures depending on their chronological stage of formation and the process of distal end fusing with the target cell membrane. This expression of the TUNTs are a culmination of cumulative NV vesicles which fuse to form TUNTs. Moreover, these TUNTs extend between two BEC membranes and are a *proviso* required for proper spatial interaction between closely approximated BECs (**Figures 3**, **6**).

Open-Ended Nanotubes

HRSEM observations show the *de novo* synthesis of the TUNTs induced by the fusion of multiple NVs and the amalgamation of its contents (**Figure 4**). The TUNTs identified in this study form within a 24–48 h period, and appear bi-directional, ultimately forming "tunneling" tubes between adjacent b.End5 cells (**Figures 5–7**). Based on the NTs described in this study there are stark disparities between the TUNTs in the current study compared to TUNTs described in the literature.

TUNTs form thin tubular channel connecting adjacent cells across the PC space, permitting cell-to-cell trafficking of biomolecules and organelles (Sáenz-de-santa-maría et al., 2017). The TUNTs in this study appear to facilitate cell membrane alignment and TJ protein interaction at the PC borders of BECs. The membranous interaction induces hemifusion of BEC membranes within the PC domain. The "tunneling" tubes formed by the TUNTs (**Figures 4**, **6**, and **7**) result in the juxtapositioning of adjacent BEC membranes suggesting that these NT ultrastructures play an integral role in the transferring of molecular signals which cause BECs to engage in proximal communication to initiate the establishment of a barrier construct. We, therefore, postulate that these fused tubular structures are a distinct category of "tunneling" NTs (**Figures 4A–C**), and are crucial to the alignment of TJ-zones and the formation of tightly, sealed PC spaces.

NT ultrastructures can give rise to open-ended, tunneling tubes, with varying diameters. According to literature, the diameters of these NTs can range between (50 and 800 nm) (Gerdes et al., 2007) in endothelial progenitor cells and rat cardiac myocytes and (500–2000 nm wide) in neural crest cells (Gerdes et al., 2007; Abounit et al., 2016) with the physical connection being 50–200 nm wide (Rustom et al., 2004). Studies conducted by Gerdes et al. (2013), further support the description of these intercellular structures, as forming transiently, not in contact with the substrate and have been observed as hovering structures within the medium.

We postulate that the PC ultrastructural NT interactions are directed by a chemogradient which in turn is generated by the paracrine contents of NVs exocytosed onto BEC membranes. We use **Figures 12A,B** to illustrate the mechanism by which we postulate NTs are attracted to adjacent cells across the paracellular space. The NV gradient is established when BECs are grown on an insert in close proximity (70–80% confluence). Initially, earlier studies, describe extending filopodia as leading edges or motile extensions of the cell membrane border, observed particularly during cell migration, as well as describing filopodial extensions as basolateral cytoplasmic projections. Earlier studies have most likely grown cells on a Petri dish or slides, and not on a surface that allows for correcting cellular orientation and their lateral engagement with each other.

The PC membranous leading edges in this study, however, have direction and are guided by exocytosed, signaling molecules secreted by NVs. The results depict the pulling of plasma membrane folds by NTs across the PC space. We, thus, infer that the sealing off of the PC space is regulated by NT transference of cytoplasmic molecular signals (**Figures 6**, **7**).

Tethering Nanotubes

In addition to the TUNTs, our study documents the emergence of a second NT, which can be likened to rope-like tethers. In

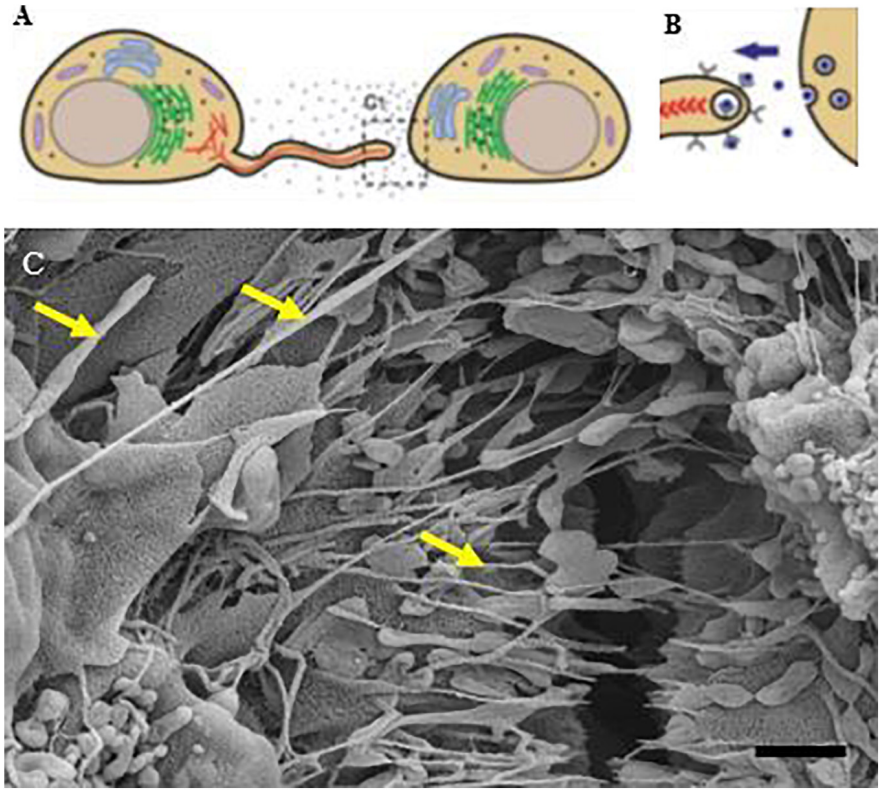

FIGURE 12 | An illustration of basolateral NT progression from membranous filopodia into "closed-ended" structures **(A,B)** (Fulga and Rørth, 2002; Gurke et al., 2008). **(C)** Depicts, morphologically, the formation of TUNTs and TENTs grown on a Millicell substrate and displaying apicolateral projecting nanotubes as seen by the "yellow arrows." Scale bar = 1,000 nm.

this study, they are denoted as tethering NTs (TENTs). TENTs protrude and pull the cell membrane toward neighboring cells over proximal distances (**Figures 9**, **10**). The extension of the membranous surplus suggests that TENTs have two functions: (i) The primary function, is to mechanically stabilize and align the PC space, so that TJs zones between adjacent cells are aligned, enabling the molecular connection between TJs of adjacent cells, and (ii) it forms a "curtain-like" leaflet over the apical PC space, which fuses with the adjacent (target) cell membrane, forming an overlapping membranous structure, covering the site of TJ and in the case of the BEC, contributes to the occlusion of the PC space, contributing to the integrity of the BBB. Speculation on the purpose of the PC membrane overlap, or membrane fold, suggests that it reduces the shear-stresses of blood flow and assist in the occlusion of the PC space, *as well as* protecting the underlying TJ occlusion zone. We show for the first time how TENTs play an important role in this process.

It is established in the literature that BECs seal their PC spaces by aligning the apicolateral zones so precisely that the TJs on the adjacent cells could align and be closely juxtaposed to each other, for inter-TJ molecular bonding to occur and seal off the PC spaces. Hitherto, it has been unclear as to how these "apicolateral" zones of TJs between two adjacent cells are aligned to allow TJs from adjacent membranes to molecularly bond to each other, creating an impermeable PC seal (Fisher and Mentor, 2019). Thus, both TENT and TUNTs play an integral role in aligning juxtaposed lateral sides of BECs and in the establishing of PC occlusion between the neighboring BECs by approximating adjacent zones of TJs so closely that molecular bonding occurs between TJs of adjacent cells (**Figures 6**, **7**).

The HRTEM experimental model utilized for BECs, grown on inserts, was identical to HRSEM, but was subjected to HRTEM tissue processing. The HRTEM images resemble the features of the *in vivo* TEM micrographs, especially with respect to membrane fold at the PC space and TJ "stitching/interaction beneath the overlapping region (Nitta et al., 2003). These *in vivo* features strongly supports the use of b.End5 cells for use in *in vitro* BBB models.

Hemifusion

In the literature, TJ (i.e., claudin-5 and occludin) localization is well documented as being restricted to the apicolateral domain of the PC space forming loop-like protein structures that are interconnected with their respective counterparts on an adjacent BEC (Nitta et al., 2003). HRSEM micrographs clearly depict the "stitching together" emulated by TJ protein-protein interaction between adjacent PC apicolateral membranes. TENTs (**Figures 7**, **8**) observably adjusts the alignment of

adjacent membranes of BEC growing on the insert membrane. Upon the juxtapositioning of the two membranes, a hemi-junction of the plasmalemma develops upon close contact. We, therefore, propose that TUNTs are requisite for this phenomenon to occur. The TUNT provides the molecular signaling and "cross-talk" between adjacent BECs which is required to facilitate preparing the lateral BEC membranes for a juxtapositioned configuration of the PC space. This direct signaling via TUNTs permits highly specialized TJ molecular zonal interaction, at its apicolateral domains (**Figures 6**, **7**). This study describes, for the first time, the features of an *in vivo* BBB model, in the development of an *in vitro* BBB (DeStefano et al., 2018; **Figure 8B**). **Figure 8B**. illustrates theoretical intercellular junctional protein complexes found within the PC space between two adjacent BEC PMs. The proximal location of these adjacent PM leaflets results in the molecular point to point interaction between closely approximated BECs within the apicolateral domain of the PC space. The intercellular interactions in this scenario suggest a strict chronological process that, when unraveled, displays the specific process whereby occlusal apicolateral TJ protein-protein interaction occurs. The partial "stitching together" of TJs are located beneath sealed-off, hemifused intercellular membrane leaflets. TENTs are essential for the formation of overlapping membranes across the PC space and are well described in *in vivo* TEM studies of the brain capillaries. The overlapping membrane across the PC space may play an important role in sealing the PC space and decreasing shear stress at the level of TJs by causing a continuous covering over TJ loci (**Figures 9**, **10**). These findings, therefore, sheds new light on TJ localization and the morphological ultrastructures reinforcing the BBB as a highly regulated and restrictive barrier.

TENTs are "rope-like" nanostructures in this study that attach themselves to the target cells' plasma membranes, expressing closed-ended, bulb-like projections, with reference to the "white circle" in **Figure 7**. It could be debated that protruding structures of this nature are likely long-filopodial protuberances, Early in the literature, reports on filopodial extensions morphing into long, slender structures, from the surface of the cell membrane denoted as cytonemes by Gerdes et al. (2007) and Kimura et al. (2012). To date, this particular structure has been observed in a few cell types, namely: T-cells, normal rat kidney (NRK) and neural crest cells (NCs) (Sowinski et al., 2008; Wang et al., 2010; Gerdes et al., 2013). Ramírez-Weber and Kornberg (1999), described filopodial intercellular processes as an established type of cell-to-cell communication.

Do Systemic Endothelial Cells Display the Same Features?

A comparison of cell-to-cell communication between systemic ECs was essential for elucidating the ultrastructural complexity of BBB development. For the purpose of this study, we have utilized the primary rat cardiac microvascular endothelial cell line (CMEC). We observed, for the first time, the cell-to-cell interaction at high-resolution of CMECs grown on an insert, similarly to b.End3 and b.End5 cells. Our results exhibited a large degree of fenestra on their cell membrane surfaces (**Figure 11A**). Concurrently, there was a marked absence of NVs on the surface of the CMEC membrane, large PC spaces and little-to-no primordial NT development, compared to BECs (**Figures 4**, **11**). These findings provide us with additional supporting evidence to infer that NTs are pivotal for the establishment of "tight" endothelial barriers and that this level of molecular and cellular anatomical organization is unique to the development of the BBB.

CONCLUSION

The novel findings in this study beg the question, "Is BBB integrity and PC occlusion solely orchestrated by TJ interaction?" In this study, we observed the presence of novel ultrastructures: A 3-D representation of a basement membrane (BM), NVs, TUNTs and TENTs. NVs play a significant role in the induction of TUNT formation, by way of paracrine communication. We describe for the first time the novel formation of intercellular NTs that are formed from the fusing of secreted vesicles to form hollow TUNTs connecting adjacent cells, presumably to facilitate the cross-talk between cells to form and align adjacent TJ zones.

The correct BEC alignment is ensured by two important features observed, for the first time, in this study: (i) the extrusion of an amorphous basement membranous structure, formed in the basal domain of BECs during monolayer establishment in culture. The BM ensures that apical and basolateral cellular orientation is achieved. The correct spatial orientation of a BEC allows for the efficient sorting of the PC TJ protein interaction within its respective domains; (ii) the induction of TUNTs bring about the eventual juxtapositioning of apicolateral BEC membranes by forming a scaffolding network of tunneling tubules which facilitates BEC alignment.

Most importantly, closed-ended TENT action results in the overlapping of membranous leaflets across the cellular cleft, establishing an occluded PC space. This study, thus, postulates that intercellular TJ protein-protein interaction is dependent on the formation of dynamic nanoscale networks. Thus, ultrastructural events (i.e., BM establishment, NV and NT formation) strictly govern the molecular underpinnings of BBB integrity and are requisite for the interaction of claudin-5 and occludin. NT-induced juxtapositioning of adjacent BEC membranes sets the precedent for TJ interaction and subsequent hemifusion of its neighboring membranes, which positively contributes to the establishment of a strictly regulated BBB.

DATA AVAILABILITY STATEMENT

All experimental data collected is archived within the University of the Western Cape (UWC) archives and is available as per UWC data and intellectual property policy guidelines and its associated copyright protection.

AUTHOR CONTRIBUTIONS

SM: investigation, methodology, data curation, formal analysis, conceptualization, and writing. DF: supervision, funding acquisition, project administration, conceptualization, and writing. Both authors contributed to the article and approved the submitted version.

FUNDING

This work was supported by the National Research Foundation (NRF) (Grant Number 116533) and the Fuch's Foundation Doctoral Scholarship. The funders had no role in study design, data collection and analysis, decision to publish, or preparation of the manuscript. This work was supported by the laboratory infrastructural and academic support provided by the Department of Medical Biosciences at the University of the Western Cape (UWC) and the Electron Microscopy Units at UWC and the University of Cape Town, South Africa.

SUPPLEMENTARY MATERIAL

The Supplementary Material for this article can be found online at: https://www.frontiersin.org/articles/10.3389/fnana.2021.661065/full#supplementary-material

Supplementary Figure 1 | An HRSEM micrograph of a b.End5 cell expressing NVs and primordial NTs on its cell membrane surface (scale bar = 200 nm).

REFERENCES

Abounit, S., Wu, J. W., Duff, K., Victoria, G. S., and Zurzolo, C. (2016). Tunneling nanotubes: a possible highway in the spreading of tau and other prion-like proteins in neurodegenerative diseases. *Prion* 10, 344–351. doi: 10.1080/19336896.2016.1223003

Cheng, L., Zhang, K., Wu, S., Cui, M., and Xu, T. (2017). Focus on mesenchymal stem cell-derived exosomes: opportunities and challenges in cell-free therapy. *Stem Cells Int.* 2017:6305295.

Datta, A., Kim, H., McGee, L., Johnson, A. E., Talwar, S., Marugan, J., et al. (2018). High-throughput screening identified selective inhibitors of exosome biogenesis and secretion: a drug repurposing strategy for advanced cancer. *Sci. Rep.* 8:8161.

Delmas, C., End, D., Rochaix, P., Favre, G., Toulas, C., and Cohen-Jonathan, E. (2003). The Farnesyltransferase inhibitor R115777 reduces Hypoxia and Matrix Metalloproteinase 2 expression in human Glioma Xenograft. *Clin. Cancer Res.* 9, 6062–6068.

DeStefano, J. G., Jamieson, J. J., Linville, R. M., and Searson, P. C. (2018). Benchmarking in vitro tissue-engineered blood–brain barrier models. *Fluids Barriers CNS* 15:32.

Dyer, L. A., and Patterson, C. (2010). Development of the endothelium: an emphasis on heterogeneity. *Semin. Thromb. Hemost.* 36, 227–235. doi: 10.1055/s-0030-1253446

Engelhardt, B., and Liebner, S. (2014). Novel insights into the development and maintenance of the blood-brain barrier. *Cell Tissue Res.* 355, 687–699. doi: 10.1007/s00441-014-1811-2

Faso, L., Trowbridge, R. S., Quan, W., Yao, X. L., Jenkins, E. C., Maciulis, A., et al. (1994). Characterization of a strain of cerebral endothelial cells derived from goat brain which retain their differentiated traits after long-term passage. *Vitr. Cell. Dev. Biol. Anim.* 30, 226–235. doi: 10.1007/bf02632044

Fisher, D. F., and Mentor, S. (2019). Are claudin-5 tight-junction proteins in the blood-brain barrier porous? *Neural Regen. Res.* 15, 1838–1839.

Fulga, T. A., and Rørth, P. (2002). Invasive cell migration is initiated by guided growth of long cellular extensions. *Nat. Cell. Biol.* 4, 715–719. doi: 10.1038/ncb848

Gerdes, H. H., Bukoreshtliev, N. V., and Barroso, J. F. V. (2007). Tunneling nanotubes: a new route for the exchange of components between animal cells. *FEBS Lett.* 581, 2194–2201. doi: 10.1016/j.febslet.2007.03.071

Gerdes, H. H., Rustom, A., and Wang, X. (2013). Tunneling nanotubes, an emerging intercellular communication route in development. *Mech. Dev.* 130, 381–387. doi: 10.1016/j.mod.2012.11.006

Gomez, G. A., McLachlan, R. W., and Yap, A. S. (2011). Productive tension: force-sensing and homeostasis of cell-cell junctions. *Trends. Cell Biol.* 21, 499–505. doi: 10.1016/j.tcb.2011.05.006

Gupta, A., Rarick, K. R., and Ramchandran, R. (2021). Established, new and emerging concepts in brain vascular development. *Front. Physiol.* 12:636736.

Gurke, S., Barroso, J. F. V., and Gerdes, H. H. (2008). The art of cellular communication: tunneling nanotubes bridge the divide. *Histochem. Cell Biol.* 129, 539–550. doi: 10.1007/s00418-008-0412-0

György, B., Szabó, T. G., Pásztói, M., Pál, Z., Misják, P., Aradi, B., et al. (2011). Membrane vesicles, current state-of-the-art: emerging role of extracellular vesicles. *Cell Mol. Life Sci.* 68, 2667–2688. doi: 10.1007/s00018-011-0689-3

Haseloff, R. F., Dithmer, S., Winkler, L., Wolburg, H., and Blasig, I. E. (2015). Transmembrane proteins of the tight junctions at the blood-brain barrier: structural and functional aspects. *Semin. Cell Dev. Biol.* 38, 16–25. doi: 10.1016/j.semcdb.2014.11.004

Hawkins, B. T., and Davis, T. P. (2005). The blood-brain barrier/neurovascular unit in health and disease. *Pharmacol. Rev.* 57, 173–185. doi: 10.1124/pr.57.2.4

Iraci, N., Leonardi, T., Gessler, F., Vega, B., and Pluchino, S. (2016). Focus on extracellular vesicles: physiological role and signaling properties of extracellular membrane vesicles. *Int. J. Mol. Sci.* 17:171. doi: 10.3390/ijms17020171

Kimura, S., Hase, K., and Ohno, H. (2012). Tunneling nanotubes: emerging view of their molecular components and formation mechanisms. *Exp. Cell Res.* 318, 1699–1706. doi: 10.1016/j.yexcr.2012.05.013

LeBleu, V. S., and Kalluri, R. (2020). Exosomes as a multicomponent biomarker platform in cancer. *Trend. Cancer* 6, 767–774. doi: 10.1016/j.trecan.2020.03.007

LeBleu, V. S., MacDonald, B., and Kalluri, R. (2007). Structure and function of basement membranes. *Exp. Biol. Med.* 232, 1121–1129.

Lucas, W. J., Ham, B. K., and Kim, J. Y. (2009). Plasmodesmata - bridging the gap between neighboring plant cells. *Trends Cell Biol.* 19, 495–503. doi: 10.1016/j.tcb.2009.07.003

Martins, T., Burgoyne, T., Kenny, B. A., Hudson, N., Futter, C. E., Ambrósio, A. F., et al. (2013). Methamphetamine-induced nitric oxide promotes vesicular transport in blood-brain barrier endothelial cells. *Neuropharmacology* 65, 74–82. doi: 10.1016/j.neuropharm.2012.08.021

Nitta, T., Hata, M., Gotoh, S., Seo, Y., Sasaki, H., Hashimoto, N., et al. (2003). Size-selective loosening of the blood-brain barrier in claudin-5-deficient mice. *J. Cell Biol.* 161, 653–660. doi: 10.1083/jcb.200302070

Okuda, K. S., and Hogan, B. M. (2020). Endothelial cell dynamics in vascular development: insights from live-imaging in Zebrafish. *Front. Physiol.* 11:842.

Purushothaman, A., Bandari, S. K., Liu, J., Mobley, J. A., Brown, E. A., and Sanderson, R. D. (2016). Fibronectin on the surface of myeloma cell-derived exosomes mediates exosome-cell interactions. *J. Biol. Chem.* 291, 1652–1663. doi: 10.1074/jbc.m115.686295

Qosa, H., Mohamed, L. A., Al Rihani, S. B., Batarseh, Y. S., Duong, Q. V., Keller, J. N., et al. (2016). High-throughput screening for identification of blood-brain barrier integrity enhancers: a drug repurposing opportunity to rectify vascular amyloid toxicity. *J. Alzheimer's Dis.* 53, 1499–1516. doi: 10.3233/jad-151179

Rajakylä, E. K., Lehtimäki, J. I., Acheva, A., Schaible, N., Lappalainen, P., Krishnan, R., et al. (2020). Assembly of peripheral actomyosin bundles in epithelial cells is dependent on the CaMKK2/AMPK pathway. *Cell Rep.* 30, 4266–4280.e4.

Ramírez-Weber, F. A., and Kornberg, T. B. (1999). Cytonemes: cellular processes that project to the principal signaling center in Drosophila imaginal discs. *Cell* 97, 599–607.

Rieu, S., Géminard, C., Rabesandratana, H., Sainte-Marie, J., and Vidal, M. (2000). Exosomes released during reticulocyte maturation bind to fibronectin via integrin α4β1. *Eur. J. Biochem.* 267, 583–590. doi: 10.1046/j.1432-1327.2000.01036.x

Risau, W., and Flamme, I. (1995). Vasculogenesis. *Annu. Rev. Cell Dev. Biol.* 11, 73–91.

Ruhrberg, C., and Bautch, V. L. (2013). Neurovascular development and links to disease. *Cell Mol. Life Sci.* 70, 1675–1684. doi: 10.1007/s00018-013-1277-5

Rustom, A., Saffrich, R., Markovic, I., Walther, P., and Gerdes, H. H. (2004). Nanotubular highways for intercellular organelle transport. *Science* 303, 1007–1010. doi: 10.1126/science.1093133

Sáenz-de-santa-maría, I., Bernardo-castiñeira, C., and Enciso, E. (2017). Control of long-distance cell-to-cell communication and autophagosome transfer in squamous cell carcinoma via tunneling nanotubes. *Oncotarget* 8, 20939–20960. doi: 10.18632/oncotarget.15467

Samanta, S., Rajasingh, S., Drosos, N., Zhou, Z., Dawn, B., and Rajasingh, J. (2018). Exosomes: new molecular targets of diseases. *Acta. Pharmacol. Sin.* 39, 501–513. doi: 10.1038/aps.2017.162

Sarrazin, S., William, C. L., and Jeffrey, D. E. (1965). Heparan sulfate proteoglycans stephane. *neoplasma* 12, 549–556.

Saunders, N. R., Dreifuss, J. J., Dziegielewska, K. M., Johansson, P. A., Habgood, M. D., Møllgård, K., et al. (2014). The rights and wrongs of blood-brain barrier permeability studies: a walk through 100 years of history. *Front. Neurosci.* 8:404.

Schwich, E., and Rebmann, V. (2018). The inner and outer qualities of extracellular vesicles for translational purposes in breast cancer. *Front. Immun.* 9:584.

Sowinski, S., Jolly, C., Berninghausen, O., Purbhoo, M. A., Chauveau, A., Köhler, K., et al. (2008). Membrane nanotubes physically connect T cells over long distances presenting a novel route for HIV-1 transmission. *Nat. Cell Biol.* 10, 211–219. doi: 10.1038/ncb1682

Tamkovich, S. N., Medicine, F., Tutanov, O., and Medicine, F. (2016). Exosomes: generation, structure, transport, biological activity, and diagnostic application. *Biochem. Suppl. Ser. A. Membr. Cell. Biol.* 10, 163–173.

Vaezi, A., Bauer, C., Vasioukhin, V., and Fuchs, E. (2002). Actin dynamics and Rho/Rock orchestrate a polarized cytoskeletal architecture in the early steps of assembly of stratified epithelium. *Dev. Cell* 3, 367–381. doi: 10.1016/s1534-5807(02)00259-9

Wang, X., Veruki, M. L., Bukoreshtliev, N. V., Hartveit, E., and Gerdes, H. (2010). Animal cells connected by nanotubes can be electrically coupled through interposed gap-junction channels. *Proc. Natl. Acad. Sci. USA.* 107, 17194–17199. doi: 10.1073/pnas.1006785107

Watanabe, T., Dohgu, S., Takata, F., Nishioku, T., Nakashima, A., Futagami, K., et al. (2013). Paracellular barrier and tight junction protein expression in the immortalized brain endothelial cell lines bEND.3, bEND.5 and mouse brain Endothelial Cell 4. *Biol. Pharm. Bull.* 36, 492–495. doi: 10.1248/bpb.b12-00915

Zhang, J., Betson, M., Erasmus, J., Zeikos, K., Bailly, M., Cramer, L. P., et al. (2005). Actin at cell-cell junctions is composed of two dynamic and functional populations. *J. Cell Sci.* 118, 5549–5562. doi: 10.1242/jcs.02639

Zhou, W., Apkarian, R., Wang, Z. L., and Joy, D. (2007). "Fundamentals of scanning electron microscopy (SEM)," in *Scanning Microscopy for Nanotechnology*, eds W. Zhou and Z. L. Wang (New York, NY: Springer).

Conflict of Interest: The authors declare that the research was conducted in the absence of any commercial or financial relationships that could be construed as a potential conflict of interest.

CHAPTER FOUR: 'THE ROLE OF CYTOSKELETAL PROTEINS IN THE FORMATION OF A FUNCTIONAL *IN VITRO* BLOOD-BRAIN BARRIER MODEL'

International Journal of
Molecular Sciences

MDPI

Article

The Role of Cytoskeletal Proteins in the Formation of a Functional In Vitro Blood-Brain Barrier Model

Shireen Mentor [1], Khayelihle Brian Makhathini [1] and David Fisher [1,2,*]

[1] Neurobiology Research Group, Department of Medical Biosciences, University of the Western Cape, Cape Town 7535, South Africa; 2746944@myuwc.ac.za (S.M.); kmakhathini@uwc.ac.za (K.B.M.)
[2] School of Health Professions, University of Missouri, Columbia, MO 65211, USA
* Correspondence: dfisher@uwc.ac.za; Tel.: +27-21-959-2185

Abstract: The brain capillary endothelium is highly regulatory, maintaining the chemical stability of the brain's microenvironment. The role of cytoskeletal proteins in tethering nanotubules (TENTs) during barrier-genesis was investigated using the established immortalized mouse brain endothelial cell line (bEnd5) as an in vitro blood-brain barrier (BBB) model. The morphology of bEnd5 cells was evaluated using both high-resolution scanning electron microscopy and immunofluorescence to evaluate treatment with depolymerizing agents Cytochalasin D for F-actin filaments and Nocodazole for α-tubulin microtubules. The effects of the depolymerizing agents were investigated on bEnd5 monolayer permeability by measuring the transendothelial electrical resistance (TEER). The data endorsed that during barrier-genesis, F-actin and α-tubulin play a cytoarchitectural role in providing both cell shape dynamics and cytoskeletal structure to TENTs forming across the paracellular space to provide cell-cell engagement. Western blot analysis of the treatments suggested a reduced expression of both proteins, coinciding with a reduction in the rates of cellular proliferation and decreased TEER. The findings endorsed that TENTs provide alignment of the paracellular (PC) spaces and tight junction (TJ) zones to occlude bEnd5 PC spaces. The identification of specific cytoskeletal structures in TENTs endorsed the postulate of their indispensable role in barrier-genesis and the maintenance of regulatory permeability across the BBB.

Keywords: nanotubules; Cytochalasin D; Nocodazole; brain endothelial cells; barrier-genesis

Citation: Mentor, S.; Makhathini, K.B.; Fisher, D. The Role of Cytoskeletal Proteins in the Formation of a Functional In Vitro Blood-Brain Barrier Model. *Int. J. Mol. Sci.* **2022**, *23*, 742. https://doi.org/10.3390/ijms23020742

Academic Editor: Hyunsoo Cho

Received: 17 November 2021
Accepted: 7 January 2022
Published: 11 January 2022

1. Introduction

The brain microvascular endothelial cells (BECs) play a critical role as an interdependent network constituting the basic angioarchitecture of the blood-brain barrier (BBB) [1]. The functionality of the BBB is closely related to the regulation of permeability and entails paracellular (PC) sealing by intercellular tight junction (TJ) protein complexes as a central feature of the barrier's physical function. How the zones of the TJs are aligned is crucial to their action. Compared to systemic endothelial cells, the apico-lateral expression of the TJs is specific, unique, and depends on the correct orientation of the BECs into the apical and basal domains [1]. The mechanics that are required for two juxtaposed BEC membranes to align in a manner that enables TJ interaction with its counterparts on adjacent cells have recently been described from an ultrastructural perspective, highlighting for the first time, the importance of nanotubules (NTs) in the physical alignment of adjacent BECs by utilizing high-resolution electron microscopy (HREM) [2]. Two types of novel NTs were discovered as a form of direct BEC–cell interaction at the apico-lateral domains of BECs and can be categorically differentiated into (i) nanovesicle (NV)-induced tunneling NTs (TUNTs) and (ii) tethering NTs (TENTs). The study illuminates the ultrastructural prowess of these NTs to generate an extracellular PC scaffolding, which facilitates TJ interaction and PC occlusion. Moreover, TENTs were described as novel nanostructural cross-bridges that emerged transiently as a supplementary means of direct cell-cell communication during immortalized mouse BEC (bEnd3/bEnd5) monolayer development in vitro, which

has become a significant feature in redefining the mechanobiology that is involved in TJ localization during in vitro BBB establishment.

Although intercellular communication has revolutionized our understanding of barriergenesis concerning BBB establishment, however, little is known about its nanoscopic development, thus limiting our understanding of the mechanobiology that is associated with its physical functionality.

Defining the BEC ultrastructural interaction is necessary when elucidating: (i) BEC proliferation dynamics, (ii) angiogenesis, and (iii) BEC permeability, which are critical parameters for ensuring a well-regulated barrier interface. It is known that the BBB is established by TJ protein-protein interactions between adjacent BECs [3–6]. Upon investigating the morphological profile of the BECs on a nanoscale, it was revealed that the barrier interface possesses a complex interactive PC engagement between the adjacent in vitro BECs growing in close proximity [2].

BECs are specifically designed to align with each other, enabling zones of apico-lateral, juxtaposed TJs to form a highly restrictive PC shunt to prevent PC permeability across brain capillaries. Furthermore, the regulatory functions of the BECs would be nullified by a permeable PC space [6].

In recent years, a novel type of cell-cell communication was observed that was based on the formation of NTs between cells. NT ultrastructures were first reported in pheochromocytoma cells and were described as actin-dependent tubules [7]. Similarly, Ma and Zhou et al. [8] under low-resolution reported the formation of membrane protrusion, which they categorized as primary "cilia". They were further described as microtubule, tubulin-based structures, protruding from in vitro BEC cell surfaces [8].

NT cross-bridge formation is a highly prevalent feature between adjacent BECs during in vitro BEC monolayer development [2]. In earlier studies, direct cell-cell communicatory NTs have been described as actin-rich NTs and/or cross-bridge NTs [9]. Although NTs were initially described in rat PC12 cells [7], it has never before been reported to play a functional role in the establishment of the BBB [2].

These recent morphological findings prompted the redefinition of the existing comprehension of barrier-genesis. Interacting BECs that line the brain capillaries, accomplish specific barrier roles, namely: regulating transcellular and PC permeability, which affects the transcellular exchange of metabolites and nutrients. This research paper reports on the cytoskeletal molecular structures, which potentially underpin the formation of TENT structure and function enabling it to generate a functional in vitro BBB model.

Cytoskeletal proteins such as actin-microfilaments have been closely associated with cellular processes such as migration, endocytosis, cytokinesis, and cytoplasmic projections and thus, it is a critical modulator of cell physiology. Moreover, actin has been reported to be the backbone of such cytoplasmic protrusions [9]. Moreover, Gurke et al. [7] reported that cytoplasmic protrusions evolve into NT-like cross-bridges, which are F-actin dependent [7]. A study by Phng et al. [10] supports these findings, reporting on the role of actin polymerization and its ability to ensure the protrusion of filopodial migration between two ECs in dorsal longitudinal anastomotic vessels and blood vein plexus formation [10].

Furthermore, a recent study on microtubules has sparked interest as these structures have been described as surface membrane protrusions on the EC and have been postulated to be critical for the functional role in vascular barrier regulation [8]. In this regard, the literature reports that the destruction of fibroblastic microtubules has a negative impact on protruding actin-rich lamellipodial-based migratory processes. [11,12]. It is further hypothesized that the microtubules are concomitant with the polymerization of actin at the cell leading edges, which induces cytoplasmic projections [11,13].

Thus, TENTs that are generated by BEC surface are membrane NT protrusions that appeared to be integral for the juxtapositioning of BECs to ensure the appropriate intercellular TJ alignment and subsequent occlusion of BEC PC spaces during the establishment of a confluent monolayer. The molecular structures, which underpin TENT cytoskeletal morphology are, however, yet to be investigated. To date, how these TENTs project themselves

across the PC space has not yet to be elucidated. This study focused on the functional role of the cytoskeletal architecture of the BEC as a critical feature governing its mechanobiology, and further postulates that the cytoskeletal proteins F-actin and α-tubulin are implicated in molecular underpinning the mechanisms of TENT formation in the bEnd5 cells.

2. Results

The study investigated the structural organization of the BECs, the cytoskeletal molecular underpinnings of microfilaments and microtubules, and their functional role in establishing BEC monolayer integrity via TENT connections. Recent high-resolution scanning electron microscopy (HR-SEM) observations in our laboratory showed that the nanoscopic morphology of the BEC confluent monolayers exhibits cytoplasmic projections, which are continuous with the leading edges of the BEC membrane (See Figure 1 below).

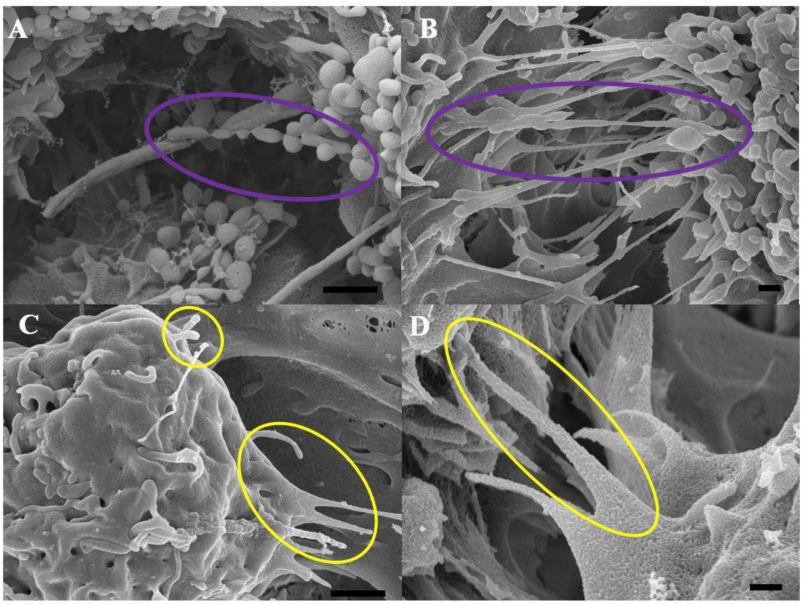

Figure 1. HR-SEM micrographs representing BEC bEnd5 NTs that are subdivided into two types: (**A**) NV-induced TUNTs indicated by the **purple** circles, scale bar 1000 nm; (**B**) TUNT formation and extension across the PC space between adjacent BECs, upon the fusion of multiple NVs, scale bar = 300 nm; (**C**) TENTs formed by the BEC membrane leading edges as indicated by the **yellow** circles, scale bar = 1000 nm; (**D**) A magnified TENT extension across the PC space between two adjacent BECs forming an occluded tent-like covering, scale bar = 300 nm.

2.1. Morphology of BEC Nanotubules at High Resolution

Figure 1A,B, shows the first category of NTs (i.e., TUNTs) which develop during the BEC monolayer establishment. TUNTs were first described in our laboratory and are formed by the fusion of a series of NVs (Figure 1A) into long, continuous cross-bridge TUNTs between adjacent BECs (Figure 1B). Figure 1C, D, shows the second category of NTs which form tether-like NT structures (i.e., TENTs) which transverse the PC spaces of juxtapositioned BECs (see **yellow circles**). The TENTs are formed by cytoplasmic projections from the BEC membrane leading edges (Figure 1C). These cytoplasmic protrusions are continuous with the cell membrane material and extend across the intercellular cleft occluding the PC space (Figure 1D). For this study, we focused on the molecular cytoskeletal functionality of TENT development.

2.2. Cytoarchitecture of the BEC

In the scanning electron micrographs, we described the formation of TENTs between adjacent BECs (Figure 1). In the immunofluorescence (IF) study, we further investigated the role of Alexa Fluor 568-stained cytoskeletal α-tubulin as the intracellular backbone

of TENTs. Figure 2A is a micrograph displaying the cytoplasmic projection of α-tubulin-rich slender microtubes between adjacent BECs. The α-tubulin within TENTs is able to project into the PC space, engaging the BEC membrane on the opposite end, and/or fully fusing with the opposite BEC membrane. Figure 2B, provides a higher magnification of the α-tubulin cytoskeletal elements of these foot-like distal ends of TENTs.

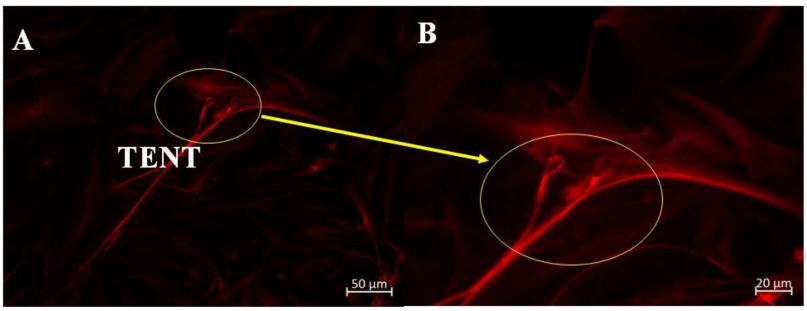

Figure 2. Alexa Fluor 568-stained α-tubulin of a non-treated bEnd3 cell. (**A**) α-tubulin interaction of cells, displaying the intramolecular profile of TENTs; (**B**) The magnification of the interaction of these α-tubulin-based TENT extending between the BECs membranes as indicated by the **yellow** circles.

In both Figure 3A,B, α-tubulin is a cytoskeletal molecular structure that is found throughout the BEC. Figure 3A, shows the extensive α-tubulin-based scaffoldings inside the cell, with long, polymerized α-tubulin molecular structures forming the central cytoskeletal structure of the TENT. Figure 3B, demonstrates that TENTs utilize α-tubulin scaffolding within the soma of the BEC to anchor and project TENTs across the PC spaces of adjacent BECs. α-tubulin, therefore, appears to be a central component of TENTs anchoring substrate which allows tethering tubules to engage with the neighboring cells. TENTs, thus project out of the BEC with a molecular backbone of α-tubulin. In Figure 3C, F-actin is more extensively distributed across the BEC, forming extensive F-actin cytoskeletal scaffolding. We also clearly observe that F-actin that is anchored on the cytoskeletal scaffolding of the BEC extends into the TENTs, forming long polymerized F-actin filamentous structures. Figure 3D shows a magnified version of the propagating F-actin-based cytoskeletal extensions between the BECs that are growing in close proximity.

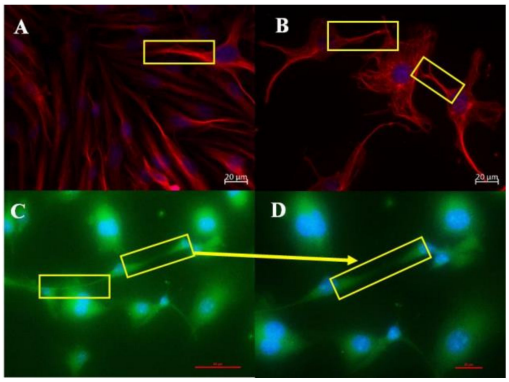

Figure 3. Immunofluorescence (IF) microscopy displays the α-tubulin and F-actin-rich cytoskeletal profile and molecular interaction between adjacent BECs that were grown on coated glass coverslips. (**A**) represents the intracellular molecular profile of α-tubulin-based cytoskeletal projections and the interaction between adjacent BECs; (**B**) Illustrates an extensive tubulin-based cytoarchitecture that is anchored inside the cell and α-tubulin-rich NT extensions from the leading edges of the BEC membranes; (**C**) Shows the intracellular molecular profile of F-actin-rich cytoskeletal projections between adjacent BECs; (**D**) Shows the magnification of F-actin-based NT extensions between adjacent BECs. The **yellow** squares indicate zones of α-tubulin interaction (**A**,**B**) and F-actin interaction (**C**,**D**) between adjacent BECs.

2.3. Chemical Perturbation of the BEC TENT Morphology

2.3.1. Effect of Cytochalasin D on TENT Morphology

The untreated BECs were able to generate intercellular TENT structures. The TENTs characteristically displayed focused development towards the targeted adjacent BEC, forming a cross-bridge scaffolding that results in a highly cross-linked PC space. In Figure 4B, treatment with Cytochalasin D resulted in an observable morphological distortion of intercellular TENTs and a decrease in BEC exosomal NVs. These exosomal NVs were prominently altered, in contrast to Figure 4A where the untreated BECs were able to generate numerous spherical NVs, which accumulated on the BEC membrane surface.

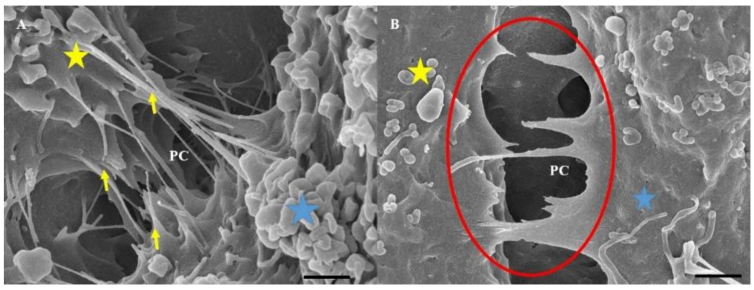

Figure 4. High-resolution scanning electron microscopy (HR-SEM) micrographical representation of the morphological deformation of cell-cell connections between adjacent BECs upon the chemical perturbation of actin polymerization utilizing a known depolymerizing agent, Cytochalasin D. (**A**) Indicates the numerous TENT interactions across the PC space between two bEnd5 cells. The micrograph clearly depicts the extensive formation of tethering-NTs which are naturally taut and project across the PC space; (**B**) A micrograph demonstrating the depolymerizing effect of Cytochalasin D on F-actin of bEnd5 cells where TENT formation is compromised forming thick, brittle-type NTs, as well as a distinct decrease in the TENT formation. An observable decrease in the number of NVs on the treated BEC membrane was seen, compared to the numerous NVs that were located on the control BEC membranes in (**A**). The **yellow** star represents cell 1, the **blue** star represents cell 2, and the paracellular space is denoted by **PC**.

The bEnd5 cells that were treated with Nocodazole failed to promote healthy NV formation and resulted in the formation of irregular shaped and flattened NVs that appeared to have collapsed on themselves. The number of cytoplasmic TENT projections in the Nocodazole-treated bEnd5 cells were distinctly less than the control (Figure 5) and displayed a PC space with a scanty NT network compared to the control conditions.

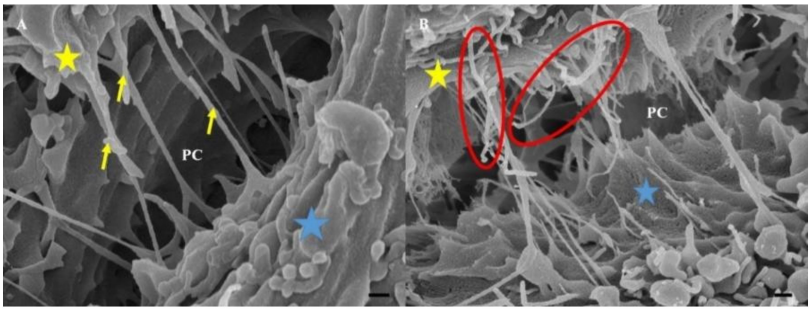

Figure 5. HR-SEM micrographical representation of the morphological deformation of cell-cell connections between adjacent BECs upon Nocodazole-induced cytoarchitectural depolymerization. (**A**) The bEnd5 TENT formation with cells that were grown in standard culture medium. The **yellow** arrows show the normal nature of PC TENTs, reflecting their bearing and tautness; (**B**) The effect of nocodazole exposure on bEnd5 NT formation relative to the control. The **yellow** star represents cell 1, the **blue** star represents cell 2, and the paracellular space is denoted by **PC**. The red circles in (**B**) indicate NTs which have lost their tautness and demonstrate the recoiling of TENTs in the Nocodazole-treated bEnd5 cell cultures.

2.3.2. Effect of Nocodazole on TENT Morphology

In Figure 5A, the untreated bEnd5 cells displayed TENTs that formed tethered attachments between the plasma membrane of cell 1 to cell 2 across the PC space. Furthermore, the TENTs exhibited a characteristically taut appearance, forming a TENT scaffold between the BECs, facilitating cell membrane alignment. In Figure 5B, upon treatment with Nocodazole, the TENTs failed to form correctly. The TENT lost its ability to directly target the juxtaposed lateral plasma membrane across the PC space, failing to form a structured NT network between the BECs due to the recoiling of the TENT structures.

2.4. Effect of Chemical Perturbation on the BEC Cytoskeleton

2.4.1. Effect of Cytochalasin D on BEC Cytoarchitecture

To investigate whether F-actin played a role in maintaining the permeability status across the BEC monolayers, confluent monolayers of bEnd5 cells were treated with selected concentrations of Cytochalasin D. In Figure 6A, the transendothelial electrical resistance (TEER) studies across the BEC confluent monolayers showed an observable decrease in TEER across all concentrations of Cytochalasin D exposure compared to the untreated (control conditions) for 12–24 h. In Figure 6B, significant suppression in the cell numbers was observed ($p < 0.001$) from 12–24 h, relative to controls. At 24 h, the lowest concentration of 0.1 µM showed no significant effects, but upon increasing concentrations of Cytochalasin D, from 0.25 µM to 1 µM, a significant decrease in the cell numbers was observed relative to the controls ($p < 0.01$). In Figure 6C, IF micrographs display the observable progression in F-actin depolymerization between adjacent BECs. The F-actin cytoskeletal extensions became progressively diminished and direct cell-cell interaction between the BECs dissipated. In Figure 6D, quantitative Western blotting analysis showed that, at 12 h exposure to Cytochalasin D (0.1–1 µM) showed a decrease in the amount of the cytoskeletal, microfilamentous protein, F-actin, relative to the control samples. F-actin decreased in a dose-dependent manner, with significant differences observed at lower (0.25 µM) and higher (1 µM) concentrations (p-value < 0.0015). At 24 h, the lower concentrations (i.e., 0.1–0.25 µM) appeared to recover relative to the control samples, however, the overall expression of F-actin remained significantly depressed relative to the control samples (p-value < 0.0186). To investigate the effect of Cytochalasin D treatment on cell division in non-confluent bEnd5 cultures, the number of treated live cells were compared to the control cell cultures that were not treated, for 12, 24, and 48 h.

2.4.2. Effect of Nocodazole on BEC Cytoarchitecture

To investigate whether α-tubulin played a role in maintaining the permeability status across the BEC monolayers, confluent monolayers of bEnd5 cells were treated with selected concentrations of Nocodazole. Figure 7A shows an increase in TEER across a confluent monolayer of bEnd5 BECs at 24 h, relative to the untreated samples. Conversely, a slight dose-related effect was evident at 48 h with a decrease in TEER upon increasing doses of Nocodazole. In Figure 7B, significant suppression in cell numbers was observed from 12–24 h across all concentrations of Nocodazole (0.25–2 µM) ($p < 0.001$), relative to the control samples. Figure 7C showed that the α-tubulin-rich population aligned along the leading edges of the BEC plasma membrane in untreated samples (controls), with effective cell-cell interaction (see the **yellow** arrows). Comparatively, the cells that were treated with Nocodazole did not exhibit α-tubulin alignment along the BEC membranous leading edges, but rather produced disorganized thread-like structures that were caused by depolymerization treatment. The depolymerization was more effective along the peripheral edges of the BEC plasma membrane (see the **red** arrows) (Figure 7C). The untreated samples displayed less pronounced polymerization at the cell center and an accumulation of α-tubulin around the nucleus. In Figure 7D, although the study was repeated in triplicate, there was no clear pattern of dose-related suppression in α-tubulin. The suppression of α-tubulin that was, however, observed relative to the control samples at 24–48 h ($p < 0.0006$), directly correlated with increasing concentrations of Nocodazole ($p < 0.0016$).

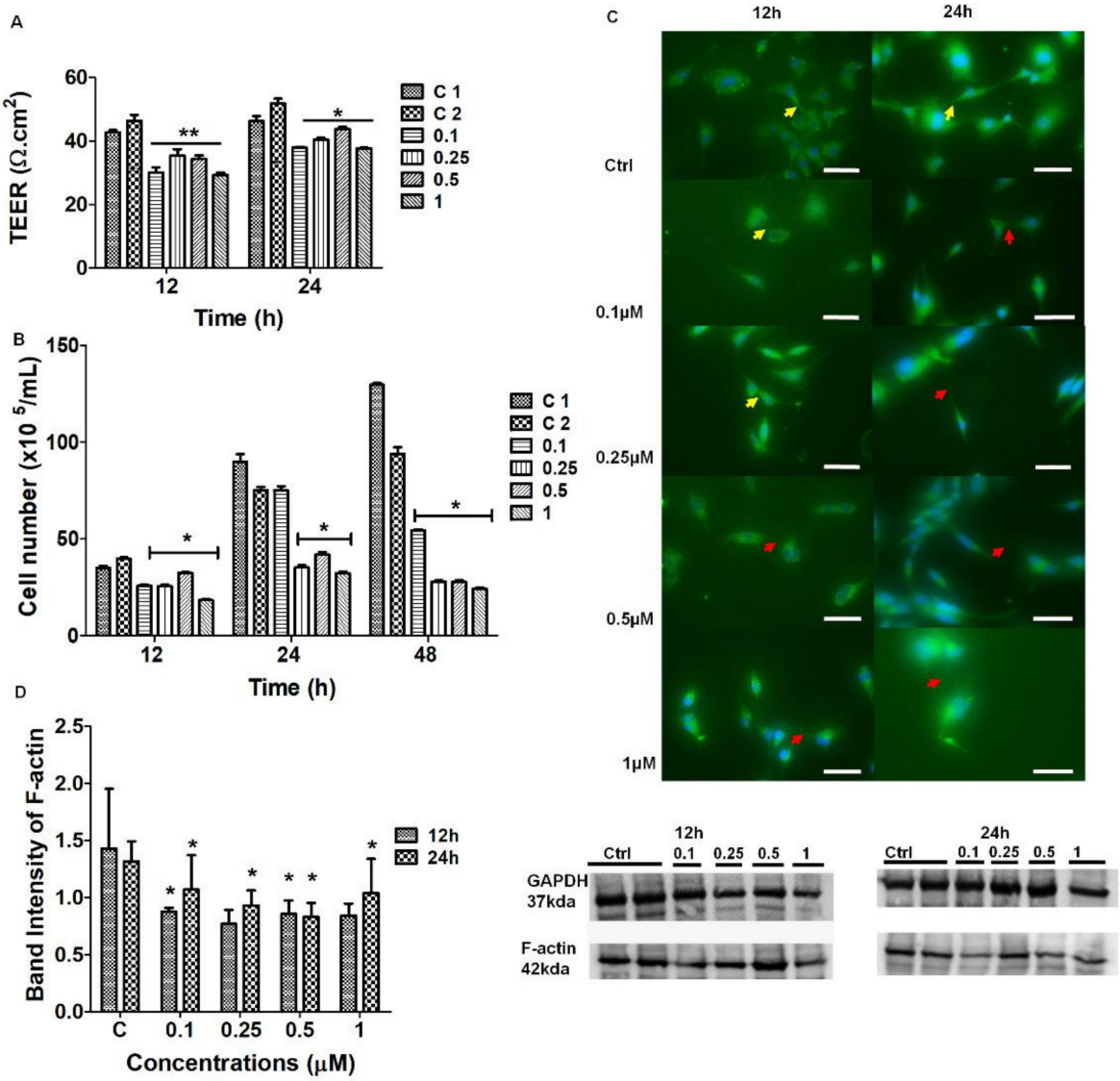

Figure 6. The effect of known depolymerizing agent Cytochalasin D on the physiological parameters of BECs. (**A**) The effect of 0.1–1 μM Cytochalasin D on the TEER across the confluent monolayers of bEnd5 BECs after 12–24 h exposure. The single asterisk * represents significant differences between the experiments and the control samples. The double asterisk (**) denotes statistical significance between the experimental samples and the vehicle control 2 (C2). The data are expressed as the mean ± SEM; (**B**) represents the effect of Cytochalasin D on bEnd5 cell numbers. The asterisks * denotes statistically significant differences between the experimental samples relative to control 1 (C1) and the vehicle control 2 (C2- with 0.1% DMSO); (**C**) Assessing the depolymerizing effect of Cytochalasin D in IF micrographs of Alexa Fluor 488 conjugated, monoclonal F-actin antibodies (Ab'), the **yellow** arrowheads indicate the regions of NT formation and the **red** arrowheads indicate the regions of depolymerization and/or intercellular gaps at the membrane leading edges between adjacent BECs, 12 h and 24 h. D (Scale bar = 50 μM) (**D**) Western blot analysis displays the effect of chemical perturbation of Cytochalasin D on F-actin expression. The asterisks * denotes statistically significant differences between the experimental samples and both control 1 and 2. The data are represented as the mean ± SEM (n = 3). Statistical significance was determined at $p < 0.05$.

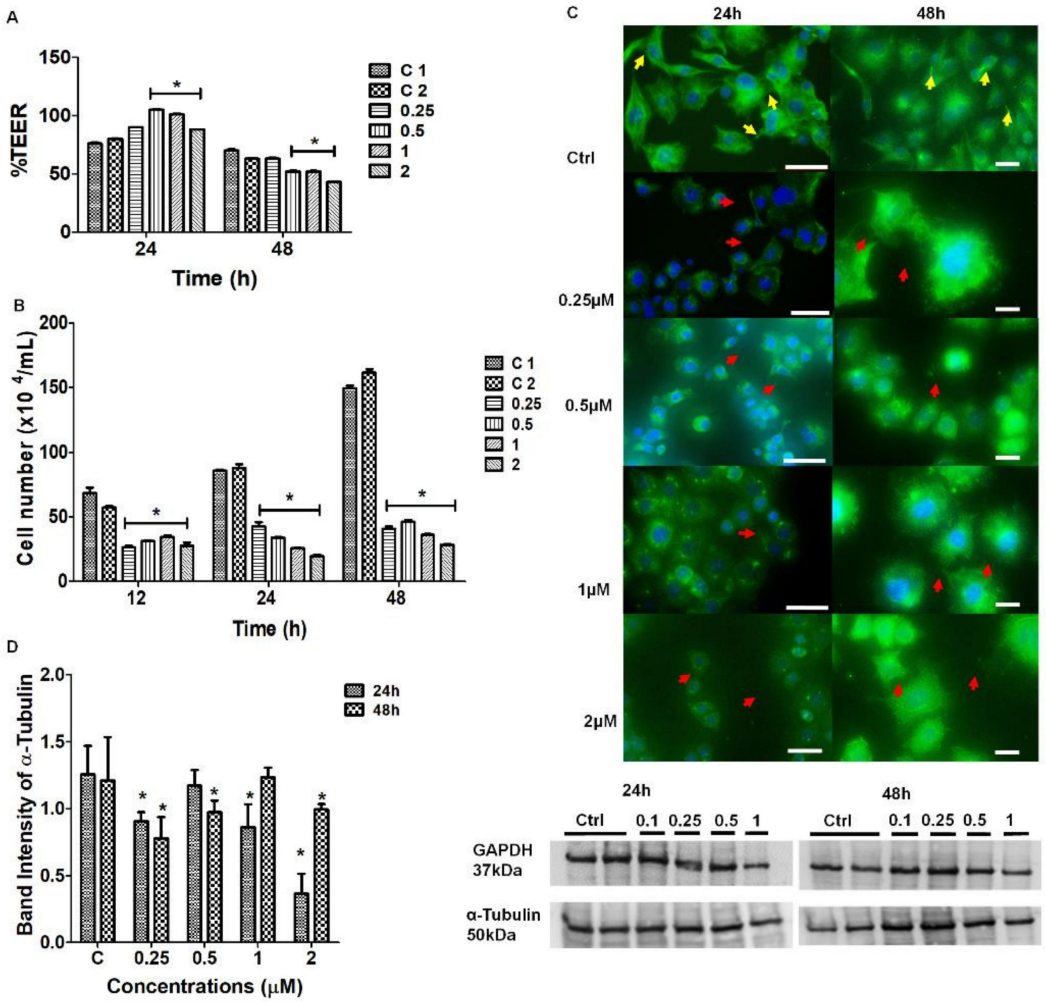

Figure 7. The effect of Nocodazole on the selected physiological parameters of bEnd5 cells. (**A**) The decreasing TEER across confluent bEnd5 cell monolayers upon treatment with 0.25–2 μM Nocodazole. The single asterisk * represents significant differences between the experiments and the untreated (control) samples. The data are expressed as the mean ± SEM; (**B**) Represents the effect of Nocodazole on bEnd5 cell numbers. The asterisk * denotes statistically significant differences between the experimental samples relative to the untreated conditions (C1) and the vehicle control 2 (C2-with 0.1% DMSO); (**C**) IF micrographs of Alexa Fluor 488 conjugated, monoclonal α-tubulin Ab' after 24–48 h Nocodazole treatment for 24 h (Scale bar = 50 μM) and 48 h (Scale bar = 20 μM). The **yellow** arrowheads indicate regions of intercellular NT formation and the **red** arrowheads indicate regions of depolymerization at the membrane leading edges between adjacent BECs; (**D**) The depolymerizing effect of Nocodazole on α-tubulin at 24 h and 48 h observed in the Western blot analysis, which showed significant suppression in protein expression relative to the controls for 24–48 h. The asterisks * denotes statistically significant differences between the experimental samples and both control 1 and 2. The data are represented as the mean ± SEM (n = 3). Statistical significance was determined at p-value < 0.05.

3. Discussion

BBB disruption is a characteristic feature of neurodegeneration [14] and alterations in BEC interactions are known to result in the failure of angiogenesis of brain capillaries with the ensuing disruption of the central nervous system (CNS) homeostasis. The metric for BBB integrity is largely founded upon its degree of impedance and selective permeability, but when it is compromised it no longer can prevent pathogens and harmful substances from crossing into the brain's microenvironment. When investigating the permeability aptitude of the BBB interface it is critical to remember that it is still essentially a physical

barrier that is primarily located at the level of the BEC. We, therefore, consider studying its physical status by exploring the HR-SEM micrographs the cellular morphology of confluent BECs at a nanoscopic level, together with the molecular cytoskeletal underpinning of these novel nanosized extracellular structures.

As more research has been implicating the BECs of the BBB as central to neurodegenerative processes [15], the importance of the BBB is that its regulatory function is closely related to the regulation of permeability through the occlusion of the PC space by TJ interaction. How these zones of juxtaposed transmembrane TJs align is crucial to their action. The transmembrane proteins are not arranged randomly across the lateral membranes of the adjacent BECs, but are arranged in narrow apico-lateral zones along the lateral borders of the BEC plasma membrane [16]. Varying morphology of adjacent BECs will result in misaligned TJ zones with juxtaposed TJs not being able to interact with each other, compromising the occlusion of the PC shunt. In view of the crucial nature of aligning zones of adjacent TJs, our HR-SEM micrographs (Figure 1) of the PC space present a view of a highly complex arrangement of NTs, which appear crucial to the formation of the PC space that would be sealed by TJs. These micrographs reiterate our previous work on the morphology of the BEC monolayers [2], by presenting the interplay of TENTs and TUNTs in the formation of a sealed PC space. In this study, we observed that cross-linking of the TENTs across the PC space seems crucial to the alignment of the lateral plasma membranes to facilitate the engagement of TJs. We wanted to further investigate what molecular cytoskeletal structures were at play in these TENTs and how these cytoskeletal structures were connected to the scaffolding cytoskeletal structures of the soma of the BEC.

We know that transmembrane TJs are attached to cytoplasmic plaque proteins (zonula occludens-1,-2,-3) that are found embedded within the soma of the BEC cytoskeleton. These transmembrane proteins are interlinked to the cytoskeleton, which provides structural support for the TJ protein complex as well as orientation [1]. Understanding the underpinning molecular mechanisms that are governing the BEC cytoskeletal dynamics and subsequent morphology is central to the maintenance of cellular orientation, allowing for aligned brain capillary EC interaction and BBB establishment.

Although Mentor and Fisher [2] described the importance of NTs in this function and described their characteristics and morphology for the first time, the role of TENTs as a causative feature in barrier generation and impedance remains to be defined. In this study the authors postulate that TENTs have a direct role in the alignment of the PC spaces between adjacent BECs, enabling juxtaposed zones of TJs to align and interact, ultimately sealing off the PC spaces. The authors proceeded to unpack this postulate, by asking "what cytoskeletal proteins are central to TENT formation and do they play a physiological role in BBB function?"

Amidst the myriad of intercellular communication, namely (i) paracrine communication; (ii) direct cell-cell contact, mediated in some cell types by gap junctions and by synaptic communication in neurons [17,18]; and (iii) direct cellular–cell communication, by way of cytoplasmic projected filipodia [9,19,20], a novel form of direct BEC–BEC communication via TUNT and TENT formation that is based on a recent HR-SEM study by Mentor and Fisher [2] has emerged. For this study, however, we have undertaken IF imaging and selected the perturbation of the polymerization of F-actin and α-tubulin approach, to understand the functional imperative of the TENTs in the developing in vitro BBB model [2].

3.1. Morphological Studies

3.1.1. Effect of Cytochalasin D on TENT Morphology

Cytochalasin D is known to block the process of F-actin polymerization by binding to the barbed (+) ends of the actin microfilaments, inhibiting its elongation [21]. This preventative action stunts cell cytokinesis (i.e., cell division following mitosis), thus actin is critical for these processes. An observable decrease in TENTs was observed on HR-SEM micrographs after treatment with Cytochalsin D. The depolymerizing effect of Cytochalasin

D may have resulted in the inhibition of TENT formation across the PC space, preventing its leading edges from extending into intercellular NT cross-bridges between adjacent BECs (Figure 4A,B).

3.1.2. Effect of Nocodazole on TENT Morphology

The treatment of bEnd5 cells with Nocodazole is a known inhibitor of α-tubulin polymerization, resulting in a loss of tautness and/or distortion in TENT formation between adjacent BECs, compared to untreated samples (controls) (Figure 5). This observation was further supported by observations of the backward folding of the TENTs, in the opposite direction of the neighboring cells (Figure 5B) relative to untreated samples (Figure 5A). The findings support the postulate that the distortion of TENTs is directly affected by the exposure to the depolymerization agent which affected its stability resulting in the failure of its directional ability to extend across the PC space and fuse with the plasma membrane of an adjacent cell. The prevention of functional NT tether formation results in the failure to mechanically engineer a convoluted/interactive PC space, ultimately preventing direct cell–cell engagement between adjacent BECs growing in close proximity during BEC bEnd5 monolayer establishment.

3.2. Cytoskeletal Studies

We used IF to investigate the cytoskeletal molecular structures in the BEC and its projection into TENTs. The IF micrographs show that the soma of the BEC has an extensive network of F-actin and α-tubulin. In the control samples, F-actin is interconnected throughout the cell cytoplasm, forming cylindrical bundles of long spiral chains while α-tubulin-based microtubules pervade the cytoplasm of the BEC, forming long chains; both form the vital components of BEC intracellular cytoarchitecture (Figure 2A,B). Furthermore, it is well known that F-actin-based microfilaments are important for actuating the endothelial barrier function and α-tubulin-rich microtubules are ubiquitous within the cell's cytoskeleton and protrude from the cells surface [8], alluding to its ability to influence the underlying mechanism of the BEC vascular barrier establishment. Our studies support this view in that the cytoskeletal molecular composition of BEC cytoplasmic extensions, TENTs, was shown to possess both F-actin and α-tubulin-rich cytoskeleton (Figure 3A,B). The microfilaments are actin-rich and are associated with myosin proteins which promote cellular movement, contraction, and cytokinesis, whereas the microtubules, which are tubulin-rich, are tubular structures that are involved in promoting cell shape, transport, and activation of the cells actin-cytoskeleton via guanosine triphosphatases (GTPases) (i.e., Rho and Rac) [12,22].

3.2.1. Effect of Cytochalasin D on the Cytoskeletal Architecture of the TENT

The chemical perturbation of cytoskeletal proteins involved treating BECs with Cytochalasin D (0.1–1 μM) to depolymerize F-actin (Figure 6). The IF micrographs exhibited a reduction in F-actin protein expression which resulted in the failure of BECs to maintain direct cell-cell contact via cytoplasmic TENT extensions (Figure 6C). These findings were endorsed by Western blot analysis which confirmed that Cytochalasin D was able to cause a dose-related suppression in the F-actin protein due to the reduction in the protein content of F-actin within the BEC cytoplasm (Figure 6D).

It is well-known that the actin-cytoskeleton plays a functional role in cell-cell contact [23]. Cytochalasin D is well known to cause the depolymerization of the F-actin-based microfilaments. The F-actin cytoskeletal protein interlinks TJ scaffolding in the cytoplasm of cells by interacting with the ZO-1 plaque proteins within the BEC [24]. Our findings suggest that any alterations in F-actin will directly affect the transmembrane TJ protein arrangement, but also compromise TENT dynamics. Our morphology study endorsed this view in that the chemically-induced alteration of the TENTs resulted in the failure of adjacent BECs to align, orientate, and juxtapose with each other to initiate apico-lateral TJ interaction. Furthermore, the IF micrographs showed a decrease in the cytoskeletal F-actin

expression, consequently affecting the degree of direct BEC–cell interaction by way of cytoplasmic F-actin protrusions on the BEC peripheral borders/leading edges of the BEC, further supporting this view. The role of F-actin appears to not only be crucial to the BEC soma morphology, but also to TENT structure and function. The depolymerization, reduction of cross-linking, disorganization, and defragmentation of F-actin-rich microfilaments could result in failed TJ anastomosis and consequently compromise the impermeability of the BECs PC spaces.

3.2.2. Effect of Nocodazole on the Cytoskeletal Architecture of the TENT

The findings in the IF studies of cytoskeletal protein α-tubulin revealed that Nocodazole, at a concentration range of 0.25–2 μM, caused both a reduction and disorganization in the arrangement of α-tubulin from its native state (Figure 7C). The distortion of the long, slender, α-tubulin-rich microtubules resulted in the failure of BEC to form membranous protrusions and subsequent cell-cell adhesion between adjacent cells that were growing in close proximity. In Figure 7D, Western Blot data and analysis showed no definite pattern and/or clear effect. Furthermore, there was no relationship between the permeability (TEER data) (Figure 7A) and protein expression. Tubulin heterodimers are the monomers of the intracellular microtubules, which are ubiquitous within the cytoskeletal backbone of all cells [25]. It is important to note that the tubulin-rich microtubules are functionally related to transport, motility, and cytokinesis during cell division [26,27]. Any structural alterations in this protein are directly associated with subcellular cytoskeletal rearrangement which directly impacts the cell morphology, disrupting the optimal functionality involved in achieving cell-cell contact which is critical for a strictly regulated barrier [23,26,28]

HR-SEM and IF studies showed that Nocodazole caused a radial reduction in α-tubulin expression (Figure 7C) directly implicates the BECs ability to make direct cell–cell contact, further contributing to the misalignment of BEC lateral plasma membranes, leading to the failure of TJ juxtaposed zones to align. The in vivo BBB requires the interaction of actin microfilaments with plaque proteins zonula occludens-1, -2, -3 (ZO-1, -2, -3) to ensure the formation of a polarized brain endothelium which ultimately drives BBB development [26]. Thus, a compromised barrier functionality of BECs implicates brain microvascular pathology and is closely linked to cytoskeletal rearrangements and actomyosin contractility, subsequently resulting in the formation of increased PC permeability between BECs.

3.3. Permeability

Barrier-genesis is central to this study. This study evaluates how F-actin and α-tubulin play a major role in NT structure and directly implicates TENTs in the regulation of permeability across the in vitro BBB model.

3.3.1. The Effect of Cytochalasin D on BEC Permeability

The TEER studies focus on the interaction of BECs with the context of a confluent monolayer, and the effects on permeability (TEER) after treatment with a depolymerizing agent. At 12–24 h, the BEC bEnd5 monolayers showed a significant, dose-dependent increase in BBB permeability ($p < 0.01$) for all concentrations of Cytochalasin D, relative to the untreated samples ($p < 0.001$) (Figure 6A). Based on these findings, we can infer that blocking the depolymerization of F-actin affects TENT formation directly by implicating the physiological prowess of BEC interaction and subsequent barrier-genesis as seen by increased permeability across our in vitro BBB model.

3.3.2. The Effect of Nocodazole D on BEC Permeability

Upon treatment with Nocodazole, the BEC TEER studies showed that within the first 24 h, the permeability increased relative to the untreated samples. At 48 h the experimental samples exhibited a significant decrease in permeability ($p < 0.001$) at the higher concentrations of Nocodazole, relative to the untreated samples (Figure 7A). It is well reported that increased vascular permeability is associated with increased pathology, especially after

the treatment with anti-cancer mitosis-blocking therapy [23]. Smurova et al. [23] reported on the ability of 100–200 nM Nocodazole to disrupt microtubules at the cell margins and transiently increase the EC permeability at the lower concentrations.

The increases in TEER within the first 24 h can be correlated with the expression of F-actin at 24 h within the IF studies. However, at 48 h there was a reduction in protein expression at the highest dose of Nocodazole, which did not parallel the decrease in TEER at the same concentration. These findings are further supported by a study conducted by Eshun-Wilson et al. [25] who reported that the state at which α-tubulin depolymerization occurs depends largely on whether the protein of interest has undergone post-translational modification through the acetylation of lysine 40 loop (K40) in α-tubulin. These conformational changes are reported to improve microtubule stability, reducing the disorder of the loops [29–31]. The variability in the rate of depolymerization of α-tubulin in TENTs that were observed in our study may, therefore, be dependent on whether the protein has undergone post-translational acetylation. Our α-tubulin data may be more varied upon treatment with Nocodazole due to the effects of post-translational acetylation.

It is conspicuous in contrasting the effects of Cytochalasin D and Nocodazole on the permeability across confluent bEnd5 monolayers, that depolymerization of F-actin had a pronounced effect of increasing the permeability, whereas depolymerization of α-tubulin had a varied effect on permeability. This suggests that F-actin and α-tubulin affect permeability across the BEC monolayers by different mechanisms. In tubular cellular structures, α-tubulin plays an important role in intracellular transport viz, in axons via the plus end-directed kinesins for anterograde transport, and dynein in dendrites [28–30]. It is, therefore, not difficult to postulate that the role that α-tubulin plays in TENTs may be related to the transfer of molecular signaling between adjacent BECs. This is endorsed by morphological evidence that indicates that the distal ends of TENTs fuse with the lateral membrane of the adjacent BEC, essentially linking the cytoplasm of the adjacent BECs. F-actin on the other hand, plays an important role in the cytoskeletal structure of BECs and is intimately involved in anchoring TJ proteins to the intracellular actin-based scaffolding via the linking proteins ZO-1/2/3 [32]. We, therefore, tentatively postulate that F-actin that is found in TENTs are more involved with the structural rigidity of the NT structure and plays an important role in both stabilizing the PC space mechanically and aligning adjacent BECs to facilitate TJ interaction. The actin-based microfilaments are localized beneath the cells' membrane, providing support to the cell's shape, promoting the movement of the cells surface (cytokinesis), migration, and cell division [33]. Thus, the ability of the BBB to form a well-regulated barrier will be compromised if the structural orientation of the BEC is altered, resulting in the potential progression of cerebromicrovascular pathology.

3.4. Effects of Cytochalasin D and Nocodazole on BEC Cell Division

This study investigated how selected inhibitors of polymerization affect BEC division. In this study, in contrast to confluent monolayers that were used in the morphology and TEER studies, non-confluent cell cultures were evaluated to elucidate the effect of depolymerizing agents on cell division. We monitored cell division of BECs, which is essential for the normal maintenance and regeneration of the BBB (e.g., especially after cerebrovascular accidents, infections, and/or inflammation), after treatment with Cytochalasin D and Nocodazole. Cytochalasin D affected BEC proliferation by causing a suppression in BEC division, relative to the untreated samples (Figure 6B). Similarly, Nocodazole treatment resulted in a significant suppression in BEC division (Figure 7B). All the treated cells showed significant suppression in BEC proliferation, thus, inferences can be made that the inhibitory effect of the compound on BEC numbers could be directly attributed to the ability of Nocodazole to disrupt α-tubulin polymer formation in a manner that negatively impacts the rate of BEC division (Figure 7B). These findings are endorsed in the literature, which reports that Nocodazole has the ability to inhibit mitosis and it is well reported that a critical requisite for cell division is appropriate mitotic spindles during mitosis [34]. The inhibition of microtubules is reported to result in cell-cycle arrest at the G_2-M phase, with

the formation of abnormal mitotic stimulants [34,35] and thus, our results endorse these findings in that Nocodazole resulted in an overall suppression in BEC division.

3.5. Synthesis

This study is focused on the concept of barrier-genesis of the brain capillary endothelium and is specifically focused on the role and mechanisms whereby TENTs affect barrier establishment of the in vitro BBB model. The findings showed the integral role of TENTs in BEC monolayer formation and, thus, by extrapolation, must form an integral part of an in vivo BBB. By logical extension, BECs that are grown close together form a strict monolayer, which is a reflection of the in vivo endothelium of the brain capillary. This in vitro complexity cannot, therefore, be an aberration of the in vivo scenario, but is rather a reflection of the complexity within the in vivo state. We found that the polymerization of F-actin and α-tubulin protein structures were ubiquitous within the TENTs. Upon chemical perturbation with Cytochalasin D and Nocodazole, we saw a breakdown in these protein structures using IF, which was supported by the morphological loss of tautness and an increase in the morphological distortion in the TENT structures. To examine how depolymerization on barrier functionality we measured TEER across the BEC bEnd5 confluent monolayers as an index for measuring the barrier integrity. TEER was affected by F-actin breakdown, whereas tubulin breakdown generated variable TEER results. Based on these findings we can infer that F-actin in TENTs is more essential for barrier-genesis than α-tubulin. Conversely, as the effects of α-tubulin on TEER were inconclusive, we propose that α-tubulin in TENTs play a role in conducting molecular signaling between adjacent BECs, as is evident by its role in other cell structures such as in axonal transport in neurons [29].

Despite TENT structures constituting both microfilaments F-actin and α-tubulin, the role of these cytoarchitectural proteins differ in terms of their direct/indirect involvement in barrier-genesis. The physical functionality of a TENT involves extensive cytoskeletal governance to ensure that adjacent BEC plasma membranes are aligned into position, allowing for TJ localization and the occlusion of the PC spaces during BBB establishment.

4. Materials and Methods

4.1. Cell Culture

The bEnd5 cell line was purchased from the European Collection of Authenticated Cell Cultures (ECACC) (Sigma-Aldrich, 96091930, St. Louis, MI, USA). The cells were cultured in Dulbecco's Modified Eagles medium (Whitehead Scientific, Cat no. BE12-719F, Stikland, South Africa), supplemented with 10% fetal bovine serum (FBS) (Celtic Molecular Diagnostics /Biowest, Cat no. S181G-500, Cape Town, South Africa, 1% Penicillin/Streptomycin (Whitehead Scientific, Cat. No. DE17-602E, South Africa), 1% non-essential amino acids (Whitehead Scientific, Cat no. BE13-114E, South Africa), and 1% sodium pyruvate (Whitehead Scientific, Cat no. BE13-115E, South Africa).

4.2. Transendothelial Electrical Resistance

A total of 24 h after seeding, 5×10^5 bEnd5 cells/insert/well on membrane inserts (Millipore/Merck, Cat no. PIHA01250, Darmstadt, Germany), in 24-well plates until they reached confluence and the cultured medium was replaced by select concentrations of depolymerizing agents: Cytochalasin D at 0.1 µM, 0.25 µM, 0.5 µM and 1 µM, relative to control samples. Nocodazole at 0.25 µM, 0.5 µM, 1 µM, and 2 µM at the humidified atmosphere of 5% CO_2 at 37 °C. Transendothelial electrical resistance (TEER) was carried out for 12 h, 24 h, and 48 h using a Millicell electrical resistance system (Millipore, Ser. No. 57318 11B, Germany). Quantitative analysis of the recorded TEER readings was achieved by employing the parameters of an appropriate equivalent circuit, which represents the electrical parameters across the in vitro BEC monolayer under investigation. The TEER values are expressed in $\Omega \cdot cm^2$ and were normalized to controls and plotted as percentage normalized resistance.

4.3. Scanning Electron Microscopy

A total of 48 h after seeding and exposing, the bEnd5 cell monolayers cells on inserts were fixed with 2.5% glutaraldehyde (Fluka/Sigma, Cat no. 49626, Darmstadt, Germany) prepared in 1X phosphate-buffered saline (PBS) (Life Technologies, Cat. no. 20012019, South Africa) for 1 h at room temperature (RT). After a thorough rinse with 1X PBS and water, the cells were dehydrated in ethanol (50–100%). This was followed by a critical point drying step for 1 h, in which ethanol was replaced by CO_2, and finally sputter coated with gold:palladium (Au:Pd). The samples were visualized by a scanning electron microscope (Zeiss-Auriga, Erfurt, Germany).

4.4. Immunocytochemistry

Immunocytochemistry detects antigens (Ag) in tissue sections utilizing immunological and chemical reactions. It is highly sensitive and specific and is able to detect a variety of protein-specific Ag in multiple animal species. The bEnd5 cells were seeded at a density of 50,000/well, on gelatin-coated glass coverslips in 12-well plates. After 24 h following cellular attachment, the cells were treated with depolymerizing agents: (i) Cytochalasin D at 0.1–1 μM and (ii) Nocodazole at (0.25–2 μM). After exposure to the drug at the respective time intervals, the samples were fixed with 4% paraformaldehyde (made in PBS pH 7.4) for 10 min at RT. The BECs were washed thrice with ice-cold 1X PBS for 5 min each. The BECs were incubated in 1% bovine serum albumin (BSA) (Sigma, Cat no. 05470-1G, Germany) which was prepared with 0.1% Triton X (Sigma-Aldrich, cat no. 9002-93-1, Germany) in PBS) for 1–2 h to permeabilize the cell membrane. Thereafter, the cells were incubated in 1%BSA, the purpose was to block unspecific binding of the antibodies. A 3% BSA solution (blocking solution) was prepared by dissolving 1.5 g BSA into the 50 mL PBS solution with 0.1% Triton X. The 0.1% Triton X solution was prepared by dissolving 50 μL in 50 mL of 3% BSA.

4.5. Immunostaining

After a 1–2 h time-lapse, the blocking solution was removed and the primary antibody (Ab') for F-actin (1:1000) (Life Technologies/ThermoFisher Scientific, Cat no. MA180729, City of Johannesburg, South Africa) and α-tubulin (1:200) (Merck Chemicals, Cat no. T8203, South Africa) was added to semi-confluent bEnd5 monolayers that were grown within 12-well plates. The Ab' was incubated on a shaker for 1h at room temperature (RT) or overnight at 4 °C. The Ab's were removed and the cell samples were washed with PBS for 5 min (min) and repeated three times. Thereafter, the cell samples were incubated with the following secondary Ab': Alexa Fluor 488-conjugated goat anti-mouse secondary Ab' (1:500) (Life Technologies/ThermoFisher Scientific, Cat no. A-11001, South Africa) and Alexa Fluor 568-conjugated goat anti-mouse secondary Ab' (1:500) (Life Technologies/ThermoFisher Scientific, Cat no. A-11011, South Africa) for 2 h. Thereafter, the secondary Ab' solution was removed and the cells were washed for 5 min with PBS three times (this step was performed under dark conditions to avoid bleaching of the fluorescent Ab').

4.6. Counterstaining with 4',6-Diamidino-2-Phenylinole (DAPI) Stain

The DAPI stain is a blue-fluorescent stain targeting double-stranded deoxyribonucleic acid (dsDNA). The binding of DAPI to dsDNA produces a ~20-fold fluorescent enhancement; this is attributed to the displacement of water molecules from both DAPI and the minor groove of the dsDNA (Larson et al., 2012). DAPI remains a popular fluorescent stain that is employed for DNA visualization and quantification. The cells were incubated with 0.1–1 μg/mL DAPI (fixed cells, grown on glass slides). A total of 1 μL of DAPI (ThermoFisher Scientific, Cat no. 62248, South Africa) was added to 10 mL of 1X PBS (Store at 4 °C under dark conditions). The DAPI stain was exposed to the fixed cells under dark conditions for 10 minutes and, thereafter, washed in 1X PBS (three times, for five minutes each). 1,4-Diazabicyclo[2.2.2]octane (DABCO) fluorogel (Sigma-Aldrich, Cat no. D27802-100G, Germany) was added to a glass slide for mounting the cell samples that

were grown on a glass coverslip. The samples were viewed using immunofluorescent (IF) microscopy (Nikon Eclipse Ts2).

4.7. Western Blot Analysis

The bEnd5 cells were allowed to grow in 75 cm^3 tissue culture flasks and were treated with different concentrations of Nocodazole (0.25 μM, 0.5 μM, 1 μM, and 2 μM) and Cytochalasin D (0.1 μM, 0.25 μM, 0.5 μM, and 1 μM) for 12 h, 24 h, and 48 h. The cells were washed in 1X PBS and trypsinized in 0.25% trypsin versene–EDTA (Whitehead Scientific, Cat no BE17-161E, South Africa). The samples were pipetted in microcentrifuge tubes and centrifuged at 1500 revolutions per minute (rpm) for 5 min RT and the supernatant was discarded. The pellet was resuspended in cold 1X PBS, on ice and centrifuged at 4000 rpm for 5 min at 4 °C. A total of 140 μL of lysis buffer was prepared by adding 250 μL of phosphatase inhibitor cocktail and 250 μL protease inhibitor cocktail to 5 mL of RIPA buffer (ThermoFisher Scientific, Lot no. VI311029 was added to each cell pellet on ice and lysed by agitation for 10–15 min, thereafter, the lysate was sonicated and centrifuged at 14,000 rpm for 10 min. The protein concentration was determined using the Thermo Scientific Nanodrop 2000/2000c spectrophotometer (ThermoFisher Scientific, USA).

The sample solutions were diluted using Laemli sample buffer (LSB) (Biorad, Cat no. 1610737) and 5% Beta mercaptoethanol (Biorad, Cat no. 1610710) to normalize the protein concentrations to 20μg/mL and denatured at 95 °C, for 5 min. The samples were run on the 10% SDS-PAGE gel at 200 V (400 mA) for about 45–50 min or until the bottom-most marker band reached the bottom of the gel. The proteins were transferred to nitrocellulose membranes for 7 min at 20 V at RT using the iblot2 transfer system (ThermoFisher Scientific, Ref. no. IB23001, South Africa) and the membranes were blocked for 2 h using 2% bovine serum albumin (BSA) or Casein blocking solution. The membranes were probed with primary monoclonal ab F-actin (1:1000, Thermofisher Scientific, USA), α-tubulin (1:2000, Sigma, Darmstadt, Germany) and GAPDH (1:4000, Invitrogen, Burlington, ON, Canada) and incubated overnight. The membrane was incubated with secondary antibody horseradish peroxidase (HRP)-conjugated goat anti-mouse secondary ab (1:10,000) for 2 h and washed three times with PBS-tween. The membrane was subjected to substrate chemiluminescence for 5 to 15 min and the BioRad ChemiDoc imaging system, version 2.4.0.03 (Lasec, South Africa) was used to view the band formation.

4.8. Trypan Blue Exclusion Assay

A cell density of 5×10^4 bEnd5 cells/well in 24-well plates were seeded and allowed to reach confluence over a 24h timeframe. Thereafter, the culture medium was replaced by the selected concentrations of depolymerizing agents: Cytochalasin D at 0.1 μM, 0.25 μM, 0.5 μM, and 1 μM, relative to the untreated (control) samples at 12–24 h; and Nocodazole at 0.25 μM, 0.5 μM, 1 μM, and 2 μM, relative to the control samples for 24–48 h, at the humidified atmosphere of 5% CO_2 at 37 °C. The cellular proliferation was investigated by utilizing the trypan blue exclusion assay to determine the effect of the selected depolymerizing agents on the rate of BEC division. A cell count was performed using the Countess III automated counter (Invitrogen), which employs built-in standardized algorithms that allow for the elimination of debris, considers cell cluster formation, and accounts for the cell size.

5. Conclusions

This study addressed the functional role that TENTs play in establishing a strictly regulated BEC monolayer. In view of the effect of F-actin treatment on confluent monolayers which produced an increase in the permeability (decrease TEER), we postulate that F-actin provides cyto-structural focus and tautness to the TENT structure. In contrast, the α-tubulin in TENTs, in addition to its structural function, as could be seen in our morphology study, does not play as prominent a role in permeability (TEER) integrity. We, therefore, postulate that it may play a role in direct cell-cell signaling across the PC space. Thus, based on the

ultrastructural and cytoarchitectural findings we postulate that TENTs not only provide tethering alignment of the PC space and TJ zones to occlude BEC PC spaces, but also play a role in direct cell-cell communication during BEC bEnd5 monolayer development. Moreover, compromising TENT formation by chemically perturbing the microfilaments and microtubules displays the dual importance of cytoskeleton proteins in providing both cell shape and transitions within BEC leading edges to form cell-cell contact points during barrier-genesis. The depolymerization of F-actin and α-tubulin negatively altered the intracellular cytoarchitecture of the BEC, changing its morphology and ability to form a well-structured BEC monolayer. The cytoskeleton is a salient feature of TENT formation as the cytoskeleton extends from the BEC soma into the TENT cytoplasmic extensions. Compromising TENT formation leads to the misalignment of adjacent BEC TJ anastomosis resulting in the failure to establish a well-regulated brain-endothelial barrier. This alludes to the integral role of NTs in monolayer development and, by extension, must form an integral part of the establishment of the in vivo BBB model. The morphological findings for TENT structures endorses the view that our in vitro BBB model is a promising method for studying BBB development. Our research, therefore, addresses a fundamental gap in how these novel NTs, TENTs play a role in the generation of the BBB endothelium in brain capillaries.

Furthermore, many neurodegenerative diseases are known to implicate BBB permeability, disrupting CNS homoeostasis. From a future perspective, we show the functional features of TENTs in BBB permeability and the usefulness of this in vitro BBB model may be important to elucidate the importance of TENTs in neurodegenerative disease progression.

Author Contributions: Conceptualization, S.M. and D.F.; methodology, S.M. and K.B.M.; validation, K.B.M.; formal analysis, S.M., DF; investigation S.M.; resources, D.F.; data curation, S.M. and D.F.; writing—original draft preparation, S.M.; writing—review and editing, S.M., D.F. and K.B.M.; visualization, S.M.; supervision, D.F.; project administration, D.F.; funding acquisition, D.F. All authors have read and agreed to the published version of the manuscript.

Funding: Funding was received from the University of the Western Cape (UWC) senate funds.

Institutional Review Board Statement: Not applicable.

Informed Consent Statement: Not applicable.

Data Availability Statement: The data is archived according to UWC policies. The data presented in this study are available on request from the corresponding author.

Acknowledgments: This work was supported by the infrastructural and academic support provided by the Department of Medical Biosciences at UWC and the Electron Microscopy Unit at the UWC, Cape Town, South Africa.

Conflicts of Interest: The authors declare no conflict of interest.

References

1. Stamatovic, S.M.; Johnson, A.M.; Keep, R.F.; Andjelkovic, A.V. Junctional proteins of the blood-brain barrier: New insights into function and dysfunction. *Tissue Barriers* **2016**, *4*, e1154641. [CrossRef] [PubMed]
2. Mentor, S.; Fisher, D. High-Resolution Insights Into the in vitro Developing Blood-Brain Barrier: Novel Morphological Features of Endothelial Nanotube Function. *Front. Neuroanat.* **2021**, *15*, 661065. [CrossRef]
3. Wolburg, H.; Lippoldt, A. Tight junctions of the blood-brain barrier: Development, composition and regulation. *Vascul. Pharmacol.* **2002**, *38*, 323–337. [CrossRef]
4. Serlin, Y.; Shelef, I.; Knyazer, B.; Friedman, A. Anatomy and physiology of the blood-brain barrier. *Semin. Cell Dev. Biol.* **2015**, *38*, 2–6. [CrossRef] [PubMed]
5. Saunders, N.R.; Habgood, M.D.; Møllgård, K.; Dziegielewska, K.M. The biological significance of brain barrier mechanisms: Help or hindrance in drug delivery to the central nervous system? *F1000Research* **2016**, *5*, 1–15. [CrossRef] [PubMed]
6. Fisher, D.; Mentor, S. Are claudin-5 tight-junction proteins in the blood-brain barrier porous? *Neural Regen. Res.* **2020**, *15*, 1838–1839. [CrossRef] [PubMed]
7. Gurke, S.; Barroso, J.F.V.; Gerdes, H.H. The art of cellular communication: Tunneling nanotubes bridge the divide. *Histochem. Cell Biol.* **2008**, *129*, 539–550. [CrossRef]
8. Ma, N.; Zhou, J. Functions of Endothelial Cilia in the Regulation of Vascular Barriers. *Front. Cell Dev. Biol.* **2020**, *8*, 626. [CrossRef]

9. Abounit, S.; Zurzolo, C. Wiring through tunneling nanotubes—From electrical signals to organelle transfer. *J. Cell Sci.* **2012**, *125*, 1089–1098. [CrossRef]
10. Phng, L.K.; Stanchi, F.; Gerhardt, H. Filopodia are dispensable for endothelial tip cell guidance. *Development* **2013**, *140*, 4031–4040. [CrossRef]
11. Bershadsky, A.; Chausovsky, A.; Becker, E.; Lyubimova, A.; Geiger, B. Involvement of microtubules in the control of adhesion-dependent signal transduction. *Curr. Biol.* **1996**, *6*, 1279–1289. [CrossRef]
12. Ballestrem, C.; Wehrle-Haller, B.; Hinz, B.; Imhof, B.A. Actin-dependent lamellipodia formation and microtubule-dependent tail retraction control-directed cell migration. *Mol. Biol. Cell* **2000**, *11*, 2999–3012. [CrossRef]
13. Best, A.; Ahmed, S.; Kozma, R.; Lim, L. The Ras-related GTPase Rac1 binds tubulin. *J. Biol. Chem.* **1996**, *271*, 3756–3762. [CrossRef] [PubMed]
14. Shi, Y.; Zhang, L.; Pu, H.; Mao, L.; Hu, X.; Jiang, X.; Xu, N.; Stetler, R.A.; Zhang, F.; Liu, X.; et al. Rapid endothelial cytoskeletal reorganization enables early blood-brain barrier disruption and long-term ischaemic reperfusion brain injury. *Nat. Commun.* **2016**, *7*, 10523. [CrossRef]
15. Cuevas, E.; Rosas-Hernandez, H.; Burks, S.M.; Ramirez-Lee, M.A.; Guzman, A.; Imam, S.Z.; Ali, S.F.; Sarkar, S. Amyloid Beta 25–35 induces blood-brain barrier disruption in vitro. *Metab. Brain Dis.* **2019**, *34*, 1365–1374. [CrossRef] [PubMed]
16. Haseloff, R.F.; Dithmer, S.; Winkler, L.; Wolburg, H.; Blasig, I.E. Transmembrane proteins of the tight junctions at the blood-brain barrier: Structural and functional aspects. In *Seminars in Cell & Developmental Biology*; Elsevier Ltd.: Amsterdam, The Netherlands, 2015; pp. 16–25. [CrossRef]
17. Lucas, W.J.; Ham, B.K.; Kim, J.Y. Plasmodesmata—Bridging the gap between neighboring plant cells. *Trends Cell Biol.* **2009**, *19*, 495–503. [CrossRef] [PubMed]
18. Maeda, S.; Tsukihara, T. Structure of the gap junction channel and its implications for its biological functions. *Cell. Mol. Life Sci.* **2011**, *68*, 1115–1129. [CrossRef]
19. Rustom, A.; Saffrich, R.; Markovic, I.; Walther, P.; Gerdes, H.H. Nanotubular Highways for Intercellular Organelle Transport. *Science* **2004**, *303*, 1007–1010. [CrossRef]
20. Ridley, A.J. Life at the leading edge. *Cell* **2011**, *145*, 1012–1022. [CrossRef]
21. Trendowski, M. Using Cytochalasins to Improve Current Chemotherapeutic Approaches. *Anti-Cancer Agents Med. Chem.* **2015**, *15*, 327–335. [CrossRef]
22. Breslin, J.W.; Zhang, X.E.; Worthylake, R.A.; Souza-Smith, F.M. Involvement of local lamellipodia in endothelial barrier function. *PLoS ONE* **2015**, *10*, e0117970. [CrossRef]
23. Smurova, K.M.; Birukova, A.A.; Verin, A.D.; Alieva, I.B. Dose-dependent effect of nocodazole on endothelial cell cytoskeleton. *Biochem. Suppl. Ser. A Membr. Cell Biol.* **2008**, *2*, 119–127. [CrossRef]
24. Van Itallie, C.M.; Tietgens, A.J.; Krystofiak, E.; Kachar, B.; Anderson, J.M. A complex of ZO-1 and the BAR-domain protein TOCA-1 regulates actin assembly at the tight junction. *Mol. Biol. Cell* **2016**, *26*, 2769–2787. [CrossRef]
25. Eshun-Wilson, L.; Zhang, R.; Portran, D.; Nachury, M.V.; Toso, D.B.; Löhr, T.; Vendruscolo, M.; Bonomi, M.; Fraser, J.S.; Nogales, E. Effects of α-tubulin acetylation on microtubule structure and stability. *Proc. Natl. Acad. Sci. USA* **2019**, *116*, 10366–10371. [CrossRef] [PubMed]
26. Revenu, C.; Streichan, S.; Donà, E.; Lecaudey, V.; Hufnagel, L.; Gilmour, D. Quantitative cell polarity imaging defines leader-to-follower transitions during collective migration and the key role of microtubule-dependent adherens junction formation. *Development* **2014**, *141*, 1282–1291. [CrossRef]
27. Straight, A.F.; Field, C.M. Microtubules, membranes and cytokinesis. *Curr. Biol.* **2000**, *10*, 760–770. [CrossRef]
28. Birukova, A.A.; Smurova, K.; Birukov, K.G.; Usatyuk, P.; Liu, F.; Kaibuchi, K.; Ricks-Cord, A.; Natarajan, V.; Alieva, I.; Garcia, J.G.N.; et al. Microtubule disassembly induces cytoskeletal remodeling and lung vascular barrier dysfunction: Role of Rho-dependent mechanisms. *J. Cell. Physiol.* **2004**, *201*, 55–70. [CrossRef] [PubMed]
29. Rolls, M.M. Neuronal polarity in Drosophila: Sorting out axons and dendrites. *Dev. Neurobiol.* **2011**, *71*, 419–429. [CrossRef]
30. Harterink, M.; van Bergeijk, P.; Allier, C.; de Haan, B.; van den Heuvel, S.; Hoogenraad, C.C.; Kapitein, L.C. Light-controlled intracellular transport in Caenorhabditis elegans. *Curr. Biol.* **2016**, *26*, R153–R154. [CrossRef]
31. Burute, M.; Kapitein, L.C. Cellular logistics: Unraveling the interplay between microtubule organization and intracellular transport. *Annu. Rev. Cell Dev. Biol.* **2019**, *35*, 29–54. [CrossRef] [PubMed]
32. Hawkins, B.T.; Davis, T.P. The Blood-Brain Barrier/Neurovascular Unit in Health and Disease. *Pharmacol. Rev.* **2005**, *57*, 173–185. [CrossRef] [PubMed]
33. Cooper, G.M. *The Cell: A Molecular Approach*, 2nd ed.; The Cytoskeleton and Cell Movement; Sinauer Associates: Sunderland, MA, USA, 2000; Chapter 11.
34. Ems-McClung, S.C.; Walczak, C.E. Kinesin-13s in mitosis: Key players in the spatial and temporal organization of spindle microtubules. *Semin. Cell Dev. Biol.* **2010**, *21*, 276–282. [CrossRef] [PubMed]
35. Kaur, R.; Kaur, G.; Gill, R.K.; Soni, R.; Bariwal, J. Recent developments in tubulin polymerization inhibitors: An overview. *Eur. J. Med. Chem.* **2014**, *87*, 89–124. [CrossRef] [PubMed]

CHAPTER FIVE: 'THE *ISM* BETWEEN ENDOTHELIAL CILIA AND ENDOTHELIAL NANOTUBULES IS AN EVOLVING CONCEPT IN THE GENESIS OF THE BBB'

International Journal of
Molecular Sciences

MDPI

Review

The *Ism* between Endothelial Cilia and Endothelial Nanotubules Is an Evolving Concept in the Genesis of the BBB

Shireen Mentor [1] and David Fisher [1,2,*]

[1] Neurobiology Research Group, Department of Medical Biosciences, University of the Western Cape, Bellville, Cape Town 7535, South Africa; 2746944@myuwc.ac.za
[2] School of Health Professions, University of Missouri, Columbia, MO 65211, USA
* Correspondence: dfisher@uwc.ac.za

Abstract: The blood–brain barrier (BBB) is fundamental in maintaining central nervous system (CNS) homeostasis by regulating the chemical environment of the underlying brain parenchyma. Brain endothelial cells (BECs) constitute the anatomical and functional basis of the BBB. Communication between adjacent BECs is critical for establishing BBB integrity, and knowledge of its nanoscopic landscape will contribute to our understanding of how juxtaposed zones of tight-junction protein interactions between BECs are aligned. The review discusses and critiques types of nanostructures contributing to the process of BBB genesis. We further critically evaluate earlier findings in light of novel high-resolution electron microscopy descriptions of nanoscopic tubules. One such phenotypic structure is BEC cytoplasmic projections, which, early in the literature, is postulated as brain capillary endothelial cilia, and is evaluated and compared to the recently discovered nanotubules (NTs) formed in the paracellular spaces between BECs during barrier-genesis. The review attempts to elucidate a myriad of unique topographical ultrastructures that have been reported to be associated with the development of the BBB, viz., structures ranging from cilia to BEC tunneling nanotubules (TUNTs) and BEC tethering nanotubules (TENTs).

Keywords: brain endothelium; tethering nanotubules; cytoplasmic projections; cilium; BBB

Citation: Mentor, S.; Fisher, D. The *Ism* between Endothelial Cilia and Endothelial Nanotubules Is an Evolving Concept in the Genesis of the BBB. *Int. J. Mol. Sci.* **2022**, *23*, 2457. https://doi.org/10.3390/ijms23052457

Academic Editor: Ana Joaquina Perez-Berna

Received: 21 January 2022
Accepted: 17 February 2022
Published: 23 February 2022

1. Introduction

The capillaries of the brain are particularly special, as they are not simply conduits for blood, but are primarily responsible for ensuring that the neurons function in a strictly regulated homeostatic interstitium. The ability to monitor and study the orientation and alignment of brain endothelial cells (BECs) during barrier establishment is limited due to the lack of qualitative, three-dimensional, nanoscopic data. These limitations have engendered the theoretical premise that the barrier-genesis of brain capillary endothelial cells (ECs) is mainly determined by paracellular interaction demarcated by the presence of intercellular tight junctions (TJs): occludin, claudin-5, junctional adhesion molecules, desmosomes and gap junctions, all of which make up the junctional complex [1] and are known to be directly linked to the BEC actin cytoskeleton via the zonula occludens-1 plaque protein [1–3].

The blood–brain barrier (BBB), in vivo, is formed by cross-talk between the cells of the neurovascular unit (NVU) (i.e., pericytes, astrocytes and BECs). The pericytes support the angiogenic features of brain capillaries and specifically have the ability to regulate brain capillary blood flow, while astrocytes regulate BEC permeability by modulating TJ expression [1,4,5]. These supporting and modulatory cells of the NVU facilitate the BEC's regulatory functions, which are expressed via the BEC endothelium, which regulates substance flux across the BBB.

BBB integrity is largely attributed to intercellular TJ protein interaction between adjacent BECs [6,7]. TJ protein complexes (i.e., claudins 1, 3, 5 and 12, occludin and zonula

occludens -1, -2, -3 (ZO-1, ZO-2, ZO-3)) serve as intercellular paracellular gatekeepers between adjacent BECs [8]. The cerebrovasculature is deemed critical for maintaining precisely regulated CNS homeostasis, by restricting the movement of substances, ions, pathogens and inflammatory cytokines from traversing the BBB [6,9,10]. The barrier role of TJ proteins is to form an intercellular protein junction complex, which occludes the paracellular shunts. These protein–protein junctions interact by a process of dimerization [11]. Three critical transmembrane proteins are occludin (65 kDa), claudin-5 (23 kDa) and junctional adhesion molecules (40 kDa), which are linked to cytoplasmic-associated proteins ZO-1, ZO-2 and ZO-3, which interact with the BEC actin cytoskeleton and form a cytoplasmic bridge connecting TJ proteins to the cytoskeleton. Claudin-5 is the major TJ protein contributing to barrier integrity and binds homotypically to the same type of claudin (-5) on the lateral membrane of an adjacent BEC [12]. However, three cellular events are requisite for dimerization to occur: (i) BEC orientation; (ii) BEC apico-lateral nanotubule (NT) expression and (iii) BEC alignment.

Identifying structural mediators of cerebromicrovascular assembly is essential to fully comprehend the morphological landscape of barrier-genesis in the brain's capillaries. As with all endothelia, BECs are orientated with reference to their basement membrane and are morphologically categorized into apical and basolateral domains. The emergence of a well-regulated brain capillary involves the intricacies of topographical, morphological cellular structures (e.g., nanotubules) across the BEC's paracellular spaces, which requires the alignment of the cytoskeleton and morphology of adjacent BECs.

These structures are crucial to the developmental framework that organizes BECs to congregate and engage each other through cross-bridge topographical nanotubular networks, which engenders cellular alignment and establishes zones of TJ interaction. This review aims to illuminate novel apico-lateral NT structures as pivotal role players in occluding BEC paracellular spaces and contrast these structures with the reported "cilia" postulated to form on BECs.

1.1. Historical Context

The literature is scarce on the subject of BEC interaction at the nanoscopic level. However, this is not unexpected as increases in microscopy resolution are commensurate with the recent technological improvements in scanning electron microscopy. Furthermore, the use of high-resolution transmission electron microscopy (HR-TEM) has established that electron-dense intercellular regions exist in the apico-lateral regions between BECs, which have been confirmed as indicative of the zones of TJs [13,14]. However, these two-dimensional interpretations of BEC paracellular spaces under-report the complexity of the paracellular interaction. In reality, the interaction within the paracellular space is highly complex and the literature describing its dynamics remains rudimentary. During the 1960s–1970s, the successful isolation and characterization of endothelial cells (ECs) in culture was developed for routine experimentation [15,16]. In 1967, the utilization of transmission electron microscopy (TEM) by Reese and Karnovsky (1967) [17] allowed for the localization of a BEC barrier, after visualizing the inability of electron-dense tracers to traverse the paracellular spaces between adjacent BECs [17]. In the 1980s, research showed a vested interest in the characterization of ECs *in vivo*, performing differential analyses within vascular beds with respect to protein expression [18]. Based on these studies, it was established that the intact endothelium displayed both ultrastructural and molecular diversity. Although it is well established that TJ localization takes place within the apico-lateral domain of the BECs, within its paracellular spaces, how the BECs engage to form the primary barrier of the BBB to regulate transendothelial solute/ion influx from the blood into the brain parenchyma is critical for understanding CNS barrier-genesis. Compromised BEC engagement results in disruption and increased permeability of the BBB and exacerbates neurodegenerative disease progression [19] and is, therefore, a good measuring index to appraise its integrity [12]. During the 1960s–1970s, the morphology of the primary cilium was first described in fibroblastic cells [15,16]; however, it was only by

the late 1990s and early 2000s that protruding cytoplasmic projections in BEC membrane surfaces were identified under both low-magnification and poor resolution (compared to current standards) and, thereafter, [2,20,21] researchers postulated these structures as endothelial cilia [22].

1.2. The Physiological Origin of the Endothelial Barrier-Genesis

The EC originates from the mesodermal germ layer during early embryonic development and is essential for capillary formation [23]. During the process of vasculogenesis, angioblasts originate in the lateral plate mesoderm, in the embryonic midline [24,25]. TJ protein genes are expressed in the embryonic stages of angiogenesis [26]. In mice, the BBB is formed on embryonic day 15.5 [27], and in humans, angiogenesis occurs at fetal week 8, with the BBB forming at 4 months [28,29]. Despite the presence of BEC TJ adhesion contact zones, which have been endorsed in the literature by freeze-fracture studies [30], the juxtaposed zones of TJs have to be aligned to be functional. Misalignment results in the inability of juxtaposed TJs to interact with each other to effectively seal the paracellular pathway [31]. The BEC establishes its polarity by way of basement membrane engagement, which allows for the juxtapositioning of the apico-lateral region of the paracellular spaces between adjacent BECs, resulting in aligned zones of TJ interaction and subsequent occlusion of the paracellular space, creating barrier separation between the inside and the outside of the brain's microenvironment. The apical membrane, which is of interest in this review, is positioned towards the external milieu/capillary lumen and there have been reports postulating the presence of cilia on the apical membranes of endothelial cells [2].

These early studies have postulated the role of endothelial cilia in either capillary flow dynamics or the genesis of the BBB [32]. These studies suggest that cilia exist on BECs and that this is functionally involved in angiogenesis and the regulation of blood flow. A landmark study by Mentor and Fisher (2021) [31] evaluated the topographical landscape of BECs in barrier formation, elucidating which topographical structures play a role in facilitating the alignment of the paracellular spaces between adjacent BECs. However, cilia were conspicuously absent. In contrast, this is the first morphological evidence that strongly suggests that NTs play an important role in BBB-genesis. Thus, we address the schism between the high-resolution scanning electron microscopy (HR-SEM)-based evidence of endothelial NT generation observed during EC monolayer development, which provided insight into the development of the brain capillary, and compare this evidence to the immunofluorescence and molecular evidence underpinning the postulate for BEC "cilia".

2. Nomenclature Clarifying Morphological Structures

The nomenclature of tubular structures has produced lots of confusion in the use of terminology for structures that extend from the plasma membrane. We, hereby, attempt to address this by describing and defining clearly the structures filopodia, cilia and the different types of NTs.

2.1. Filopodia

Historically, cytoplasmic protrusions emerging from cells were denoted as filopodial extensions between adjacent cells. The term filopodia has its roots in the term pseudopodia, implying "false-feet". The filopodia, when broken down, implies a family of a specific type of foot-like structure, viz., an extension from a parental body (i.e., the cell) [33]. The filopodia are thought to be involved in the migration of the BECs crucial for the repair of the capillaries (viz. as seen in the *in vitro* scratch assays, or following an *in vivo* cerebrovascular accident). To date, filopodial structures have sometimes been incorrectly associated with tunnelling nanotubule (TUNT) formation [34–36]. In terms of dimensions, the size of filopodia is in the micrometer range (80 µm in length; see Table 1) and, therefore, by definition, they should not be categorized together with nano-sized morphological structures. It is, therefore, incorrect to refer to these structures as "nano"-tubules, as seen in Figure 1.

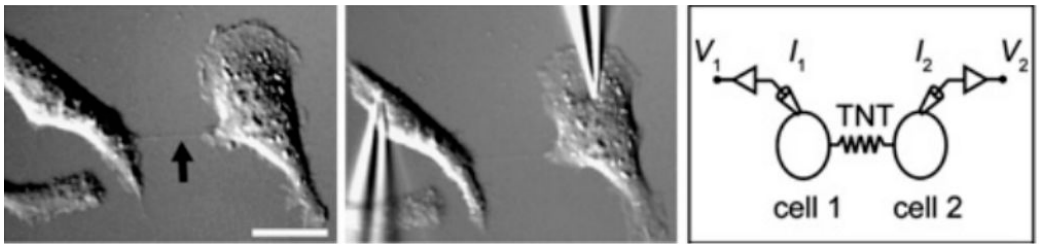

Figure 1. A micrograph illustrating filopodial "TNT" (tunnelling nanotubule) extensions between two normal rat kidney (NRK) epithelial cells (black arrow) (**Right**); during electrophysiological recordings (**Left**). Scale bar = 20 µm. V_1 and V_2 denote voltage applied to cell 1 and cell 2, and I_1 and I_2 denote the current injected into cell 1 and cell 2. These experiments indicated that filopodia electrically connect cells [37].

An electrical coupling study, reported in NRK cells, illustrated the ability to apply an electrical voltage to one cell and monitor its ability to conduct a current from cell to cell, across filopodia (TNTs), using patch-clamping techniques, suggesting that cells are able to communicate via these filopodia using electrical signaling (Figure 1). Furthermore, the filopodia are f-actin-based intercellular conduits that play a functional role in direct intercellular communication, spanning lengths of 10–80 µm. These filopodial-like f-actin-rich protrusions form intercellular cross-bridge networks. This was indeed the first tubular structure proposed that was reported to be involved in cell–cell interaction [34]. A study by Dieriks et al. (2017) [38] reported that filopodia possess a "cargoing" function between *in vitro* neuroblastoma cells implicated in Parkinson's disease (i.e., SH-SY5Y, human cell line). Furthermore, work describing the role of filopodial-like structures in brain tumors in mice showed the functional importance of tubular connections *in vivo* [38,39]. BEC filopodial structures are typically seen between cells grown on glass or in a Petri dish and, in terms of dimensions, are fundamentally in the micrometer range (see Table 1) and function primarily in terms of intercellular communication or migration.

Table 1. Comparison between filopodial and BEC NTs.

	Filopodia	**BEC NT**
Size	**µm**	**nm**
Diameter	200–400 nm [40,41]	50–100 nm [31]
Length	80 µm [42]	<1000 nm [31]
Location	Basolateral domain of cultured mouse melanoma cells [43]	Apico-lateral domain of cultured mouse BECs [31]

2.2. Cilia

Between the late 1990s and early 2000s, protruding cytoplasmic projections in BEC membrane surfaces were identified and, thereafter, [2,20,21] postulated these structures as endothelial cilia [22]. These reports stated that these endothelial cilia-like structures may be critical for vascular remodeling upon identifying cilia-like structures during vascular development (i.e., vasculogenesis and angiogenesis). However, how do we identify membrane protrusions as cilia?

By definition, the archetypical cilium is an apico-lateral-based structure, with a highly structured set of microtubules. These internal cytoskeletal microtubules are easily identified by TEM (see Figure 2). The typical conformation of its axoneme is constituted by nine pairs of post-translational, acetylated peripheral microtubules, which are arranged according to its motility status. Non-motile, primary cilia are present in mammalian cells (i.e., fibroblasts, epithelial and muscle cells) [44], which have a 9 + 0 arrangement of microtubules within their

axoneme; conversely, the motile cilia contain a 9 + 2 microtubule arrangement [2,21,45–47]. Generically, the cilium is rooted at its base by a basal body, which is derived from the centriole of the centrosome [48], the latter structure being essential for nucleating the mitotic spindle during cell division. During mitosis, the cilium is resorbed to release the centrioles, and cilio-genesis commences after the completion of cytokinesis [16,49] (Figure 2).

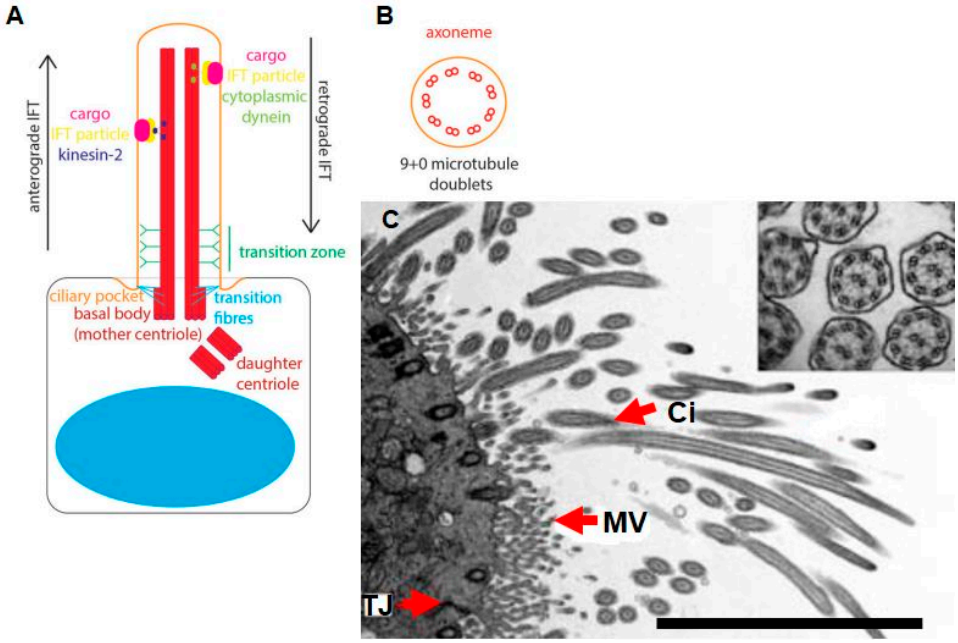

Figure 2. A schematic illustration of cytoplasmic protruding cilia, originating from the cell centrosome. (**A**) A typical primary cilium projecting from the cell surface, comprising cargo, viz., intraflagellar transport particles: kinesin-2 and cytoplasmic dyein; (**B**) a cross-section of a non-motile cilium, which assumes a 9 + 0 formation of microtubule doublets [16]; (**C**) a TEM image of tracheal epithelium and a cross-section of tracheal cilium displaying a 9 + 2 conformation. Ci denotes cilia, MV denotes microvilli and TJ denotes epithelial tight junctions. Scale bar = 8 μm [50].

The authors of Figure 2A–C give a strong rationale for defining cilia, namely that they have clearly seen this conformation via HR-TEM and thus have ascribed this function and structure to the cilium, based on micrographical data. Many differentiated mammalian cells have been reported to produce primary cilial extensions, which possess chemosensory and mechanosensory functions to respond to external stimuli, and thus are classified as organelles that function in integrative signaling from extracellular signals, promoting physiological functioning within cells [2,45,51,52]; however, to date, the exact nature of ciliary mechanosensory functions in BECs remains moot as no empirical data have been supplied to support this premise. The proverbial "elephant in the room" is that no one has reported an HR-TEM micrograph of the cytoskeletal structure of a BEC cilium. Given the extensive occurrence of immunofluorescence "evidence" reported for BEC cilia, it should be routine to use HR-TEM to identify BEC cilia.

2.3. Nanotubules

In contrast, nanotubules (NTs) are involved in cell–cell interaction across the paracellular spaces between adjacent BECs and, in terms of dimensions, are less than 1000 nM, and they are involved in the mechanical stabilization and alignment of the paracellular space, as well as intercellular communication. Before the study by Mentor and Fisher (2021) [31], existing reports of cytoplasmic projections failed to resolve the role of cytoplasmic-based NT projections between BECs during BBB formation. This study described the BEC NT as an expressed topographical structure on the apical surfaces of BECs. Furthermore, two novel NTs were described: nanovesicle (NV)-derived tunnelling NTs (TUNTs) and rope-like

tethering NTs (TENTs), which extend across the paracellular spaces between adjacent BECs during monolayer development. The TENT plays a crucial role in aligning adjacent BECs to facilitate the interaction of TJ zones between juxtaposed lateral BEC membranes and promotes cell–cell hemifusion/TJ interaction. Moreover, TENTs play a key role in the formation of the typical overlapping apical membrane regions of BECs, which shield TJ loci and reinforce paracellular occlusion, subsequently contributing to BEC monolayer integrity [31].

Moreover, BECs possess NVs, which are extruded onto the surfaces of BECs growing in close proximity. Some of these NVs are extruded from the cell membrane and possess a specific surface topography that is distinctly different from the plasma membrane. These NVs display a propensity to fuse together, forming a tube (tunnelling-nanotubule: TUNT) between BECs, which connects the lateral membranes of two adjacent cells. The significance of these NVs is that they are hollow and devoid of cytoskeletal structures. It is, therefore, inferable that the NVs possess the same molecular contents, which are involved in intercellular signaling processes, triggering the same morphological/molecular signals, which bring about BEC alignment during brain capillary endothelial development [31]. The NVs are thus secreted to form tubes, which connect two adjacent cells, with their ends incorporated into the BEC membrane, providing identical signaling between cells.

2.4. Postulational Brain Endothelial Cell Primary Cilium

Cilia are reported to be associated with quiescent cells, while cells that are involved in the cell cycle are non-ciliated (this is because the basal body of cilia forms the centrosomal bodies during cell division, and only after cells enter their quiescent phase do these centriole-derived basal bodies become available for ciliogenesis). Cilia are described as hair-like and/or flagellar structures that form on the cell surfaces of eukaryotes through the process of ciliogenesis [47,53]. Postulated cilia of the vascular endothelium are reported to extend into the lumen of the blood vessel and respond to sensory stimuli (i.e., extracellular stimuli) [29,45]. These "primary cilia" are described to be functionally involved in vascular barriers by exhibiting a sensory function that allows for the transmission of extracellular signals into the vascular endothelial cell, contributing to blood vessel function, through sensing blood flow and cell migration [2,22,32,45]. The index by which to conclude that an extracellular organelle extending from the plasma membrane of a BEC is in fact cilia requires that the following criteria be taken into consideration: is it an extracellular organelle adjoined with the plasma membrane, and are these extensions structured with a 9 + 2 or 9 + 0 microtubule cytoarchitecture; are these structures associated/anchored with a basal body and are they motile and/or sensory? [54,55]. Transmission electron micrographs support the presence of (9 + 0; 9 + 2) microtubule doublets in cross-sections of tracheal, intestinal and bronchiole epithelia [56]; however, evidence of this microtubule conformation in BECs has yet to be observed or reported in the literature.

Mohieldin et al. (2016) [51] reviewed primary cilia, postulated in blood vessels of mouse arteries and blood vessels of human patients (Figure 3).

In this review, the authors [57,58] postulate a mechanosensory function for primary endothelial cilia that is due to polycytin proteins (i.e., polycytin-1 and polycytin-2), which are reported to respond to changes in blood pressure or shear stress within the blood vessels, triggered by changes to the influx of calcium. The study, however, fails to concretize these postulates with empirical data (i.e., graphical and/or micrographical findings) and, thus, the role for BEC cilia has not been supported with concrete data. Endothelial cilia in cardiac arteries thus remain a postulate.

Postulated EC cilia have also been suggested to play a role in extracellular fluid mechanics in an intracellular signaling cascade, which activates endothelial nitric oxide synthase (eNOS) and results in vasodilation [51]. Furthermore, with respect to blood pressure and blood flow dynamics, it is well established that sphincters within the walls of arterioles and pre-capillary arterioles regulate the flow of blood through capillaries using neural and local mechanisms of vasodilation and vasoconstriction [59,60], which is driven

by the eNOS system and has never been linked to cilia's mechanisms of action. One critical function of the BEC is to regulate the flux of substances across the BBB; thus, it is unlikely that the primary cilium is at the nexus between fluid dynamics and vessel dilation of the brain' capillary ECs as the capillary lacks contractile elements and thus is not involved in modulating blood vessel diameter. The function of capillary diameter regulation is not the role of the endothelial cell, but rather the role of the pericytes of the BBB. This is well established in the literature [61].

Eisa-Beygi et al. (2018) [22] showed the emergence of cilia in early cranial vessels assembling during angiogenesis in hindbrain capillaries in a study utilizing zebrafish. "Cilia" distribution was seen in ECs upon intercrossing several tissue-specific transgenic reporter lines (i.e., *Tg(kdrl:mCherry-CAAX)*^{y171} (Figure 4) [62], which enabled the labeling of EC membranes to demonstrate the distribution of EC cilia [40]. The aim of this study was to measure flow velocity and shear stress. After 24 h, green fluorescent protein (GFP)-probed cilia were observed throughout the blood vessel, within the primordial midbrain channel, predominantly accumulating at the boundaries of intravascular spaces (Figure 4).

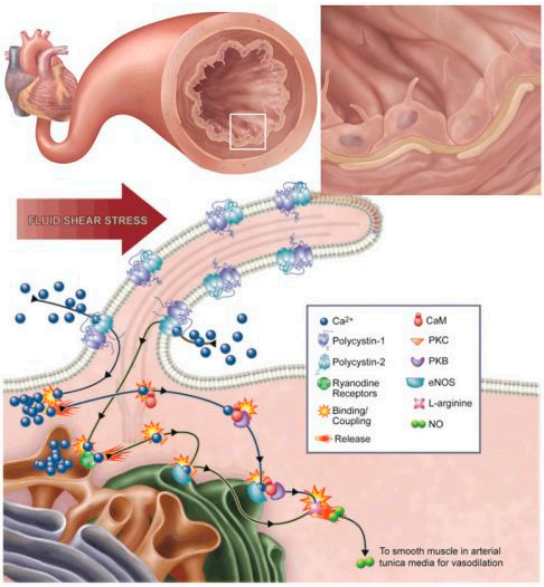

Figure 3. An illustration postulates endothelial primary cilia as regulators of blood pressure through nitric oxide production, which is transferred to the smooth muscle in arterial tunica media [51].

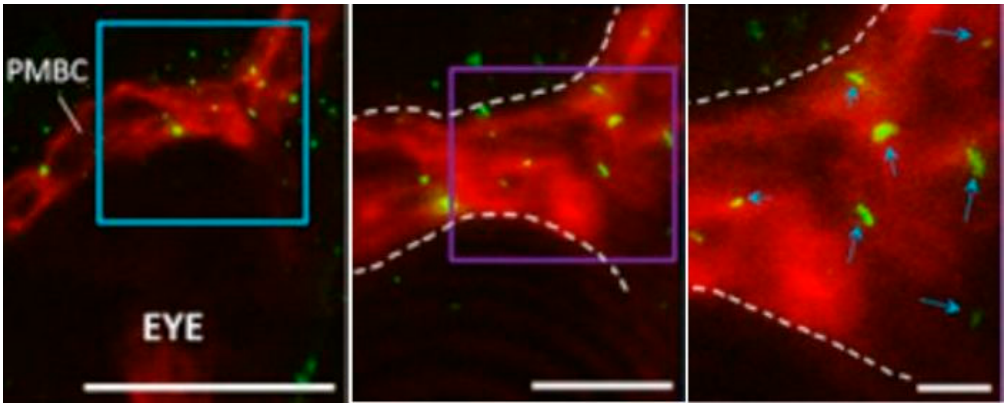

Figure 4. Determination of "cilia" distribution on EC membranes of primordial cerebral vessels. Confocal micrographs of GFP-labeled primordial midbrain channel in transgenic line *Tg (kdrl:mCherry-CAAX)*^{y171} and *(bactin::Arll3b:GFP)* to help label EC membranes. Scale bar = 40 μm [22].

Furthermore, low-resolution imaging was performed, utilizing confocal microscopy to visualize the characterized distribution of cilia in BECs. "Cilia" were found to be distributed around the edges of the cell, projecting into the intravascular spaces (Figure 5 below).

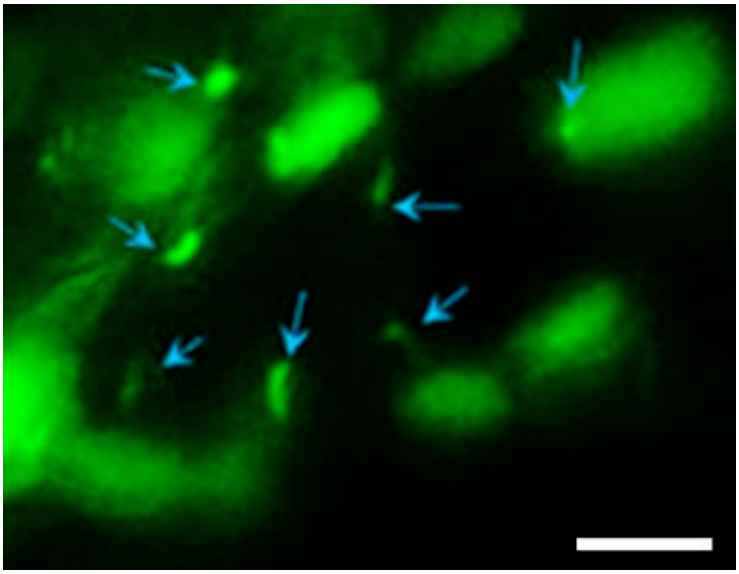

Figure 5. Photomicrograph of primary cilia, denoted by blue arrows. An illustration of GFP-labeled cilial extensions within primordial midbrain channels. Scale bar = 5 μm [22].

GFP refers to the gene that produces green fluorescent protein. The authors suggest that structures labeled with GFP are cilia (Figure 5) [22], which play a functional role in the early stages of cerebral–vascular morphogenesis; however, biologists normally use GFP as a generic protein marker. GFP can attach to and mark proteins with fluorescence, enabling scientists to see the presence of the particular protein in an organic structure. This type of fluorescent marking cannot explicitly identify cilia per se. This is evident as much more than just the "cilia" has been tagged with GFP fluorescence (Figure 5). Control of EC behavior and morphology is critical during vascular formation and remodeling; however, at such a low resolution, it is implausible to clearly identify a distinctive cytoskeletal profile of cilia. Furthermore, at this resolution, it is also unclear whether one can show the 9 + 2 cytoskeletal structure of the cilium, and supporting evidence from TEM microscopy has never produced proof to suggest the presence of endothelial cilia. What is clear is that GFP fluorescence extends from the soma of the BEC into these projections. This indicates that the protein-based cytoskeletal structure of the BEC projects into the tubular projection. This cytoskeletal immunofluorescence (IF) has also been described for TENTs in BECs, but, in the case of TENTs, clear HR-SEM micrographs support the IF-based evidence for TENTs.

GFP staining does not emphatically make a cytoplasmic projection a cilium—it simply implies that it is a tubulin-based structure and not "cilia" *per se*. Furthermore, nowhere do we see presented evidence of a 9 + 0/9 + 2 cross-sectional conformation.

Moreover, a study by Antal et al. (2017) [52] reported on mammalian cells possessing a primary cilium, which is generated during growth arrest of the cell. It further presumed that many single-layered epithelia possess a primary cilium, excluding the small intestine and the colon. Moreover, adenylate cyclase type III (AC3)-positive cilia were reported to be found in cells of mesenchymal origin, namely smooth muscle cells and ECs. AC3 is an enzyme involved in the synthesis of cyclic adenosine monophosphate from adenosine triphosphate and is found on the plasma membranes of the neuronal primary cilium. It was first reported to be present on olfactory neurons and has since been found in endothelial cells *in vitro* (Figure 6), which is in addition to the hypothesis that primary cilia may play a role in the regeneration of select mesenchymal cells. However, to date, there have been little to no postulations on the potential

role of AC3-positive cilia in BECs. AC3-based identification of cilia needs to be corroborated by additional evidence, viz., HR-TEM, as, on its own, it does not prove the presence of cilia.

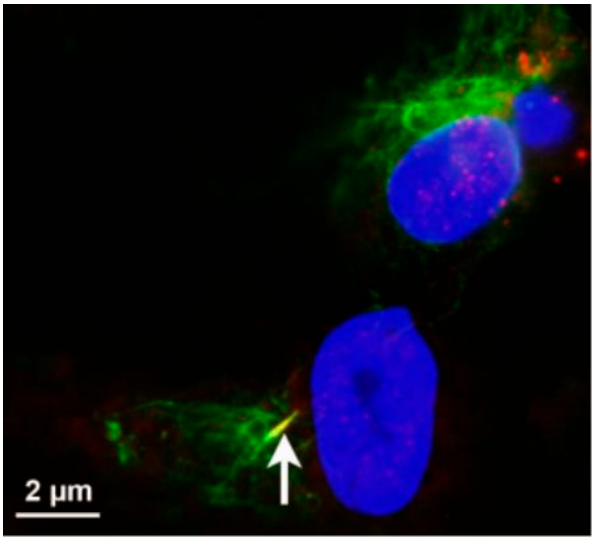

Figure 6. Immunofluorescence (IF) illustration of EC "cilium-like structures". The white arrow exhibits a gamma-tubulin AC3-positive tubular structure, which is postulated to be a cilium [52].

The "cilium" in Figure 6 was identified using immunocytochemistry, by studying the molecular dynamics of the cytoskeletal protein tubulin. The authors propose that an EC is able to display a singular acetylated tubulin-positive cilium. It is presumed that cilia are engendered from tubulin, which extends between two adjacent ECs [52].

Based on the cytoarchitectural dynamics of TENT structures, it is highly debatable that tubulin, which is ubiquitous within the cell's cytoskeleton, results in a single cytoplasmic projection. Based on the molecular dynamics of tethering NTs (TENTs), tubulin extends directly into the membranous protrusions from the BEC plasma membrane surface into TENTs between adjacent BECs (see Figure 7). In Figure 7, HR-SEM findings strongly suggest that focusing on a single projection negates the vastly complex physical functionality of cytoplasmic projections, which concentrate along the BEC membrane's leading edges, facilitating cell–cell engagement during BEC monolayer formation.

In addition, the study by Mohieldin et al. (2016) [51], suggests that the presence of primary "cilia" correlates with the onset of angiogenesis, suggesting that "cilia" are critical in the early processes of new blood vessel formation and damage to the "cilia" induces an array of vascular diseases [22,51,63]. Despite references that allude to the functionality of the EC primary cilium, namely its mechanosensing ability at the blood–tissue interface [45], the notion that BECs of cerebromicrovascular beds possess cilial-like structures within their lumen is difficult to conceive, as capillary pressure is directly proportional to blood pressure, which drives blood flow through the capillary, and thus the postulate that cilia on BECs are responsible for sensing/regulating capillary blood flow simply introduces an entirely new dynamic and/or obstruction to the functionality capillary flow dynamics that is not currently supported by empirical data. Nowhere do these postulates on ciliary function and blood flow of shear stress address the role of the pericyte in regulating local capillary blood flow.

A study by (Ma and Zhou et al., 2020) and (Kallakuri et al., 2015) [35,64] reported that "cilia" are present in the vascular ECs of zebrafish brains; however, in the absence of high-definition morphological clarity around these structures, it is understandable how its description of cilium structures could be misconstrued. These presumed cilia structures are likely being misidentified. Given these observations, it may be of interest to re-evaluate the data that have postulated the presence of EC "cilia" in light of new HR-SEM-based evidence in BEC endothelia [31].

Given the contention that these endothelial structures may be "cilia", it is important to note that, in the literature, there is a wide array of actin-based NT structures, which are denoted as TENTs, intercellular cross-bridges, NT highways and cytoplasmic projections. The most widely reported function of the NTs is their ability to cargo proteins, DNA, RNA, organelles and viruses [65]. However, the physical functionality of NTs in BBB construction is described for the first time in the *in vitro* BBB model [31,66]. The study addresses the functional role of actin and tubulin in the cytoskeletal structure of the TENT [66].

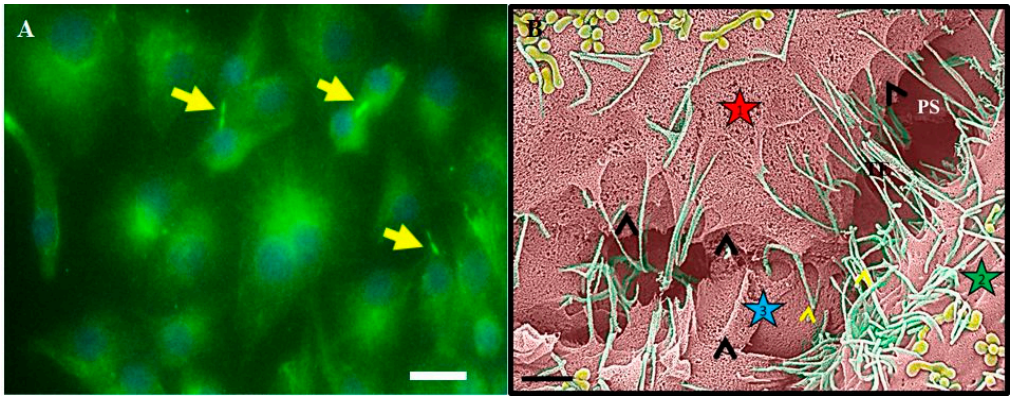

Figure 7. The cytoarchitectural organization of primordial cytoplasmic projections. (**A**) The formation of TENT extensions by cytoplasmic extension of α-tubulin in BEC bEnd5 cells, from the BEC leading membranous edges. The yellow arrows indicate TENT extensions, scale bar 20 µm [66]. (**B**) TENT formation on the apico-lateral surfaces of the BEC bEnd5 plasma membrane [31]. PS denotes the paracellular space; the stars represent cells 1, 2 and 3. The black arrows indicate areas of continuous membrane leading edges of BECs, governed by cytoplasmic projections, which develop into thin rope-like tethers. Scale bar 1000 nm.

2.5. TENTs

In a recent HR-SEM study by Mentor and Fisher (2021) [31], numerous cytoplasmic projecting nanostructures, denoted as BEC nanotubules (TENTs), were described (Figure 7A,B). In these studies, NTs are further divided into two membranous extensions: (i) tunneling NTs (TUNTs) and (ii) tethering NTs (TENTs) [31]. In contrast to the extrapolated evidence for postulated endothelial cilia, the authors use HR-SEM [31] to depict a highly dynamic set of apical and apico-lateral nano-projections from the BEC membrane. These high-definition photomicrographs have led to the postulate that tunneling NTs (TUNTs) and tethering NTs (TENTs) exhibit an ability to facilitate the alignment and localization of TJ proteins between adjacent BECs in culture, which is the hallmark of BBB establishment [31]. Tethering nanostructures are of interest in this review as they are observed extensions from the plasma membranes of BECs. These overlapping, tent-like structures progress to form slender ropes that play a role in the occlusion of the paracellular shunt between adjacent BECs and were, thus, denoted as TENTs. TENTs are observed as cellular protrusions, which are continuous with the apical and apico-lateral regions of BEC membranous leading edges and are, thus, extensions of the BEC phospholipid bilayer [28]. Furthermore, in a study by Mentor et al. (2022) [66], it was found that the ultrastructural TENT is governed by select cytoskeletal proteins (i.e., f-actin and α-tubulin). These findings endorse the influence of the TENT on endothelial barrier-genesis as the cytoskeleton is directly linked to the junctional and plaque TJ proteins, strongly suggesting that TENTs are critical in the alignment and interaction of BEC–cell junctions to form a well-regulated vascular barrier.

In the study by Mentor and Fisher (2021) [31], BEC TENTs were qualitatively evaluated using HR-SEM to generate a three-dimensional map to investigate its morphogenesis during BEC monolayer establishment. Furthermore, a supporting study by Mentor et al. (2022) [66] utilized depolymerizing agents (Cytochalasin D and Nocodazole) to suppress the expression of cytoskeletal proteins f-actin and tubulin during BEC monolayer devel-

opment, using immortalized mouse BECs (bEnd5) as an *in vitro* BBB model. In this study, interactions between adjacent BEC membranes were suggested to be facilitated by f-actin-rich microfilaments and α-tubulin-rich microtubules and were further proven to be the intracellular backbone of BEC TENTs [66].

The discovery of the TENT creates the contention between postulated EC cilia and ubiquitous BEC NTs. In view of the discovery of the BEC TENT, we question if indeed cilia are found on the surfaces of BECs, as a separate class of cytoplasmic projections. Despite having studied thousands of BECs under high-resolution microscopy and finding no evidence for apical cilia, one cannot exclude the possibility that they exist. However, if they are integral to the physiological function of the BEC or the brain capillary, then routine observation should clearly lead to their observation and, currently, this is not the case. Secondly, transmission electron microscopy (TEM) studies have been carried out on BECs for decades, leading to clarification of the molecular occlusion of the paracellular space by TJs, yet none have identified cilia. Even though the absence of cilia identified by HR-TEM/HR-SEM does not preclude their presence, it is essential that collaborated evidence is obtained before we start to ascribe postulated functions to these low-resolution, low-magnified structural extensions from the soma of BECs.

In Figure 7, cytoplasmic extensions are pervasive within BEC paracellular spaces, forming cell–cell networks and resulting in BEC membrane juxtapositioning, which further promotes TJ localization and the establishment of a highly restrictive BEC monolayer [66]. It is noteworthy, at this stage, to compare our documented IF micrographs of TENTs with those described in Figures 5 and 6 as cilia. These same NT structures seen with HR-SEM (Figure 7B) clearly do not depict "cilia".

The cytoplasm is a polyphase material and its dynamic nature has been insinuated to be central to the cytomechanics of cell shape, migration and division [67]. Furthermore, the role of cytoskeletal elements in TENT formation is a critical aspect of cytoplasmic modifications during BEC monolayer development. Based on the empirical findings in Figure 7 [66], TENTs are α-tubulin- and f-actin-rich tethering structures.

2.6. The Role of I-BAR Proteins' Nano-Tubular Formation

The role of f-actin in "membrane shaping" is key to cellular processes such as transcytosis, cell division, filopodial protrusions and NT formation [31,34,36]. The formation of membranous structures is endorsed by the role of regulators of membrane curvature, which is a family of proteins that comprises the crescent-shaped Bin/Amphiphysin/Rvs (BAR) domain [68].

I-BAR domains cause membranes to inversely/negatively curve towards the extracellular environment. I-BAR domains contain the actin-bundling protein with BAR domain-containing adaptor protein 2 (BAIAP2) homology (i.e., referred to as ABBA protein), which is associated with membrane protrusions. Furthermore, I-BAR domains have been reported to produce tubules within a range of 40–80 nm in diameter in *Escherichia coli* BL21 (DE3) cells [69]. The cell membrane, thus, becomes curved, allowing for (i) tubular carriers (i.e., lamellipodia/filopodia) and (ii) TENTs/TUNTs to form from flat membranes (Figure 8). These postulates are supported by the polymerization of actin polymers that are closely associated with protrusions that bring about cell membrane extensions [43,70].

The filopodia are rich in actin and their protruding extensions and are governed by cell membrane deformation by the I-BAR proteins, resulting in the negative curvature of the membrane away from the cell's cytoplasm [43].

Synthesis:

It appears that the TENT and "cilia" possess identical entrails of microtubule conformation, which begs the question, "were the postulated cilial structures actually developing primordial TENTs?" Given the low-magnification and low-resolution of these postulated cilia, was it simply a case of misinterpreting the visual and fluorescent data? The overall structure, function and localization of these two cytoplasmic variants could likely be narrowed down to cytoskeletal semantics. TENTs are inclined to accrue and develop on the apical and/or apico-lateral

plasma membranes of BECs and, in their early stage of development, resemble cilial structures. However, they mature into cytoplasmic projections, which form a tethering scaffold across the paracellular space of adjacent BECs during monolayer development, which is crucial for membrane alignment, interaction and the consequential occlusion of the paracellular space. Little is known about the sequential development of cilia structures. Moreover, given the HR-SEM evidence on TENTs, it has become clear that the TENTs are abundant on BECs during monolayer development. According to fluorescent-based observations, postulated cilia should be abundant on the apical surface of BECs, but when studied using either HR-TEM or HR –SEM, this is not observed. This critical review aims to show the contrast between primordial TENTs and structures identified largely through IF or molecular studies, which are postulated as "cilia". Both the postulated cilia and the TENTs are projections from the BEC apico-lateral membrane surface. Both have cytoskeletal structures, which include f-actin and/or tubulin. However, actual HR-SEM and HR-TEM evidence does not suggest that these structures are cilia, as they have no defined cilia microtubular cytoskeletal structure (9 + 2). Given that primordial TENTs, or newly developed TENTs, are short f-actin/tubulin extensions and that the evidence for cilia consists of mostly IF observations, it is easy to see why they may be misconstrued as "cilia" (Figure 9A).

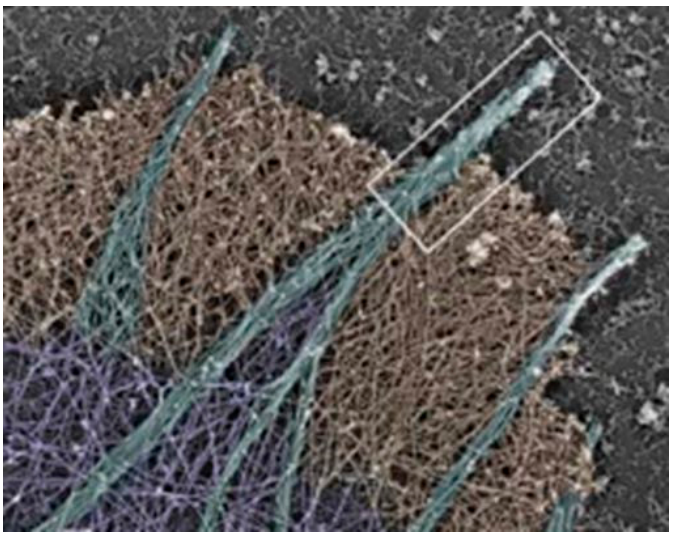

Figure 8. Electron micrograph of actin-based membranous protrusions from leading edges of cultured mouse melanoma cells as denoted by the white rectangle [43].

HR-SEM illuminates TENT development in an *in vitro* BBB model in Figure 9A. These cilia-like structures (early developing TENTs) are merely in a primordial state and, when fully developed, form TENTs [31].

Figure 9B emphatically illustrates a projecting "cilial" structure on the membrane surface of an EC [71]. Thus, we lean towards the postulate that cilia are in fact primordial versions of much more progressive TENTs.

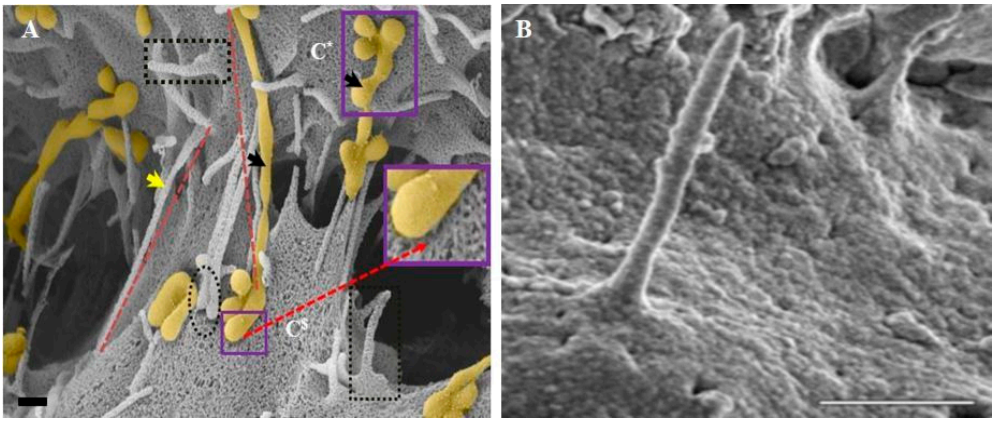

Figure 9. TENT development on the apical surface of BEC bEnd5 plasma membrane surfaces. (**A**) Early/primordial TENT development on the plasma membrane surface of the BEC at high magnification, represented in the black perforated boxes. C* denotes the membrane of cell one, C$ denotes cell two, the yellow arrow denotes a fully formed TENT structure extending across the paracellular space between two adjacent BECs and the black arrows denotes nanovesicle-induced TUNT structures. Scale bar = 200 nm [31]. (**B**) A SEM photomicrograph of proposed primary endothelial cilium at high magnification. Scale bar = 1 µm [71]. Note the similarity between the primordial TENT (perforated square) in (**A**) to the postulated cilium in (**B**).

3. Conclusions

The TENT and its primordial counterparts appear to be cellular protrusions that extend from the BEC membrane surface chemical stimulations. The cytoplasmic projections, both earlier (postulated cilia) and currently (primordial TENTs), appear to be identical with reference to the cytoarchitecture dynamics of the cell–cell extension features, which are governed by a cytoskeleton backbone (i.e., f-actin and α-tubulin). Furthermore, these cytoskeleton proteins act in concert to promote nanostructural TENT formation. HR-SEM studies have endorsed the observations of the transient formation of primordial TENTs, which develop into mature TENT nanostructures. Furthermore, HR-SEM scrutiny of thousands of BECs has yet to produce one observation of an authentic cilium or groups of cilia. To date, characteristic TENT features are unique to BECs. TENTs are essential for intercellular communication, facilitating BEC alignment and intercellular communication during endothelial barrier-genesis. The presence of TENTs is suggested to ensure the stability of the brain's vascular barrier and thus it is naturally instinctive to speculate that the previously postulated cilia are in fact primordial TENTs due to their intimate molecular association and their dimension similarities. Despite BECs employing tubules as a mechanism of transcytosis, no experimental evidence has emphatically described the step-by-step documentation of BEC primary "cilia" development; however, the progression of the BEC TENT into matured tethers during BEC monolayer development has been emphatically demonstrated. TENTs are infinitesimal in nature and form transiently, and thus their morphogenesis has only been discovered recently, at HR. This review illuminates these apico-lateral structures as pivotal in occluding BEC spaces, by the formation of highly restrictive, polarized endothelial sheets during BEC monolayer formation. TENTs are suggested to be critical for angiogenesis and subsequent barrier-genesis and, thus, represent promising therapeutic targets in the treatment of cerebrovascular disorders. It is, therefore, our considered perspective that the "cilia" postulated by the earlier studies suffered from not having access to high-definition microscopy, and thus, under relatively low resolution and low magnification, these cellular projections were simply misconstrued TENT or TUNTs.

Author Contributions: Conceptualization, S.M. and D.F.; validation, D.F.; resources, S.M.; data curation, S.M. and D.F.; writing—original draft preparation, S.M.; writing—review and editing, S.M.

and D.F.; visualization, S.M.; supervision, D.F.; project administration, D.F.; funding acquisition, D.F. All authors have read and agreed to the published version of the manuscript.

Funding: This research received no external funding. Funding was received from the University of the Western Cape (UWC) Senate funds.

Institutional Review Board Statement: Not applicable.

Informed Consent Statement: Not applicable.

Data Availability Statement: The data are archived according to UWC policies. All relevant data presented in this study are available upon request from the corresponding author.

Acknowledgments: This work was academically supported by the Department of Medical Biosciences at UWC and the Electron Microscopy Unit at the UWC, Cape Town, South Africa.

Conflicts of Interest: The authors declare no conflict of interest.

Abbreviations

Selected Abbreviations:

AC3	Adenylate cyclase type III
BBB	Blood–brain barrier
BEC	Brain endothelial cell
CNS	Central nervous system
EC	Endothelial cell
GFP	Green fluorescent protein
HR-SEM	High-resolution scanning electron microscopy
HR-TEM	High-resolution transmission electron microscopy
NT	Nanotubule
NV	Nanovesicle
TENT	Tethering nanotubule
TJ	Tight junction
TUNT	Tunneling nanotubule

References

1. Menaceur, C.; Gosselet, F.; Fenart, L.; Saint-Pol, J. The Blood–Brain Barrier, an Evolving Concept Based on Technological Advances and Cell–Cell Communications. *Cells* **2021**, *11*, 133. [CrossRef] [PubMed]
2. Cao, X.; Surma, M.; Simons, K. Polarized sorting and trafficking in epithelial cells. *Cell Res.* **2012**, *22*, 793–805. [CrossRef] [PubMed]
3. Langen, U.H.; Ayloo, S.; Gu, C. Development and Cell Biology of the Blood-Brain Barrier. *Annu. Rev. Cell Dev. Biol.* **2019**, *35*, 591–613. [CrossRef] [PubMed]
4. Wolburg, H.; Lippoldt, A. Tight junctions of the blood–brain barrier: Development, composition and regulation. *Vasc. Pharmacol.* **2002**, *38*, 323–337. [CrossRef]
5. Saint-Pol, J.; Gosselet, F.; Duban-Deweer, S.; Pottiez, G.; Karamanos, Y. Targeting and Crossing the Blood-Brain Barrier with Extracellular Vesicles. *Cells* **2020**, *9*, 851. [CrossRef]
6. Naranjo, O.; Osborne, O.; Torices, S.; Toborek, M. *in vivo* Targeting of the Neurovascular Unit: Challenges and Advancements. *Cell. Mol. Neurobiol.* **2021**. [CrossRef]
7. Serlin, Y.; Shelef, I.; Knyazer, B.; Friedman, A. Anatomy and physiology of the blood–brain barrier. *Semin. Cell Dev. Biol.* **2015**, *38*, 2–6. [CrossRef]
8. Banks, W.A.; Kovac, A.; Morofuji, Y. Neurovascular unit crosstalk: Pericytes and astrocytes modify cytokine secretion patterns of brain endothelial cells. *J. Cereb. Blood Flow Metab.* **2018**, *38*, 1104–1118. [CrossRef]
9. Brown, J.A.; Pensabene, V.; Markov, D.A.; Allwardt, V.; Neely, M.D.; Shi, M.; Britt, C.M.; Hoilett, O.S.; Yang, Q.; Brewer, B.M.; et al. Recreating blood-brain barrier physiology and structure on chip: A novel neurovascular microfluidic bioreactor. *Biomicrofluidics* **2015**, *9*, 054124. [CrossRef]
10. Erickson, M.A.; Wilson, M.; Banks, W.A. *In Vitro* modeling of blood–brain barrier and interface functions in neuroimmune communication. *Fluids Barriers CNS* **2020**, *17*, 26. [CrossRef]
11. Rajagopal, N.; Nangia, S. Obtaining Protein Association Energy Landscape for Integral Membrane Proteins. *J. Chem. Theory Comput.* **2019**, *15*, 6444–6455. [CrossRef] [PubMed]
12. Kadry, H.; Noorani, B.; Cucullo, L. A blood–brain barrier overview on structure, function, impairment, and biomarkers of integrity. *Fluids Barriers CNS* **2020**, *17*, 69. [CrossRef] [PubMed]

13. Martins, G.G.; Kolega, J. Endothelial cell protrusion and migration in three-dimensional collagen matrices. *Cell Motil. Cytoskelet.* **2006**, *63*, 101–115. [CrossRef] [PubMed]
14. Hladky, S.B.; Barrand, M.A. Mechanisms of fluid movement into, through and out of the brain: Evaluation of the evidence. *Fluids Barriers CNS* **2014**, *11*, 26. [CrossRef] [PubMed]
15. Sorokin, S. Centrioles and the formation of rudimentary cilia by fibroblasts and smooth muscle cells. *J. Cell Biol.* **1962**, *15*, 363–377. [CrossRef]
16. Wheway, G.; Nazlamova, L.; Hancock, J.T. Signaling through the Primary Cilium. *Front. Cell Dev. Biol.* **2018**, *6*, 8. [CrossRef]
17. Reese, T.S.; Karnovsky, M.J. Fine structural localization of a blood-brain barrier to exogenous peroxidase. *J. Cell Biol.* **1967**, *34*, 207–217. [CrossRef]
18. Aird, W.C. Phenotypic Heterogeneity of the Endothelium: II. Representative vascular beds. *Circ. Res.* **2007**, *100*, 174–190. [CrossRef]
19. Wu, Y.-C.; Sonninen, T.-M.; Peltonen, S.; Koistinaho, J. Lehtonen, Šárka Blood–Brain Barrier and Neurodegenerative Diseases—Modeling with iPSC-Derived Brain Cells. *Int. J. Mol. Sci.* **2021**, *22*, 7710. [CrossRef]
20. Händel, M.; Schulz, S.; Stanarius, A.; Schreff, M.; Erdtmann-Vourliotis, M.; Schmidt, H.; Wolf, G.; Höllt, V. Selective targeting of somatostatin receptor 3 to neuronal cilia. *Neuroscience* **1999**, *89*, 909–926. [CrossRef]
21. Gerdes, J.M.; Davis, E.E.; Katsanis, N. The Vertebrate Primary Cilium in Development, Homeostasis, and Disease. *Cell* **2009**, *137*, 32–45. [CrossRef] [PubMed]
22. Eisa-Beygi, S.; Benslimane, F.M.; El-Rass, S.; Prabhudesai, S.; Abdelrasoul, M.K.A.; Simpson, P.M.; Yalcin, H.C.; Burrows, P.E.; Ramchandran, R. Characterization of Endothelial Cilia Distribution During Cerebral-Vascular Development in Zebrafish (Danio rerio). *Arter. Thromb. Vasc. Biol.* **2018**, *38*, 2806–2818. [CrossRef] [PubMed]
23. Dyer, L.A.; Patterson, C. Development of the Endothelium: An Emphasis on Heterogeneity. *Semin. Thromb. Hemost.* **2010**, *36*, 227–235. [CrossRef] [PubMed]
24. Risau, W. Developing brain produces an angiogenesis factor. *Proc. Natl. Acad. Sci. USA* **1986**, *83*, 3855–3859. [CrossRef] [PubMed]
25. Okuda, K.S.; Hogan, B.M. Endothelial Cell Dynamics in Vascular Development: Insights from Live-Imaging in Zebrafish. *Front. Physiol.* **2020**, *11*, 842. [CrossRef]
26. Daneman, R.; Agalliu, D.; Zhou, L.; Kuhnert, F.; Kuo, C.J.; Barres, B.A. Wnt/β-catenin signaling is required for CNS, but not non-CNS, angiogenesis. *Proc. Natl. Acad. Sci. USA* **2009**, *106*, 641–646. [CrossRef]
27. Ben-Zvi, A.; Lacoste, B.; Kur, E.; Andreone, B.J.; Mayshar, Y.; Yan, H.; Gu, C. Mfsd2a is critical for the formation and function of the blood–brain barrier. *Nature* **2014**, *509*, 507–511. [CrossRef]
28. Marín-Padilla, M. The human brain intracerebral microvascular system: Development and structure. *Front. Neuroanat.* **2012**, *6*, 38. [CrossRef]
29. Ihezie, S.A.; Mathew, I.E.; McBride, D.W.; Dienel, A.; Blackburn, S.L.; Pandit, P.K.T. Epigenetics in blood–brain barrier disruption. *Fluids Barriers CNS* **2021**, *18*, 17. [CrossRef]
30. Haseloff, R.F.; Dithmer, S.; Winkler, L.; Wolburg, H.; Blasig, I.E. Transmembrane proteins of the tight junctions at the blood–brain barrier: Structural and functional aspects. *Semin. Cell Dev. Biol.* **2015**, *38*, 16–25. [CrossRef]
31. Mentor, S.; Fisher, D. High-Resolution Insights Into the *in vitro* Developing Blood-Brain Barrier: Novel Morphological Features of Endothelial Nanotube Function. *Front. Neuroanat.* **2021**, *15*, 661065. [CrossRef] [PubMed]
32. Ma, N.; Zhou, J. Functions of Endothelial Cilia in the Regulation of Vascular Barriers. *Front. Cell Dev. Biol.* **2020**, *8*, 626. [CrossRef] [PubMed]
33. Fukui, Y.; Inoué, S. Amoeboid Movement Anchored by Eupodia, New Actin-Rich Knobby Feet in *Dictyostelium*. *Cell Motil. Cytoskelet.* **2008**, *354*, 787–802.
34. Rustom, A.; Saffrich, R.; Markovic, I.; Walther, P.; Gerdes, H.-H. Nanotubular Highways for Intercellular Organelle Transport. *Science* **2004**, *303*, 1007–1010. [CrossRef] [PubMed]
35. Gerdes, H.-H.; Carvalho, R.N. Intercellular transfer mediated by tunneling nanotubes. *Curr. Opin. Cell Biol.* **2008**, *20*, 470–475. [CrossRef] [PubMed]
36. Gurke, S.; Barroso, J.F.V.; Gerdes, H.-H. The art of cellular communication: Tunneling nanotubes bridge the divide. *Histochem. Cell Biol.* **2008**, *129*, 539–550. [CrossRef]
37. Wang, X.; Veruki, M.L.; Bukoreshtliev, N.V.; Hartveit, E.; Gerdes, H.-H. Animal cells connected by nanotubes can be electrically coupled through interposed gap-junction channels. *Proc. Natl. Acad. Sci. USA* **2010**, *107*, 17194–17199. [CrossRef]
38. Dieriks, B.V.; Park, T.I.-H.; Fourie, C.; Faull, R.L.M.; Dragunow, M.; Curtis, M.A. α-synuclein transfer through tunneling nanotubes occurs in SH-SY5Y cells and primary brain pericytes from Parkinson's disease patients. *Sci. Rep.* **2017**, *7*, srep42984. [CrossRef]
39. Osswald, M.; Jung, E.; Sahm, F.; Solecki, G.; Venkataramani, V.; Blaes, J.; Weil, S.; Horstmann, H.; Wiestler, B.; Syed, M.; et al. Brain tumour cells interconnect to a functional and resistant network. *Nature* **2015**, *528*, 93–98. [CrossRef]
40. Salas-Vidal, E.; Lomelí, H. Imaging filopodia dynamics in the mouse blastocyst. *Dev. Biol.* **2004**, *265*, 75–89. [CrossRef]
41. Abounit, S.; Zurzolo, C. Wiring through tunneling nanotubes—From electrical signals to organelle transfer. *J. Cell Sci.* **2012**, *125*, 1089–1098. [CrossRef] [PubMed]
42. Miller, J.; Fraser, S.E.; McClay, D. Dynamics of thin filopodia during sea urchin gastrulation. *Development* **1995**, *121*, 2501–2511. [CrossRef]

43. Svitkina, T. The Actin Cytoskeleton and Actin-Based Motility. *Cold Spring Harb. Perspect. Biol.* **2018**, *10*, a018267. [CrossRef] [PubMed]
44. Venkatesh, D. Primary cilia. *J. Oral Maxillofac. Pathol.* **2017**, *21*, 8–10. [CrossRef] [PubMed]
45. Pala, R.; AlOmari, N.; Nauli, S.M. Primary Cilium-Dependent Signaling Mechanisms. *Int. J. Mol. Sci.* **2017**, *18*, 2272. [CrossRef]
46. Satir, P.; Christensen, S.T. Overview of Structure and Function of Mammalian Cilia. *Annu. Rev. Physiol.* **2007**, *69*, 377–400. [CrossRef]
47. Ma, R.; Kutchy, N.A.; Chen, L.; Meigs, D.D.; Hu, G. Primary cilia and ciliary signaling pathways in aging and age-related brain disorders. *Neurobiol. Dis.* **2021**, *163*, 105607. [CrossRef]
48. Nigg, E.A.; Stearns, T. The centrosome cycle: Centriole biogenesis, duplication and inherent asymmetries. *Nat. Cell Biol.* **2011**, *13*, 1154–1160. [CrossRef]
49. Basten, S.G.; Giles, R.H. Functional aspects of primary cilia in signaling, cell cycle and tumorigenesis. *Cilia* **2013**, *2*, 6. [CrossRef]
50. Henning, A.; Schneider, M.; Bur, M.; Blank, F.; Gehr, P.; Lehr, C.-M. Embryonic Chicken Trachea as a New *In Vitro* Model for the Investigation of Mucociliary Particle Clearance in the Airways. *AAPS PharmSciTech* **2008**, *9*, 521–527. [CrossRef]
51. Mohieldin, A.; Zubayer, H.; Al Omran, A.; Saternos, H.; Zarban, A.; Nauli, S.; AbouAlaiwi, W. Vascular Endothelial Primary Cilia: Mechanosensation and Hypertension. *Curr. Hypertens. Rev.* **2016**, *12*, 57–67. [CrossRef] [PubMed]
52. Antal, M.C.; Bénardais, K.; Samama, B.; Auger, C.; Schini-Kerth, V.; Ghandour, S.; Boehm, N. Adenylate Cyclase Type III Is Not a Ubiquitous Marker for All Primary Cilia during Development. *PLoS ONE* **2017**, *12*, e0170756. [CrossRef] [PubMed]
53. Ishikawa, H.; Marshall, W.F. Intraflagellar Transport and Ciliary Dynamics. *Cold Spring Harb. Perspect. Biol.* **2017**, *9*, a021998. [CrossRef] [PubMed]
54. Garcia, G., 3rd; Raleigh, D.R.; Reiter, J.F. How the Ciliary Membrane Is Organized Inside-Out to Communicate Outside-In. *Curr. Biol.* **2018**, *28*, R421–R434. [CrossRef] [PubMed]
55. Park, S.M.; Jang, H.J.; Lee, J.H. Roles of Primary Cilia in the Developing Brain. *Front. Cell. Neurosci.* **2019**, *13*, 218. [CrossRef]
56. Zhang, M.; Assouline, J.G. Cilia containing 9 + 2 structures grown from immortalized cells. *Cell Res.* **2007**, *17*, 537–545. [CrossRef]
57. Alaiwi, W.A.A.; Lo, S.T.; Nauli, S.M. Primary Cilia: Highly Sophisticated Biological Sensors. *Sensors* **2009**, *9*, 7003–7020. [CrossRef]
58. Nauli, S.M.; Kawanabe, Y.; Kaminski, J.J.; Pearce, W.J.; Ingber, D.E.; Zhou, J. Endothelial Cilia Are Fluid Shear Sensors That Regulate Calcium Signaling and Nitric Oxide Production Through Polycystin-1. *Circulation* **2008**, *117*, 1161–1171. [CrossRef]
59. Anderson, B.G.; Anderson, W.D. Scanning electron microscopy of microcorrosion casts; intracranial and abdominal microvasculature in domestic animals. *Am. J. Anat.* **1978**, *153*, 523–536. [CrossRef]
60. Itoh, Y.; Suzuki, N. Control of Brain Capillary Blood Flow. *J. Cereb. Blood Flow Metab.* **2012**, *32*, 1167–1176. [CrossRef]
61. Attwell, D.; Mishra, A.; Hall, C.N.; O'Farrell, F.M.; Dalkara, T. What is a pericyte? *J. Cereb. Blood Flow Metab.* **2016**, *36*, 451–455. [CrossRef] [PubMed]
62. Fujita, M.; Cha, Y.R.; Pham, V.N.; Sakurai, A.; Roman, B.; Gutkind, J.S.; Weinstein, B.M. Assembly and patterning of the vascular network of the vertebrate hindbrain. *Development* **2011**, *138*, 1705–1715. [CrossRef] [PubMed]
63. Luu, V.Z.; Chowdhury, B.; Al-Omran, M.; Hess, D.A.; Verma, S. Role of endothelial primary cilia as fluid mechanosensors on vascular health. *Atherosclerosis* **2018**, *275*, 196–204. [CrossRef] [PubMed]
64. Kallakuri, S.; Yu, J.A.; Li, J.; Li, Y.; Weinstein, B.M.; Nicoli, S.; Sun, Z. Endothelial Cilia Are Essential for Developmental Vascular Integrity in Zebrafish. *J. Am. Soc. Nephrol.* **2014**, *26*, 864–875. [CrossRef]
65. Acquistapace, A.; Bru, T.; Lesault, P.-F.; Figeac, F.; Coudert, A.E.; le Coz, O.; Christov, C.; Baudin, X.; Auber, F.; Yiou, R.; et al. Human Mesenchymal Stem Cells Reprogram Adult Cardiomyocytes Toward a Progenitor-Like State Through Partial Cell Fusion and Mitochondria Transfer. *Stem Cells* **2011**, *29*, 812–824. [CrossRef]
66. Mentor, S.; Makhathini, K.B.; Fisher, D. The Role of Cytoskeletal Proteins in the Formation of a Functional *In Vitro* Blood-Brain Barrier Model. *Int. J. Mol. Sci.* **2022**, *23*, 742. [CrossRef]
67. Charras, G.T.; Coughlin, M.; Mitchison, T.J.; Mahadevan, L. Life and Times of a Cellular Bleb. *Biophys. J.* **2008**, *94*, 1836–1853. [CrossRef]
68. Leite, D.M.; Matias, D.; Battaglia, G. The Role of BAR Proteins and the Glycocalyx in Brain Endothelium Transcytosis. *Cells* **2020**, *9*, 2685. [CrossRef]
69. Barooji, Y.F.; Rørvig-Lund, A.; Semsey, S.; Reihani, S.N.S.; Bendix, P.M. Dynamics of membrane nanotubes coated with I-BAR. *Sci. Rep.* **2016**, *6*, 30054. [CrossRef]
70. Pollard, T.D.; Borisy, G.G. Cellular Motility Driven by Assembly and Disassembly of Actin Filaments. *Cell* **2003**, *112*, 453–465. [CrossRef]
71. Dummer, A.; Poelma, C.; DeRuiter, M.C.; Goumans, M.-J.T.H.; Hierck, B.P. Measuring the primary cilium length: Improved method for unbiased high-throughput analysis. *Cilia* **2016**, *5*, 7. [CrossRef] [PubMed]

CHAPTER SIX: GENERAL DISCUSSION

The physiological motivation for this research study was to establish the role of nanostructures on the permeability of the *in vitro* BBB. This work demonstrates the novel, yet integral role of NTs within the context of BEC bEnd5 monolayer development as the cellular basis of the *in vitro* BBB. The study, for the first time, observes and re-counts the step-by-step morphogenesis of the BEC from singular cells to the establishment of a confluent monolayer on a nanoscale.

Utilizing high-resolution electron microscopy (HR-EM) as a tool, for investigating cellular morphology illuminated the complexity of the BEC monolayer. This complexity was analyzed. For the first time we observed an extracellular matrix extrude from singular, sparsely located BECs grown cellulose insert membranes. As the cells grew to confluence, the intercellular spaces became progressively convoluted, expressing an array of nanostructures. These novel BEC nanostructures, were comprised of nanovesicles (NVs), tunneling nanotubules (TUNTs) and tethering nanotubules (TENTs) in developing BEC bEnd5 cells in culture (Mentor and Fisher, 2021).

The NVs exhibited a highly porous appearance and have been postulated to generate chemoattractant and/or paracrine gradients between BECs growing in close proximity. Furthermore, another variant of NVs were able to fuse together, forming TUNTs, which connected juxtaposed BEC membranes of opposing cells. TUNTs function in aligning adjacent BECs and in so doing, chemically aligns the adjacent TJ zones, facilitating the juxtapositions of apico-lateral membrane domains in order

to bring about TJ zones of engagement. The significance of the NV-induced TUNT structures is its hollow interior, which is devoid of cytoskeletal structures. We postulate that NVs contain molecular signals, which bring about the alignment of the BECs. Since these NVs possess identical surface topography and are extrude from the same cells, we further postulate that they possess the same molecular contents, which trigger the same morphological and/or molecular signals in juxtapositioned cells (Mentor and Fisher, 2021).

Another category of nanotubules (NT) discovered was the tethering NT (TENT), which extends across the PC spaces of adjacent BECs. We observed a continuation of the outer plasma membranes amorphous material, forming a tent-link structure across the PC spaces. The TENT assembles as a cytoplasmic projection from the leading edges of BEC apico-lateral membranes and is likened to tethers/"tents", which spans across the entire PC shunt. The TENT, therefore, appears to be critical for reinforcing the occlusion of the BEC PC spaces (Mentor and Fisher, 2021).

A critical question that arose was, "what made it possible for tethering NTs (TENTs) to assume its functional morphology?" We investigated the cytoskeletal structure of the TENT utilizing immunofluorescence. For the first time we saw that the NTs contain f-actin and α-tubulin, furthermore, these cytoskeletal proteins were anchored to the soma of the BECs and extended into the TENT structure (Mentor *et al.*, 2022).

To endorse the physical functionality of the TENTs, we suppress its molecular underpinnings, by inducing depolymerization of the cytoskeletal proteins (i.e., f-actin and α-tubulin) using polymerizing suppressive agents Cytochalasin D and

Nocodazole (Mentor *et al*, 2022). The objective was to evaluate the relevance of BEC cytoarchitecture in TENT development.

The depolymerization of the select cytoskeletal proteins was confirmed using immunoblotting analysis showed a decrease in f-actin protein quantity, however, α-tubulin protein quantity remain variable.

Furthermore, we differentially investigated the implications of cytoskeletal protein suppression on select physiological parameters, namely: permeability, cell division, percent cell viability, percent cell toxicity and morphologically. The main thrust of this study was to determine NT relevance in BBB functionality. We observed major effects on BEC permeability upon f-actin depolymerization. TEER was the measuring index for BEC monolayer integrity/permeability. TEER data suggests that a breakdown in f-actin caused an increase in bEnd5 monolayer permeability, endorsing the role of f-actin in promoting shape to the BEC and associated NT projections, in addition to its, known, influence on intercellular TJ protein arrangement between BECs. The depolymerization of α-tubulin has a suppressed effect on BBB BEC permeability. By extrapolation of the HR-SEM and IF microscopy findings, α-tubulin assumes a more prominent role in signal transfer rather than influencing barrier integrity (Mentor *et al.*, 2022).

From the cell division findings, we infer that an inhibition in BEC numbers prevent the formation of a nanostructural scaffolding between adjacent BECs, which alters its ability to communicate in close proximity in order to establish a well-regulated, impermeable BEC barrier.

The hallmark for proper BBB functionality is its permeability status. Given the morphological information influencing BEC monolayer establishment, it was prudent to evaluate the role of NTs in facilitating the occlusion of the PC spaces between brain capillary bEnd5s as a critical event in establishing monolayer integrity. It is evident from the data on NTs that it forms an integral part of the *in vivo* BBB. By extension, cells grown close together forms a strict monolayer, which is reflective of the BBB *in situ* and its complexity, with respect to its morphogenesis cannot merely be organized in an *in vitro* model and, thus, choosing a suitable membrane substrate for BEC orientation and growth, in culture, is pivotal when studying its barrier-forming properties.

Transcribing the snapshot development of BEC ultrastructural dynamics and inculcating the mechanobiology governing its formation consolidates its physical functionality as critical for BEC alignment and, subsequent TJ localization during BBB establishment.

A thorough scrutiny of the literature revealed that researchers have previously reported on their observations of tiny, cytoplasmic projecting structures that appeared to be endothelial "cilia," under low-magnification (Eisa-Beigy *et al.*, 2018; Mohieldien *et al.*, 2016; Antal *et al.*, 2017). The structures had actin and/or tubulin, but no 9+2 conformation has seen in typical primary cilia (Cao *et al.*, 2012; Pala *et al.*, 2017).This lead us to attempt finding cilia by utilizing HREM on BEC monocultures. In view of the novel complexity of the BEC NTs it was naturally prudent to reassess the literature and critically evaluate the postulated BEC "cilia" in view of the new evidence emanating from this research study. The question thus was, "is it really cilia?" We critically discuss and review this notion at length in a

review paper, which highlights the misperception between endothelial cilia and endothelial nanotubes (NTs), by challenging rudimentary, physiological reasons why cilia within the endothelial vasculature are highly unlikely (Chapter 5).

The evaluation of the BBB is critical in order to understand neurodegenerative diseases progression. To date, the inability to manipulate the BBB persists hitherto our poor understanding of BBB establishment. The nanoscopic findings in this study invites novel descriptions and/or definitions for BBB development from a nanoscopic perspective.

CHAPTER SEVEN: GENERAL CONCLUSIONS AND RECOMMENDATIONS

7.1 General Conclusions

Recent work on nanotubules (NTs) have shown that a suitable basement membrane substrate is critical for developing an effective BEC monolayer establishment and/or barrier-genesis. High-resolution electron microscopy (HREM) and immunofluorescence imaging promoted the effective appraisal of cell-cell communication through direct, membranous NT formation, generated from the leading edges of the BEC plasma membranes.

Upon studying the cytoskeletal underpinnings of these NTs, by selective chemical perturbation/depolymerization of known cytoskeletal proteins (i.e. actin and tubulin), it is emphatic that the targeted proteins form the cytoarchitectural backbone governing the functional morphology of the tethering NT (TENT). Furthermore, the accumulation of NVs on the BEC cell surface and its amalgamation from mono-vesicles, to bi-vesicles, tri-vesicles and ultimately tubular structures, which span the PC pathway between adjacent BECs, has lead to the postulate that NVs induce a second ilk of NTs denoted as the tunneling NT (TUNTs). TUNTs and TENTs are not restricted to transport of cargo, but rather function as conduits (i.e. TUNTs) conveying chemotactic signals between cells and rope-like TENT ultrastructures, which bring adjacent BECs into alignment during BEC monolayer formation by generating overlapping membranous regions resulting in the occlusion of PC shunts.

The existence of these NT ultrastructures suggest that BECs are able to communicate with each other in a direct manner, thus, NTs may play a critical role in direct inter-endothelial interaction and subsequent barrier-genesis. Furthermore, TENT generation depends on the polymerization of f-actin and α-tubulin, which constitute the molecular, mechanistic underpinnings of BEC TENT cytoplasmic projections.

High-resolution (HR) imaging has illuminated unprecedented, nanostructural membranous, projections facilitating BEC interaction. BEC NT signalling and mechanics are found to be important events enabling the juxtapositioning of adjacent BEC membranes, which promotes highly specialized TJ engagement. Based on the research findings we can infer that BEC NTs are critical for processes such as angiogenesis and subsequent barrier-genesis. Moreover, TENTs and TUNTs may set new avenues for elucidating structural and functional imperatives in both the physiology and pathophysiology of BBB establishment.

Furthermore, early snapshots of BBB establishment *in vitro* provides a basis for potential prediction of neurodegenerative disease onset, making NTs a new target for future treatment and prevention of brain disease progression.

7.2 Recommendations

In order to understand the significance of BEC NV generation during *in vitro* BBB development it is naturally prudent to inhibit its expression to determine its significance in regulating the rate of BEC monolayer establishment. The use of Tipifarnib, an inhibitor of NV biogenesis will allow us to investigate the effect of NVs on cell-cell communication during BEC monolayer development.

Effect Tipifarnib in the inhibition of nanovesicle biogenesis

Tipifarnib is potential therapeutic agent utilized in advanced cancer treatment. **Figure 7.1.** shows the chemical structure of Tipifarnib. It functions by selectively inhibiting farnesyltransferase (FTase). FTase is an enzyme which functions in catalyzing the post-translational attachment of farnesyl groups (i.e., farnesylation) to signal proteins that are required for localization to the cell membranes (Datta *et al.*, 2018; Gilardi *et al.*, 2020).

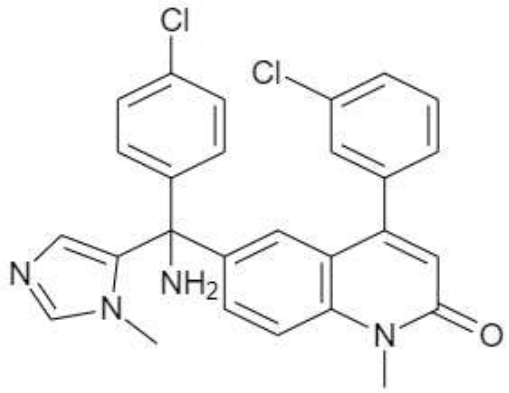

Figure 7.1. The chemical structure of Tipifarnib.

Tipifarnib (0–250nM) has been reported to cause dose-dependent decreases in NV/exosomal markers (i.e. ALIX, nSMase2, and Rab27a) in both C4-2B and PC-3 prostate cancer cells (Datta *et al*., 2018). For future study, we will focus on the effect of Tipifarnib as a potent inhibitor of NV/exosomal biogenesis in an immortalized mouse BEC line (bEnd5). Isolating the NVs and investigating its contents, would provide useful information with respect to the nature of the molecular signals released between BECs during cell-cell communication during monolayer establishment. Understanding both the nature of NVs/exosomes and isolating its contents is critical when elucidating molecular and morphological

phenomena/cellular events during barrier-genesis. It is known that exosomes are rich in RNA cargo (i.e. micro RNA, messenger RNA, transfer RNA etc.) (Squadrito *et al.*, 2014). Identifying specific BEC exosome/NV contents will provide useful information about the NV potential to form TUNTs and will facilitate our understanding of its functionality in forming a chemical signaling gradient during BEC communication.

REFERENCES

Antal, M. C., Bénardais, K., Samama, B., Auger, C., Schini-Kerth, V., Ghandour, S., Boehm, N. (2017). Adenylate cyclase type III is not a ubiquitous marker for all primary cilia during development. *PLoS ONE*, 12(1): 1–13. doi: 10.1371/journal.pone.0170756.

Cao, X., Surma, M. A., and Simons, K. (2012). Polarized sorting and trafficking in epithelial cells. *Cell Res*earch, 22(5): 793–805. doi: 10.1038/cr.2012.64.

Datta, A., Kim, H., McGee, L., Johnson A.E., Talwar S., Marugan J., Southall N., Hu X., Lal, M., Mondal, D., Ferrer, M., Abdel-Mageed, A.B. (2018). High-throughput screening identified selective inhibitors of exosome biogenesis and secretion: A drug repurposing strategy for advanced cancer. *Scientific reports*, 8(1): 1–13. doi: 10.1038/s41598-018-26411-7.

Eisa-beygi, S., Benslimane, F.M., El-Rass, S., Prabhudesai, S., Abdelrasoul, M.K.A., Simpson, P.M., Yalcin, H.C, Burrows, P.E., Ramchandran, R. (2018). Characterization of endothelial cilia distribution during cerebral-vascular development in zebrafish (*Danio rerio*). *HHS Public Access*, 38(12): 2806–2818. doi: 10.1161/ATVBAHA.118.311231.

Gilardi, M., Wang, Z., Proietto, M., Chillà, A., Calleja-Valera, J.L., Goto, Y., Vanoni, M., Janes, M.R., Mikulski, Z., Gualberto, A., Molinolo, A.A., Ferrara, N., Gutkind, J.S., Burrows, F. (2020). Tipifarnib as a precision therapy for HRAS - mutant head and neck squamous cell carcinomas. *Molecular cancer therapeutics*, 19 (9): 1784–1796. doi: 10.1158/1535-7163.MCT-19-0958.

Mentor, S., and Fisher, D. (2021). High-resolution insights into the *in vitro*

developing blood-brain barrier: Novel morphological features of endothelial nanotube function. *Frontiers in Neuroanat*omy 15: 1–15. doi: 10.3389/fnana.2021.661065.

Mentor S., Makhathini, K.B., Fisher, D. (2022). The role of cytoskeletal proteins in the formation of a functional *in vitro* blood-brain barrier model. *International journal of molecular science*, 23(2):742. doi: 10.3390/ijms23020742.

Mentor S., Cummings F., and Fisher D. (2022). Preparation of biological monolayers for producing high-resolution scanning electron micrographs. *PLoS ONE* (in press). dx.doi: 10.17504/protocols.io.bw37pgrn.

Mentor S., and Fisher D. (2022). The *ism* between endothelial cilia and endothelial nanotubules is an evolving concept in the genesis of the BBB. *International journal of molecular sciences*. 23 (5):1-16. doi:10.3390/ijms23052457.

Mohieldin, A. M., Saad, Z.H., Al Omran, A., Saternos, H.C., Zarban, A.A., Abou-Alaiwi, W.A., Nauli, S. (2016). Vascular endothelial primary cilia: Mechanosensation and hypertension. *Current Hypertension Reviews*, 12: 57–67. doi:10.2174/1573402111666150630140615.

Pala, R., Alomari, N., and Nauli, S. M. (2017). Primary cilium-dependent signaling mechanisms. *International. journal of molecular science*, 18(11). doi: 10.3390/ijms18112272.

Squadrito, M. L., Baer C., Burdet F., Maderna C., Gilfillan G.D., Lyle R., Ibberson M., De Palma, M. (2014). Endogenous RNAs modulate microRNA sorting to exosomes and transfer to acceptor cells. *Cell reports*, 8(5): 1432–1446. doi: 10.1016/j.celrep.2014.07.035.